UTS UNIVERSITY OF TECHNOLOGY SYDNEY

Classification of Spinal Cord Injured EMG Data for Locomotion Recovery

by Raymond Quong Yueng Chia

Thesis submitted in fulfilment of the requirements for the degree of

Doctor of Philosophy

under the supervision of Prof. Chin-Teng Lin and Dr. Yu-Kai Wang

University of Technology Sydney
Faculty of Engineering and Information Technology

October 2024

CERTIFICATE OF ORIGINAL AUTHORSHIP

I, *Raymond Chia* declare that this thesis is submitted in fulfilment of the requirements for the award of Doctor of Philosophy, in the *School of Computer Science*, *Faculty of Engineering and Information Technology* at the University of Technology Sydney.

This thesis is wholly my own work unless otherwise referenced or acknowledged. In addition, I certify that all information sources and literature used are indicated in the thesis.

This document has not been submitted for qualifications at any other academic institution. This research is supported by the Australian Government Research Training Program.

SIGNATURE: Production Note: Signature removed prior to publication.

Raymond Chia

DATE: 10th October, 2024

PLACE: Sydney, Australia

Abstract

A century ago, neuroscientists first noticed reflexively driven rhythmic behaviour in decerebrate cats. These observations led to the discovery of reflex and feedforward locomotion activity driven only by peripheral sensory feedback, namely the locomotor central pattern generator (CPG). Since then, even with limited descending brain input, we have seen extensive evidence of the spinal cord's capacity for use-dependence motor learning. Indeed, the spinal cord, without supraspinal descending input, can generate complex coordinated motor tasks with the appropriate neural environment and training. More and more evidence supports the idea of the spinal cord participating in preparation, execution, and adaptation events to express a responsive and coordinated sensorimotor system.

The following question was asked: "What is the appropriate neural environment in the spinal cord for use-dependent motor learning?". An extensive data set from an experiment performed on spinally transected rats in an enriched cage environment was analysed. The study looked at different combinations of pharmacological and electrical stimulation therapies after 6 weeks of training. Firstly, hindlimb step-like activity was logged during 6-hour recording intervals with a rule-based algorithm using only sparse electromyogram (EMG) ankle flexor and extensor activity. The algorithm results performed better at false positive rejection compared to existing methods in the literature.

The classification algorithm was improved by implementing multi-label deep learning network methodologies and trained on pre-processed continuous wavelet transform

(CWT) inputs. Complete deep learning classification analysis included implementing state-of-the-art vision transformers and domain invariant adversarial learning with depthwise separable convolutional neural networks. Results suggested greater spatiotemporal representations in vision transformers compared to depthwise separable convolutional neural networks.

Deep learning results were improved by incorporating curriculum learning with domain adaptation across subjects. Results were compared against self-supervised contrastive learning after pretraining from task-relevant EMG open-source datasets. Pretraining feature extraction layers before linearly training the classification layer with temporally aware domain adversarial strategy successfully bridged long- and short-term information across subjects.

From these captured step-like events, analysis of the EMG and motor-evoked potential (MEP) activity infer how the neurological state of the spinal cord affects spontaneous step-like events without any sensory input from treadmill activity. Combining quipazine (serotonin agonist), strychnine (glycine antagonist), and electrical stimulation most effectively elevated the locomotor neural networks towards a functional state, promoting a more significant number of 'self-training' events. MEPs, captured during detected hindlimb locomotion, contained spiking activity in middle and late responses strongly correlated to the functional state of the spinal cord.

A biologically constrained spiking neural network (SNN) model was developed to explain the mechanisms of sensory and neuromodulation integration in the flexor reflex circuit. The effects of body-weight-supported (BWS) locomotion, serotonin agonists, and electrical stimulation were investigated in a simulated inhibition-dominant SCI neural environment. Modulating the neural environment to reach a balanced excitation and inhibition state enabled the propagation of phasic flexion activation. The model explains the mechanistic basis of BWS for locomotion recovery.

Finally, future works are suggested, such as collecting pathological locomotion data from human subjects and incorporating extensor reflex circuity in the SNN. The proposed design allows interrogation of the origins and reasons for the emergence of polysynaptic late responses in MEPs during locomotor recovery.

Dedication

This thesis is dedicated to my mother who inspired and nurtured a young boy's scientific mind and a young man's character. I hope this work adds to the ever-growing evidence of your love for science and your children.

ACKNOWLEDGMENTS

I would like to sincerely thank my supervisor, Prof. Chin-Teng Lin, and co-supervisor, Dr. Yu-Kai Wang, for their tutelage and support during the later years of my PhD journey at the University of Technology Sydney (UTS). I am sure the decision to take on a student from a dissolved lab was not easy. For that, you have my greatest gratitude to have invited me into your space and provided the opportunity to complete my PhD under your supervision.

I would like to thank all the lab members in Computational Intelligence and Brain-Computer Interfaces (CIBCI) group for welcoming me in to your community. It was a lovely change to engage in scientific discussion, debug engineering issues, and receive support from people in similar circumstance. A special mention goes to Avinash, Charles, Howe, Jia, Minh, and Yanqiu.

Thank you to Prof Alaina Ammit, David Beins, and Dr Sinead O'Reilly for their support and guidance during the challenging transition of losing a supervisory panel.

I truly wish to emphasise the gratitude I have for my previous co-supervisor, Prof. Victor R Edgerton. My scientific rigour and independence as a researcher was seeded under your guidance. Thank you for showing me that one can be as intellectual and impactful as yourself, but also even more kind, generous, and gracious. Thank you to the 2018-2020 lab members of Edgerton Lab. You made a foreign and completely new environment feel closer to home. A special mention to Dr. Parag Gad for his mentorship and guidance in my early scientific career.

Thank you to all the friends back in LA, I hope to see you all soon and in good health. A special thank you to Michael Liu and Mrinal Neil Rath, thank you for your warmth and support over the years.

I would also like to acknowledge Prof. Bryce Vissel, had you not taken me on I would never have had the chance to have an experience like this. Thank you for committing to my scientific progress and your moral and financial support in the early years of my PhD.

I want to acknowledgement UTS School of Computer Science for their staff and support, especially to Matthew Gaston your support using the iHPC was critical. Thank you to the Research Training Program (RTP) scheme from the Department of Education and Training for funding my stipend.

I wish to thank all my friends who kept me sane. Namely Dom, Jeremy, Aidan, Chalin, and my partner Maybelle, for their support, laughter, and kinship.

Lastly, I could not have completed this journey without the support of my family, Terence, Veronica, and Kymberley Chia. Thank you for nurturing me and laying the foundation I needed to grow, learn, and cultivate a sense of wonder for the unknown. Your unconditional love has shaped me into the person I am today.

List of Publications

Related to the Thesis :

1. Chia, R., Zhong, H., Vissel, B., Edgerton, V. R., & Gad, P. (2020). Novel activity detection algorithm to characterize spontaneous stepping during multimodal spinal neuromodulation after mid-thoracic spinal cord injury in rats. In Frontiers in Systems Neuroscience (Vol. 13, Issue 82). https://doi.org/10.3389/fnsys.2019.00082

2. Chia, R., & Lin, C. (2024). Deep learning approach to multi-domain pathological locomotion and standing classification in sparse EMG signals. (In Draft)

3. Chia, R., & Lin, C. (2024). Biologically-Constrained Spiking Neural Network for Neuromodulation in Locomotor Recovery after Spinal Cord Injury (Under Review)

Others :

4. Chia, R., Nguyen, M., Liu, J., Zhu, H., Jin, C., Nguyen, V., Singh, A., Lin, C. (2024). Towards using Head-Worn Kinematic Data for Respiration Rate Estimation. (Under Review)

5. Chia, R., Nguyen, M., Liu, J., Zhu, H., Lin, C. (2024). Transfer learning for robust inter-subject cognitive work-load estimation. (In Draft)

Table of Contents

List of Figures

Figure **Page**

List of Tables

CHAPTER 1

INTRODUCTION

Spinal cord injury (SCI) can severly diminish somatic and autonomic nervous system capabilities. Symptoms vary depending on the location and severity of the lesion. Severe damage can lead to loss of voluntary sensorimotor control from the waist (paraplegia) or neck (tetraplegia) down. Adjustment to this new lifestyle is jarring and difficult, often involving the management of secondary effects such as pressure ulcers, bone fractures, depression, and pain syndromes (Sezer et al., 2015; Nas et al., 2015). SCI cases commonly present in young men, leading to a lifetime of reduced quality of life and economic burden (Ding et al., 2005).

The economic burden on these populations and their communities is incredibly costly, reaching lifetime medical expenses in the millions (Berkowitz et al., 1998; Collie et al., 2010). If treatment could improve muscle function in just 10% of people with SCI, it could offer $3.5 billion in cost savings for the Australian economy (Australia, 2020). Aiming to achieve voluntary activation of the spinal locomotor central pattern generator (CPG) is a potential recovery pathway towards walking activity (Rossignol and Frigon, 2011). Though the methods to achieve such a goal are under ongoing investigation (Minassian

et al., 2017).

Locomotor centres of the spinal cord establish a disproportionately inhibitory environment upon losing supraspinal (from the brain) descending input (Edgerton et al., 2008). Spinal cord stimulation via electrodes coupled to the skin, or epidurally, and pharmacological treatment offer some potential for recovering sensorimotor control (Harkema et al., 2011; Gad et al., 2018; Rabchevsky et al., 2011; Courtine et al., 2009).

The heterogenous nature of each person's injury requires granular balancing of the appropriate neuromodulation to elicit a safe and efficacious response (James et al., 2018). Robust and task-specific neurological measurement emerges as a method to better understand the causal effects of therapies and rehabilitation outcomes.

1.1 Research Problems

This thesis highlights two gaps in the field of neuromodulation for locomotion recovery. There is no immediate method for monitoring neural activity while undergoing treatment. Mechanistic explanations of neuromodulatory therapies lack the ability to describe subject-specific responses and adaptations while undergoing neuromodulation.

Two fundamental neurological principles can be leveraged to improve the field of neuromodulation. Firstly, the expression of sensorimotor activity is task-dependent (Hodgson et al., 1994; Fong et al., 2005; Taccola et al., 2018; Dietz and Fouad, 2014). This property intrinsically links the requirement for measurement and detection of task-specific activity. Secondly, the motoneuron (MN) is the final common pathway of sensorimotor circuitry (Brownstone and Bui, 2010). Thus, MN activity can be interpreted as the convolutional output of sensorimotor neural states (Edgerton and Gad, 2022).

The detailed works in this dissertation aim to exploit the measurement of invasive electromyogram (EMG) recordings during pathological gait by first developing reliable and subject-invariant classification algorithms for monitoring stepping and standing

rodent activity. By analysing extracted windows of activity, we determine the effects of various synergies between pharmacological and electrical stimulation therapies. Evidence suggests that the re-balancing of spinal neural circuitry by modulating excitation and inhibition at a sub-threshold level facilitates the functional state of locomotor networks.

1.2 Thesis Organisation

This thesis presents an in-depth literature review to develop an appreciation and understanding of the complexity of neuromodulation and the available measurement tools. The materials section describes the specific data set and labelling process to facilitate the development of the relevant work. Most of the work delves into extracting unilateral step and bilateral standing events in stochastic, multi-domain biosignals. Firstly, a new adaptive thresholding and rule-based algorithm is presented and compared against previously studied machine learning methodologies. The detection methods undergo improvements through innovative applications of deep learning methodologies, including vision transformers and transfer learning. Lastly, the thesis analyses the extracted events from the data set and proposes potential mechanisms and biomarkers for monitoring neural recovery after SCI.

- Chapter 2 reviews the historical and current perspectives of key concepts behind neurological recovery and neuromodulation. The structure and physiology of the spinal cord and CPG are briefly introduced. Furthermore, we delve into the mechanisms of neuroplasticity and examine its role in sensorimotor recovery following SCI. Finally, neuromodulation technology and methods to measure the effects of therapies are discussed.

- Chapter 3 summarises the main data set used for this thesis, describing the

instruments, surgical procedures, and recording methods. The method of manual labelling and the resulting distribution are also included.

- Chapter 4 introduces an adaptive threshold and rule-based algorithm to detect pathological unilateral stepping and bilateral standing events. The chapter compares the new algorithm with machine learning approaches. Previously reported and newly suggested methods failed to reliably predict pathological gait and standing events. The proposed rule-based algorithm was most successful in rejecting false positives.

- Chapter 5 aims to improve upon the results of Chapter 4 in two ways. Firstly, the requirement for handcrafted feature extraction across domains should be reduced through domain adaptation. Secondly, the first investigations will be performed on the effect of vision transformers in extracting long-distance representations of spatiotemporal-dependent locomotor activity.

  - Vision transformers encode spatiotemporal information towards locomotor relevant latent representations.
  - Domain adversarial neural networks failed to converge upon relevant locomotion and standing activity features across therapy domains.

- Chapter 6 presents curriculum learning from locomotor phase to whole gait as a new and efficacious method to classify pathological gait patterns. The new method was applied to inter-subject domain adaptation techniques. The conjunction of curriculum learning with domain adaptation bridged the inter-subject domain gap more successfully than self-supervised contrastive learning techniques.

- Chapter 7 analyses the extracted event data during pathological gait under multimodal therapies. Including serotonergic agonists appears critical to enabling

locomotor activity initiated only through sensory afferent activity. Combining serotonergic agonists, glycinergic inhibitors, and electrical stimulation tunes the neural environment towards a more excitable state. Finally, late responses (LRs) in motor evoked potentials (MEPs) suggest a correlation with local spinal circuitry and response to neuromodulation therapies.

- Chapter 8 details the design of a biologically constrained spiking neural network (SNN) of the flexor reflex circuit. The excitatory and inhibitory effects of neuromodulation with phasic proprioceptive afferents are investigated. Simulating an SCI and body-weight-supported locomotion environment provides results that elucidate the impact of balancing excitation and inhibition for successful locomotor recovery.

- Chapter 9 discusses potential future work to scale detection methods towards human studies using wearable electrode-embedded EMG sensors. An in-depth model of the locomotor CPG is designed with biologically constrained architecture. Future directions of further SNN modelling to provide a mechanistic explanation of the emergence of LRs in MEPs are discussed.

- Chapter 10 summarises the main contributions of this thesis and its implications for neurological recovery monitoring.

CHAPTER 2

Historical and Current Perspectives of Spinal Cord Locomotion Recovery

This chapter aims to summarise the anatomical and physiological aspects of the spinal cord and highlight the impact of spinal cord injury in a health-conscious and socioeconomic context. Core concepts in neuroplasticity, neurological recovery, and stereotyped responses in the spinal cord are explored, offering readers insights into current perspectives of sensorimotor networks. A broad review of the electrophysiological and genetic investigations to unravel the neuronal substrate of locomotion is included, as well as how this information leads to the development of targetted neuromodulatory therapies to recover sensorimotor function after SCI. The effects of these therapies will be covered across both animal and human studies. Finally, methods to map neurological changes to behavioural recovery using assessment and wearable tools are discussed.

2.1 The Spinal Cord

The text below summarises the core spinal anatomy and physiology necessary for a healthy human sensorimotor spinal cord. These structures and functions will reappear throughout the thesis and only core information will be included.

2.1.1 Anatomy

The spinal cord is responsible for communication between the brain and the body. Pulses of electrochemical signals, carrying sensory and motor information, constantly travel up and down the spinal cord (Catala and Kubis, 2013; Nógrádi and Vrbová, 2013). Despite protection by the bony vertebrae column, traumatic damage could lead to impaired neurological communication. To this extent, the severity and location of a SCI play a major role in the remaining motor and sensory function (Catala and Kubis, 2013).

The spinal cord contains 8 cervical, 12 thoracic, 5 lumbar, 5 sacral, and coccygeal spinal segments in the adult human and 33 vertebrae, 7 cervical, 12 thoracic, 5 lumbar, 5 sacral, and 4 coccygeal, see fig. 2.2. The bony structures of the vertebral column protect the spinal cord, while intervertebral discs allow smooth motion along the vertebral column. The spinal cord is covered by three fibrous membranes, the outermost dura mater, arachnoid, and innermost pia mater. See fig. 2.1 for a visual representation of the spinal cord gross anatomy. The cervical (C3-T1) and lumbar (L1-S2) vertebral enlargements contain a large population of neurons that innervate the arms and legs, respectively. The spinal cord is topographically organised, where motor and sensory neurons are mapped based on the distance from the trunk and function. Sensory nerve roots at certain spinal levels innervate specific body regions, known as a dermatome, see fig. 2.2. Similarly, motor nerve roots innervate specific regions known as a myotome.

The spinal cord is composed of an H-shaped grey matter cross-section, surrounded by white matter (see figs. 2.1 and 2.3). The white matter consists of the densely myelinated

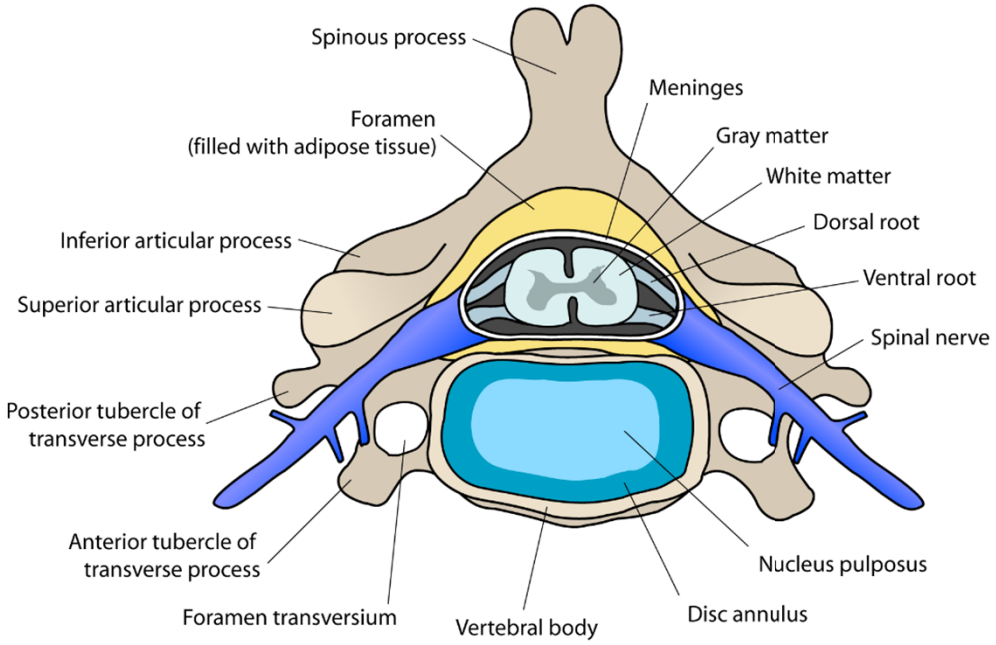

Figure 2.1: A cross-sectional view of the spinal cord, outlining protective features such as the vertebral body, vertebral disk, meninges and the major features such as the dorsal and ventral roots, and grey and white matter. Image ©Wikimedia user debivort `https://commons.wikimedia.org/wiki/File:Cervical_vertebra_english.png`.

white matter of the spinal cord, providing efficient sensory and motor information communication across multiple segments and towards the cortex. Grey matter consists of motor and sensory neurons, interneurons, and neuropils (glial cells and unmyelinated axons). The grey matter cross-section structure is organised into left and right dorsal and ventral horns. The dorsal horns contain most of the interneurons of the spinal cord, while ventral horns contain predominantly MN cell bodies.

Afferent signals arrive at the dorsal roots before synapsing to the spinal interneurons, where complex sensory processing functions occur. Efferent muscle contractive control synapse from ventral horn neuron pools. Running axially along the spinal cord is the central canal, filled with cerebrospinal fluid (CSF). The ventral and dorsal roots coalesce into two bundles and enter the dorsal root ganglion (DRG) in the intervertebral foramen,

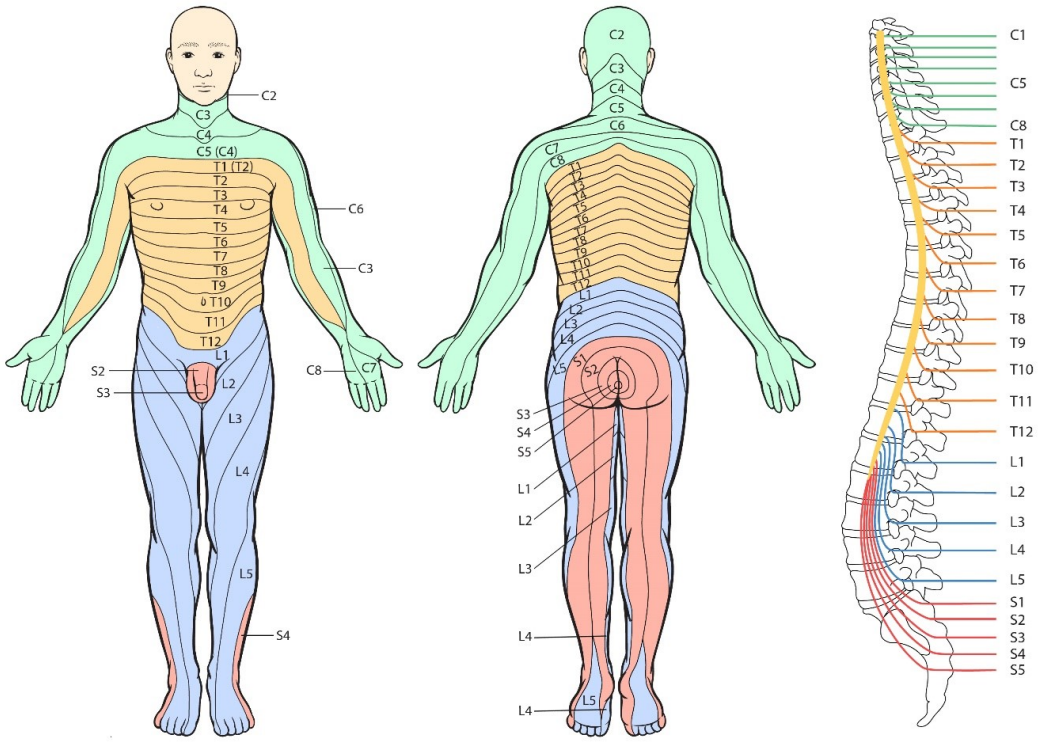

Figure 2.2: An approximate schematic of the sensory innervation mapped on the human body. Images ©Janet Fong, 2009 `http://www.aic.cuhk.edu.hk/web8/Hi%20res/dermatome.jpg`

where they exit and form the spinal nerve trunk. These break off into plexuses and eventually form the peripheral nerves (Nógrádi and Vrbová, 2013; Thau et al., 2021).

The grey matter in the spinal cord is organised by sections, called spinal laminae (of Rexed) see fig. 2.3. These sections are partitioned into 10 layers, designated by Roman numerals (I-X). At a high level, laminae I, II, and V receive noxious stimuli input; III and IV receive light-touch and position-related inputs; and laminae VI respond to mechanical signals from the joints and skin. Laminae VII exists in thoracic and upper lumbar segments from which preganglionic sympathetic fibres project and give rise to the cells of Clarke's column (posterior spinocerebellar tract). Laminae VIII and IX are somatotopically arranged and contain α– and γ–MNs and interneurons (INs). Lamina X surrounds the central canal and contains axons that cross to the opposite side of the

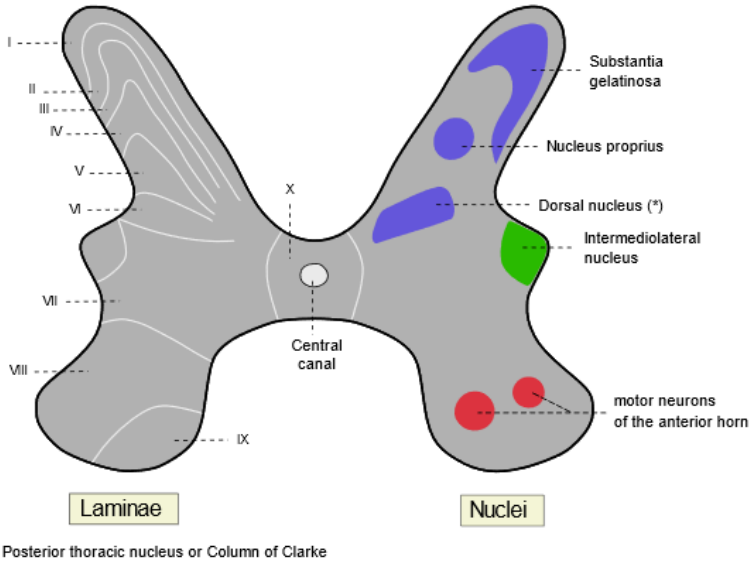

Figure 2.3: Organisation of the grey matter in the spinal cord by Rexed Laminae. Images ©User: Polarlys, 2006 https://commons.wikimedia.org/wiki/File:Medulla_spinalis_-_Substantia_grisea_-_English.svg

spinal cord (Sabharwal, 2013; Ganapathy et al., 2021). Refer to tables 2.1 and 2.2 for a summary of anatomical organsiation and projection of myelinated spinal tracts and table 2.3 for correlated laminae position and functional mapping. The dorsal column sensory tracts are modality organised with mechano- and propriosensory specific axon diameters (Niu et al., 2013). These organised structures are preserved across multiple mammalian species including rat, feline, canine, monkey, and human (Al-Chalabi et al., 2021).

The white matter holds densely myelinated tracts and rapidly delivers sensorimotor information to and from other spinal segments, cortical structures, and peripheral nerves. Ascending tracts include the spinothalamic, spinocerebellar, and dorsal column-medial lemniscal tracts (Al-Chalabi et al., 2021; Harrow-Mortelliti et al., 2021). Descending tracts include the corticospinal, vestibulospinal, tectospinal, and reticulospinal tracts (Sengul and Watson, 2012a; Harrow-Mortelliti et al., 2021; Sabharwal, 2013).

Table 2.1: A high-level summary of the various descending myelinated tracts longitudinally running through the spinal cord (Nógrádi and Vrbová, 2013; Sengul and Watson, 2012a,b).

Name	**Information**	**Originates**	**Termination**
Corticospinal tract	Contralateral voluntary movement	Motor cortex	Ventral horn
Rubrospinal tract	Motor function	Red nucleus of the midbrain	Laminae V – VII, mainly cervical and lumbosacral enlargements
Tectospinal tract	Coordinating head and eye movements	Midbrain	Laminae V – VIII
Vestibulospinal tract	Coordinating head and eye movements and maintain upright and balanced posture	Lateral and medial vestibular nuclei	Laminae VII – VIII of the ventral horn and terminate at α- and γ-motoneurons of laminae IX
Reticulospinal tract	Modulate preparatory, sensory information and spinal reflexes	Brainstem reticular formation	Laminae I, V, and VI – IX.

Table 2.2: A high-level summary of the various ascending myelinated tracts longitudinally running through the spinal cord (Nógrádi and Vrbová, 2013; Sengul and Watson, 2012a,b).

Name	**Information**	**Originates**	**Termination**
Dorsal Column Medial Leminiscal (Fasciculus Gacilis and Faciculus Cuneatus)	Dorsal and ventral columns carrying mechano- and propriosensory information	Nucleus dorsalis of Clarke column; laminae V and VII of the lumbosacral spinal cord.	Cerebellum
Spinothalamic tracts	Crude touch, pressure, pain, and temperature information	Laminae I, V, VII, and VIII	Thalamus
Spinocerebellar tract	Pain, touch, and temperature. Proprioceptive information	Laminae IV, V, and VII	Cerebellum

Table 2.3: A high-level summary of the laminae correlated functions in the spinal cord (Sabharwal, 2013; Ganapathy et al., 2021; Nógrádi and Vrbová, 2013; Sengul and Watson, 2012a,b).

Lamina	**Function**	**Synapse**
I – II	Axons carrying noxious and temperature signals synapse here.	Cross the midline via the anterior white commissure and ascend via the lateral spinothalamic tract.
III – IV	Processes vibration and pressure touch sensation. Carries proprioceptive impulses	Synapses to spinothalamic tract and carries proprioceptive impulses to the cerebral cortex via the dorsal medial lemniscus pathway.
V	A high number of dendritic interconnections receive sensory afferents from cutaneous, muscle, mechanical, and visceral nociceptors. Best suited for sensory integration	Many of the Rexed lamina V cells project to the brain stem and the thalamus via the contralateral and ipsilateral spinothalamic tract. Descending corticospinal and rubrospinal fibres synapse upon its cells.
VI	Propriospinal neurons or interneurons that target ventral horn MNs	Receiving sensory afferent input, rubrospinal fibres, tectospinal fibres, and other heterogenous INs.
VII	Premotor interneurons projecting to MNs. Involved in excitation and inhibition of different muscles	Receiving sensory afferent input, rubrospinal fibres, vestibulospinal fibres, tectospinal fibres, and other heterogenous INs.
VIII	Propriospinal interneurons play a role in coordination. Long pathways connect cervical and lumbar enlargements.	Receiving sensory afferent input, vestibulospinal fibres, and other heterogenous INs.
IX	α- and small γ-MNs, β-MNs and the remainder are INs	Receiving sensory afferent input, corticospinal tract, vestibulospinal fibres, and other heterogenous INs.
X	Receive somatic and visceral afferents with Aδ and C-fibres, plays a role in nociception and visceroception	Receiving sensory afferent input, and other heterogenous INs.

Propriospinal fibres in the white matter connect multiple segments of spinal cords (Sengul and Watson, 2012b; Jankowska et al., 1974). These axons connect ventral and dorsal horns, cervical and lumbar enlargements, and provide bilateral projections between the left and right sides of the spinal cord (Taccola et al., 2018). These are numerically dominant structures in the spinal cord and have heterogenous morphology. For a thorough review of the propriospinal system, see (Taccola et al., 2018; Laliberte et al., 2019; Flynn et al., 2011). For up-to-date morphology on spinal cord neurons and their pathways, see (Arle et al., 2019).

Spinal motoneurons are organised in columns across the rostrocaudal axis described as the median (MMC), lateral (LMC), hypaxial (HMC) motor columns, and the preganglionic column (PGC) (Stifani, 2014). Other spinal columns include the spinal accessory column (SAC) and the phrenic motor column (PMC). Of interest to sensorimotor recovery and the organisation of MNs in peripheral limb activity are the MMC and LMC. MMC MNs are located in the ventromedial region of the spinal cord and are mainly involved in the maintenance of body posture. LMC MNs are located ventrolaterally and connect to muscles of the appendages, limited to C5–T1 and L1–L5 vertebral levels (Stifani, 2014).

LMC MNs have medial-lateral populations topographically mapped such that medial MNs target the ventral portion of a limb and lateral MNs target dorsal limb muscles (Kania et al., 2000; Tosney et al., 1995). Moreover, LMC MNs have dorsal-ventral organisation and distally innervated muscles located more dorsally than proximal muscles (Bikoff et al., 2016). Similar topographical mapping has been observed in premotor neurons within the spinal cord where premotor INs segragate according to flexor-extensor (Tripodi et al., 2011) and distal-proximal (Goetz et al., 2015) muscle groups, see fig. 2.4.

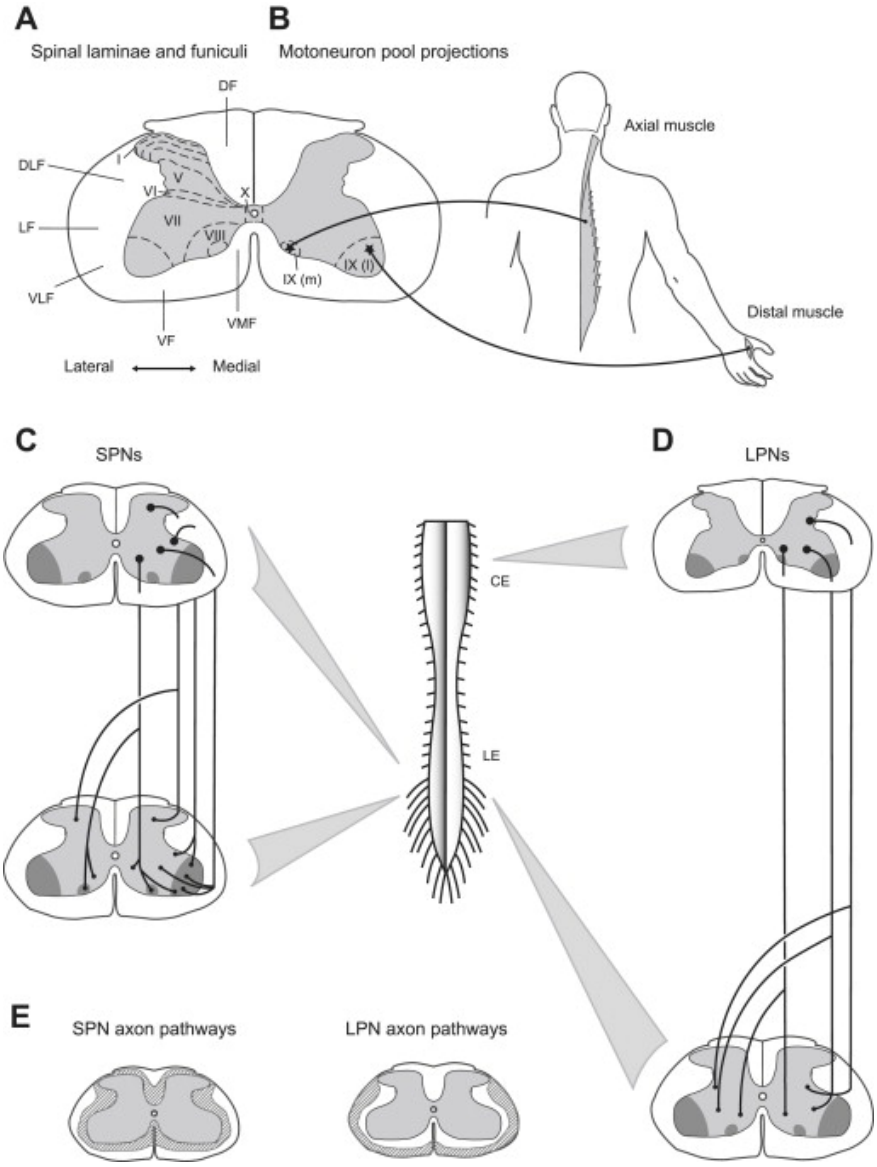

Figure 2.4: Organisation of the spinal cord and major propriospinal circuits, reused with permission from (Flynn et al., 2011). **A** and **B** shows the cross-section of the spinal cord and the laminae distribution and the relationship between lateral-medial and axial-distal innervation respectively. **C** and **D** illustrates the short (SPN) and long propriospinal neurons (LPNs) respectively, their projection patterns, and termination sites. **E** SPN axons are contained deeper in the spinal cord and are present across all funiculi of grey matter. LPN axons are superficial and predominantly present in lateral ventral and funiculi. SPN pathways spread across shorter distances in the vertebrae while LPNs communicate across cervical and lumbar enlargements.

The above summary details distinct spatial premotor and MN topographical mappings within the spinal cord. MN pools innervate specific muscles and receive preferential

information from descending and sensory inputs. Knowledge of the intended and affected neuronal populations assist with developing fine-tuned and specific neuromodulation therapies (Capogrosso et al., 2013).

2.1.2 Physiology

The action potential (AP) is the core underpinning neural mechanism of how CNS functions and different neural systems communicate. Neuron APs propagate in an all-or-nothing response along nervous tissue and facilitate neuronal communication via electrical and chemical transmission (Mortimer and Bhadra, 2018). A single soma maintains a baseline resting potential until it receives inputs via dendrites (Grider et al., 2024). Input potentials may be initiated by presynaptic neurons, external perturbations of sensory neurons, or spontaneously in pacemaker potentials. The latter case may lead to complex bursting patterns at differing frequencies (Nógrádi and Vrbová, 2013). Upon reaching threshold, an AP fires away from the cell body, down the axon hillock (see fig. 2.5 for illustration).

Table 2.4: Dorsal and ventral organisation or sensorimotor neurons in the spinal cord.

Position	**Name**	**Fibre Type**	**Information**
Dorsal	Muscle Spindle	Group Ia; Aα	Stretch Velocity
Dorsal	Muscle Spindle	Group II; Aβ	Stretch
Dorsal	Golgi Tendon	Group Ib; Aα	Tension Changes
Ventral	α-motoneuron	Aα	Extrafusal motor unit recruitment
Ventral	γ-motoneuron	Aγ	Intrafusal motor unit recruitment

Current educational standards explain voluntary motion as efferent signals travelling from the primary motor cortex down the spinal cord to synapse at MN pools. MN cell bodies are located in the ventral horn of the spinal cord and synapse at the neuromuscular

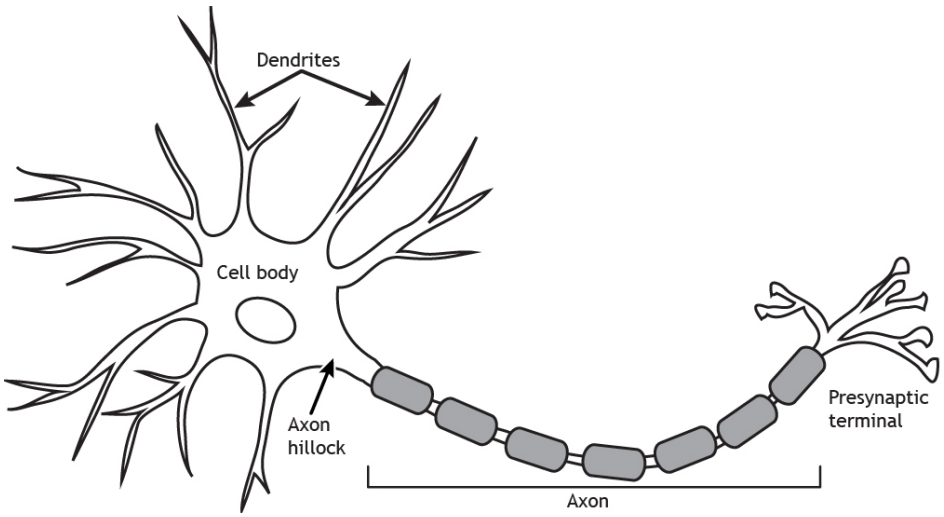

Figure 2.5: An illustration of a typical neuron. The cell body, or soma, receives information from other neurons. The dendrites conduct this information towards the soma. Action potentials fire away from the soma, down the axon, before reaching the presynaptic terminal. 'Neuron' by Casey Henley is licensed under a Creative Commons Attribution Non-Commercial Share-Alike (CC-BY-NC-SA) 4.0 International License. Image `https://openbooks.lib.msu.edu/app/uploads/sites/6/2020/11/Neuron.jpg`.

junction to several motor units. The spinal cord is precisely organised, separated by motor or sensory function in the ventral and dorsal regions respectively (see fig. 2.6). Information regarding key fibres and their function is summarised in table 2.4.

As the muscle contracts, afferent proprioceptive information is constantly relayed to the dorsal root ganglion (DRG). The DRG integrates sensory information and fires APs to IN structures which diverge to both the cortex and reflexive neural networks. The most fundamental is the reciprocal inhibition reflex (see fig. 2.7). Ia inhibitory INs receive Ia muscle spindle afferent input and produce a disynaptic inhibition on antagonist muscles (Hochman, 2007). The number of synapses involved in a reflexive motor process determines the magnitude and kinematic speed of the reflex. With greater recruitment comes greater dynamics. Stretch reflexes such as the knee jerk are categorised under a monosynaptic reflex whilst more complex motion with many synapses are described as polysynaptic. Historically, these reflexive activities were thought to be automatic, local responses in the spinal cord. However, as we will delve into later, modern research

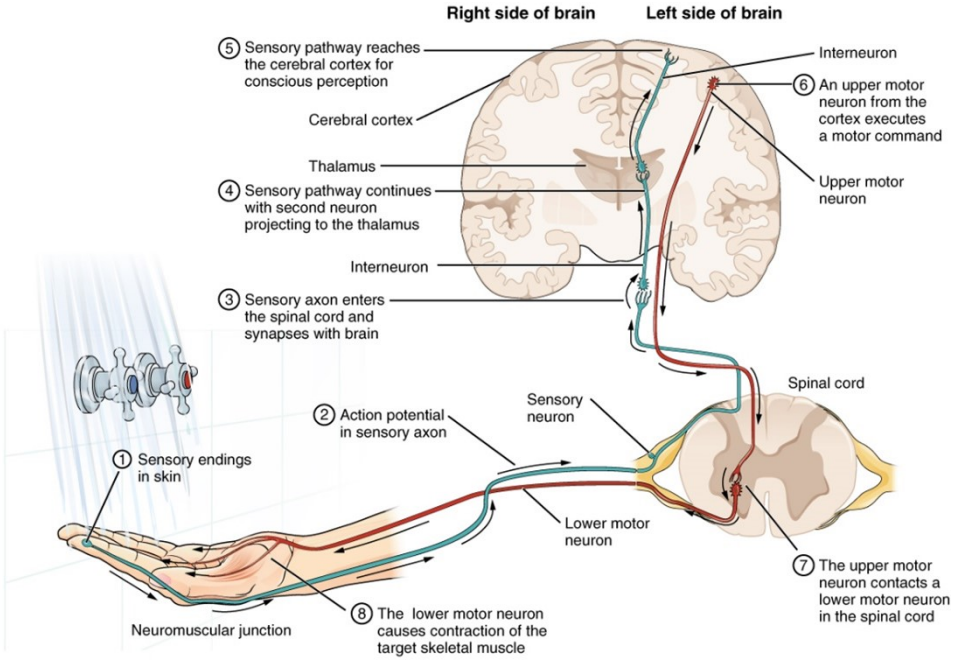

Figure 2.6: A graphical representation of voluntary movement and feedback of sensory information while testing the temperature of the water. Mechanosensory and thermoreceptive afferent fibres enter the spinal cord dorsally to inform the brain of the conditions of the external environment. Information regarding heat and pain is processed in the cerebral cortex. The voluntary motor efferent signal descends the spinal cord, exits at the ventral horn, and contracts the target muscle to act. Image ©Wikimedia user OpenStax `https://commons.wikimedia.org/wiki/File:1212_Sensory_Neuron_Test_Water.jpg`

highlights the complex integrative role of spinal cord reflexive circuits in coordinated sensorimotor function.

Able-bodied human proprioception is consciously and subconsciously sensed with dependence on the conscious attention of the person (Johnson et al., 2008). To give the reader an intuitive example, consider raising one's arm (Cordo and Nashner, 1982). The arm movement itself is voluntary and consciously perceivable. The force and stretch can be experienced through the shoulder, together with the tactile sensation and sound of fabric, the sight of the motion, and perhaps even the cooling of the skin. Now, one might repeat the motion but also focus on the sensation in the lower back and legs. One may notice some anticipatory muscle activity there. Interestingly, the same anticipatory

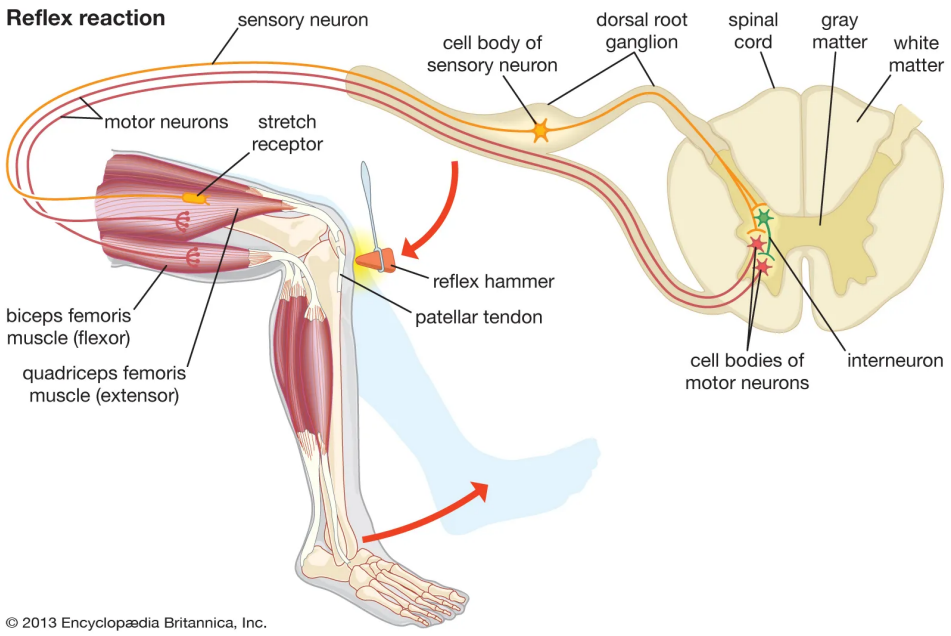

Figure 2.7: An example of the monosynaptic knee-jerk reflex. The hammer strikes the patella tendon, invoking a stretch in the intrafusal muscle spindles. The sudden change in muscle length sends an afferent signal to the DRG where an inhibitory and excitatory signal is synapsed at an interneuron. To keep the muscle taut, the quadriceps flex (excite) and the hamstrings relax (inhibit). Image ©Encyclopedia Britannica `https://www.britannica.com/science/knee-jerk-reflex`

activities become absent after exposure to microgravity environments (Layne et al., 2001; Layne and Spooner, 1990).

2.2 Spinal Cord Injury

Spinal cord injury (SCI) refers to damage to any part of the spinal cord and can be broken down into either primary or secondary injury mechanisms. Primary injury refers to the immediate physical injury to the spinal cord resulting from laceration, contusion, compression, and contraction of the neural tissue (Farooqui, 2010; Oyinbo, 2011). Pathological changes from primary injury mechanisms include severed axons, direct mechanical cell damage, rapid cell death and ruptured blood vessels (Oyinbo, 2011). Secondary injury is responsible for the expansion of the injury site and limiting

recovery potential (Dumont et al., 2001). Rehabilitation therapies aim to harness the regenerative and plastic capabilities of the nervous system and reduce the burden of injury (Dumont et al., 2001; Ding et al., 2005; Oyinbo, 2011).

2.2.1 Symptoms and Implications

In the event of SCI, damage to nervous tissue can result in several clinical loss of voluntary control and sensation. Paralysis commonly leads to secondary impairments such as respiratory, cardiovascular, urinary and bowel complications, spasticity, pain syndromes, pressure ulcers, osteoporosis, bone fractures, emotional disorders and loss of independence (Sezer et al., 2015; Nas et al., 2015; Migliorini et al., 2008). Activities of daily living (ADLs) become especially challenging for those with cervical SCI (Dickson et al., 2008). Due to these impairments, the effects of SCI have an immense impact on the person and surrounding community. Feelings of depression, anxiety, clinical-level stress, or post-traumatic stress disorder are common mental health problems in SCI populations (Migliorini et al., 2008).

The social, functional, and economic impact of a severe high-level injury at a relatively young age greatly influence the quality of life of friends, family and the individual (Trieschmann, 1988). To quantify the burden of disease, a metric known as the 'disability weight' is used (Salomon et al., 2015; van Hedel and Dietz, 2010). Disability weight is measured on a scale from 0, implicative of full health and 1, equivalent to death. The Global Burden of Disease 2013 study estimates a spinal cord lesion at the neck level to be 0.589 (treated) and 0.732 (untreated) (Salomon et al., 2015). Spinal cord injury can significantly reduce one's quality of life and introduce a high sense of burden from a young age.

2.2.2 Statistics

As of 2015, traumatic SCI affects an estimated 23.0 cases per million, ranging from 3.6 to 195 per million, worldwide (Jazayeri et al., 2015; Massetti and Stein, 2018). Most are young men, aged 16 to 30 years old (Ding et al., 2005). Commonly presented cases include incomplete tetraplegia (41%), incomplete paraplegia (19%), complete paraplegia (18%) and complete tetraplegia (12%) (Massetti and Stein, 2018). SCI management requires significant healthcare resources and takes a substantial emotional and financial burden on patients, families, and the community (Diop et al., 2021; Anderson, 2004). The treatment and lifetime medical costs can range from $1.47 million to $3 million CAD per person (Public Health Agency of Canada, 2013). In the US, the total annual economic burden of SCI is close to $18.5 billion USD (Berkowitz et al., 1998). A report commissioned by Spinal Cure Australia and Insurance and Care NSW (icare) details the financial burden to the goverment, individuals and their families, and losses in broader economic productivity with healthcare costs estimated at $3.7 billion AUD per annum (Australia, 2020) matching similar estimates from past research (Collie et al., 2010).

2.2.3 Severity

The severity of SCI follows the grading as per the International Standards for Neurological and Functional Classification of Spinal Cord Injury (ISCSCI-92), endorsed by the American Spinal Injury Association (ASIA) (Maynard et al., 1997). The paper recommends a series of motor and sensory scores, the ASIA Impairment Scale, clinical syndromes, and the Functional Independence Measure as an approach for assessing the impact of SCI on the individual's daily life activities and functions. The ASIA Impairment Scale (AIS) categorises complete injury as the absence of sensory and motor function and is defined as per table 2.5

There are SCI clinicians who view clinically complete SCI cases to be 'absolutely'

Table 2.5: ASIA Impairment Scale (AIS) in brief (Maynard et al., 1997)

AIS	Description
A	Complete; no sensory or motor function preserved in sacral segments S4-S5
B	Incomplete; sensory but not motor function is preserved below the neurological level and includes the sacral segments S4-S5.
C	Incomplete; motor function is preserved below the neurological level, and more than half of key muscles below the neurological level have a muscle grade less than 3.
D	Incomplete; motor function is preserved below the neurological level, and at least half of key muscles below the neurological level have a muscle grade greater than or equal to 3.
E	Normal; sensory and motor function is normal

complete (Dimitrijevic and Kakulas, 2020; Maynard et al., 1997). Despite this, research has consistently shown remaining sensorimotor function, even in chronic complete SCI patients, below the spinal lesion (Heald et al., 2017; Harkema et al., 2011; Gerasimenko et al., 2015a; Gad et al., 2018; Gerasimenko et al., 2015c).

From the above information, one could conclude that SCI significantly impacts the quality of life for many young adults and their communities. Thus, developing safe and efficacious therapies not only improves the quality of life of those affected but reduces the economic burden of healthcare systems.

2.2.4 Current Methods for Recovery

All SCI patients undergo a spontaneous recovery stage usually within the first 3 months after the lesion with a small amount of recovery occurring up to even 18 months or longer (Fawcett et al., 2007; Weidner et al., 2001; Steeves et al., 2011). This stage of recovery is also facilitated by modern-day surgical procedures, pharmacological treatments and physical therapy, reviewed in (Cadotte and Fehlings, 2011; Onifer et al., 2011; Kirshblum et al., 2007). Recovery gains may be attributed to neurological mechanisms between

axons spared from injury and intrinsic spinal cord circuits that relay information past lesion sites (Courtine et al., 2008).

Traditionally, rehabilitation focuses on functional restoration by maximising residual motor skills through therapeutic exercise or overcoming losses with compensation or assistive devices (Asín Prieto et al., 2016). Present-day neurorehabilitation paradigms emphasise functional neuro-recovery by taking advantage of remaining neural connections, plasticity, and repair mechanisms (Curt et al., 2008; Musselman et al., 2018; Cadotte et al., 2012). Regaining control and independence in the daily lives of patients with SCI is considered the primary goal for rehabilitation (Nas et al., 2015). To enable the patient to achieve their goals, short, and long-term functional milestones are developed by considering the severity and location of injury as well as the patient's desires (Nas et al., 2015; Kirshblum et al., 2007).

Physical and occupational therapy dosage is positively associated with the motor functional change in a sigmoidal fashion, such that improvements exponentially increased before reaching an asymptotic limit (Truchon et al., 2017). Efficiently increasing the therapy intensity and resource utilisation could reduce patient costs if the optimal strategy is applied to the patient (Truchon et al., 2017). While the extent of spontaneous recovery is significantly greater in incomplete lesion populations than in complete, patients that have tetraplegia demonstrate more recovery gain than those with paraplegia (Spiess et al., 2009; Kirshblum et al., 2004; Marino et al., 1999). These improvements are generally seen immediately below the lesion with a low probability of bringing functional benefits (Fawcett et al., 2007). This thesis focuses on the functional recovery of motor activity in SCI patients and its neuroscientific basis.

2.3 Neuroplasticity

Neuroplasticity is the adaptive or maladaptive changes within neuronal circuits that reflect the nervous system's reorganisation (Dietz and Fouad, 2014). Physiologically, neuroplasticity can be described as changes in synaptic formations and synaptic strength arising from intracellular property dynamics (Luft et al., 2016; Lüscher and Malenka, 2012). Spike time-dependent plasticity (STDP) has been demonstrated as the synaptic learning rule across multiple species, from insects to humans (Caporale and Dan, 2008). STDP describes the mechanism of presynaptic neuron firing, timing, and firing rate relative to the timing of action potential in the postsynaptic neuron (Froemke and Dan, 2002). In short, STDP is the Hebbian learning rule often summarised as the long-term potentiation and depression of synaptic strength according to the order and temporal interval between pre- and postsynaptic spikes (Hebb, 2005).

In the case of SCI, spontaneous recovery of sensorimotor functions has been attributed to factors such as the resolution of neuropraxia and re-myelination of spared axons (Dietz and Fouad, 2014; Heckman and Enoka, 2012). However, the following criteria must be met for non-maladaptive connections to be made. Firstly, cells must be alive or replaced (neural or tissue transplantation). The neural environment must be permissive for axonal growth. Correct signalling to select the desired target must be provided, and axonal re-myelination must be allowed (Asín Prieto et al., 2016).

The behavioural adaptations from neurorehabilitation recovery can be attributed to the abovementioned points. These adaptations to a post-lesion environment can occur within the spinal cord (Ding et al., 2005; Courtine et al., 2008). For example, spinal adaptation due to postural asymmetry of the hindlegs from cerebellar hemispheric lesion persisted after spinal transection (Di Giorgio, 1929). Similarly, extensive behavioural modification training created long-lasting changes in the H-reflex expression, which continued even after spinal transection (Wolpaw and Tennissen, 2001; Wolpaw and Carp,

1990).

In an isolated spinal cord, sensory afferents dominate the inflow of neural encoded information (Edgerton and Roy, 2009a). Repetitive task-specific training aims to leverage the sensory afferents and has been shown to improve synaptic efficacy and the expression of the trained behaviour (de Leon et al., 2001; Rossignol et al., 2006). After severe SCI in rats, providing appropriate afferent input to spinal circuits directs sprouting above and below the lesion, resulting in improved functional outputs (Goldshmit et al., 2008). Conversely, sprouting without direction from task-specific training leads to neurological dysfunction (Beauparlant et al., 2013). Successes in task-specific functional recovery have been replicated in cats (Rossignol et al., 2002) and non-human primate models (Courtine et al., 2007a; Capogrosso et al., 2016).

Studies incorporating functional magnetic resonance imaging (fMRI) have reported dynamic reorganization of the CNS following SCI (Oni-Orisan et al., 2016; Cadotte et al., 2012). Specifically, incomplete SCI subjects report an increased number of inter-spinal connections and an increase in the average number of active voxels in dermatomes of normal sensation in chronic SCI patients relative to healthy controls. Additionally, patients that reported full recovery from incomplete SCI maintained the increased degree of inter-spinal connections (Cadotte et al., 2012).

In humans, intense and repetitive training after SCI has been shown to promote cortical plasticity (Lynskey et al., 2008). Active exercise (i.e., overground locomotion, manual-assisted and robot-assisted partial weight training, repetitive upper limb training) requires patients to perform assisted or unassisted active movement (Hubli and Dietz, 2013). Voluntarily initiating motor activity reinforces functionally relevant synapses across cortical efferents, spinal neurons, and sensory afferents (Cote et al., 2017).

Of course, the limitation of this paradigm is that active voluntary exercise can only be performed by patients with some level of pre-existing motor function. Intentional

movement attempts reward subjects with greater rehabilitative gains over passive exercise (Gill et al., 2020b; Capogrosso et al., 2016; Wagner et al., 2018; Bonizzato et al., 2018). Thus, voluntary activation of sub-lesion neural circuits can be difficult for severely injured patients without the appropriate neural environment. Neuromodulation paradigms, such as Electrical Stimulation (ES), aim to enhance functional mobility by recruiting the body's existing neural pathways, allowing patients to practice activities that were not previously accessible (Lynskey et al., 2008; Edgerton et al., 2001a, 2004).

Developing new efficacious therapies to enable inaccessible neural circuitry is a worthwhile pursuit. Moreover, a high-intensity programme is pivotal to providing robust motor function improvement (Wolbrecht et al., 2008; Marchal-Crespo and Reinkensmeyer, 2009; Reinkensmeyer et al., 2012, 2016; Lotze and Cohen, 2006). Therefore, reliably mapping neurological states to functional outputs offers an equally important opportunity.

2.4 Sensory Integration in Spinal Sensorimotor Circuits

Spinal reflexes have historically been considered involuntary components restricted to invariable, stereotyped, and unmodifiable sensorimotor responses (Arber, 2012; Jankowska, 2013a). Edgerton and his team have proposed an alternative perspective on locomotor CPG: Sensory-informed feedforward coordination of motor pools is the primary mechanism for spinal locomotion (Edgerton et al., 2001a, 2004; Roy et al., 2012; Gerasimenko et al., 2017, 2016b). This feedforward capability has been observed throughout multiple motor tasks across species and is hypothesised to be attributable to both development and experience (Edgerton et al., 2001b; Bernstein, 1966). When investigating the neuroanatomical implications of Bernstein's motor laws, successful and smooth motor activity required spatially separated biological neuromotor groups to act in a predetermined

relationship (Whiting and Bernshtein, 1984). That is to say, in a feedforward, preparatory manner. The themes of feedforward spinal sensorimotor mechanisms will be further explored.

2.4.1 Central Pattern Generator

The common perception of the CNS considers the brain the primary control system of nearly all neurological functions (Thau et al., 2021). A solely cortical approach to motor control overlooks the time required for movement planning and execution and the adaptations computed from sensory feedback (Andrew, 2016; Whiting and Bernshtein, 1984; Strominger et al., 2012).

With many neuronal connections, processing time and cumulative errors can significantly hinder convergence towards an optimal movement pattern. This case was emphasised by the degrees of freedom problem. With the presence of biomechanical (Bernstein, 1966) and neurological (Hennig et al., 2018; Pham et al., 2020) redundancies, a continuous barrage of sensory inputs, and ever-changing working environments, motor control derived purely from cortical processing would simply be too slow for smooth, robust, and responsive movement (Andrew, 2016). When researching functional sensorimotor activity after traumatic injury to the spinal cord, it is natural to question how the brain and spinal cord bidirectionally interact with the PNS. The discussion surrounding biological sensorimotor control systems remains contentious, with many iterations and new hypotheses discussed across a multidisciplinary lens (Kandel et al., 2000; Merel et al., 2019; Gerasimenko et al., 2017; Latash et al., 2010; Dhawale et al., 2017; Wolpert et al., 1995; Shenoy et al., 2013; Escobar-Juárez et al., 2016; Orban De Xivry and Ethier, 2008).

So far, we discussed reflexes as a mechanism for reducing cortical computational load by accounting for movement smoothening, rapid stereotyped protective responses,

and resistance against perturbation (Sherrington, 1906, 1910). However, a more elegant proposal for solving sensorimotor neural resourcing may be the motor primitive model. Motor primitives off-load cortical sensorimotor processing tasks to smaller modular units that locally regulate and structure neural activity (Bizzi et al., 1991; Giszter and Hart, 2013; Giszter, 2015; Hart and Giszter, 2010; Flash and Hochner, 2005; Grau, 2014; Edgerton et al., 2004; Mussa-Ivaldi and Bizzi, 2000).

Motor primitive hypotheses are early in development and are accepted as a possible explanation for primitive, rhythmic motor behaviours such as walking, swimming, and standing. However, a model based solely on reflexes or synergies contradicts the Bernsteinean perspective of movement indeterminacy (Whiting and Bernshtein, 1984). Complex and practised movements such as playing a musical instrument, dancing, or ballistic motions cannot be completely predicted in a synergy-only hypothesis. Perhaps stereotyped, feedforward movements can only be performed in an experience-specific context, where ensembles of afferent and endogenous activity integrate to converge on the neural map that becomes a movement. The structure and mechanisms of the CPG are important considerations when researching the clinical impact of neuromodulation on SCI.

Pearson (1993) identifies three potential core roles of afferent feedback in the locomotor CPG. (1) The reinforcement of CPG activity, particularly during load-bearing activity. (2) Timing of motor output with particular regard to displacement and force. (3) Facilitation of phase transition. Spinal animals undergoing step-training on a treadmill showcase the ability of the lumbosacral spinal cord to combine multisensory inputs, adapt, and output locomotion (Roy et al., 2012). Coordinated and adaptable locomotion indicates the significant role of Golgi tendon organs, cutaneous, and muscle spindle afferent input (Van De Crommert et al., 1998; Rossignol et al., 2006; Rossignol and Frigon, 2011).

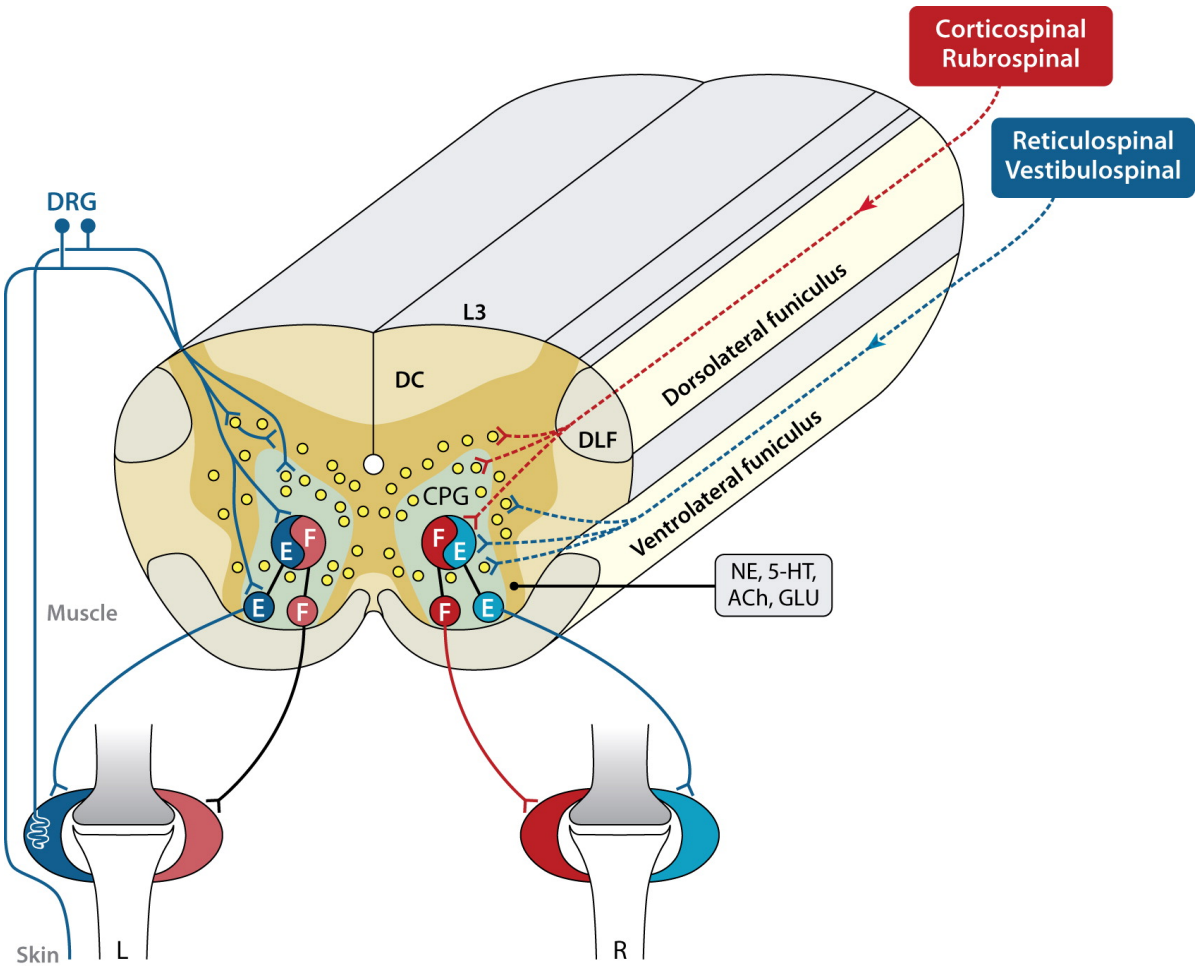

Rossignol S, Frigon A. 2011.
Annu. Rev. Neurosci. 34:413–40

Figure 2.8: Illustration of the existing idea behind the locomotor CPG in the lumbar spinal segment (L3-L4). The CPG produces the alternating activity between flexors (F) and extensors (E), coordinating in a bilateral fashion. Some interneurons transmit directly to MNs while receiving afferent and efferent activity. Several neurotransmitters have been found to transmit in the CPG including, norepinephrine (NE), serotonin (5-HT), glutamate (GLU), GABA, or acetylcholine (ACh). Sensory afferents project bidirectionally along the rostrocaudal axis. With permissions from Rossignol and Frigon (2011).

Sensory inputs from skin mechanoreceptors of the foot are involved in foot positioning (Bouyer and Rossignol, 2003; Barbeau and Rossignol, 1987; Belanger et al., 1996), locomotor expression (Abraham et al., 1985; Duysens, 1977; Forssberg et al., 1980a, 1975; Labella et al., 1992), and corrections (Bouyer and Rossignol, 2003; Duysens, 1977; Dietz, 2002; Forssberg, 1979; Park et al., 2019; Choi et al., 2016). Cutaneous inputs also have gain-modulating properties during the postural correction in locomotion (Bolton and Misiaszek, 2009; Mouchnino and Blouin, 2013) and have some involvement in the reinforcement of extensor activity (Duysens and Pearson, 1976; Guertin et al., 1995).

Muscle stretch (Group II) and stretch-velocity (Group Ia) proprioceptive afferent information, particularly in muscles of the hip joint, are important for locomotor initiation and phase adjustments (Sherrington, 1910; Kriellaars et al., 1994; Grillner and Rossignol, 1978; Andersson et al., 1978; Andersson and Grillner, 1981; Dietz, 2002). Dense quadriceps and sartorius group II afferents assist with step frequency, locomotion entrainment, and phase-transition sensitivity (Edgley and Jankowska, 1987; Andersson and Grillner, 1981; Pearson, 2008; Akazawa et al., 1982). A significant phasic reflex modulation in muscle stretch pathways maintains limb stability and force production (Zehr and Stein, 1999; Brooke et al., 1997).

Force input (Group Ib) is an essential sensory signal to locomotor pattern and standing (Zehr and Stein, 1999; Conway et al., 1987; Duysens and Pearson, 1980; Dietz, 2002). More specifically, sensing extensor force load has been proposed as a crucial input for locomotion entrainment (Duysens and Pearson, 1980; Pearson et al., 1992) and resetting the locomotion cycle (Conway et al., 1987; Gossard et al., 1994). A higher number of active INs and MNs were detected after load-bearing step training, suggesting load activity as a strong promoter of locomotor circuitry recruitment (Duru et al., 2015; Courtine et al., 2009).

Golgi tendon organs discharge maximally during stance and are positively corre-

lated to force output (Prochazka et al., 1989; Donelan and Pearson, 2004; Pearson and Collins, 1993). Concurrently, the extensor Ia and Ib afferent signals shape the amplitude, duration, and timing of ipsilateral extensor activity (Guertin et al., 1995). The locomotor spinal network uses sense-driven ipsilateral activation to maintain a high level of integration and adaptability (Forssberg et al., 1980b; Martinez et al., 2012).

The CPG's precise architecture and evolutionary function remain contentious (Rancic and Gosgnach, 2021; Grillner, 2021). However, the isolated spinal cord clearly contains complex circuitry that integrates incoming sensory information to produce stereotyped motor output.

2.4.2 The Smart Spinal Cord

Research across species has documented the spinal cord's capacity to integrate complex sensory inputs and produce adaptable, coordinated motor responses (Stuart and Hultborn, 2008; Hodgson et al., 1994; Edgerton et al., 1997b, 2001b, 2004, 2008; Edgerton and Roy, 2009a; Gerasimenko et al., 2016a, 2017; Wolpaw and Tennissen, 2001). Sensory integration and spinal IN pathways shape task-specific synaptic reorganisation during locomotor training (Kobayakawa et al., 2019). Thus, sensory integration in spinal pathways has a reinforcement role during locomotor recovery. While it is intuitive to consider trans-lesional axonal regrowth responsible for locomotion recovery in the spinal cord, results from retrograde labelling show no regeneration (Tillakaratne et al., 2010).

Other explanations for locomotor recovery through treadmill training after SCI have also been proposed. Such explanations include improved muscle strength, spontaneous recovery, and non-specific increased excitability (Rossignol and Frigon, 2011; Van De Crommert et al., 1998; Harnie et al., 2019). However, these effects improve functional output, spinal learning and adaptable sensory-driven spinal neural circuitry drive recovery.

2.4.2.1 Proprioceptive and Cutaneous Afferent Inputs

The spinal cord, receiving suitable excitation and step-training, can explore and reinforce specific efficacious sensory afferent integration pathways (Ichiyama et al., 2008a). Locomotor training with neuromodulation therapy enables spinal circuits to use sensory information to flexibly compute new motor and postural activity solutions without cortical input (Gerasimenko et al., 2017). Sensory information is sufficient to guide speed, direction adaptation and strength of load-bearing connections (Ichiyama et al., 2005; Minassian et al., 2013; Musienko et al., 2013). Moreover, variability during task-specific training can complement synchronous activation of spinal circuits via sensory afferent inputs (Shah et al., 2012; Rossignol and Drew, 1986; Shah et al., 2012; Ichiyama et al., 2008a; Edgerton et al., 2001a). Not providing sufficient variability can reduce coordination and range of motion (Edgerton and Roy, 2009b).

However, a lack of variation during training can disrupt the stereotyped progression of activation in locomotor CPGs (Ziegler et al., 2010). Even introducing environmental and mechanical perturbations after complete SCI, the spinal cord adapts to ensure smooth and uninterrupted locomotion (de Leon et al., 2002; Edgerton et al., 2001a; Timoszyk et al., 2002; Zhong et al., 2012; Chopin and Buerger, 1976).

Work in the upper limb has suggested that traditional, intrinsic spinal expression of CPG does not appear necessary for sub-threshold electrical stimulation to facilitate learning (Gad et al., 2018; Kumru et al., 2021). It is hypothesised that the spinal cord can compute errors from the planned output, adapt local circuitry through plastic changes, and restore coordinated motor function (Gerasimenko et al., 2017). The spinal circuitry achieves this by accommodating intrinsic variability and guiding adaptive mechanisms towards specialised pathways (Edgerton and Roy, 2009b; Courtine et al., 2009; Ichiyama et al., 2008a; Edgerton et al., 2008).

Edgerton and Roy (2012) argues that the CNS takes a ‘snapshot’ of cutaneous and

proprioceptive sensory information, then 'decides' what neurons to excite and inhibit as appropriate. Similar to that of an image being captured by the eye rather than processed by a singular pixel. In a more granular lens, the recent review (Edgerton and Gad, 2022) suggests sensory ensembles as input to select phase-specific combinations of interneurons to activate the next set of MNs to continue the stepping cycle. These state-dependent sensorimotor pathways have also been discussed in cortical dynamic representations as well (Shenoy et al., 2013; Hayashi et al., 2020).

Across species, including humans, body weight loading modulates motor pool activity (De Guzman et al., 1991; Edgerton et al., 1991; Wolpaw and Tennissen, 2001; Conway et al., 1987; de Leon et al., 1999). It is not the unique properties of CPG networks that generate rhythmicity and coordinated motor output but the dynamics of sensory ensembles. Like animal models, humans express a sensory-driven phasic response through the step-cycle, especially in the extensors (Courtine et al., 2009; Conway et al., 1987; Grillner and Dubuc, 1988; Forssberg et al., 1980a). Moreover, load-bearing and gravity-related sensory information reduces excitability or increases inhibition of spinal locomotor circuits (Gerasimenko et al., 2015b). These phasic modulations are hypothesised to be driven by presynaptic inhibition circuitry, gating further extensor activity whilst initiating flexor activation (Fink et al., 2014; Willis, 2006; Eccles et al., 1962).

Inhibitory neurons have a dominant effect in the lumbosacral spinal cord, hindering the propagation of sensory input towards locomotion entrainment after SCI (Edgerton et al., 2008). These inhibitory neurons may become dominant after reduced descending activity. Strong excitatory neurons require strong inhibitory inputs, while only small excitation is required for inhibitory neurons (Lee et al., 2019). It seems natural to address the inhibitory imbalance after injury. Notably, neuromodulation's role in presynaptic inhibition has yet to be thoroughly investigated (Lalonde and Bui, 2021).

Interestingly, γ-MNs undergo more extensive synaptic plasticity than α-MNs after spinal transection (Al'joboori et al., 2020). Indicating that γ-MN pathways significantly influence spinal learning and locomotor expression. The gating of sensory inflow has a considerable effect on integrating sensory information and generating smooth, controlled movements.

Flexible sensory-driven adaptations to continue stereotyped behaviour are thought to be shared across the CNS (Makino et al., 2016). Dynamical system representation, the representation of a system by first-order differential equations (Shenoy et al., 2013), and population reduction, pruning vast neural populations for a task, (Courtine et al., 2009; Ichiyama et al., 2008a) maybe a common feature in learning-driven changes in population encoding, reducing overlaps in space and time representation (Makino et al., 2016). After SCI, the delivery of timely sensory input to locomotor circuits becomes much more important. However, some descending information often bypasses the lesion and has some effect on spinal circuit modulation (Gill et al., 2020b).

2.4.2.2 Descending Command and Sensory Integration in the Spinal Cord

Spinal INs express pre-movement delay activity in the intact spinal cord, resembling supraspinal neuronal activity (Prut and Fetz, 1999). Thus, supraspinal commands may work to prepare motor actions, including the modulation of afferent information from the periphery to spinal and supraspinal levels (Cordo and Nashner, 1982). Alternatively, movement preparation may be embedded into the sensorimotor processes, co-occurring over distributed neural regions (Edgerton and Roy, 2012). This section briefly discusses the key research in uncovering the integration of descending volitional and ascending sensory activity.

Overlapping descending commands and sensory input synergise to elicit motor responses greater than the sum of either input (Gerasimenko et al., 2016a; Militskova et al., 2020; Mahrous et al., 2019). By increasing the excitability of the lumbar spinal

cord, simply imagining or observing locomotion activity can initiate rhythmic muscle activation in healthy humans (Gerasimenko et al., 2018). These effects are so strong that intentional participation with body-weight support can activate lower extremity muscles in chronic complete SCI human subjects receiving ES (Gill et al., 2020b). To promote stronger connections between cortical and spinal neurons, timed Transcranial Magnetic Stimulation (TMS) and PNS pulses enhance bidirectional neural activity after SCI, improving hand and lower limb function (Bunday and Perez, 2012; Bunday et al., 2018; Urbin et al., 2017; Jo and Perez, 2020). The paired TMS and PNS protocol promotes passive Hebbian-like activity by targeting weakened corticospinal connections after SCI (Benavides et al., 2020; Jo and Perez, 2019; Christiansen and Perez, 2018; Federico and Perez, 2017; Baker and Perez, 2017).

The role of sensory feedback heightens after SCI, most likely from loss of supraspinal structures (Rossignol and Frigon, 2011). Jiang et al. (2016) found competitive interactions between proprioceptive and corticospinal axons that participate in the organisation of mature corticospinal axons and spinal motor circuits. By eliminating descending cortical input, the spinal circuit increases corticospinal contacts. Conversely, eliminating primary afferent fibre input results in a greater number of afferent contacts with spinal neurons. Competitive interactions do not mean one source becomes more important than the other; neurons utilise whatever reliable inputs they receive.

Ascending and descending information synergistically modulate the spinal circuits at a cellular level. Further work is required to track these changes before, during, and after movement execution. In summary, findings across animal and human studies support the hypothesis of the electrically activated neural pathways elevating the excitability of spinal circuitry to enable activation by supraspinal and sensory inputs.

2.4.3 Activity Dependent Recovery

Afferent information can robustly reorganise functional connections among spinal sensorimotor networks and refine them to specific acute and chronic pathways (Edgerton and Roy, 2009a). Researching approaches aimed at maximising function after SCI and uncovering the mechanisms of activity-dependent plasticity within the spinal cord is a logical starting point for understanding the acquisition and maintenance of skilled behaviour (Wolpaw and Tennissen, 2001; Edgerton et al., 2001a, 2008, 1997a; Edgerton and Roy, 2009b).

The chronic transected spinal cord can generate full weight-bearing hindlimb stepping or standing by exposing the spinal circuits to the appropriate sensory information (de Leon et al., 1999; Dietz and Muller, 2004). However, cats trained to stand had poor locomotor capability and vice versa (De Leon et al., 1998a,b). Adaptations include modifications in the glycinergic pathways that provide inhibition. (Edgerton et al., 2001a). Inhibitory circuits, mediated mainly through glycine and GABA, modulated to recover locomotion (Caron et al., 2020; Koch et al., 2017). Moreover, these circuits are present even if the animal has not been trained to step. The ability of spinal circuitry to interpret sensory input for locomotor entrainment is partly mediated by glycinergic inhibition (de Leon et al., 2001). Neuromodulation techniques have been shown to excite muscle groups and induce locomotion (Wenger et al., 2016). It may seem desirable to artificially control muscles to express some activity; however, neuromodulation therapies must work harmoniously with sensory inputs (Edgerton et al., 2008; Formento et al., 2018) to recover and train remaining pathways. Notably, returning polysynaptic sensory-driven pathways to motorneurons appear to coincide with the return of locomotor function in spinal rats (Lavrov et al., 2008a; Rattay et al., 2000; Murg et al., 2000).

Poor stepping performance was correlated with spinal rats that did not exhibit polysynaptic activation from rostral lumbosacral networks (Gerasimenko et al., 2019). Addi-

tionally, electrically stimulated bilateral hindlimb locomotor activity required at least 5% body weight support during treadmill stepping, suggesting exogenous stimulation alone was insufficient to induce hindlimb locomotion (Ichiyama et al., 2005). However, by combining electrical stimulation with incoming sensory inputs in concert, chronically spinal rats may sufficiently integrate sensory information and output functional motor expression of coordinated locomotion.

Animal models with affected proprioceptive afferents appear incapable of the sensory-driven adaptation (Takeoka et al., 2014; Takeoka and Arber, 2019; Akay et al., 2014). Receiving appropriate sensory feedback appears critical to locomotor recovery. Combining ensemble sensory information and intrinsic activity allows the spinal cord to readily adjust parameters such as speed and step direction (Musienko et al., 2013), weight loading (Gerasimenko et al., 2019), novel perturbations (Ziegler et al., 2010), and force fields (Timoszyk et al., 2002). Thus, the spinal cord can solve problems for locomotion in real time based on continual incoming peripheral information.

2.5 Neuromodulation of the Injured Spinal Cord

Several extensive reviews have been written on the effect of neuromodulation and sensorimotor recovery following SCI (Calvert et al., 2019; Megia Garcia et al., 2020; Hofer and Schwab, 2019; Zheng et al., 2020; Edgerton and Roy, 2012; van den Brand et al., 2015; Christiansen and Perez, 2018; Cote et al., 2017; Minassian et al., 2017; Courtine and Sofroniew, 2019; Gerasimenko et al., 2008; Roy et al., 2012; Taccola et al., 2018; Young, 2015; Pizzolato et al., 2021). Each of these papers discusses key factors of neuromodulation in sensorimotor recovery. This section briefly summarises strategies and relationships between neuromodulation and sensorimotor recovery.

It has long been established that neuromodulatory intervention can improve functional recovery in SCI animal and human models (van den Brand et al., 2015; Roy et al.,

2012; Hofer and Schwab, 2019; Gerasimenko et al., 2008; Taccola et al., 2018). However, there is a disconnect between the research and the clinical domain. While research suggests neuromodulation, in addition to activity-dependent therapy, outperforms traditional rehabilitation protocols, many scientists discuss the need for further validation and clinical trials testing the efficacy and safety of neuromodulatory techniques (Calvert et al., 2019; Megia Garcia et al., 2020; Zheng et al., 2020; Cote et al., 2017; Hofer and Schwab, 2019). More specifically, there is a need for clinical studies focusing on clinical impact, efficacy of electrical stimulation protocols. These studies, paired with animal studies and neurological biomarker exploration, will be critical in further understanding functional activity recovery after SCI (Seanez and Capogrosso, 2021).

The mechanisms of action and tools to track neuromodulation therapy progress are still in contention. Electrical stimulation has been shown to enhance neuroregeneration, regulate neural networks, and build muscle strength and voluntary movement after SCI (Calvert et al., 2019; Megia Garcia et al., 2020; Zheng et al., 2020). Clinical adoption of neuromodulation requires in-depth understanding of the synergy between CPG, sensory inputs, activity-dependent plasticity, and modulation techniques (Taccola et al., 2018; Minassian et al., 2017, 2016; Minassian and Hofstoetter, 2016).

The transition towards clinical adoption will require a robust method to measure the causal effects of neuromodulation towards sensorimotor recovery. Researching the effect of neuromodulation and developing new tools to measure the interactions between therapy and spinal cord circuity will be critical to developing safe and efficacious therapies. Several scientists encourage the extension of modern engineering and the neuroscientific findings of sensorimotor control in the spinal cord to develop new therapies (Pizzolato et al., 2021; Zheng et al., 2020; Edgerton and Roy, 2012; Courtine and Sofroniew, 2019).

Sensorimotor recovery aims to leverage neuromodulation to promote a desired function. Adjusting the neural environment to a functional state has enabled voluntary

activation of sub-lesional networks (Gill et al., 2020b; Sayenko et al., 2019). Historically, this has been accomplished through electrical or pharmacological interventions (Courtine and Sofroniew, 2019). This section discusses the history and advancements of neuromodulation towards the recovery of locomotion post-spinal injury.

2.5.1 Electrical Stimulation

Initial work using Electrical Stimulation (ES) on decerebrate cats (Brown, 1911; Grillner and Zangger, 1975; Grillner and Rossignol, 1978; Iwahara et al., 1992) kickstarted the investigation of the spinal locomotor CPG. Initial CPG studies induced a 'fictive' locomotion pattern by stimulating the lumbosacral spinal cord above the motor threshold at a specific frequency. Fictive locomotion could only be achieved by accurately positioning electrodes and selecting appropriate stimulation configurations (Minassian et al., 2007; de Leon et al., 1999). Uncertainty regarding locomotor CPG activation via electrical stimulation continues to persist (Calvert et al., 2019; Minassian et al., 2017).

An obvious step is to question if similar effects can be elicited in humans. ES was initially applied to the epidural space of the spinal cord to inhibit ascending nociceptive signals travelling along the large dorsal column fibres (Mekhail et al., 2018; Buffart et al., 2009). By adapting pain stimulation protocols to a different frequency and delivered charge, ES reduced spasticity in SCI subjects (Dimitrijevic et al., 1986; Pinter et al., 2000). Further tuning stimulation parameters initiated stereotyped rhythmic or tonic activity in paraplegic humans (Dimitrijevic et al., 1998). Human research studies began to pivot towards recovering voluntary locomotor activity after SCI. By combining activity-dependent rehabilitation and epidural stimulation, adults with chronic motor complete SCI recovered assisted standing, voluntary leg movements, and locomotor-like activation (Harkema et al., 2011; Angeli et al., 2014). With these new techniques available, research efforts into other sensorimotor activities proliferated; see table 2.6 and table 2.7. SCI

Table 2.6: A summary of ES parameters and applicable protocols along the spinal cord and relevant frequencies.

Reference	**Function**	**Location**	**Frequency**
Minassian et al. (2004) Jilge et al. (2004) Dimitrijevic et al. (1998)	Tonic extension	T10 – L1	5 – 15Hz
Minassian et al. (2004) Dimitrijevic et al. (1998)	Rhythmic movement	T10 – L1	25 – 60Hz
Greiner et al. (2021)	Reach and pull	C5 – T1	10, 20, 50, 100Hz
Benavides et al. (2020)	Upper limb function	C5 – C6	30Hz and 5kHz carrier
Gad et al. (2018)	Grip strength	C3 – C7	30Hz
Lu et al. (2016)	Grip control	C5 – T1	5, 10, 20, 30Hz
McPherson et al. (2015)	Reaching	C6 – C8	<100Hz
Kreydin et al. (2020) Herrity et al. (2018)	Overactive bladder	T11 – L1 L1 – S1	30Hz
Gill et al. (2020a)	Trunk stability	T11 – L1	20 – 25Hz
Rath et al. (2018)	Trunk stability	T11 – L1	30Hz@T11, 15Hz@L1, 10kHz carrier
DiMarco et al. (2014)	Coughing	T9 – T11	50Hz

human subjects can leverage the benefits of ES towards stepping and standing activity (Harkema et al., 2011; Angeli et al., 2014). Some subjects recover enough control to stand overground while bearing body weight (Rejc et al., 2015; Gad et al., 2017) or execute voluntary activation without ES facilitation (Rejc et al., 2017a).

Task-specific functional recovery requires unique stimulation protocols for each activity (table 2.6). For example, even in the same stimulation region, the same standing frequency does not appear to facilitate recovery for stepping (Minassian et al., 2004). The

vast stimulation options and the requirement for patient-specific optimisation present an interesting issue. The modulatory effect of spinal cord stimulation is significantly affected by the minor changes in stimulation parameters and electrode location (Angeli et al., 2014; Gad et al., 2013a; Alam et al., 2015; Wagner et al., 2018). A daunting task of subject-specific fine-tuning emerges when provided with the multidimensional challenge of stimulating the nervous system of activity-dependent recovery (Gad et al., 2013a; Desautels et al., 2015; Sui et al., 2017). Furthering engineering advancements will reduce the fatigue and burden on the clinician and subject.

Stimulation timing must also be considered when applying an electric field to the epidural space of the spinal cord for effective motor recovery. Some results suggest spatiotemporally triggered stimulation significantly improved motor recovery compared to a continual stimulation waveform (Hsieh and Giszter, 2011). Similarly, continual assistance via robotic manipulation yielded poorer recovery when compared to assist-as-needed protocols (Mounis et al., 2017; Ziegler et al., 2010). Notably, timing the delivery of epidural stimuli according to the onset of locomotion signalling in the brain restored weight-bearing locomotion, outperforming continuous stimulation (Capogrosso et al., 2016).

2.5.1.1 Proposed Mechanisms

While these observations are important to decipher the role of ES of the spinal cord in motor function recovery, the exact mechanisms are still in question. Taccola et al. (2018) proposed a hypothesis where ES does not induce movement via dorsal root activation but enables movement. Enabled movement can be understood as bringing the locomotor networks to a more excitable state such that appropriate sensory inputs can initiate coordinated movement. It is important to recognise that sensory information significantly influences neural plasticity after SCI (Edgerton et al., 2008). Numerous studies provide evidence of proprioceptive information's significant influence on circuit reorganisation

during recovery (Takeoka and Arber, 2019; Takeoka et al., 2014; Takeoka, 2020; Edgerton et al., 2008). Interrupting these signals may fail to recover locomotive function (Formento et al., 2018).

Electrophysiological work suggests that spinal cord electrical stimulation excites sensory afferent dorsal roots and their axonal branches (Murg et al., 2000; Jilge et al., 2004; Courtine et al., 2009; Hofstoetter et al., 2018). Furthermore, computational studies show large diameter, low threshold dorsal root fibres were more readily excited than ventral roots (Rattay et al., 2000; Minassian et al., 2004). Human studies suggest ES increases the baseline level of excitability in CPG locomotor neurons of the spinal cord, thus reducing the threshold for small descending or afferent signals to activate CPG mechanics (Angeli et al., 2014; Danner et al., 2015). Similar to hypotheses suggested in (Edgerton et al., 1997a; de Leon et al., 1999; Tillakaratne et al., 2002). Other research suggests interleaved stimulation targets, though it is unclear what percentage of the observed modulation is attributable to neural structures outside dorsal roots (Cheng et al., 2019; Lavrov et al., 2008b; Taccola et al., 2018). The predominant view in literature maintains that the electrical activation of locomotor circuits is achieved via dorsal root pathways.

The synergistic effects between neuromodulation and incoming sensory ensembles are key to understanding the mechanisms of neurorehabilitation (Formento et al., 2018; Gad et al., 2013c). Increasing the net excitability of the locomotor network allows weak endogenous stimuli (e.g. afferents) to generate rhythmic patterns (Gad et al., 2013c; Etlin et al., 2010). Formento et al. (2018) designed a lower threshold stimulation strategy that employed lower amplitude but higher frequency parameters. Upon stimulation, the electrical field only recruited a limited number of proprioceptive afferents and allowed a summation of excitatory postsynaptic potentials (EPSPs) in motoneurons, thus increasing overall excitation. However, all nonrecruited afferents were still able to de-

liver sensory information. This allows the computation of necessary proprioceptive and mechanosensory information in central neural networks and greater spatial selectivity and modulation of stimulation bursts without increasing the amplitude. It would appear beneficial for sub-threshold electrical neurostimulation for more natural sensory integration. Interestingly, a recent paper analysing computational models of neural tissue shows that endogenous fields (of internal origin) can significantly affect neural oscillation by applying only weak electric fields (Cakan and Obermayer, 2020).

Despite the gaps in understanding, researchers have been able to leverage these proposed sites of activation to develop stimulation protocols for humans with SCI, resulting in the recovery of voluntary sensorimotor control (Wagner et al., 2018; Alam et al., 2020; Gad et al., 2018; Gill et al., 2018; Gad et al., 2017). There have been many advancements in the clinical application of ES. However, the gaps in understanding the mechanisms of action, especially understanding how endogenous and exogenous signals coordinate in concert to produce elevated functional states, remain unsolved.

2.5.2 Pharmacology

Many studies modulate the activity of neurotransmitter receptor activity for neurorehabilitation of SCI via pharmacological agents in the rat (Fong et al., 2005; Gad et al., 2013c, 2015; Duru et al., 2015), cat (reviewed in (Rossignol et al., 2001)), monkey (Courtine et al., 2005, 2007b, 2008, 2009; Capogrosso et al., 2016; Barra et al., 2018), and human subjects (Fung et al., 1990; Radhakrishna et al., 2017; Rabchevsky et al., 2011) (reviewed in (Domingo et al., 2012) and section 4 of (Barbeau et al., 1999)). Numerous neurotransmitter pathways have been identified to influence spinal locomotor pattern generators differently. These include GABA, glycine, glutamate, serotonin, dopamine, and noradrenaline (Minassian et al., 2017; Barbeau et al., 1999; Barbeau and Rossignol, 1991). Pharmacologically modulating these pathways has been proposed to enable

weight-bearing stepping post-SCI for a broader range of task-specific training (de Leon et al., 2001; Pizzolato et al., 2021). The section below focuses on pharmacological neuromodulation mechanisms and specific targets to facilitate neurological recovery in SCI. One important takeaway is the recognition of multiple neurotransmitter pathways affecting the behaviour of locomotion expression across multiple species (Barbeau et al., 1999; Minassian et al., 2017; Taccola et al., 2018).

2.5.2.1 GABA and Glycine

Reducing the dominant inhibition in locomotor networks after chronic SCI facilitates spinal learning (de Leon et al., 1999; Lalonde and Bui, 2021). Stepping ability in cats unresponsive to step-training or only received stand-training was significantly improved by reducing glycinergic activity (de Leon et al., 1999; Edgerton et al., 2004). Results suggest glycinergic pathways as a dominant inhibitor of locomotion activity (fig. 2.9). Reducing the likelihood of glycine activation enabled the activation of locomotion-relevant circuitry.

Improvement of stepping may occur by blocking abnormally high levels of inhibition resulting from complete SCI. Tillakaratne et al. (2002) presented further evidence of the role of inhibition in stepping where the GABA synthetic enzyme, GAD67, in the spinal cord was higher in non-trained spinal cats than in step-trained spinal cats. These were observed within as little as one week of training. Cellular mapping of GAD67 also suggests that the spinal cord of both stand and non-step-trained spinal cats have selectively higher inhibitory potential than that of step-trained spinal cats. Similarly, the stepping ability of poorly stepping spinal cats can be dramatically improved by the administration of bicuculline, a GABAA receptor antagonist. Reduced inhibition in GABAergic systems may facilitate locomotor spinal learning. GABA-mediated actions in the spinal cord include pre-synaptic inhibition of primary afferent fibres and post-synaptic inhibition of interneurons, sensory neurons, and motoneurons (Alvarez et al.,

1996).

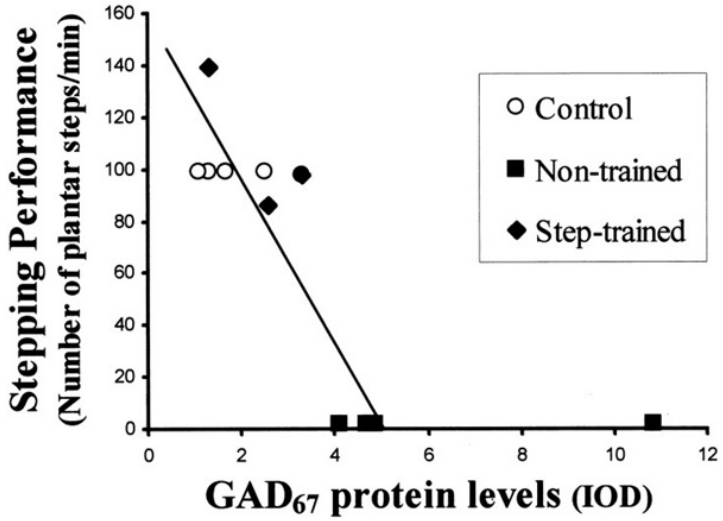

Figure 2.9: Effect of step training on expressed GABAergic interneurons of spinal cats (Tillakaratne et al., 2002). Step-trained spinal cats saw a reduction in GABAergic activity compared to non-trained and control groups. Reduced inhibition was correlated with stepping performance. Copyright 2002 Society for Neuroscience.

2.5.2.2 Serotonin

Serotonergic pathways originate from the brain stem, commonly projecting to lamina II and motoneurons in the ventral horn. Serotonin project from brainstem and midbrain inputs (Feraboli-Lohnherr et al., 1999, 1997) and descend via two parallel pathways (Hornung, 2003). The dorsolateral path terminates in the dorsal horn, while ventromedial tracks terminate in both the intermediate and ventral horn (Hornung, 2003). Serotonin innervated neurons appear critical to the propagation of the locomotor CPG (Jacobs and Fornal, 1993; Kathe et al., 2022).

Brainstem-derived 5-HT_2 receptors maintain motoneuron excitability by regulating persistent calcium currents (Hultborn et al., 2003; Jacobs et al., 2002; Perrier, 2005; Hounsgaard et al., 1988). Analysis of these 5-HT_2 receptors post spinal hemisection revealed transformations in receptor activity to facilitate persistent inward currents without significant 5-HT binding, thus allowing motoneurons to generate sustained

muscle contractions and recovery motor functions like locomotion (Murray et al., 2010). Combining robotic assistance with quipazine, a serotonin agonist, resulted in significant recovery with longer and stronger stance phases (Fong et al., 2005; Antri et al., 2003). Introducing 5-HT inverse agonists impaired locomotion, suggesting recovery of 5-HT activity is crucial for spontaneous recovery of hindlimb motor function after partial SCI.

Activating serotonin receptors in the locomotor neural circuits induce rhythmic activity in paralysed hindlimbs of transected rats (Landry et al., 2006; Fouad et al., 2010). During treadmill locomotion, increased serotonergic activity evoked greater step coordination and EMG burst amplitude (Feraboli-Lohnherr et al., 1999; Kim et al., 2001; Gackière and Vinay, 2014). Notably, Fong et al. (2005) discovered that sub-threshold dosage facilitates stepping rather than directly activating stepping networks.

During voluntary locomotion function testing in adult rats, administering serotonin antagonists left animals in a paralysis-like state (Cabaj et al., 2017). If 5-HT_7 receptors are blocked, flexor and extensor INs receive disrupted afferent feedback, potentially attributing to paralysed state (Gerasimenko et al., 2009). Similar results studying locomotor patterns and cutaneous reflex in flexor groups have been reported, specifically greater weight support and increased step length with increased cutaneous reflex excitability (Barbeau and Rossignol, 1990; Gackière and Vinay, 2014). These results suggest that serotonergic drugs mediate increased excitability of spinal neurons and are different from noradrenergic agonists (i.e. clonidine), indicating a subclass of neuronal influence in locomotor function and reflex activity (Gackière and Vinay, 2014).

Serotonin effects in the injured spinal cord are widespread and have been targeted as a method for recovery of locomotion (Ghosh and Pearse, 2014; Cabaj et al., 2017; Courtine et al., 2009; Husch et al., 2012). Given the presence of tonic descending serotonin input and its pivotal role in shaping the locomotor circuitry, returning serotonergic input to spinal circuits may be an intuitive way to restore the locomotion in the injured spinal

cord (Schmidt and Jordan, 2000; Jean-Francois et al., 2013; Gackière and Vinay, 2014; Capelli et al., 2017).

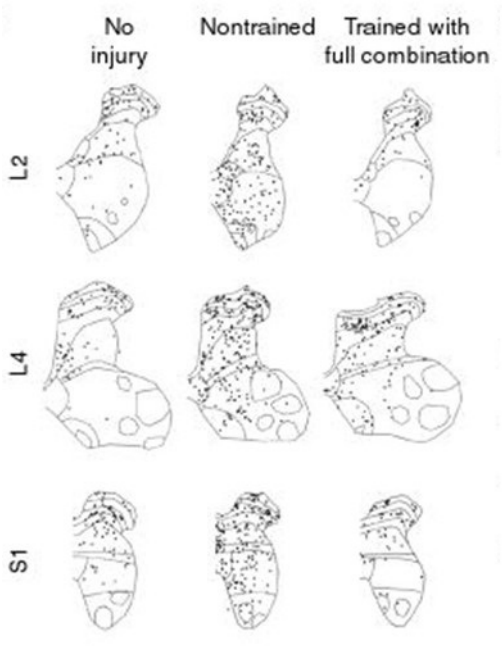

Figure 2.10: Active neurons identified with c-FOS shortly after continuous stepping with synergistic serotonin agonists and ES on rodents (Courtine et al., 2009). Nontrained rodents after injury had a greater number of FOS-positive cells than trained and uninjured groups.

Combinatorial interventions induce unique functional states correlated with distinct locomotion patterns and monosynaptic excitability in spinal rats, see fig. 2.10, (Han et al., 2008; Courtine et al., 2005; Gerasimenko et al., 2007). Moreover, introducing ES and N-methyl-D-aspartate (NMDA) (Van Den Brand et al., 2012) and selective inhibitory presynaptic blockers (Taccola et al., 2020) in conjunction with treadmill training achieved intraspinal plasticity, bypassing lesions and restoring locomotor function after paralysis. Synergistic electropharmacological interventions may enable specific modulation of specific spinal neural circuit components that differentially affect locomotor expression. However, subject-specific responses and longitudinal adaptations evoked from these interventions remain elusive.

With rich literature on animal models, it was natural to transfer towards human models and apply similar methodologies to test efficacy and safety. SCI human subjects can leverage the benefits of ES towards stepping and standing activity (Harkema et al., 2011; Angeli et al., 2014). Some subjects recover enough control to stand overground while bearing body weight (Rejc et al., 2015). Other subjects present voluntary activation improvements without ES facilitation (Rejc et al., 2017a). However, similar to non-human animal models (Hodgson et al., 1994), human spinal cord neural circuits are task-specific in their recovery after SCI (Rejc et al., 2017b). Focusing on a singular task does not effectively transfer functional capabilities to another task (De Leon et al., 1998b; Rejc et al., 2017b; De Leon et al., 1998a; Edgerton et al., 1997a; Gerasimenko et al., 2015a). A summary of human studies for different functions is provided in table 2.7. Studies were screened for (1) human subjects with SCI, (2) ES or pharmacological neuromodulation, and (3) methods to include a targetted sensorimotor function and assessment of response. It is still unclear how to ascertain the optimal dosage to reduce side effects while maximising sensorimotor recovery gains (Radhakrishna et al., 2017).

In summary, neuromodulatory inputs to the injured spinal cord have been shown to work in concert and facilitate greater recovery than independent therapies alone. There is a knowledge gap in the extent to which these synergistic effects work, the physiological processes behind these therapies, and their role in neural plasticity. Careful consideration must be given before assuming heightened excitation and increased likelihood of neuroplasticity leads to positive change (Maier et al., 2009).

Although current methods have improved the quality of life for SCI patients, the mechanisms, reliable monitoring, and prediction of subject suitability still need to be determined. Comparing short- and long-term clinical outcomes remains challenging (Rahman et al., 2022). To close this gap, I suggest developing relevant and specific tools to monitor the ongoing effects of neuromodulation.

Table 2.7: A summary of neuromodulation studies performed on human subjects. Studies were filtered by human subject and different applications of neuromodulation therapies for subjects with SCI.

Reference	**Function**	**AIS**	**Neurotherapy**
Harkema et al. (2011)	Stepping and standing	A	ES
Angeli et al. (2014)	Voluntary movement	A and B	ES
Rejc et al. (2017a)	Voluntary movement	B	ES
Rejc et al. (2015)	Standing	A and B	ES
Rejc et al. (2017b)	Standing	A and B	ES
Gerasimenko et al. (2015a)	Stepping	B	ES
Angeli et al. (2018)	Stepping	A, B, and C	ES
Gill et al. (2018)	Stepping	A	ES
Wagner et al. (2018)	Stepping	C and D	ES
Gad et al. (2017)	Stepping	A	Buspirone + ES
Gill et al. (2020b)	Stepping	A	ES
Sayenko et al. (2019)	Standing	A, B, and C	ES
Lorach et al. (2023)	Stepping	B	ES
Freyvert et al. (2018)	Hand function	B	Buspirone + ES
Gad et al. (2018)	Hand function	B and C	ES
Lu et al. (2016)	Hand function	B	ES
Inanici et al. (2018)	Hand and arm function	B and C	ES
Inanici et al. (2021)	Hand and arm function	B, C, and D	ES
Kreydin et al. (2020)	Bladder sensorimotor function	A and C	ES
Gad et al. (2020)	Respiratory function	A	ES
Darrow et al. (2019)	Autonomic function	A and B	ES
Rath et al. (2018)	Trunk stability	A and C	ES
DiMarco et al. (2014)	Coughing	–	ES
Fung et al. (1990)	Stepping	Incomplete injury	Clonidine (α-adrenergic agonist)
Wainberg et al. (1990)	Spasticity and stepping	–	Cyproheptadine (serotonin antagonist)
Dietz et al. (1995)	Stepping	Incomplete and complete	Baclofen (GABA agonist)
Radhakrishna et al. (2017)	Stepping	A and B	Buspirone/levodopa/carbidopa

2.6 Activity Monitoring

Patient monitoring has provided an integral method for informing clinicians on the effect of prescribed intervention towards recovery progress. Knowing the neurological state and behavioural outputs equips clinicians with information to develop efficacious and efficient recovery protocols. Clinicians could provide greater patient care if given access to patient activity performance outside the controlled clinical environment. In uninjured populations, the spatiotemporal locomotor characteristics of individual walking are expressed more variably when comparing out-of-clinic and in-clinic environments (Prajapati et al., 2011; Toda et al., 2020; Albert et al., 2017).

Wearable and ambient sensing technology has been considered the most intuitive and effective strategy to perform these measurements (Burns and Adeli, 2017; Nizam Uddin, 2012; Pantelopoulos and Bourbakis, 2010; Patel et al., 2012; Pathak et al., 2021). While patient monitoring is critical to understanding the therapy effects, gathering sufficient patient data and developing robust classification techniques remains a challenge (Burns and Adeli, 2017; Schmid et al., 2021; Jayaraman et al., 2018; Schneider et al., 2018). Secondly, more attention needs to be given to mapping the neurological state to the behavioural output during recovery (De Fazio et al., 2023).

The scientific enquiry into how these neural adaptations occur over a chronic timescale has been challenging due to population variability and difficulty in accessing and gathering relevant datasets (Johnson and Picard, 2020). In spinal cord injury recovery, classifying behavioural activity and identifying a reliable and generalisable biomarker using wearable technology for recovery and neuromodulation therapy response remains elusive. The following section presents the state of functional assessment, activity classification, and biomarker investigations regarding locomotion recovery after SCI.

2.6.1 Assessment Tools

SCI subjects admitted to rehabilitation are often assigned some metric (or several metrics) to assess how different protocols affect recovery. These are typically adapted according to the goals the subject wishes to achieve. For example, hand-and-arm functional assessment may use the Box and Block Test (Kontson et al., 2017), and bladder and bowel function may be assessed by the Qualiveen and Short-From Qualiveen (Tate et al., 2020). A more holistic assessment may incorporate the Spinal Cord Independence Measure or the equivalent, Functional Independence Measure (Harvey, 2016).

For locomotor function, a standard 10-meter walk test or Walking Index for Spinal Cord Injury may be used to gain insight into subject progress (van Hedel and Dietz, 2010). While these assessments offer high-level functional information regarding the patient's response to rehabilitation, little can be extrapolated about the patient's neurological response and state. Lower-level information can build a better picture for physicians to develop case-specific protocols to maximise recovery outcomes. From a scientific perspective, these assessments offer little information if one wishes to map neural states to functional outcomes. Currently, the 'best' tool to measure gait control is unknown (Buckley et al., 2019). Several tests, subject-specific biomarkers, and uncontrolled continuous measurement will likely be key tools to diagnose and monitor neurological conditions and behaviour outputs.

Secondly, the in-person, practical assessments are predominantly performed within the clinic, limiting the clinician to information gained within that specific time frame and conditions. Due to the nature of paralysis, moving around and physically reaching a clinic is much more demanding. Limiting the subject's exposure to unnecessary burdens may give the patient a more positive experience during their rehabilitation process (Syed et al., 2013). Access to healthcare infrastructure is even more demanding for regional and remote patients. In Australia, remote healthcare services have a significantly lower

population threshold for care than in densely populated areas.

Additionally, these remote communities are disproportionately admitted to hospitals, compared to their more densely populated city counterparts (Thomas et al., 2015; Australian Institute of Health and Welfare, 2022). The onset of the COVID-19 pandemic has highlighted the necessity and benefits of telemonitoring in conjunction with at-home healthcare services (Australia, 2021). Commercially, the western market has seen huge interest in wearable devices with the wearable technology industry reaching a USD 99.5 billion evaluation in 2022 (GlobalData, 2023).

Separate from telehealth's economic and reduced burden benefit, much more information can be gained out-of-clinic monitoring that may not be captured while in front of a practitioner. How the patient performs at home, at work, or during transfers may offer critical insights missed because the patient forgot or does not consider an event important. Knowing the performance of tasks outside the clinic creates opportunities for rapid feedback, personalised therapy, and reduction in overall healthcare cost (Burns and Adeli, 2017; Nizam Uddin, 2012; Pantelopoulos and Bourbakis, 2010; Patel et al., 2012; Wang et al., 2017, 2014; Andersson et al., 1978).

While evidence supports the use and continual improvement of wearable technology, several limitations must be considered when attempting to deploy these systems in practice.

2.6.2 Challenges in Activity Recognition

Wearables to monitor movement and disease-related information are heterogeneous, non-standardised, and lack evidence for reliability, responsiveness, and sensitivity to longitudinal changes (Johansson et al., 2018; Celik et al., 2021). These are further exacerbated by inconsistencies across experiment protocols, classification techniques, and analysis methodologies (Celik et al., 2021; Balbinot et al., 2021). For these reasons,

it is challenging to establish conclusive interpretations of the evidence.

Inter-subject variability is a challenge commonly faced by researchers and engineers developing classification models for activity recognition (Barshan and Yurtman, 2016). As expected, performance has often degraded when introduced to heterogenous subject populations, multi-day recordings, and variable activities (Balbinot et al., 2021; Zhou et al., 2020; Côté-Allard et al., 2019; Albuquerque et al., 2020). Care should be taken when extrapolating utility from studies with limited sample pooling and homogenous activities across shorter time scales.

One method to account for population variability and improve confidence in study results is to gather an immense amount of data. Access to these vast datasets would also assist in the development of more generalisable machine learning models (Mitchell et al., 2021). However, this has famously been the Achilles Heel of medical research and one of the reasons why the advancements in machine learning appear to lag behind the other domains such as language modelling and computer vision (Fawaz et al., 2018; Ismail Fawaz et al., 2019; Miotto et al., 2018). Currently, no single open-source SCI activity dataset is available for scientists and engineers to use as a platform for development and benchmarking.

Many gait detection algorithms succeed in healthy populace evaluation, but it would be naïve to suggest that healthy population gait findings translate to an injured population (Den Otter et al., 2007; Jayaraman et al., 2018; Terashi et al., 2020). Though comparable accuracy has been previously reported using IMUs placed on the foot and shank, data was only collected in a laboratory environment without any neuromodulation (Jasiewicz et al., 2006; Werner et al., 2021). It is uncertain if the same accuracy could be attained if subjects were given a set of separate tasks to perform or receiving rehabilitation therapies over a longer recording period. Additionally, kinematic activity prediction with IMU sensing cannot inherently record neurological change directly. Ar-

guments for kinematic sensing alone may include reducing the number of sensors and improving usability, compliance, and battery performance (Celik et al., 2021; Johansson et al., 2018). While these are tenable arguments, accepting these conditions comes at the expense of fine-tuning neuromodulatory stimulus in short time scales that require timely precision for efficacious neurological recovery (Moraud et al., 2016; Formento et al., 2018; Lorach et al., 2023; Rowald et al., 2022). Loss of these functions would be considered undesirable, especially considering the strong activity-dependent adaptations, as discussed in section 2.4 and section 2.3.

With these challenges outlined, there is an obvious need for more openly available datasets across healthy and neurologically impaired populations. Until these datasets become more available and the culture of openly sharing ethical and relevant experimental data becomes more prevalent, alternative techniques must be developed to advance the field of robust activity classification techniques. This thesis will aim to develop new methods to classify locomotor events in neurologically injured populations. While intuitive to monitor the return of the activity of interest, I do not believe such high-level information is sufficient as an indicator for novel neuromodulation rehabilitation progress.

2.6.3 Biomarkers for Neuromodulation Therapy

Several questions naturally arise with the success of volitional sensorimotor recovery via neuromodulation therapy in chronic SCI human subjects. These encompass topics such as safety and efficacy, subject response prediction, dose-response relationships, and persistence of therapy effects (Lorach et al., 2023; Rowald et al., 2022). Currently, no gold standard exists for quantifying ambulatory function (van Hedel and Dietz, 2010; Nguyen et al., 2021). Kinematic coordination, timing, strength, range-of-motion, and balance measures have been traditionally used to monitor change over time (Jayaraman et al., 2018; Harbeau et al., 2002; Mignardot et al., 2017; Hubli and Dietz, 2013). These

measures have informed researchers on the impacts of rehabilitation protocols towards positively adaptive plastic changes in the neural environment (Reinkensmeyer et al., 2016; Ying et al., 2005).

Observing kinematic changes provides information on how different neuromodulation therapies correlate with the movement expression; it can be tempting to simply suggest these are sufficient measurement methods (Colombo et al., 2008; Nizam Uddin, 2012; Garro et al., 2021). Changes to the applied neuromodulation protocol would occur only after several kinematic events. Current state-of-the-art epidural spinal cord stimulation devices adapt applied therapy at millisecond time scales, so monitoring and modulating the sensorimotor system to the same degree would seem natural (Brooker et al., 2021; Wenger et al., 2016). Thus, at small time scales, kinematic measurements will have limited utility.

Electrophysiological measurements offer direct measurements of the CNS at millisecond-level resolution. Common EMG properties include amplitude peaks, onset/offset timing, number of recruited motor units, synergies, co-contraction index, power spectral density, sample entropy, and zero-crossings (Balbinot et al., 2021; Levy et al., 1987; Jo and Perez, 2020). Some have monitored the changes in electroencephalography (EEG) specific frequency bands of the central area and parietal lobe (Simis et al., 2021). Temporal and frequency features such as those listed above are simple to compute and understand. A subject that previously had no volitional control of supra-lesional networks receiving neuromodulation therapies would likely measure changes across these feature spaces (Wolpaw and Tennissen, 2001).

Intuitively, electrophysiological signals provide close coupling to neurological adaptation that occurs due to activity-dependent plasticity and neuromodulation therapy. The electrochemical coupling method between the neurological system and sensitive recording equipment makes it difficult to use in a chronic out-of-lab setting (Krucoff

et al., 2016; Xiong et al., 2021). Additionally, high-level temporal and frequency data, such as those extracted from amplitude analysis and power spectral bands, can only provide limited information on the adaptations occurring at the network level. If effective neuromodulation therapies require micrometre fidelity at millisecond precision, an in-depth understanding of the interactions between the spinal neural network and neuromodulatory device is warranted (Squair et al., 2021).

The groundwork for such biomarkers has been laid by scientists studying the interactions of neuromodulation with ensembles of sensory afferent signals (Gerasimenko et al., 2006; Lavrov et al., 2006; Gad et al., 2015; Formento et al., 2018). Motor-evoked potentials (MEPs) from the CNS shed light on integrating sensory and neuromodulatory information (Atkinson et al., 2020; Musienko et al., 2007; Calvert et al., 2021; Gerasimenko et al., 2018; Urbin et al., 2017).

Pharmacological and electrical modulation of the injured spinal cord have uncovered new techniques to evoke locomotion activity (Gerasimenko et al., 2016a). However, the most appropriate method to elicit these responses is convoluted and requires tuning towards each subject (Desautels et al., 2015). The methods to measure the response to each neuromodulation therapy are coarse and antiquated (Johansson et al., 2018; Celik et al., 2021). Additionally, our understanding of the mechanisms of action remains incomplete (Zhang et al., 2021). New techniques to classify pathological expressions of movement are required to improve these areas. These new methods could offer insights into predicting therapy responses promptly, further optimising recovery. Secondly, computational techniques offer a flexible and novel method for uncovering the mechanistic effects of neuromodulation (Capogrosso et al., 2013; Edlund, 2019; Rybak et al., 2006). Expanding biologically constrained models to investigate trains of sensory input in conjunction with neuromodulatory stimulus can offer novel insights into the inner workings of the locomotor CPG.

CHAPTER 3

MATERIALS

A large portion of this thesis was based on the data collected by Dr. Parag Gad, Dr. Mrinal Neil Rath, Dr. Hui Zhong, and Prof. V Reggie Edgerton from the University of California, Los Angeles who were kind enough to share their data with me while I was a Visiting Graduate Researcher at Prof. Edgerton's lab. I go on to use their immense EMG and video data set for analysis. The data consists for 4 spinally transected female rats who underwent spinal cord electrode and EMG electrode implantation. The rats received bipedal locomotion and standing training on a rat body weight supporting treadmill device. During training and cage-roaming conditions, rats received combinations of sub-threshold epidural electrical stimulation, Quipazine (serotonin agonist), and Strychnine (glycinergic antagonist). The remainder of this chapter details the methodology performed to gather electrophysiological and Infra-Red (IR) video data to monitor the locomotion and standing activity of spinally transected rats in a free-roaming cage environment.

3.1 Animal Preparation and Care

Data were obtained from 4 adult female Sprague Dawley rats (270 – 300 g body weight). Pre- and post-surgical animal care procedures are described in Roy et al. (1992). The rats were housed individually in cages with food and water provided *ad libitum*. All survival surgical procedures were conducted under aspetic conditions and with the rats deeply anesthetised with isoflurane gas (1.5 – 2%) administered via facemask. All procedures described hence forth are in accordance with the national Institute of Health Guide for the Care and Use of Laboratory Animals and approved by the Animal Research Committee at UCLA.

3.2 Head Connector and Intramuscular EMG Electrode Implantation

A small incision was made at the midline of the skull. The muscles and fascia were retracted laterally, small grooves were made in the skull with a scalpel, and the skull was dried thoroughly. Two amphenol head connectors with Teflon-coated stainless steel wires (AS 632, Cooner Wire, Chatsworth, CA) were securely attached to the skull with screws and dental cement as described previously (Ichiyama et al., 2008a). The tibialis anterior (TA, ankle flexor) and soleus (Sol, ankle extensor) muscles were implanted bilaterally with intramuscular EMG recording electrodes (Roy et al., 1992). Skin and fascial incisions were made to expose the belly of each muscle. Two wires extending from the skull-mounted connector were routed subcutaneously to each muscle. The wires were inserted into the muscle belly with a 23-gauge needle, and a small notch (0.5-1.0 mm) was removed from the insulation of each wire to expose the conductor and form the recording electrodes. The wires were secured within the belly of each muscle via a suture on the wire at its entrance into and exit from the muscle belly. The proper placement of

the electrodes was verified during the surgery by stimulation through the head connector and postmortem via dissection.

3.3 Spinal Cord Transection and Electrode Implantation Procedures and Post-Surgical Animal Care

A partial laminectomy was performed to expose the T8 – T9 spinal cord, and then a complete spinal cord transection to include the dura, was performed with microscissors. Two surgeons verified the completeness of the transection by lifting the cut ends of the spinal cord with fine forceps and passing a glass probe through the lesion site. Gel foam was inserted into the gap created by the transection as a coagulant and to separate the cut ends of the spinal cord. For epidural electrode implantation, partial laminectomies were performed to expose the spinal cord levels L2 and S1. Two Teflon-coated stainless steel wires from the head connector were passed under the spinous processes and above the dura mater of the remaining vertebrae between the partial laminectomy sites. After a small portion (~1-mm notch) of the Teflon coating was removed and the conductor was exposed on the surface facing the spinal cord, the electrodes were sutured to the dura mater at the midline of the spinal cord above and below the electrode sites with 8.0 Ethilon suture (Ethicon, New Brunswick, NJ). Two common ground (indifferent EMG and ES) wires (~1 cm of the Teflon removed distally) were inserted subcutaneously in the mid-back region on the right side (EMG) and midline (ES) close to the tail. All wires (for both EMG and ES) were coiled in the back region to provide stress relief. All incision areas were irrigated liberally with warm, sterile saline. All surgical sites were closed in layers with 5.0 Vicryl (Ethicon) for all muscle and connective tissue layers and for the skin incisions in the hind-limbs and 5.0 Ethilon for the back skin incision.

Buprenex (0.01-0.05mg/kg sc every 8 to 12 hrs) was used to provide analgesia. Analgesics were initiated before completion of the surgery and continued for a minimum of 2 days. The rats were allowed to recover fully from anesthesia in an incubator. The rats were housed individually in cages that had ample CareFresh bedding, and the bladders of the spinal rats were expressed manually three times daily for the first 2 weeks after surgery and two times daily thereafter. The hind-limbs of the spinal rats were moved passively through a full range of motion once per day to maintain joint mobility. All of these procedures have been described in detail previously (Courtine et al., 2009).

3.4 Training Procedures

All rats were trained for bipedal stepping and standing on a motor driven rodent body weight supporting treadmill for 5 days/week, 20 min/day for 6 weeks starting at 12 days post-injury (dpi), including the days of testing (de Leon et al., 2002). Temporal training specifications were selected on the basis of near normal step cycle trajectory recovery during partial weight bearing stepping after SCI in rats when compared to control groups (Heng and de Leon, 2009). Spinally transected rats reach a plateau of recovery after 6–7 weeks of step training (Courtine et al., 2009; Gad et al., 2013c). Bipolar ES between L2 and S1 (current flowing from L2 to S1) at frequency of 40 Hz, pulse width 0.2 ms was used in combination with quipazine (0.3 mg/kg; (Ichiyama et al., 2008b; Courtine et al., 2009)) and strychnine (0.5 mg/kg; (de Leon et al., 1999; Gad et al., 2013c)) injected intraperitoneally 10 min before each training/testing session. ES was only delivered during the 20min/day training periods as described previously (Ichiyama et al., 2005). Chronic step training was used to train and reinforce locomotor neural networks that generate spontaneous cage activity (Gad et al., 2013a). At the early stages of training, ES intensity was set at threshold or at super-threshold to invoke locomotive activity (Gerasimenko et al., 2008). As training continued, the stimulation intensity

was gradually reduced, dependent upon the stepping performance of each rat until the stimulation intensity was just below threshold.

3.5 Stimulation and Testing Procedures

The threshold for eliciting muscle twitch and corresponding time linked EMG response in the soleus was identified and set to 1.8 to 2 V (Ichiyama et al., 2005). The sub-threshold level was set to 20% below the motor threshold during the recording of spontaneous cage activity, between 1.4 and 1.6 V. ES was delivered only during the training and testing periods. Each rat prior to testing was injected intraperitoneally with the same volume described during training (see section 3.4). Quipazine has shown immediate restoration of locomotion activity during robotic treadmill training (Fong et al., 2005). Quipazine dosages used in the present study effectively enable full weight-bearing treadmill locomotion in spinally transected rats with enhanced stepping ability in synergy with ES (Courtine et al., 2009). Quipazine enabled locomotor movement occurrence reaches a plateau after a dosage of 0.3 mg/kg (Ichiyama et al., 2008b). Similarly, strychnine was administered using the same dosages in the training procedures at doses known to facilitate stepping after spinal transection during weight-bearing locomotion 30 min after administration (Hart, 1971; de Leon et al., 1999). Rats were injected 10min prior to beginning of spontaneous cage activity testing, with the prescribed neuromodulating pharmacology. The spontaneous activity of the spinal rats were determined in their home cage. Spinal rats that had previously been trained to step on a treadmill in presence of strychnine (Strych) and quipazine (Quip) were tested under 5 different conditions i.e., no ES (Pre), ES, ES+Quip (qES), ES+Strych (sES) and ES+Quip+Strych (sqES). The head connector was coupled to a set of amplifiers and a stimulator.

The swivel arrangement was attached to allow the rats to roam freely in the cage. There was food distributed throughout the cage floor to encourage movement and ex-

ploration. IR video data were recorded using a camcorder for select conditions. EMG data were amplified and recorded using custom LabView-based data acquisition software with a sampling frequency of 10kHz. Data were recorded continuously for 6 hrs between 8pm and 2am, i.e. the active period of time for rats. One out of the 20 experiments (n=4 rats, 5 experiments/rat) were conducted every night and were randomized with at least one day's gap between two successive recordings for a rat and all 20 experiments were completed within 3 weeks. Note that the first 20 minutes EMG recordings for rat 1 in the sqES and all recording channels for rats 2 and 4 for the ES only case were corrupted and unable to be used.

3.6 Labelling

With a lack of footswitch, marker labelling, or ground reaction force (GRF) data, a manual labelling process of the EMG data was performed with cross-validation of IR video footage. A custom software was developed to highlight the periods of identified locomotion and standing events selectively. The specified data sections were later saved into a file for downstream processing. A time-consuming process of manually collecting data sets across animals, times, and therapies while cross-validating with manually scrubbed IR footage was performed. Refer to fig. 3.1 for a reference of the custom software graphical user interface.

To assist with the operator's decision for successful locomotor activity, a Gaussian Mixture Model (GMM) was trained across the selected times for labelling. Signals of the left and right TA or SOL were concatenated contralaterally for the same muscle group and used to train a GMM for each muscle group. Data for each muscle group was normalised and processed to generate the envelope. Digital signal processing steps are detailed in section 4.2.1. Taking the envelope, the signal was downsampled from 10kHz to 1kHz, and the first differential was calculated. The non-differentiated and

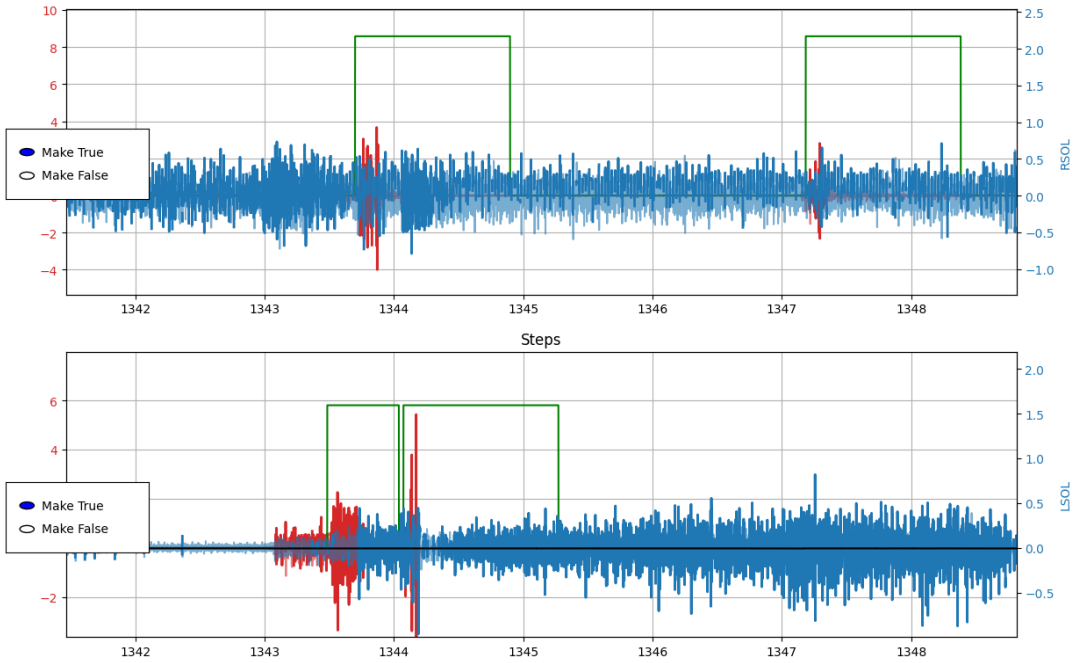

Figure 3.1: An example of the custom labelling developed to assist with manually detecting and segmenting locomotor and standing events while scrubbing synchronised IR video feeds. Signal plots with lower opacity were considered inactive by a trained 2 cluster GMM. In red is the TA activity, and in blue is the SOL activity. The top subplot displays right side data, and the bottom displays left side data.

differentiated data was used to train the GMM to approximate a binary estimation of active or non-active muscle. Note that this process was not used to generate the online proposed locomotion detection algorithm but to inform the operator of the likelihood of active or non-active recordings.

The manual labelling process created 125 min of labelled EMG stand and locomotion data, split into 5 min sections across different animal subjects, periods, and therapies (sqES, qES, sES, ES, and Pre).

3.6.1 Data Set Distribution

The labelled data set displays an incredible imbalance between positive and negative labels across stepping and standing events fig. 3.2. The right steps and left steps are

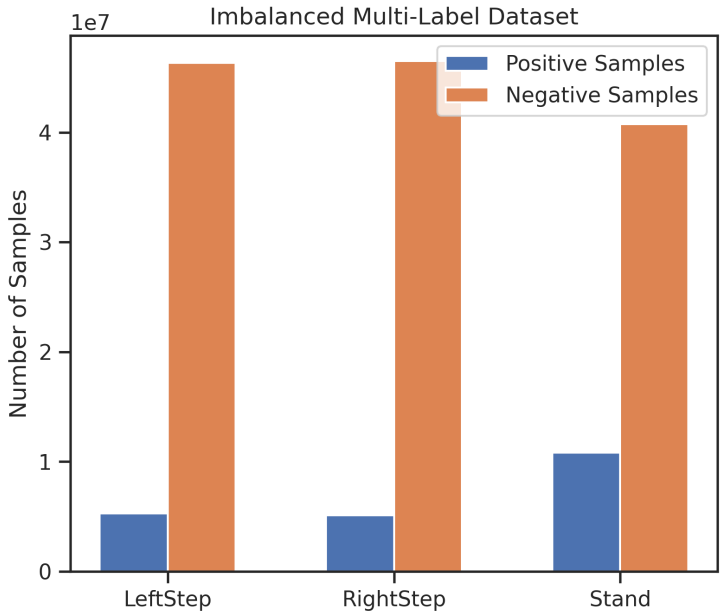

Figure 3.2: Bar plot of the distribution of datapoints which are registered a positive and negative labels for the respective activity.

relatively similar (n_{right} = 810676 and n_{left} = 91492), while stand events are more than double left or right stepping label counts (n_{stand} = 2511446). Calculating the same information from the extracted feature data from the complete data set revealed similar distributions ($n_{left,win}$ = 1765, $n_{right,win}$= 1562, $n_{stand,win}$ = 3062).

3.7 Relevant Equations

(3.1) $$\text{Macro F1} = \frac{1}{N}\sum_{i=1}^{N} \text{F1}_i$$

(3.2) $$\text{Weighted F1} = \sum_{i=1}^{N} w_i \times \text{F1}_i w_i = \frac{\text{No. of samples in class } i}{\text{Total no. of samples}}$$

$$\text{F1 score} = \frac{2 \cdot \text{precision} \cdot \text{recall}}{\text{precision} + \text{recall}} \tag{3.3}$$

$$\text{Precision} = \frac{\text{True Positives}}{\text{True Positives} + \text{False Positives}} \tag{3.4}$$

$$\text{Recall} = \frac{\text{True Positives}}{\text{True Positives} + \text{False Negatives}} \tag{3.5}$$

$$\text{softmax} = \sigma(x_i) = \frac{e^{x_i}}{\sum_{j=1}^{K} e^{x_j}} \quad for\ i = 1, 2, \ldots, K \tag{3.6}$$

$$\text{Relu}(x) = \max(0, x) \tag{3.7}$$

$$\text{Sigmoid}(x) = \frac{1}{1 + e^{-x}} \tag{3.8}$$

$$\text{GeLu}(x) = xP(X \leq x),\ P(X) \sim N(0, 1) \tag{3.9}$$

$$\text{Cross Entropy} = -(y \log(p) + (1 - y) \log(1 - p)) \tag{3.10}$$

$$\text{Multiclass Cross Entropy} = -\sum_{c=1}^{M} y_{o,c} \log(p_{o,c}) \tag{3.11}$$

$$\text{L2 norm} = \lambda \sum_{1}^{n} w_i^2 \tag{3.12}$$

CHAPTER 4

Novel Classification Algorithm of Step and Stand Events During Spinal Neuromodulation

Neural circuitry reorganises upon introducing neuromodulatory therapy and task-specific locomotor training. Monitoring the neural effects of the rehabilitation protocols and neuromodulation therapies seems intuitive to ensure safety and efficacy towards subjects. This opportunity needs to be addressed in the existing literature. Standard methods for identifying locomotor activity use kinematic sensing. Available neurological sensing has only been performed in closed, controlled laboratory environments, such as on a treadmill or across flat ground. As far as I am aware, no efforts have been made to pursue out-of-lab neural monitoring activity while subjects with neuro-pathological gait undergo therapy. I aim to investigate the efficacy of existing methodologies in locomotion classification on pathological gait rats undergoing multimodal spinal neuromodulation. I hypothesise that non-linear methods are sufficient to detect locomotion events in pathological gait under different therapy domains. I suggest a spatiotemporal rule-based algorithm and compare multiple machine-learning methods for time-series classification of unilateral stepping and standing events in manually

labelled 4-channel EMG data. Results from the experiment show poor classification performance in all tested algorithms. The novel rule-based algorithm outperformed existing methods in rejecting false positives. Relevant identified features for each label and reasons for poor performance are discussed.

4.1 Background

Several variables have been suggested as significant markers within the scope of SCI sensorimotor rehabilitation. These can be broken down into kinematic and electrophysiological monitoring (Burns and Adeli, 2017). In this section, I will refine the scope of previous works to locomotion rehabilitation and related tasks only.

Several strategies have been used to measure spatiotemporal gait metrics algorithmically. Analysis of kinematic information is an intuitive lens through which clinicians and engineers can peer. Recording activity via small, energy-efficient, and reliable inertial motion units (IMUs) appears as an obvious pathway to monitor the recovery of sensorimotor function. A common method is to isolate the plane of analysis to a single side, reducing the complexity of the problem (Greene et al., 2010; Jasiewicz et al., 2006; Storm et al., 2016; Catalfamo et al., 2010). Machine learning models using IMU sensors have accurate classification performance during in lab environments but reduce by nearly 40% when used out of the lab (Albert et al., 2017). Adding multiple sensors offers extra information to improve machine learning accuracies (Salarian et al., 2004; Chen et al., 2015).

While these methods provide adequate classification accuracies both in and out of the lab setting, they are naïve to the underlying neurological changes occurring due to the effects of therapy. An argument can be made that kinematic measurements effectively express the neurological state. However, the time course to see behavioural change is long with little sensitivity to subject response (Donati et al., 2016; Angeli et al., 2018). It

would be beneficial to predict the subject response to therapy rather than invest months of rehabilitation effort before learning what adaptations were introduced. Access to nervous system activity would be more informative than only kinematic activity.

Morbidoni et al. (2019) offers the first look at identifying gait phases with surface EMG (sEMG) data. Data was prepared with a signal envelope and sliding window process before passing left and right concatenated data into multilayer perceptron with Rectified Linear Unit (ReLu) activation functions. Similar methodologies were applied using sEMG data using statistical, temporal, and frequency features for treadmill walking (Nazmi et al., 2019) and compressed muscle synergy matrices for overground walking (Park et al., 2023). While the results show promise in burst detection, they do not present a solution for pathological locomotion detection or out-of-lab environments. That said, recent effort has been made to detect gait phase events in cerebral-palsy hemiplegic children (Morbidoni et al., 2021).

Kyeong et al. (2019) performed a gait experiment for human-robot interaction using sensor fusion methods with sEMG, ground reaction force, load-cell, and rotary encoders. Statistical, frequency-time domain and spatial features were extracted to train a Bayesian linear discriminant analysis (BLDA) model. As expected, the highest locomotion classification accuracy results were acquired with sensor fusion across all sensors. EMG alone with all 5 ipsilateral sEMG electrodes scored ~80%. Reducing the number of channels to only the tibialis anterior (TA) and gastrocnemius (GM) only resulted in ~67% accuracy.

Huang et al. (2009) aimed to develop an EMG pattern recognition algorithm to assist in the control of active artificial legs by classifying gait phases. The post-heel-strike and toe-off and pre-heel-strike and toe-off phases of gait were incorporated to develop a more reliable classification system. The authors extracted statistical, frequency-domain features to train an ANN and LDA classifier for each desired phase. Singular phase

detection outperformed whole stride classification with either classifier.

A simple if this then that (ITTT) algorithm using high energy spectrograms from multi-channel EMG successfully detected multiclass walking by tuning hyperparameters for participant-specific profiles (Joshi et al., 2015). Interestingly, in contrast to Kyeong et al. (2019), TA and GM activity had the strongest discriminating power to classify locomotor modes.

So far, the most prominent method has been preprocessing segmented data and extracting multiple features across statistical, temporal, and frequency domains before applying a non-linear models. Assessing this pipeline with SCI pathological gait has yet to be performed.

As far as I know, there is no any existing literature regarding the classification of locomotor activity in SCI EMG data over a chronic period while free-romaing. In this study, I aim to bridge this gap and develop a simple digital signal processing pipeline followed by the rule-based algorithm for readily scalable online classification of locomotor activity in spinal transected rats undergoing multimodal therapies. This chapter aims to investigate how existing digital signal processing techniques will perform to generalise locomotor activity across treatments and chronic recordings. I hypothesise non-linear techniques will best classify multi-label stepping and standing activity.

4.2 Methods

4.2.1 Digital Signal Processing

The raw EMG signal, across all channels, was filtered with a third-order Butterworth bandpass filter with cut-off frequencies of 30 – 1000 Hz. This attenuates DC offset and higher frequency noise. An envelope was extracted by feeding the filtered signal into a Teiger Keiser Energy Operator (TKEO) known to improve burst detection in EMG signals

Table 4.1: Summary of presented algorithms and sensors used to estimate locomotion activity

Author	**Assessment Environment**	**Sensor**	**Algorithm**
Greene et al. (2010)	Lab setting	IMU	Sliding threshold and peak detection
Jasiewicz et al. (2006)	Lab setting	IMU	Peak detection
Storm et al. (2016)	Indoor and outdoor	IMU	Peak detection
Catalfamo et al. (2010)	Indoor and outdoor	IMU	Zero-crossing, ITTT
Salarian et al. (2004)	Lab setting	IMU	Peak detection
Albert et al. (2017)	Lab and home setting	IMU	SVM, NB, LR, KNN, RF
Chen et al. (2015)	Lab setting	IMU, Pressure	LDA, QDA, LR
Huang et al. (2009)	Lab setting	EMG	LDA, ANN
Morbidoni et al. (2019)	Lab setting	EMG	ANN
Nazmi et al. (2019)	Treadmill	EMG	ANN
Kyeong et al. (2019)	Lab setting	EMG, GRF, Load-Cell, Encoder	BLDA
Park et al. (2023)	Treadmill	EMG	RF, KNN, SVM, ANN

Inertial Motion Unit (IMU); If-This-Then-That (ITTT); Support Vector Machine (SVM); Naïve Bayes (NB); Logistic Regression (LR); K-Nearest-Neighbours (KNN); Random Forest (RF); Linear Discriminant Analysis (LDA); Quadratic Discriminant Analysis (QDA); ANN (Artificial Neural Network); Bayesian Linear Discriminant Analysis (BLDA); Ground Reaction Force (GRF)

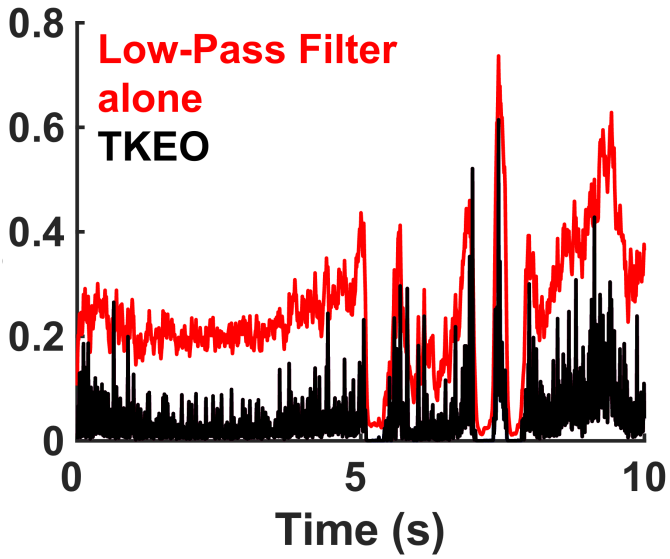

Figure 4.1: The TKEO step pushes the envelope activity closer to zero with lower delay than the lowpass filter

(Solnik et al., 2010). The TKEO output was smoothened using a first-order Butterworth lowpass filter with a cut-off frequency of 50Hz fig. 4.1.

The data was broken up into 10-sec bins to determine the activity threshold across each channel. An adaptive threshold sampling method determined the rest period throughout each 10-sec bin. Envelope data were first averaged into 10ms windows, and a minimum window was selected as the first region of interest. A sliding window procedure, combined with non-linear dual-thresholding, was implemented to determine the entire rest period within the 10-sec bin.

The end of rest was set if the first differential magnitude of 0.1mV/s or a logarithmic threshold of 300 $\log(mV)$ was reached. It was found that during the slower, more gradual ramping of EMG activity, first-order differential values were not sufficiently sensitive. To account for this slow ramping, a logarithmic threshold was considered. This enables the software to have a whole period of low 'rest-activity' established if either threshold is reached in either direction.

The mean and standard deviation of the detected rest intervals were used to set the

adaptive thresholding. A scalar constant was multiplied by the standard deviation and summed with the mean value for each channel. The constant, K, was set dependent on the target muscle, where TA was 6, and SOL was 3.

$$threshold = \mu_{rest} + K\sigma_{rest} \tag{4.1}$$

Finally, a time criterion was implemented for each channel to consider valid bursting activity. If the TA activity above the threshold was < 0.1s, and SOL activity above the threshold was < 0.3s, then it was not considered for further processing. These values were set based on previous literature studying the recovery of swing and stance phase during treadmill locomotion using the same neuromodulation therapies (Gad et al., 2015). For an example of the thresholding techniques, see fig. 4.3.

4.2.2 Rule-Based Algorithm

A relative difference signal between a min-max normalised TA and SOL was calculated from the extracted envelope fig. 4.3. The relative difference signal was used as a representation of coordination between flexion and extension of the ankle. It was assumed that if the signal was positive and within an identified burst, the joint had greater flexion force. Conversely, if the same were to be said for the negative magnitudes of the signal, a greater extension force was acting on the joint. A peak during the positive signal region indicates a switch between a flexion phase and an extension phase. Thus, if the peak was followed by registered bursting extensor activity and the relative difference signal was negative, then this was considered a successful transition from flexion to extension.

A peak detection process was performed to indicate the flexion phase and the beginning of a step cycle. The flexion phase can be rapid and seen as a sharp change in the relative difference signal. A minimum peak detection threshold was set to 0.01 to ensure

that only adequate activity was considered. Secondly, switching must be temporally constrained. Otherwise, any extension activity occurring too slowly after the swing phase may be registered as a positive event. A step was only recorded if a negative signal followed a positive peak while the SOL was active within a temporal threshold of 0.5s. Finally, a minimum period of 0.2s was set between local maxima to ensure that only the last local maxima within the TA burst were selected. Standing events were defined as the paired SOL bursting activity reaching a time threshold 0.6s (Gad et al., 2015). See fig. 4.2 for a complete reference to the algorithm. We will name this proposed rule-based algorithm Thresholding Offline Kinematic and EMG Data Analysis (TOKEDA).

4.2.3 Machine Learning

To increase the potential for successful window classification, a larger sliding window length of 0.14s was used with 20% overlap to generate the feature set used to train the machine learning models (Huang et al., 2009; Park et al., 2023). Several frequency, statistical, and signal-relevant features were extracted from each window for each channel. These include peak-to-peak values, max and min values, skew, kurtosis, integrated EMG, mean, standard deviation, root mean square, max frequency, spectral density, and spectral entropy, see table 4.2.

Features were input to LDA, LR, and SVM models to classify EMG locomotion activity. This study will also include KNN and XGBoost models for comparison. Linear models were trained using the One-Vs-All strategy. Their hyperparameters were tuned using 3 K-Fold cross validation. See table 4.3 for full details. XGBoost models were trained using an NVIDIA Quadro RTX 6000 Passive graphics card to reduce computation time. The remaining classification models and signal processing pipelines were completed on Intel Xeon Gold 6238R 2.2GHz 28-core CPU with 38.5MB L3 Cache.

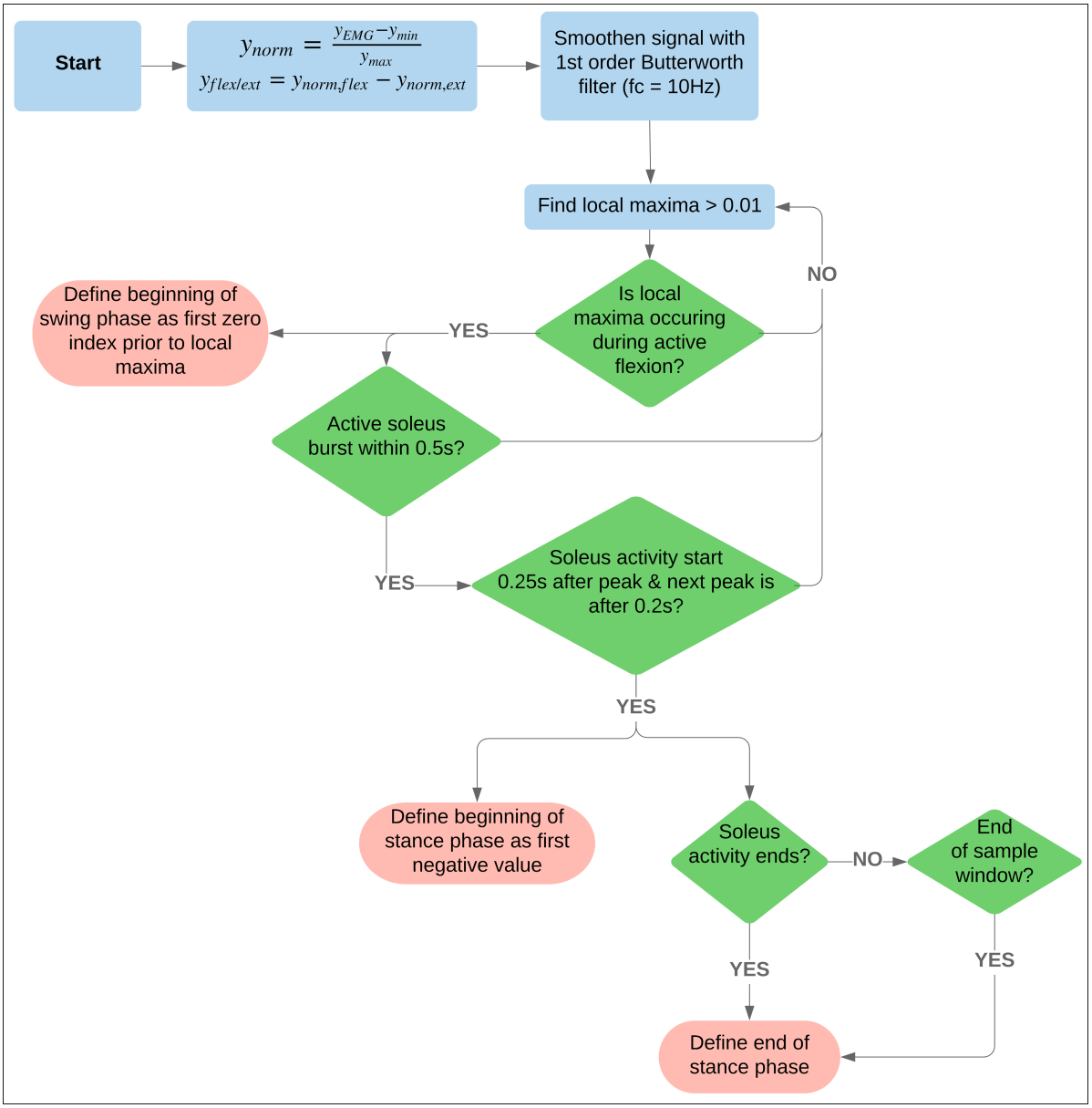

Figure 4.2: Illustration of the algorithm process and rules before classifying a sequence of EMG data as a step.

Table 4.2: Statistical, time, and frequency domain features extracted from a window size of 0.14s and overlap of 20%. These features formed an input vector for machine learning input.

Feature	Equation
Mean	$\bar{x} = \frac{1}{N}\sum_{i=1}^{N} x_i$
Standard Deviation	$SD = \sqrt{\frac{1}{N}\sum_{i=1}^{N}(x_i - \bar{x})^2}$
Kurtosis	$K = \frac{\frac{1}{N}\sum_{i=1}^{N}(x_i - \bar{x})^4}{SD^4}$
Skewness	$S = \frac{\frac{1}{N}\sum_{i=1}^{N}(x_i - \bar{x})^3}{SD^3}$
Root Mean Square	$RMS = \sqrt{\frac{1}{N}\sum_{i=1}^{N} x_i^2}$
Peak-to-Peak Value	$PPV = \max(x) - \min(x)$
Relative Difference	$RelDiff = envelope_{Flex} - envelope_{Ext}$
Max Frequency	$f_{\max} = \frac{\text{index}_{\max} \cdot f_{\text{sample}}}{N}$
Spectral Density	$S(\omega) = \lim_{T\to\infty} \frac{E[\lvert X(\omega)\rvert^2]}{T}$
Spectral Entropy	$H = -\sum_{i=1}^{N} P_i \log_2(P_i)$

4.2.4 Statistics

The classification accuracy will be reported concerning each classified window. F1 scores, precision, and recall will be used to compare the multiclass performance for left and right steps and standing events. F1 scores are commonly used to evaluate classification accuracy by combining precision and recall scores. Macro F1 scores can be interpreted as the averaged F1-score for each label, without considering the proportion of the label in the data set, see section 3.7.

The labelled data sets were split into partitions of 0.6/0.2/0.2 for train, validation, and test sets, respectively. To find the representative accuracy of the tested algorithms,

Table 4.3: Summary of machine learning models used in this study and their respective hyperparameters, tuners, and scorers.

Model	Parameters	Tuner	Scorer
KNN	power = 1, 2 leaf_size = 10, 30, 100, 300 weights=uniform, distance	GridSearchCV	F1-Score
LDA	tolerance=0.0001, 0.0003 C=0.1, 0.3, 1.0 class weights=None, balanced max_iter=300, 1000, 3000	GridSearchCV	F1-Score
LR	tolerance=0.0001, 0.0003 C=0.1, 0.3, 1.0 class_weights=None, balanced max_iter=300, 1000, 3000	GridSearchCV	F1-Score
SVM	tolerance=0.0001, 0.0003 C=1, 10 class_weights=None, balanced max_iter=300, 1000, 3000	GridSearchCV	F1-Score
XGBoost	max_trials=20 max_depth=3, 5, 6, 10, 15, 20 learning_rate=0.01, 0.1, 0.2, 0.3 n_estimators=100, 500, 1000 colsample_bytree=0.1, 0.4, 1.0 colsample_bylevel=0.1, 0.4, 1.0 subsample = 0.5, 0.6, 0.7, 0.8, 0.9	RandomizedSearchCV	F1-Score

a series of set time-windowed labels were found by performing the sliding window procedure through the test data label set. The sliding window contained a 3-sec window size and no overlap. All windows that did not contain any information were rejected. This is to determine the accuracy within a time window, focusing on assessing the performance of our classifier during specific temporal segments of interest. The reported results used the same test set, shared between machine learning and digital signal processing approaches.

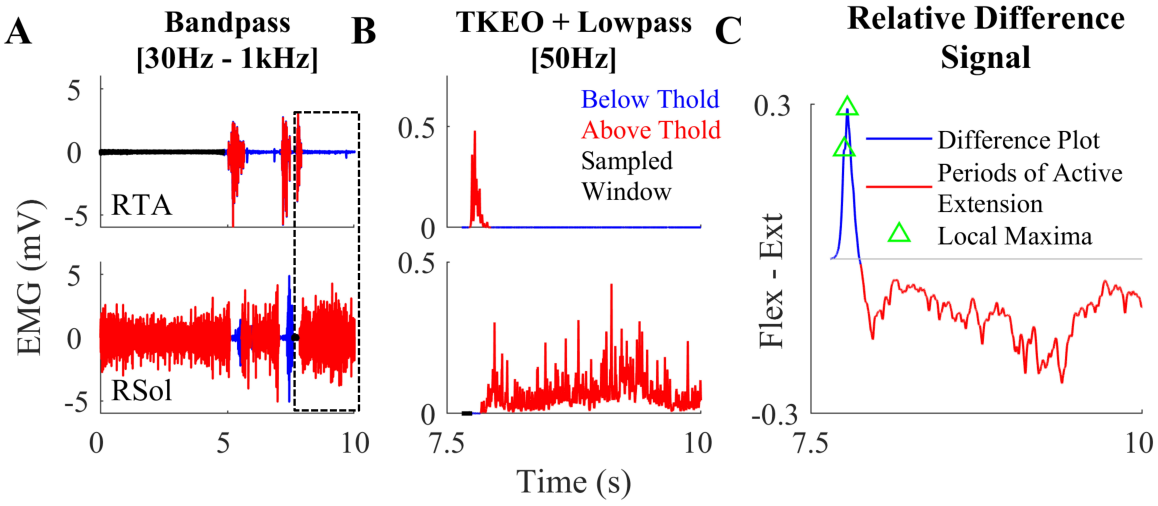

Figure 4.3: **A)** Representative band-pass filtering of TA and Sol. The boxed area shows a close-up example of the thresholding and the normalized difference plot used to characterise step-like activity. Regions of the signal below threshold (blue), above threshold (red) and rest (black) were recorded. **B)** TKEO signal conditioned, rectified and smoothed EMG signal from the TA and Sol muscle of a spinal rat during spontaneous cage activity. A representative example of a singular hind-limb step within the first hr of recording spontaneous activity. **C)** The relative difference between the normalized values of the TA and Sol from **B)**. The grey line y-axis = zero. The blue line is a trace of the relative difference plot and in red is the periods of active extension, identified through thresholding. Green triangles represent points of local maxima during active flexion. These features were used to detect spontaneous hind-limb step-like activity.

4.3 Results

Without analysing the time windowed accuracy and submitting the proposed rule-based algorithm to the entire data set, TOKEDA yielded success in rejecting negative examples, outperforming the machine learning models in precision. However, struggled to identify the true positives. The macro evaluations are summarised in table 4.4.

The machine learning models differentiated in their ability to discriminate between positive and negative examples. LDA, KNN, and XGB models reached relatively equivalent precision and recall scores. XGB model yielded the highest F1-score overall with the greatest precision and recall among the aforementioned balanced models. Although LR and SVM models reported the second and third highest F1-score, care must be taken if

Table 4.4: Macro metrics for complete and time-windowed evaluation of machine learning models compared with TOKEDA pipeline using the entire test data set.

	Precision		Recall		F1-score	
Model	Complete	Windowed	Complete	Windowed	Complete	Windowed
KNN	0.48	0.52	0.46	0.25	0.46	0.33
LDA	0.53	0.33	0.43	0.19	0.47	0.23
SVM	0.40	0.39	0.61	0.28	0.48	0.32
XGB	0.55	0.51	0.48	0.25	0.51	0.34
LR	0.38	0.40	0.70	0.33	0.49	0.36
TOKEDA	0.59	0.42	0.10	0.06	0.17	0.10

Table 4.5: Left step label evaluation of machine learning models compared with TOKEDA pipeline in both complete and time-windowed test datasets.

	Precision		Recall		F1-score	
Model	Complete	Windowed	Complete	Windowed	Complete	Windowed
KNN	0.41	0.43	0.36	0.22	0.38	0.29
LDA	0.49	0.14	0.34	0.11	0.40	0.12
SVM	0.37	0.27	0.55	0.22	0.44	0.24
XGB	0.49	0.44	0.34	0.18	0.40	0.25
LR	0.33	0.29	0.70	0.25	0.45	0.27
TOKEDA	0.40	0.36	0.09	0.06	0.15	0.10

one were to base the evaluation solely on the macro F1-score. While LR and SVM models performed better than the other models in recalling the positive windows, they failed to reject negative examples.

Closer inspection of the results in tables 4.5 to 4.7 provide a more granular view. TOKEDA reports the greatest result while classifying the right steps compared to the other labels. TOKEDA precision results for right steps yield 0.74, nearly double the different models for right stepping. However, it suffers in recall evaluations, leading to a poor F1 score. TOKEDA precision for left step and standing labels did not outperform the machine learning techniques.

Time-windowed data were extracted to test only relevant 3-sec windows on the respective methodologies. These sectioned results are seen in table 4.4. Model evaluations from time windowed sections are significantly different; see fig. 4.4.

Table 4.6: Right step label evaluation of machine learning models compared with TOKEDA pipeline in both complete and time-windowed test datasets.

	Precision		Recall		F1-score	
Model	Complete	Windowed	Complete	Windowed	Complete	Windowed
KNN	0.43	0.42	0.31	0.21	0.36	0.28
LDA	0.40	0.15	0.35	0.18	0.38	0.16
SVM	0.33	0.24	0.42	0.19	0.37	0.21
XGB	0.45	0.42	0.32	0.22	0.37	0.29
LR	0.30	0.27	0.53	0.30	0.39	0.28
TOKEDA	0.74	0.20	0.15	0.05	0.26	0.07

Table 4.7: Stand label evaluation of machine learning models compared with TOKEDA pipeline in both complete and time-windowed test datasets.

	Precision		Recall		F1-score	
Model	Complete	Windowed	Complete	Windowed	Complete	Windowed
KNN	0.60	0.72	0.71	0.31	0.65	0.43
LDA	0.69	0.72	0.60	0.27	0.64	0.39
SVM	0.50	0.65	0.85	0.43	0.63	0.51
XGB	0.72	0.66	0.77	0.35	0.75	0.46
LR	0.51	0.64	0.86	0.43	0.64	0.52
TOKEDA	0.62	0.72	0.06	0.07	0.10	0.12

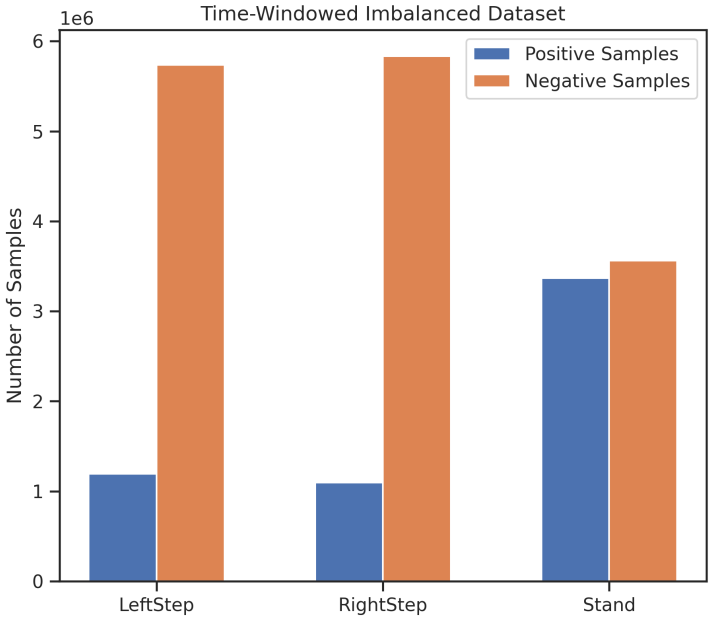

Figure 4.4: A bar plot representation of the time-windowed data set

Table 4.8: Irrelevant features, as determined from the Benjamini-Hochberg procedure for left stepping, right stepping, and standing labels

Label	Feature	p-value
Left Step	fmax_{CH1}	0.05
	mean_{CH2}	0.20
	skew_{CH3}	0.26
	mean_{CH1}	0.43
	mean_{CH3}	0.46
	mean_{CH0}	0.57
	fmax_{CH3}	0.76
	fmax_{CH0}	0.90
	fmax_{CH2}	0.93
Right Step	mean_{CH1}	0.27
	fmax_{CH3}	0.27
	fmax_{CH2}	0.43
	skew_{CH1}	0.58
	mean_{CH3}	0.78
	fmax_{CH0}	0.83
	mean_{CH2}	0.88
Stand	skew_{CH2}	0.17
	fmax_{CH1}	0.24
	fmax_{CH3}	0.25
	fmax_{CH0}	0.27
	mean_{CH0}	0.32
	fmax_{CH2}	0.44
	mean_{CH1}	0.68
	mean_{CH3}	0.73
	mean_{CH2}	0.86

KNN, SVM, XGB, and LR retained similar precision values ($range_{\max} = 0.04$). However, recall metrics dropped for each of these models. LDA and TOKEDA suffered a reduction in both precision and recall when challenged with time-windowed evaluation, resulting in a 0.24 and 0.07 drop in F1 score, respectively. Closer inspection of tables 4.5 to 4.7 indicates success in standing classification has the dominant contributor to F1 scores.

TOKEDA struggles with the top performers in total or time-windowed data sets,

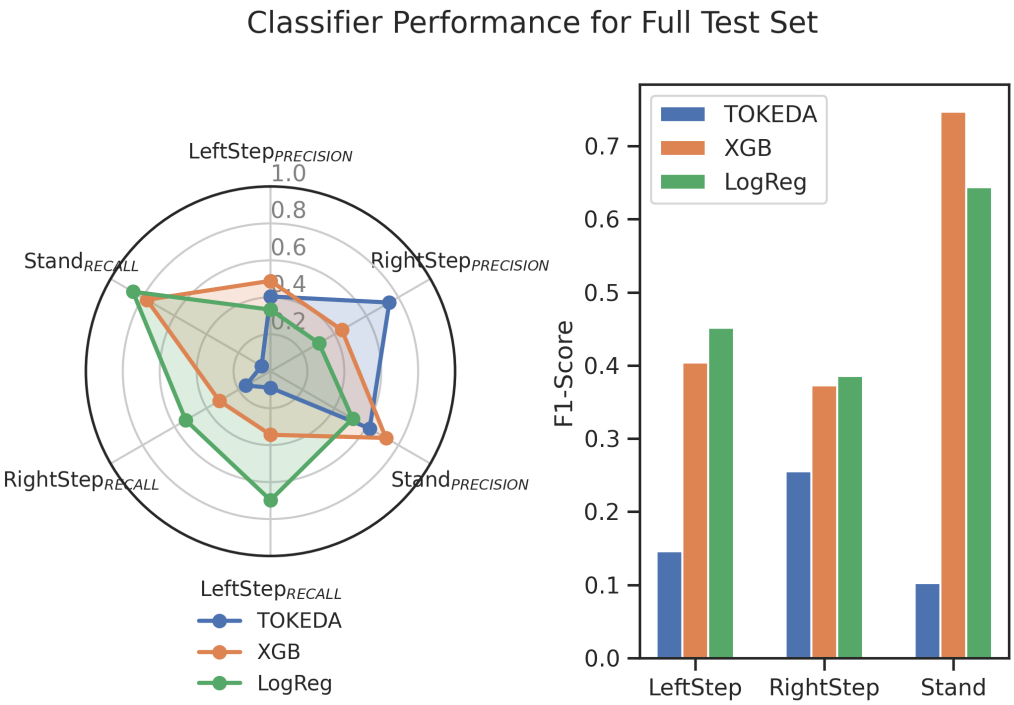

Figure 4.5: A spider and bar graph to illustrate the differences between the performance of select models. The left shows the spider plot of different labels and their precision and recall. The right displays the F1-scores for different labels and models.

which have a strong bias towards the right step and stand false-positive rejections. The top performers in either test case category show a greater spread in their labelling compared to TOKEDA. However, within the model, the spread is significantly smaller and skewed towards stand label false negative rejection figs. 4.5 and 4.6.

4.4 Discussion

Presented are the results of standard machine learning techniques compared with a novel online adaptive rule-based digital signal processing pipeline to classify chronic, cage-roaming rodent locomotor activity. This chapter describes the methodology of classifying a labelled time series data set in stochastic, multi-domain, and free-roaming environments for spinally transected rats. I developed a digital signal processing rule-based algorithm,

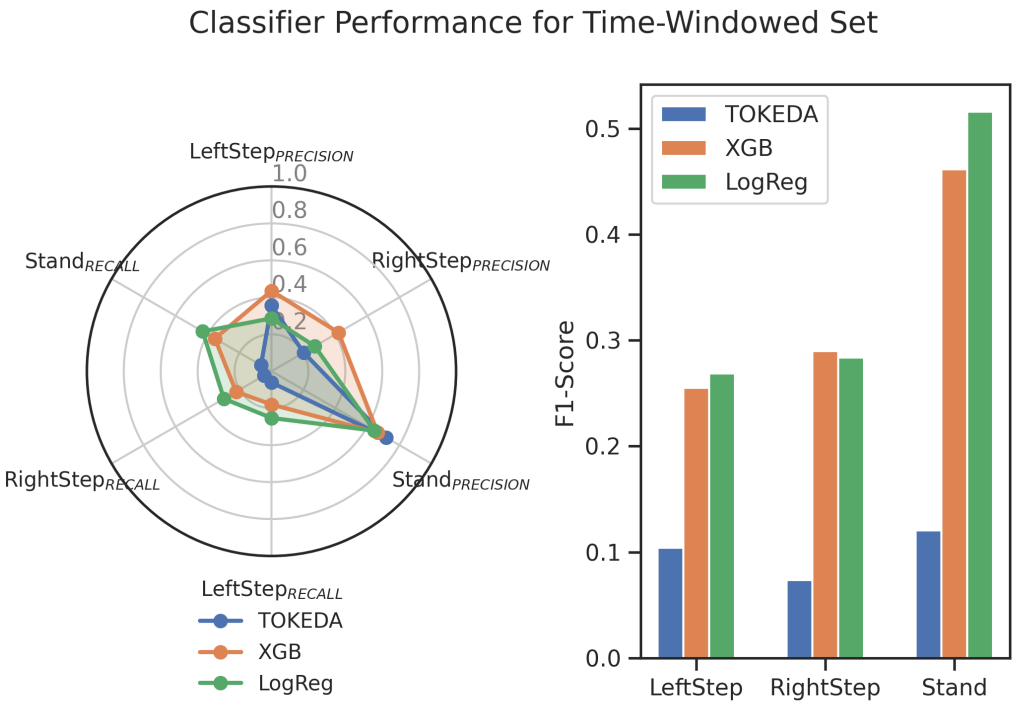

Figure 4.6: Spider and bar graph of select models to highlight the performance differences for time-windowed data sets.

TOKEDA, to classify multi-label data without needing to re-run the algorithm multiple times as a One-Vs-All strategy. A set of features to feed into machine learning models were designed to compress and represent locomotion activity in hindlimb EMG signals. Several linear and non-linear machine learning algorithms were tuned and trained with the One-Vs-All strategy to perform multi-label classification of stepping and standing events. The non-linear classifier, XGBoost, was the best performing machine learning model.

This is the first study on animal locomotor and standing classification using EMG data in a chronic, cage-roaming setting. Although previous studies have presented other strategies for detecting rat activity within a caged setting. These include the use of vibration/tilt sensing (Ganea et al., 2007), IR beams (Clarke et al., 1985), IR and non-IR video tracking (Aragao Rda et al., 2011; Gad et al., 2013b; York et al., 2013), capacitive flooring (Pernold et al., 2019), optical touch sensors (Mendes et al., 2015), RFID (Redfern

et al., 2017), and radar technology (Martin and Unwin, 1980; Rose et al., 1985; Young et al., 1996; Genewsky et al., 2017).

Detecting spontaneous self-recovering movement after paralysis outside a controlled clinical environment has rarely been explored quantitatively. This may be due to the limitation of securely attaching sensors or markers at specific locations. The antennas attached to a rat have tracked gross body movements through a maze of tubes (Starkey et al., 2014). It was shown that self-motivated training within an 'enriched environment' led to superior performance in skilled movement compared to restricted task-specific training. This 'RatTrack' system allows for testing self-initiated and task-specific training and dose responses. While the mentioned efforts can be extended in the direction of automation, each of these methods cannot directly measure the neuromotor parameters. TOKEDA relies solely on chronically implanted EMG electrodes for sensing to assess in vivo responses to different combinations of electrical and pharmacological neuromodulatory interventions. Access to neuromuscular activity synchronised with stimulation pulses directly linked to behaviours provides a direct and realistic measurement of reorganising neural networks throughout a chronic period as the nervous system becomes more functional (Courtine et al., 2008).

It is technically becoming more feasible to chronically record EMG from many muscles to detect how the reorganisation of neuronal networks that control locomotion can be focused on the patterns of coordination of flexion/extension, abduction/adduction and non-repetitive tasks such as grip and pinch manoeuvres as well as repetitive tasks such as cycling etc. Moreover, the ability to measure the state of the locomotive neural circuitry to determine the direct relationship between the treatment provided and the underlying neuronal mechanics serves as detailed insight as the subject undergoes training, providing the opportunity to adjust treatments to maintain an enabling effect, maximising activity-dependent recovery.

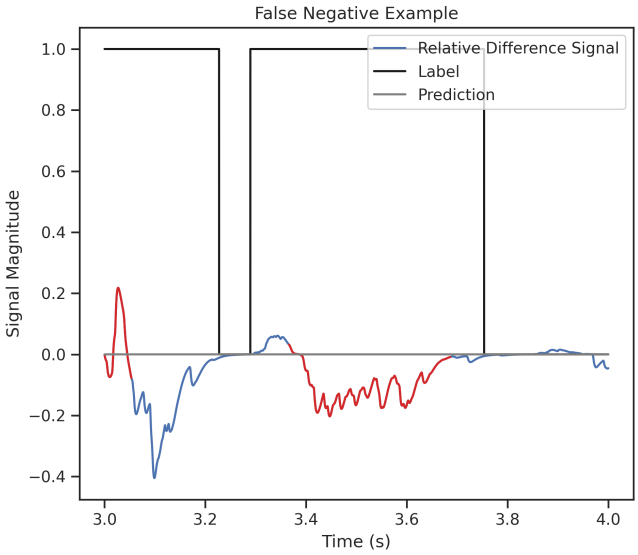

Figure 4.7: TOKEDA example of a false negative event. This occurred due to the way the relative difference signal encodes deactivation of the flexor muscle. The flexor and extensor magnitude for coordinated transition was not met due to the adaptive threshold.

The ability to record chronically for 6-hrs in a natural setting highlights the functional and electrophysiological changes over time and could lead to a valuable biomarker of recovery post paralysis. Spinal circuits controlling stepping and standing (locomotion and posture) can be improved after SCI by practising those tasks, i.e., by increasing the activation of those circuits (Ahissar and Hochstein, 1997; Bayona et al., 2005). Developing methods to improve the classification accuracy and analyse the stepping data towards investigating the possibility of a bio-marker for recovery is a logical step forward.

TOKEDA successfully rejected false positives for right stepping and standing but failed to do the same for left step events. The algorithm also accepted false negatives and thus missed several true positive points in the data set fig. 4.7. A strong skew towards stand detection was uncovered when testing the time-windowed data set. Results suggest that current machine learning and digital signal processing methodologies must be more robust and accurate to feasibly capture locomotor events in complex, open environments expressing pathological gait.

Previous effort to determine classification error between non-disabled and transfemoral amputee participants showed dissimilar EMG patterns between groups (Huang et al., 2009). Results from the investigation suggested sufficient neural information for accurate classification across various locomotion modes in both subject pools. Although the amputee's EMG patterns were not similar to able-bodied subjects, their algorithm results could adapt to each individual. The adaptive threshold developed in this work successfully registered active and non-active muscle groups spatiotemporally manner figs. 4.1 and 4.3. Future endeavours aiming to classify locomotion in pathological gait may succeed more if a similar 'divide-and-conquer' approach is taken.

The machine learning models resulted in greater evaluation metrics, especially in XGBoost and Logistic Regression models table 4.4. The results from these models suggest a bias towards standing event labelling. This is expected due to the skew towards stand data. While the One-Vs-All strategy reduces the impacts of skewed labelling, the sheer volume of standing events may provide a more probable successful classification than step data. Another interpretation can be made, where the standing data was more linear compared to stepping data. Mapping these representations has yet to be done before, and it is unclear if this information can be extracted from only 4 channel antagonist muscle groups.

To ascertain the features machine learning models used to detect relevant features, a Principle Component Analysis (PCA) and Benjamini-Hochberg method was implemented fig. 4.8 and table 4.8. From this data, the most variance was encoded in the frequency domain, specifically in the max frequency of the window. These effects were less significant in channels 1 and 3, corresponding to the soleus activity in the right and left hindlimb respectively. The relevance tables between the left and right stepping indicate that almost all features were significant concerning the labels ($p < 0.000001$).

Values shown by the tables table 4.8 only detail the irrelevant features. From this,

most maximal frequency features and mean values do not contribute to the label outputs, and yet max frequency in each window explains most of the variance after linear compression fig. 4.8. This is an unexpected finding, as one would expect the greater frequency activity to indicate more motoneuronal firing, thus correlating with stepping and standing activity. On the polar end, the most relevant features for stepping were peak-to-peak, standard deviation, and root-mean-square features.

Standing relevant features ranked magnitude related information, such as integrated EMG and root-mean-square, near the top. However, the p-value differences between these most relevant features were negligible. The results in Gad et al. (2015) may explain the frequency irrelevance. After combinatory pharmacology and electrical stimulation were introduced, frequencies during stepping became more balanced and attenuated at lower frequencies.

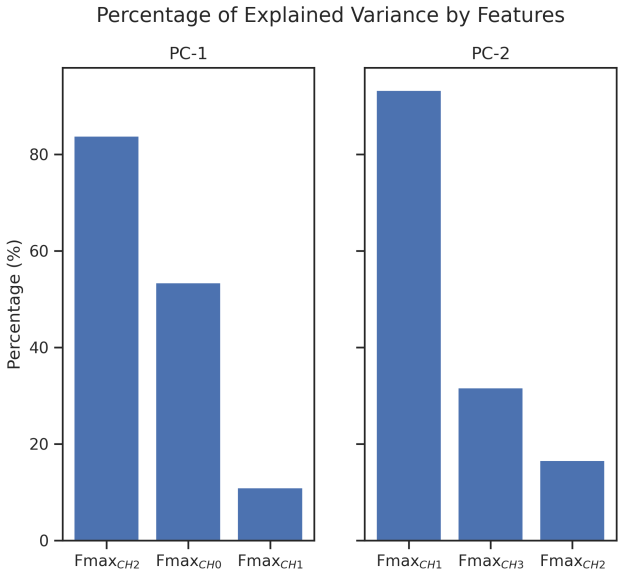

Figure 4.8: Percentage of explained variance in 2 component PCA, using features described in table 4.2

Time-series classification with imbalanced data sets has been a consistent challenge in biosignal analysis (Zhao et al., 2018; Kumar et al., 2022). This difficulty stems from the nature of biological signal tracking and the diversity of available data. Several issues

arise when adopting machine learning techniques that fit biological data. One major challenge is developing valid and reliable biomarkers that are suitable for the target population (Kempsell et al., 2016; Richens et al., 2020; McDermott et al., 2013). Although developing these biomarkers is valuable, the process is often time-consuming and costly (de Graaf et al., 2018). Additionally, much of of the data is either difficult to access or completely opaque (Kempsell et al., 2016; Fahr et al., 2019).

Biological systems are rarely static, and in the case of pathological nervous systems, this is particularly the case. This may be due to environmental, pathological, or endogenous variables that are difficult to capture section 4.1. An element of human cognition is almost always required when interpreting time-series data (Längkvist et al., 2014). This variable is often lost or compressed when working with machine learning methodologies. All previous attempts outlined above, using machine learning, have approached the problem in this fashion. For this reason, the TOKEDA methodology was conceived with built-in spatiotemporal dependencies. However, the method yielded poor results compared to XGBoost and logistic regression.

How salient features contributed to step and standing classification was investigated with SHapley Additive exPlanations (SHAP) (Lundberg and Lee, 2017). SHAP values use game theory to assign credit for a model's prediction to each feature and can help explain the output of machine learning models. Logistic regression heavily relied on higher Sol IEMG values for left and right step classification (see fig. 4.9). During left step events, the classifier mistakenly prioritised the contralateral Sol IEMG variable and negatively weighted left TA IEMG feature values. Mistaken channel attribution may also mean that many left-step events coincided with right steps and provide an explanation for the slightly poorer classifier performance in left vs right stepping. The left TA activity, ranked second by SHAP values, provided information similar to that of the right Sol IEMG. High SD and RMS values in right Sol negatively influenced the

prediction output, in line with expected outcomes. Intuitively, RMS and SD of the left and right SOL channels return high SHAP values with high magnitude for standing classification.

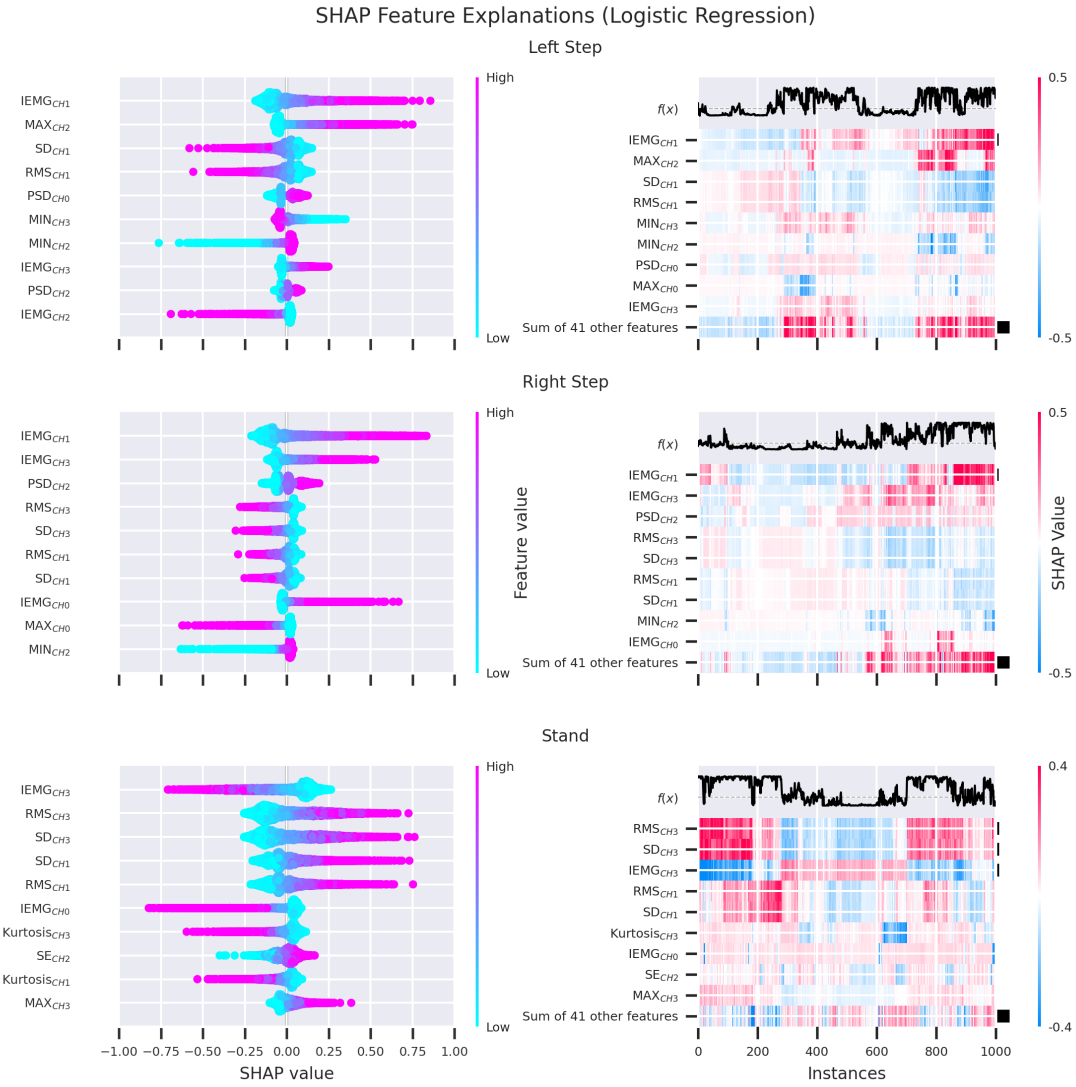

Figure 4.9: Top-10 SHAP feature analysis with beeswarm (left) and heatmap (right) plots for logistic regression. Temporal and frequency activity in the left and right side contributed to the classification of step activity. Mainly temporal amplitude features contributed to the classification of standing activity. Heatmap activations indicate the contribution of each feature to the logistic regression model output ($f(x)$). Note channels 0 – 4 indicate TA and Sol electrodes from right to left.

XGBoost SHAP values for ranked features exhibited a smaller spread than the

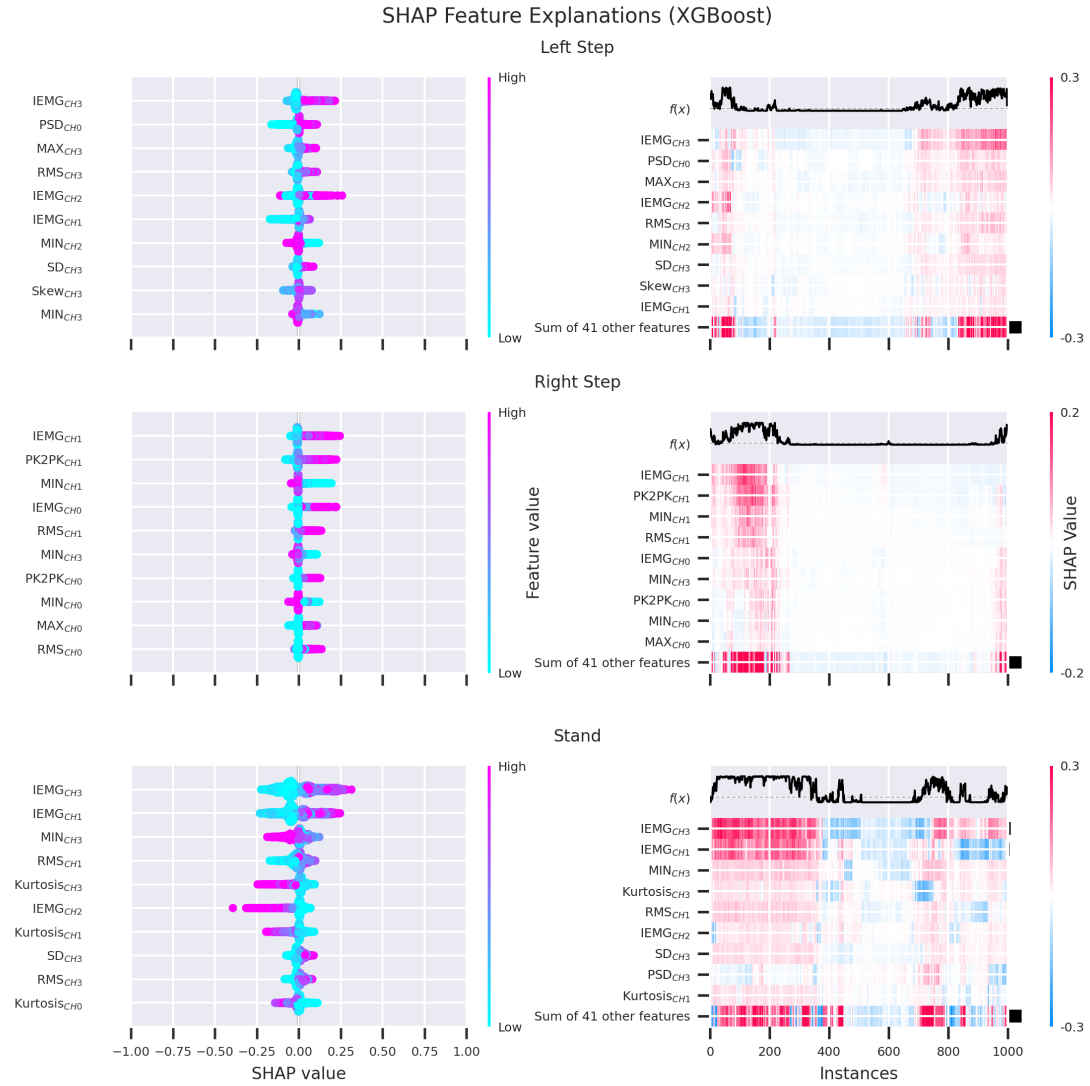

Figure 4.10: Top-10 SHAP feature analysis with beeswarm (left) and heatmap (right) plots of XGBoost. Temporal activity contributed to the classification of left step activity whilst a mixture of temporal, statistical, and frequency features contribute to left step activity. Temporal and statistical features contributed to the classification of standing activity. Heatmap activations indicate the contribution of each feature to the logistic regression model output ($f(x)$).

Logistic Regression feature explanations (see fig. 4.10). The left step classification developed positive SHAP values for IEMG, RMS and max features in the left channel data with greater contribution from the Sol channel. Min right Sol features were inversely attributed such that lower min values returned positive SHAP values. The inverse

Table 4.9: EMG burst classification comparisons between gaussian mixture model and online adaptive thresholding for right TA (RTA), right Sol (RSOL), left TA (LTA), left Sol (LSOL).

	RTA	RSOL	LTA	LSOL
F1-Score	0.13	0.41	0.16	0.44
Precision	0.36	0.53	0.33	0.66
Recall	0.08	0.33	0.11	0.33

relationship between SHAP values and minimum left Sol values was also correctly associated. The right step XGBoost classification positively associated IEMG, peak-to-peak, RMS, and max information from right channel data. However, PSD TA and IEMG Sol right channel information was mistakenly utilised for left step classification. Similar to logistic regression SHAP analysis, right step classification may have outperformed left step classification due to the model correctly learning relationships for right step activity. Intuitively, stand classification contributes positively to SHAP value from the left and right Sol IEMG features. Sol channel kurtosis negatively contributes to stand classification, reducing the probability of positive labelling. SHAP values increased with lower kurtosis; this could be interpreted as smaller deviations or outliers in the windowed data led to a higher likelihood of stand events.

Finally, to investigate the reason for small recall in the rule-based TOKEDA algorithm, the adaptive thresholding digital signal process was compared against the Gaussian mixture model for burst classification, refer to table 4.9. While the Sol burst activity in both left and right achieved strong false positive rejection, many real positives in the TA channel were missed. The TOKEDA process requires the initial detection of a TA burst. The strict threshold criteria of TA bursts stop the digital signal process from the beginning and may explain the poor recall performance in the TOKEDA algorithm. However, TOKEDA achieved a competitive precision score by prioritising false-positive rejections.

4.5 Conclusion

In this chapter, I approach the problem of time-series classification of locomotion and standing activity in 4 spinal transected rats receiving multiple forms of neuromodulatory therapy while roaming in an enriched cage environment. The proposed pipeline rapidly utilised adaptive online thresholding mechanisms with temporal constraints to capture spatiotemporal information. It was hypothesised that linear techniques would suffer poor classification results due to the stochastic nature of EMG activity and behavioural variations from overground locomotion. The results from this study only partially support this hypothesis. XGBoost, a non-linear methodology, and logistic regression, a linear methodology, were revealed as the top-performing classifiers. Future work to improve the performance of this classification task may incorporate feature selection methods such as dynamic time warping or state-of-the-art deep learning methodologies.

CHAPTER 5

Deep Learning Methodologies for Stochastic EMG Time-Series Multi-Label Classification

Deep learning has seen immense growth in the past decade, and only recently has the life-science stream sought to exploit the representational power of deep learning models. While state-of-the-art (SOTA) techniques have shown tremendous promise in natural language processing and image classification, time-series biosignal analysis has historically shown a delay in advancements. Scientists and engineers have developed impressive handcraft feature sets for specific subjects and domains that offer poor scalability and generalising power. The noisy, high-dimensional complexity of biomedical datasets is a difficult scope to work within. To advance the field of biosignal time-series classification, I consider the works of domain adaptation across therapies and incorporate the Vision Transformer as a secondary tool to develop long-distance representations in EMG continuous wavelet transformed (CWT) data. CWT inputs were stacked along the feature dimension, and multiple models were trained. I hypothesise that mixing depthwise separable convolutional operations in vision

transformers will best encode the cross-channel and spatiotemporal information of a locomotor events. Results suggest depthwise separable convolutions do perform better for standing activity. However, suffer in representing the cross-channel time requirements of locomotor activity. Vision transformers encode more robust spatiotemporal information across channels to classify locomotor activity compared to convolutional networks. I discuss the reasons for the results and suggest future advancements in biosignal analysis in a deep learning context.

5.1 Introduction

In 1895, Willem Einthoven invented the electrocardiogram (ECG) as a clinical diagnostic tool to measure the electrical activity of heart muscles and represent the cardiac cycle in polarization and depolarisation of the myocardium (Silipo and Marchesi, 1998). Multiple systems have been developed since, including electroencephalography (EEG), reporting brain electrochemical activity via micro-voltage changes from the scalp (Bajaj and Pachori, 2013). EMG measures the electrical potential generated from motoneuronal activity, activating the voltage-gated calcium channels in muscular tissue (Karthick et al., 2016; Kuo and Ehrlich, 2015). Photoplethysmography (PPG) encodes representations of the volumetric changes of an organ over time via light absorption (Alian and Shelley, 2014). Electrical, mechanical, thermal, and other biosignals, transduced via an appropriate sensor selection, enables the estimated measure of physiological data over time.

These signals all measure the adaptation of some physiological activity over continuous time, discretised through an analogue-to-digital converter. It is through the dimension of time that the characteristics and meaning of the signal are captured. Physiological biosignals are incredibly complex, with individual specific time-dependent information, dynamically changing depending on the equipment setup, physiological

state, and environment factors (Idri et al., 2018; Miotto et al., 2018).

Traditionally, signal processing methodologies, feature extraction, and classification techniques seen in chapter 4 were performed to extrapolate the information of interest. However, these processes are time-consuming and lack reliability (Längkvist et al., 2014). Handcrafting feature sets also make it difficult to generalise between data sets and adapt across different domains (Koelstra et al., 2012; Krishnan and Athavale, 2018). One method to approach the non-linear and dynamic nature of biosignal analysis is to harness the processing power of neural networks, capable of non-linear transformations and extracting features from raw multivariate time-series data (Fawaz et al., 2018).

While computer science has endeavoured to develop neural networks and exploit representation learning for complex tasks since the 1950s, the life sciences have only recently seen advancements in deep learning relevancy, see fig. 5.1. Deep learning offers to encode significant volumes of information, allowing researchers and users to extrapolate the information they require from an otherwise noisy, high-dimensional, and complex data set (Deserno and Marx, 2016). Thus, deep learning and the comprehensive data collected through decades of healthcare industry physicians and public health infrastructure have opened doors to data mining for extracting hidden knowledge behind medical tasks (Esfandiari et al., 2014).

Artificial neural networks (ANNs) have their roots embedded in a multidisciplinary stream. Some consider Aristotle's attempts to understand the brain in 300 BC as the first step towards neuroscience and the development of the neural networks of today (Wang and Raj, 2017). Early works by critical neuroscientists helped form early conceptions of deep learning. Cajal and Golgi are considered to be the first neuroscientists in history. Original work by Cajal, using the famous 'la reazione nera – the black reaction' developed by Golgi, gathered the first histological slides of the nerve cell, awarding Golgi and Cajal with a shared Nobel Prize in 1906 (Yuste, 2015; Ghosh, 2020). Works by the likes of

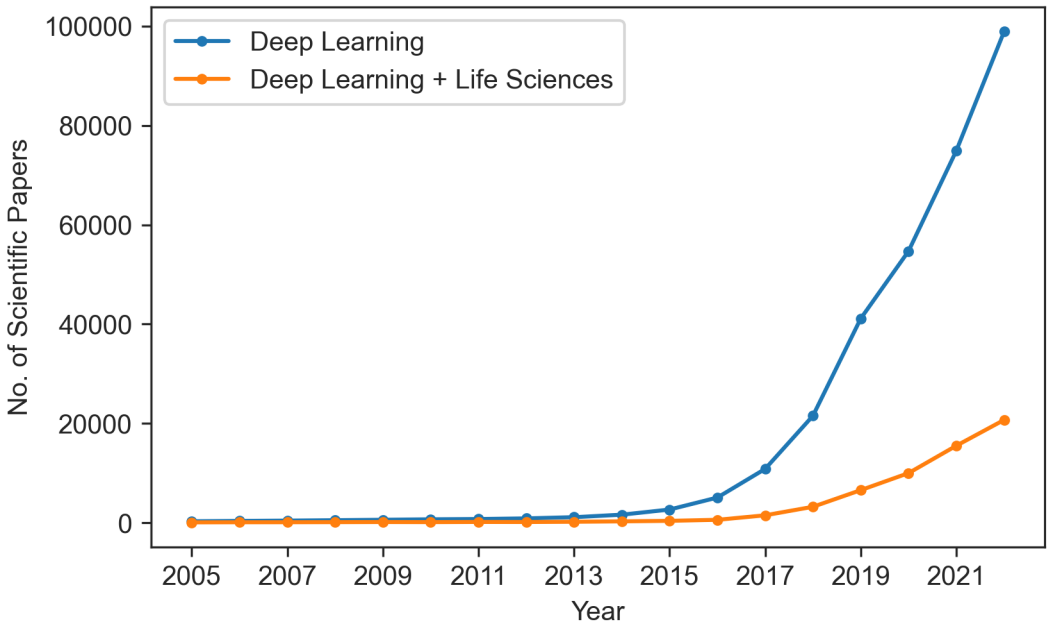

Figure 5.1: Deep learning popularity over time, compared to the inclusion of deep learning techniques in life sciences. Deep learning differentiates from machine learning in requiring three or more layers. Adapted and updated image from Bacciu et al. (2018).

Donald Hebb, Alan Hodgkin, Andrew Huxley, Warren McCulloch, and Walter Pitts paved the way towards the development of the first perceptron in 1958 by, at the time, research psychologist Frank Rosenblatt, who later on became associate professor of neurobiology and behaviour at Cornell University (Hebb, 2005; McCulloch and Pitts, 1943; Hodgkin and Huxley, 1952; Rosenblatt, 1958). Since then, multi-layer perceptions, convolutional neural networks, recurrent neural networks, transformer networks, and new SOTA models in development have seen incredible coverage in research and commercial contexts (Alzubaidi et al., 2021).

Deep learning towards diagnostics and monitoring has received significant attention in the biomedical space (Gérardin et al., 2022; Wosiak et al., 2018). Multiple applications exploiting the representational power of deep learning have been presented, especially in diagnostics (Aggarwal et al., 2021; Suzuki, 2017). Medical image classification has seen an incredible rise in research coverage with many researchers adopting the successes of

image processing in convolutional neural networks (CNNs) to classify medical imaging data (Sarvamangala and Kulkarni, 2022). Three techniques have been reported to classify medical images successfully: training a CNN from scratch, using pre-trained CNN features, and unsupervised CNN pre-training with supervised fine-tuning (Shin et al., 2016). The depth of latent representation in immense data volumes gives deep learning the edge of traditional machine learning approaches. Recently, research effort has gone towards applying augmentation techniques to upscale and develop robust deep learning models in small data set contexts, such as personalised models (Iwana and Uchida, 2021). Yoo et al. (2014) applied feature extraction of MRI data towards multiple sclerosis lesion segmentation using unsupervised learning, followed by random forest supervised classification. CNNs have been used widely in cancerous lesion identification, diagnosis, and segmentation (Ciompi et al., 2015; Suzuki et al., 2004, 2010).

With similar taxonomy to CNNs, time-related classification and prediction using recurrent neural networks (RNNs) has received a lot of attention (Wang et al., 2021; Miotto et al., 2018; Ganapathy et al., 2018). Applications have encompassed the use of deep belief networks (Liu et al., 2014) and autoencoders (Hu et al., 2016; Rajan and Thiagarajan, 2018) for early Alzheimer's onset prediction. Long short-term memory (LSTM) cells using multi-channel fusion have been used to make medical prediction models in diverse healthcare scenarios such as blood glucose level prediction (Rabby et al., 2021) and medical event prediction (Liu et al., 2022). Similarly, gated recurrent units have been applied to predict heart failure (Choi et al., 2017).

While RNNs introduce an element of time into latent space representation, they struggle to perform on long time series with limited channels and have not been commonly utilised for time-series classification tasks (Ismail Fawaz et al., 2019). Capturing the transformation of the physiological state from one slice of time to another is valuable when developing protocols, practising prevention, and patient monitoring (Wang et al.,

2021; Miotto et al., 2018; Ganapathy et al., 2018).

Characterising and classifying SCI subject rehabilitation recovery, activity tracking, and compliance are critical variables for clinicians to properly regime and develop protocols for the patient's success (Bonato, 2010; Cao et al., 2020; Burns and Adeli, 2017; Brogioli et al., 2017). Moreover, they are necessary to understand the dose-response of therapeutic interventions and inform of the safety and efficacy of such interventions. The question then arises: If traditional methodologies to track pathological gait and standing events struggle to perform, how do deep learning methods compare?

5.2 Background

In this study, I aim to perform discriminative classification on stochastic multi-label EMG data, detailed in chapters 3 and 4. I compare multiple deep-learning methodologies and analyse the performance of convolutional and vision transformer models. This section contains previous deep-learning EMG classification methods in pathological and healthy locomotion detection.

5.2.1 Deep Learning for EMG Classification

Multilayered ANNs using features extracted from multivariate EMG signals have previously shown promise for classifying overground locomotion for uninjured populations (Morbidoni et al., 2019; Huang et al., 2009; Negi et al., 2020). Recently the work has been extended to intra- and inter-subject gait phase prediction in cerebral palsy hemiplegic children (Morbidoni et al., 2021). However, improvements to the representational power of ANNs have been made possible by way of CNNs (Ismail Fawaz et al., 2019).

Multilayered CNN1D approaches have been used to represent IMU kinematic information in sliding window segmentation for locomotion classification towards exoskeleton and robotic prostheses (Lu et al., 2020; Kim et al., 2021). Similar approaches to feature

extraction were applied in large CNN models, namely AlexNet and VGG16, to sample sEMG data, transform a window of data into a 2D representation with short-time Fourier Transform (STFT) or continuous wavelet transforms (CWT) before downsampling the data (Demir et al., 2019; Krizhevsky et al., 2012; Simonyan and Zisserman, 2015). These approaches were also studied in upper-limb gesture detection (Duan et al., 2019; Ozdemir et al., 2022; Huang and Chen, 2019; Savithri et al., 2021; Shanmuganathan et al., 2020; Nahid et al., 2020; Rahimian et al., 2020; Côté-Allard et al., 2019). Such strategies aimed to take advantage of pre-trained ImageNet weights for more generalised feature extaction. This is an interesting approach considering EMG spectrogram information should look very dissimilar to typical content within the ImageNet database but results showcase the latent representational power held within deep learning networks (Deng et al., 2009).

As far as I am aware, there have yet to be deep-learning studies on the classification of spinal cord injured pathological gait. While my data set does not incorporate human activity, I develop the first case towards locomotion classification in SCI pathological gait.

5.2.2 Advancements in Deep Learning

I will discuss several critical advancements in deep learning time-series classification relevant to the stochastic nature of the data set at hand. These will include transformers, vision transformers, and domain adaptation.

From several CNN architectures, residual networks have ranked as a top performer across multivariate time-series datasets (Ismail Fawaz et al., 2019). With this information in mind, I briefly summarise the development of Residual, Inception, and Xception models (He et al., 2015; Szegedy et al., 2016; Chollet, 2017). Residual Networks (ResNet) apply skip connections to avoid degradation of information as more layers are added into a

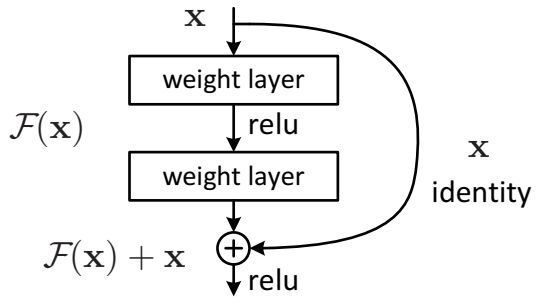

Figure 5.2: Illustration of a skip connection of residual CNN, from the original paper (He et al., 2015). These connections aim to reduce the effects of vanishing gradients.

neural network, also known as the vanishing gradient problem fig. 5.2. This enables extensive learning towards more generalised latent representations for deep learning classification.

Inception was suggested to avoid representational bottlenecks and allow high dimensionality without increasing computational expense (Szegedy et al., 2016). The design introduces using multiple filter sizes, rather than a single size, in a single block, which were then concatenated and passed to the next layer. Thus, capturing various local information. Finally, the Xception model builds upon the foundations of CNN, ResNet, and Inception by replacing all convolutional layers with depthwise separable convolutional layers (Chollet, 2017). These layers map cross-channel correlations and perform spatial convolutions within a singular channel, entirely decoupling the convolutional mapping, as opposed to other CNN architectures that perform cross-channel correlations simultaneously with spatial correlations. This is completed by calculating a 1x1 convolution after performing channel-wise spatial convolutions.

Despite recurrent design, LSTM has had difficulty with long time-series data and maintaining relevance in forecast prediction over discriminative tasks (Zouitni et al., 2023). To summarise, LSTM networks suffer from three main problems: inability to parallelise due to sequential computation, no explicit long- and short-range dependency modelling, and linear positional encoding between information. Transformer networks

were introduced in natural language processing to fill the long-distance representation difficulties with LSTM (Vaswani et al., 2017). The transformer architecture begins by positionally encoding the input sequence using the phase properties of different frequencies in sine and cosine waves. The wavelengths progress from 2π to $10000 \cdot 2\pi$, creating positional embedding as a linear function of PE_{pos}.

$$PE_{(pos,2i)} = \sin(pos/10000^{2i/d_{model}}) \tag{5.1}$$

$$PE_{(pos,2i+1)} = \cos(pos/10000^{2i/d_{model}}) \tag{5.2}$$

The encoded inputs are fed into a stack of layers, each containing cells specified in fig. 5.3. The multi-head self-attention mechanism consists of feeding inputs as values, keys, and queries, each linearly mapped into a scaled dot-product operation. The mathematical function is described below in eq. (5.3) where Q, K, and V are the queries, keys, and values respectively and d_k is a scaling factor. Intuitively, the attention scores compute the similarity between the query and the key applied to the value. One example is the search engine context, where the operator inputs a query to be listed a series of keys. The most relevant of these keys are weighted according to some value. A multi-head attention mechanism can attend to different subspace representations by performing this operation multiple times. Implementing positional encoding allows for positional dependencies across each head. A residual connection is included from the encoder cell to prevent information degradation, mitigating the effects of the vanishing gradient problem (He et al., 2015). The decoder output feeds into a linear projection before applying SoftMax activation.

$$Attention(Q,K,V) = softmax(\frac{QK^T}{\sqrt{d_k}})V \tag{5.3}$$

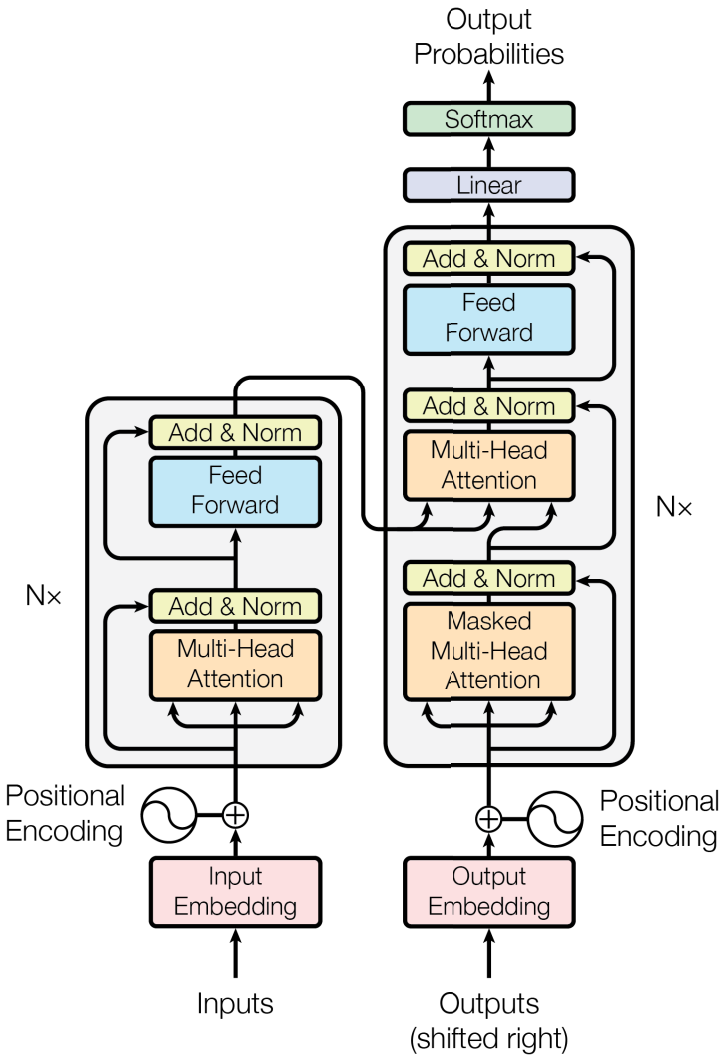

Figure 5.3: The Transformer model architecture, as specified in Vaswani et al. (2017). On the left is the encoder stack, which performs self-attention. On the right is the decoder stack, which performs attention operation on the output of the encoder stack.

Having briefly covered the architectures and underlying principles of deep CNN models and Transformer networks, I now discuss the recent research efforts into vision transformers (Dosovitskiy et al., 2021). This work has since seen many adaptations, including additional depthwise separable convolutional layers between attention layers, performing cross-covariance to operations for cross-channel similarity, and self-supervised semantic segmentation (Wu et al., 2021b; El-Nouby et al., 2021; Caron et al., 2021). The vision transformer model uses the same attention mechanisms as the original

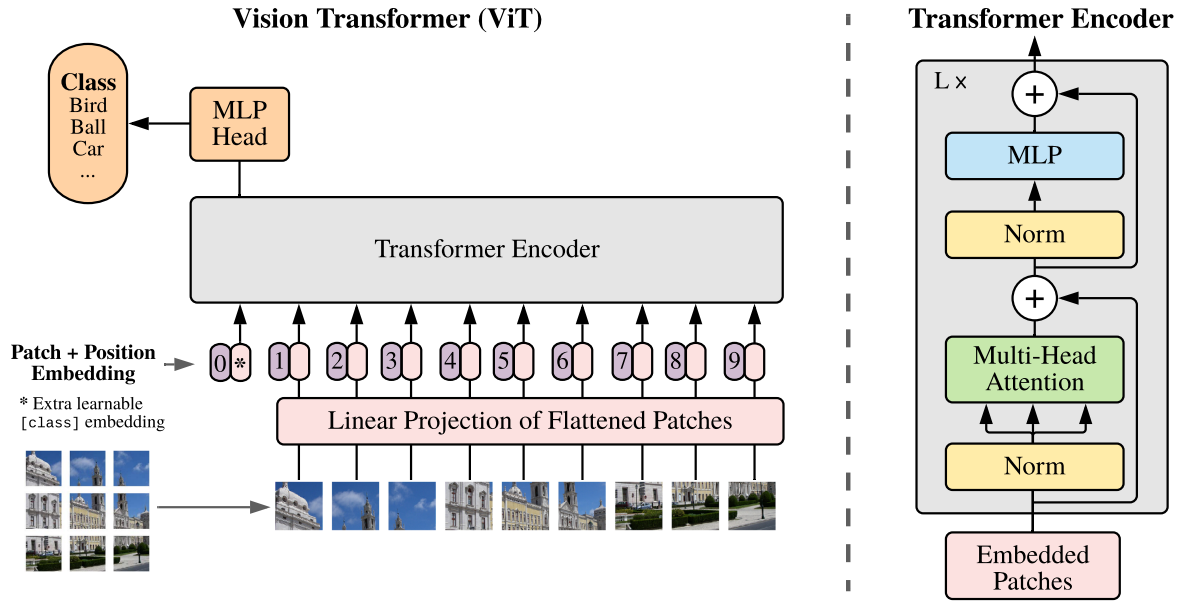

Figure 5.4: The Vision Transformer model architecture as described in Dosovitskiy et al. (2021).

design with slight variations in the implementation. Firstly, the positional embedding is performed by the 'patching' operation, which crops the image into multiple patches before linear projection to the transformer encoder layer. An embedded 'class' token is concatenated at the beginning of the flattened patch sequence. The key difference in the vision transformer encoder is the pre-normalisation step that occurs before the multi-head attention and multilayer perceptron block.

Wu et al. (2021b) combined the ideas from the Xception model to the vision transformer to create the convolutional vision transformer (CvT). The model first removes the need for patch embedding and is replaced with a convolutional layer to form a convolutional patch projection. The intuition behind this was to encode the details of each patch from the embedding stage with overlapping spatial footprints, enabling a deeper representation of complex patterns. The convolutional embedding reoccurs between transformer layers. A depthwise separable convolutional operation is performed on the query, key, and value matrices within each transformer block before completing the attention step. By replacing the linear projection between attention layers, the

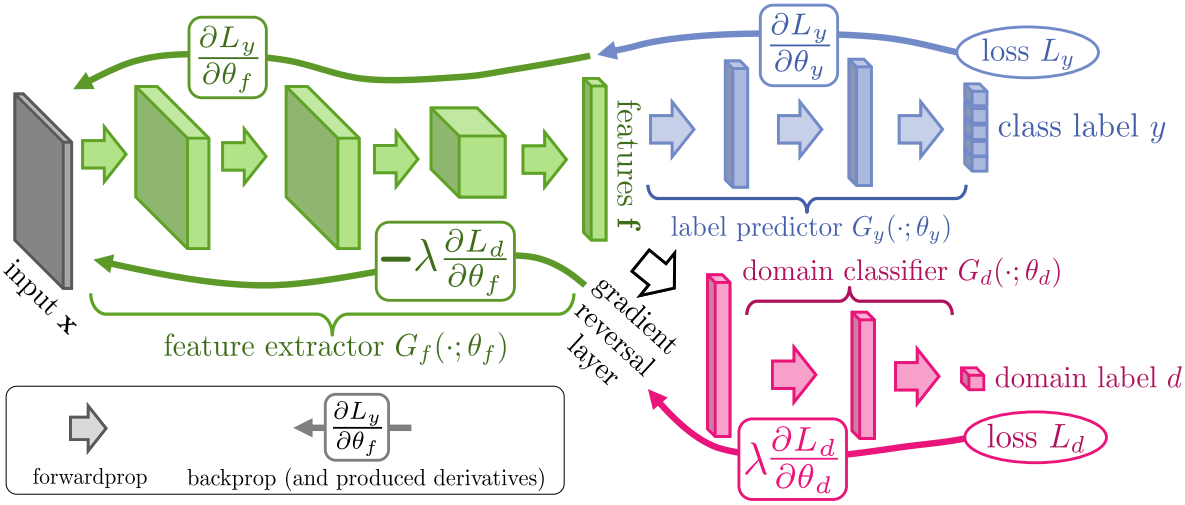

Figure 5.5: Domain adversarial neural network architecture with the goal of 'confusing' the feature extractor sufficiently to learn domain invariant representations of the data set, image from the original paper (Ganin et al., 2016).

authors hypothesised a mapping of local spatial information to higher-order semantic representation. With similar motivations to Wu et al. (2021b), a second approach to depth-wise self-attention was introduced as the cross-covariance image transformer (XCiT) (El-Nouby et al., 2021). XCiT involves computing the self-attention function along the feature dimension by reversing the matrices K and Q in the scaled dot-product operation. Furthermore, the authors suggest l_2 normalising and learnable temperature scaling, τ, to limit the magnitude of query and key matrices to enhance stability during training with a variable number of tokens.

$$\text{XC-}Attention(Q,K,V) = softmax(\frac{K^T Q}{\tau})V \tag{5.4}$$

Finally, domain adaptation was initially suggested to generalise feature representations across various domains (Ganin et al., 2016). The mathematical underpinnings are described in detail in Levi et al. (2021). The basic principle operates on 3 loss functions to converge domain adversarial neural networks towards domain invariant representations

eq. (5.5). Inputs to the classifier consist of the source and target (adversarial) domain fig. 5.5. These are concatenated before passing into the feature extractor network. The feature extractor attaches to a label classifier and a domain classifier. The job of the label classifier is to correctly output the source labels, while the job of the domain classifier is to output the domain of each sample correctly. Applying a gradient reversal process to domain classification samples forces the domain loss to increase while trying to converge onto the source loss eq. (5.5).

Levi et al. (2021) mathematically defined the losses towards domain-invariant adversarial learning (DIAL). I summarise the key components below. Let $G_f(\cdot;\theta_f)$ as the feature network output with parameters θ_f and $G_y(\cdot;\theta_f)$ as label classifier, and $G_d(\cdot;\theta_d)$ as the domain classifier with parameters θ_d. For a given training set $(x_i, y_i)_{i=1}^n$ with adversarial (adv) samples as $(x_i, y_i)_{i=1}^n$ the source (src) loss can be defined as the following:

$$L_{src}^{y} = \frac{1}{n}\sum_{i=1}^{n} CE(G_y(G_f(x_i;\theta_f);\theta_y), y_i)$$
$$L_{adv}^{CE} = \frac{1}{n}\sum_{i=1}^{n} CE(G_y(G_f(x_i';\theta_f);\theta_y), y_i)$$

$$L_{src}^{d} = \frac{1}{n}\sum_{i=1}^{n} CE(G_d(G_f(x_i;\theta_f);\theta_d), d_i)$$
$$L_{adv}^{d} = \frac{1}{n}\sum_{i=1}^{n} CE(G_d(G_f(x_i';\theta_f);\theta_d), d_i),$$

$$DIAL_{CE} = L_{adv}^{y} + \lambda L_{adv}^{CE} - r(L_{src}^{d} + L_{adv}^{d}) \tag{5.5}$$

Note L represents the loss calculation from cross-entropy (CE), per section 3.7.

In eq. (5.5), the r parameter is a hyperparameter used to enforce domain-invariant representation as training progresses, scalably increasing the losses in the domain space. As far as I know, only Côté-Allard et al. (2021) has utilised domain adversarial training to perform EMG classification. The authors prescribed different calibration sessions as domains to train from, reporting more robust classification over multiple days, an area of significant interest for wearable sensing.

In this study, I aim first to investigate convolutional and vision transformer neural network classification performance on sparse EMG channel recordings for ipsilateral locomotion and bilateral standing events in spinally transected rats. Secondly, I report on the effect of domain adaptation between therapies using domain adversarial neural network strategy. By structuring EMG windows as CWT transforms and stacking along the channel dimension, I hypothesise the Xception and CvT models to best perform by capturing cross-channel latent representations. Moreover, I hypothesise that CvT outperforms Xception by the robust encoding of local to global semantic information within a CWT frame.

5.3 Methods

Pre-processing follows similar steps as section 4.2. Bandpass filtering and standard normalisation were repeated with the same values. A CWT with Generalised Morse Wavelet (GMW) was performed to transform the multichannel signal into a 3D representation fig. 5.6. The first dimension contained the number of scales, the second-dimension time, and the third dimension contained each channel. To hasten the processing speed, I used the package 'ssqueezepy', reducing computational processing 10-fold (Muradeli, 2020). Further optimisations included pre-calculating the scales used to feed into CWT by log-piecewise scaling and batch multiprocessing filtered multichannel data. Batched window labelling was calculated by taking the median of each label. Performing CWT increases

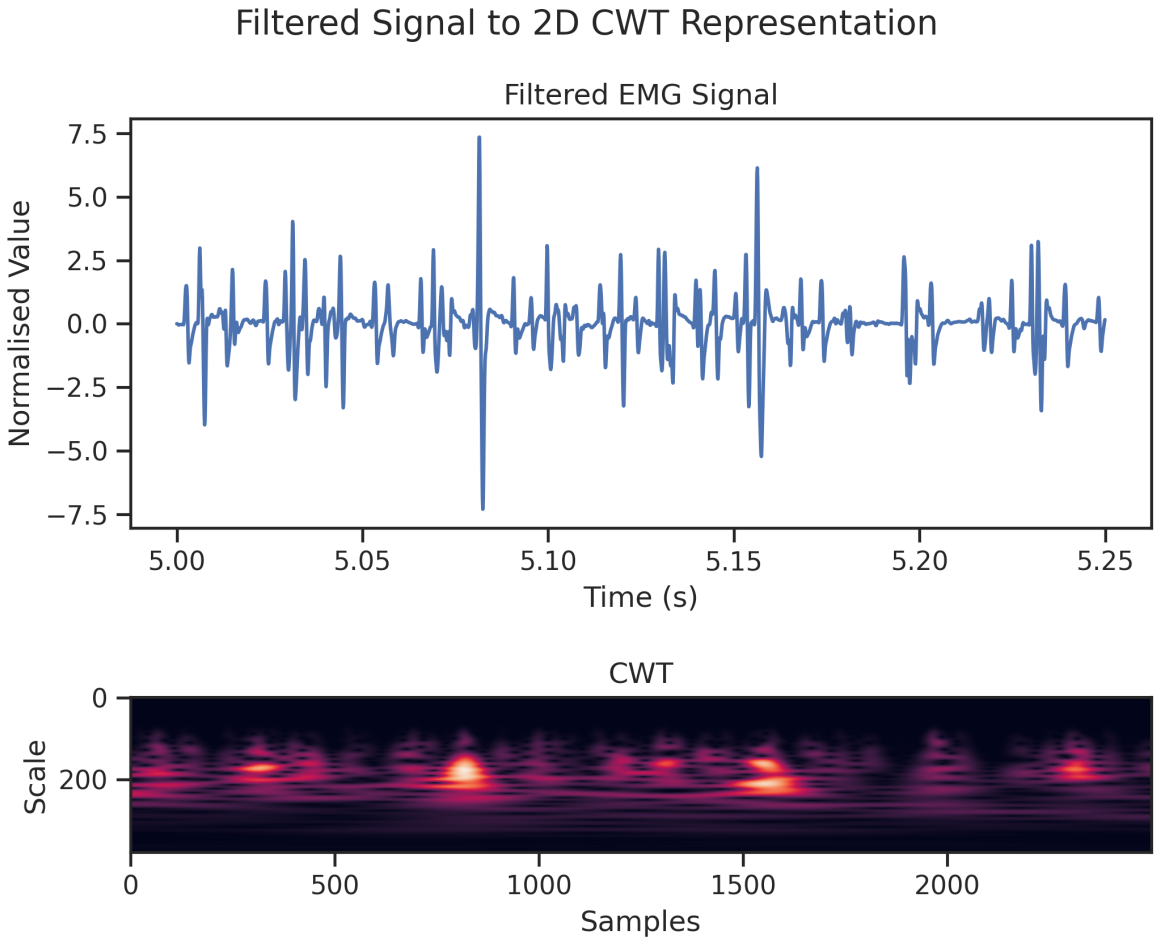

Figure 5.6: Bandpass and standard normalised EMG channel signals were continuous wavelet transformed with GMW and stacked along the 'feature' or 'channel' axis.

the data set by a factor equal to the number of scales calculated for the transform. The number of scales varied according to the window size but averaged close to 250. To reduce memory constraints, deterministic pre-processing output encoded files of size 200MB into non-volatile memory. An input buffer decoded the files before batching, shuffling, and pre-fetching, improving computational speeds and reducing training time. A shuffle buffer size of 100 batches was filled and reshuffled each iteration to enhance stability during training.

A hybrid CNN2D-BiLSTM model defined in table 5.1 was developed with stateful

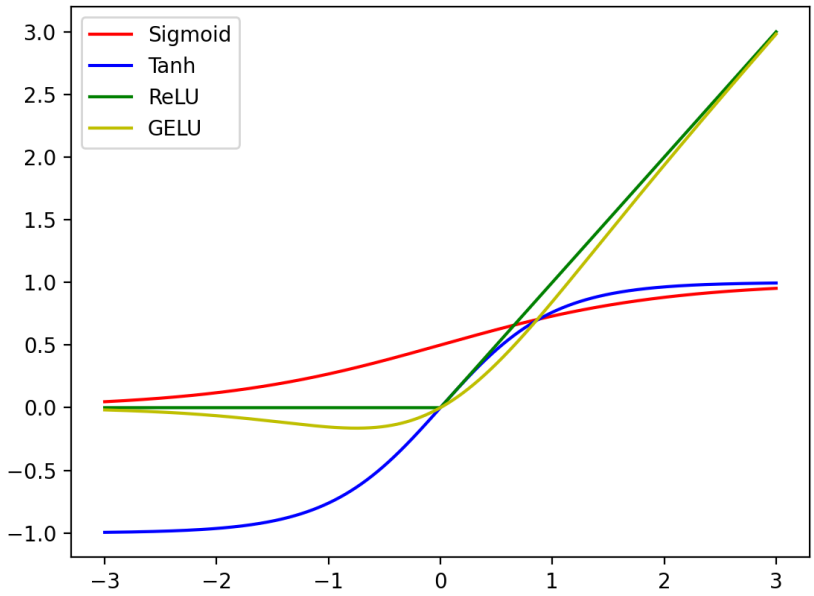

Figure 5.7: Illustration of different activation functions used in this study. Image from Qi et al. (2023).

BiLSTM cells, each returning full sequences before being concatenated for dense multi-layer perceptron (MLP) processing. BiLSTM units were initialised with tanh activation and recurrent sigmoid activation, meeting requirements for cuDNN implementation, see fig. 5.7. This study did not modify the CNN-only networks from the original works (He et al., 2015; Szegedy et al., 2016; Chollet, 2017). Vision transformers will follow the same naming convention as the original works. The ViT, XCiT, and CvT models will be used to test against the hypothesis (Dosovitskiy et al., 2021; El-Nouby et al., 2021; Wu et al., 2021b). Model architectures each are summarised in tables 5.2 to 5.4. For image representations of the mechanisms behind each model, see figs. 5.4, 5.8 and 5.9. CvT models were trained with and without the class (CLS) token. Only the results without the CLS token are outlined below. CNN models were trained with a batch size of 12, and ViT models were trained with a batch size of 8.

Source and target domains for DIAL were split by inclusion and exclusion of quipazine

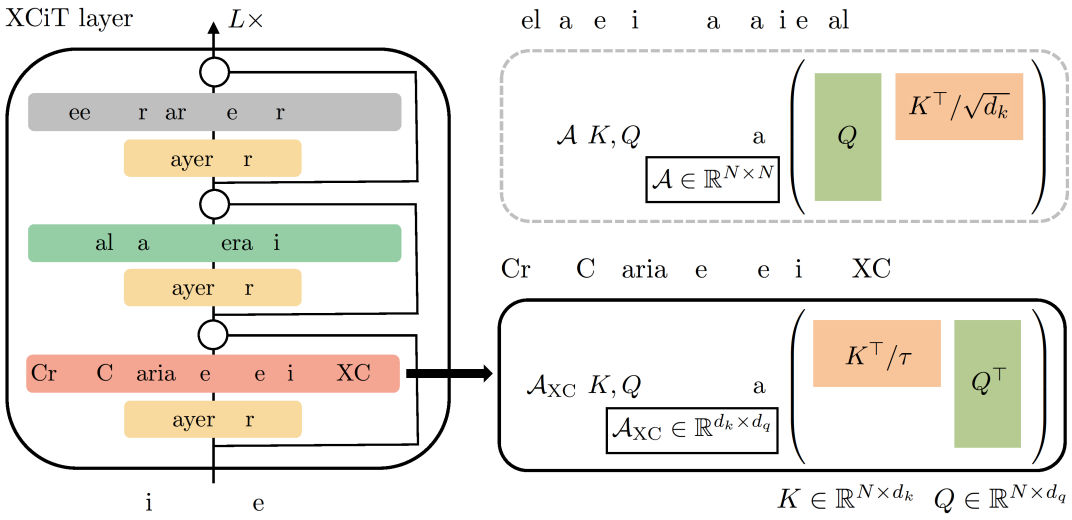

Figure 5.8: Illustration of the adapted vision transformer layer, scaled dot-product operations are now performed across each channel. Image from El-Nouby et al. (2021).

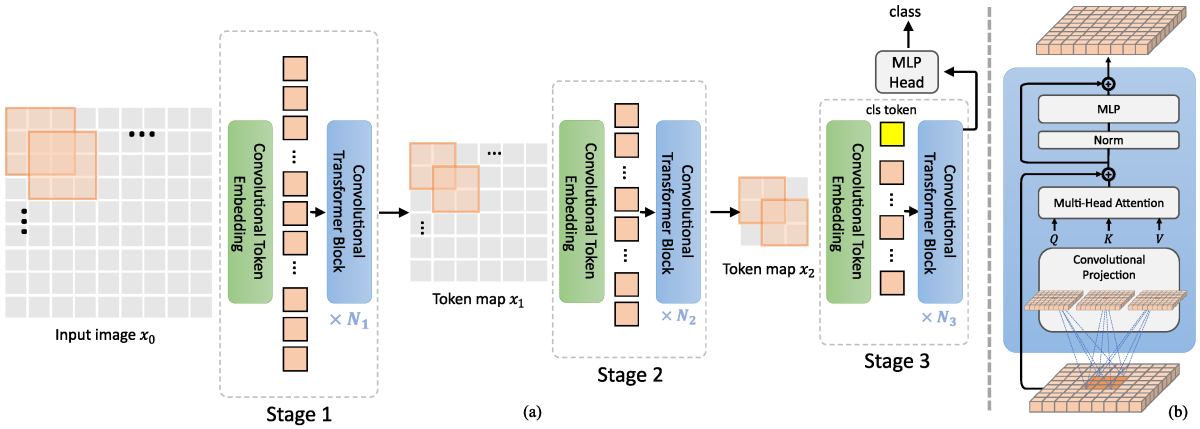

Figure 5.9: Illustration of the CvT network. Note the convolutional embeddings between transformer layers, and depthwise separable mapping of Q, K, and V matrices, prior to scaled dot-product operations are now performed across each channel. Image from Wu et al. (2021b).

Table 5.1: Hybrid 3-layer CNN2D-BiLSTM model. The notation follows as batch size, height, width, and variable dimension 'd'. 'fc' stands for fully connected.

Layer Name	CNN2D-BiLSTM
conv_1	2×2, 32, stride 1
batch normalisation	
maxpooling 2d	5×5, stride 1
dropout	0.4
reshape	b h w d → b h (w d)
bilstm	32-d, tanh
dropout	0.4
flatten	b h (w d) → b (h w d)
dense	32-d fc, relu
dense	3-d fc, sigmoid

in the applied therapies. This was informed by the frequency-dependent change in neuromuscular expression upon introducing the serotonin agonist to spinally transected rodents during locomotion training on a weight-supported treadmill (Gad et al., 2015). The same preprocessing steps to prepare CWT input data were applied to the source (with quipazine) and target (without quipazine) domains. Brief experimentation with matching source and target domain labels to develop a representational bridge between domains found no difference in evaluation results. Thus, both source and target domain labels were shuffled independently.

The feature-extracting model was selected based on the performance of the tested CNNs, choosing the model with the lowest loss. Preparing the model for DIAL involved building the feature extractor and truncating the classifying layer. For ResNet, Inception, and Xception models, this meant including the top input layer until the last global average pooling stage but excluding the penultimate fully-connected classifying layer

Table 5.2: ViT architecture with linear projections and GeLu activation in the final MLP output layer (Dosovitskiy et al., 2021).

Layer Name	ViT
linear projection	1024
embedding dropout	0.1
number of heads	16
layer depth	6
transformer dropout	0.1
mlp output dimension	2048

Table 5.3: XCiT architecture with convolutional patch projections and fourier positional encoding. GeLu activation was applied in the MLP and convolutional patch projection layers (El-Nouby et al., 2021).

Layer Name	XCiT
convolutional embedding dimension	768
embedding dropout	0.0
number of heads	12
transformer layer depth	12
class attention layer depth	2
transformer dropout	0.0
mlp output dimension	3072

(He et al., 2015; Szegedy et al., 2016; Chollet, 2017). In the case of the custom hybrid model, the final sigmoid activated fully connected layer would be excluded table 5.1.

The final pooling layer of the feature extractor, before the output layer, was connected to an MLP label classifier and a gradient-reversed MLP domain classifier with scaling function ‘r’ fig. 5.5 and eq. (5.5). The label classifier was a 128-d, ReLu-activated MLP,

Table 5.4: CvT architecture with convolutional overlap embedding (Wu et al., 2021b). Each attention block maps query, key, and values with depthwise separable convolutions before attending with scaled dot-product operations. GeLu activations were applied in MLP output layer.

Layer Name	CvT
cvt_1	embed: 7×7, 64, stride 4 Q: 3×3, 64, stride 1 K, V: 3×3, 64, stride 2 heads: 1 depth: 1 mlp multiplier: 4
cvt_2	embed: 3×3, 192, stride 2 Q: 3×3, 192, stride 1 K, V: 3×3, 192, stride 2 heads: 3 depth: 2 mlp multiplier: 4
cvt_3	embed: 3×3, 384, stride 2 Q: 3×3, 384, stride 1 K, V: 3×3, 384, stride 2 heads: 6 depth: 10 mlp multiplier: 4

connected to the final output sigmoid-activated layer with 3 classes. The domain classifier was a 64-d to 32-d, ReLu activated MLP with a 0.5 dropout layer, see table 5.5. This now fully describes the domain adversarial neural network (DANN). Class weights for the adversarial, or target, domain were set to 0. The scaling factor, 'r', was kept as 1. Training the DANN followed the same steps as the other models but with a split source and target domain data set preparation. All hyperparameters were set per table 5.6.

After training the DANN with source and target domain samples and reaching 20 epochs, the label classifier section of the model was re-compiled without the domain adversarial, gradient-reversal layers. The feature extractor model layers were 'frozen',

Table 5.5: Summary of the domain adversarial neural network (DANN), built on top of the feature extractor network. Feature representations from the extractor are global average pooled before passing into label and domain dense layers.

Layer Name	DANN
feature extractor	
label dense 1	128-d fc, relu
label dense output	3-d fc, sigmoid
domain dense 1	64-d fc, relu
domain dense 2	32-d fc, relu
dropout	0.5
domain dense output	3-d fc, sigmoid

Table 5.6: List of the hyperparameter specifications used for training and testing of each deep learning network. The Adam optimiser is defined in Kingma and Ba (2017). All vision transformers downsampled to the specified size. Only ViT used a 50x50 patch size. The remaining vision transformer models performed convolutional patch embedding.

Hyperparameter	Value
learning rate	1×10^{-7}
loss	Multiclass Binary Cross Entropy
optimiser	Adam
CNN downsample	(scale size/2, window size/2)
ViT downsample	(150, 1500)
ViT patch size	(50, 50)

meaning all trainable variables became fixed. Finally, fine-tuned with supervised learning over the entire source and target data set was completed using the hyperparameter settings in table 5.6.

Tensorflow v2.12.0 framework was used to train all deep learning models (Wagner and

Smith, 2008). Training, validation, and testing data were split with 60%/20%/20% ratios. All deep learning models used the Adam optimiser, with a learning rate of 1×10^{-7}, and a sigmoid activation dense output unit, see table 5.6 for full hyperparameter specifications. Deep learning models were trained using NVIDIA Quadro RTX 6000 Passive graphics cards for minimally 20 epochs. A post-analysis of the training history was completed to ascertain if the model should undergo further training in iterations of 10 epochs. All code was written on Python 3.8 (Van Rossum and Drake, 2009).

To determine the effect of window size and window shift, a hybrid CNN2D-BiLSTM network was trained up to 20 epochs across 0.1 – 0.8ms window sizes and proportional window shifting between 25 – 100%. The learning rate was set to 1×10^{-6} and a batch size of 2. The minimum validation loss sampled from all epochs was used to determine the effect of window sizing and shifting on classification results.

The below metrics were recorded during the training and validation procedure for all models. The multiclass binary cross entropy was set as the loss variable to minimise. Precision, recall, and area-under-curve (AUC) were also recorded. The AUC is the interpolated area of the true positive rate, eq. (3.5), against the false positive rate.

$$\text{False Positive Rate} = \frac{\text{False Positive}}{\text{False Postive} + \text{True Negative}} \tag{5.6}$$

To find the representative accuracy of the tested algorithms, a series of set time-windowed labels were found by performing the sliding window procedure through the test data label set. The sliding window contained a 3-sec window size and 25% overlap. All windows that did not have any event activity were rejected. This process determines the accuracy within a time window, focusing on assessing the performance of our classifier during specific temporal segments of interest.

All train, validation, test data sets, and analysis methods followed the same structure

as specified in section 4.2.

5.4 Results

The window size and stride study are displayed in fig. 5.10. The figure suggests no relationship between the performance of our hybrid CNN2D-BiLSTM model and window size or shift. A Tukey's honest significance test confirmed these results and returned no significance in any pairs ($p > 0.1$). Fixing the analysis to only a single window size of 0.2s with varying window shift produced lower validation loss with higher percentage of overlapping samples with no difference for fig. 5.11. Using 50% overlap recorded no difference in yielding lower validation loss across window sizes. To reduce computational load a window size of 0.25s and sliding overlap of 75% was used to perform CWT and deep learning classification.

Evaluation across the entire data set using macro calculated metrics is shown in table 5.7. Analysing F1 scores, the top-2 models were made of Xception and ResNet50. ResNet101, DANN, ViT, and CvT placed third in the F1-score evaluation. ViT recorded the highest precision, followed by Xception, then ResNet50. The CNN2D-BiLSTM hybrid model reported the highest recall, followed by Xception and ResNet50. The highest-performing model was the Xception deep learning network from these metrics.

Using Xception as a feature extraction network, the DANN model was trained with the parameters specified in table 5.5. DANN model results are reported along the bottom row in table 5.7. No improvement was observed in the recall values, although precision was reduced by 0.11.

All models reported an improvement in macro evaluation metrics by separating the test data set into periods of 3-sec windows and rejecting any window without labelled event activity. Notably, the F1 scores of CNN2D-BiLSTM and Inception model improved by 0.16 and 0.15, respectively. The third largest gain of 0.1 was seen by ViT and DANN

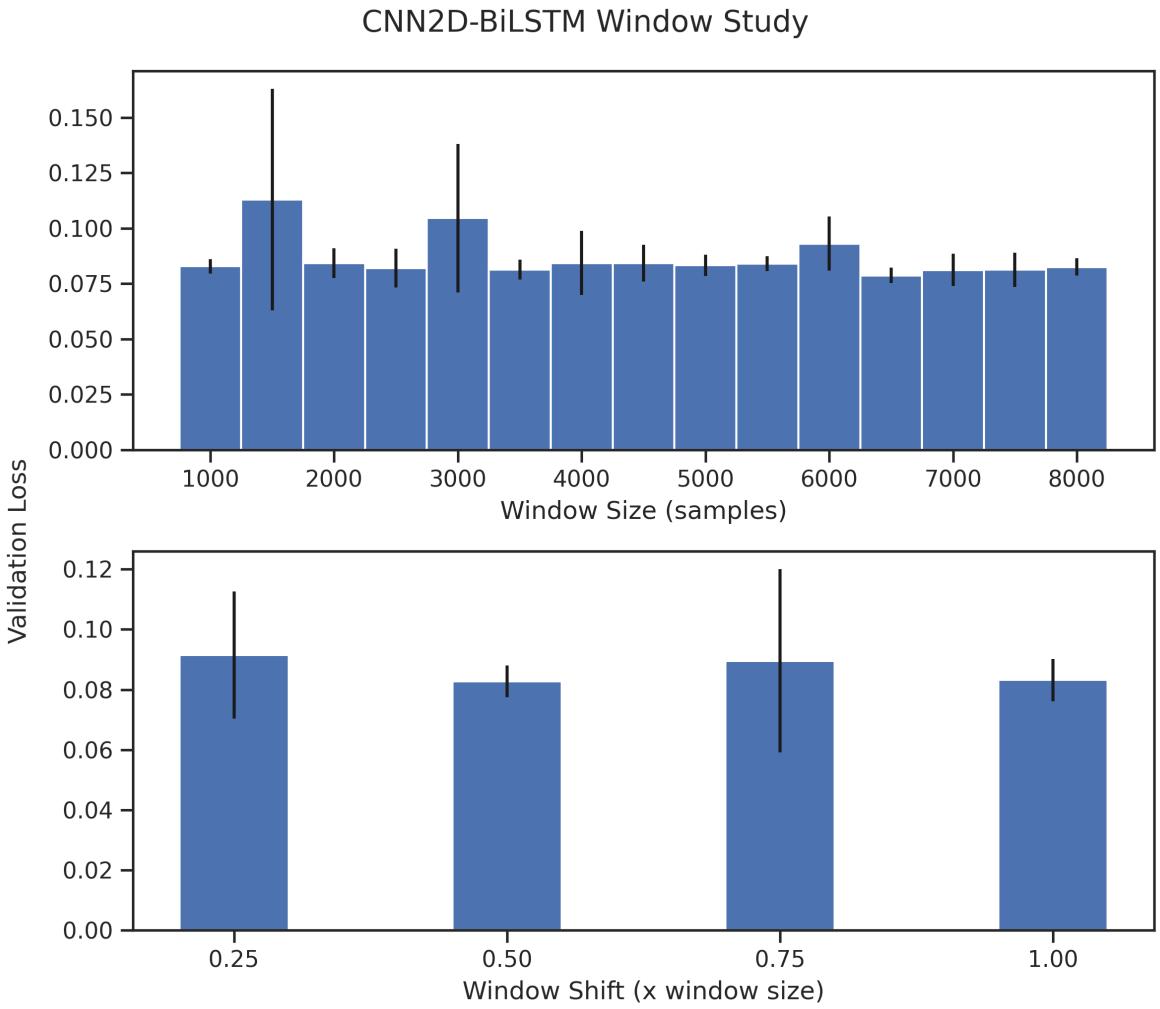

Figure 5.10: Sliding window size and shift results from the CNN2D-BiLSTM training experiment. There are no significant differences in validation losses across any parameter.

models; see table 5.8. Xception and ResNet50 consistently ranked high in their full and time-windowed data sets evaluation scores. ViT and CvT were evaluated equally on F1 scores but differed in precision and recall metrics across full and time-windowed data sets. The two highest-performing models were the Xception and ResNet50. The Xception model more accurately detected left stepping and standing activity over ResNet50 see figs. 5.12 and 5.13.

Between the vision transformer models, ViT and CvT resulted in correctly classifying stepping and standing events. ViT more reliably detected stepping activity over standing

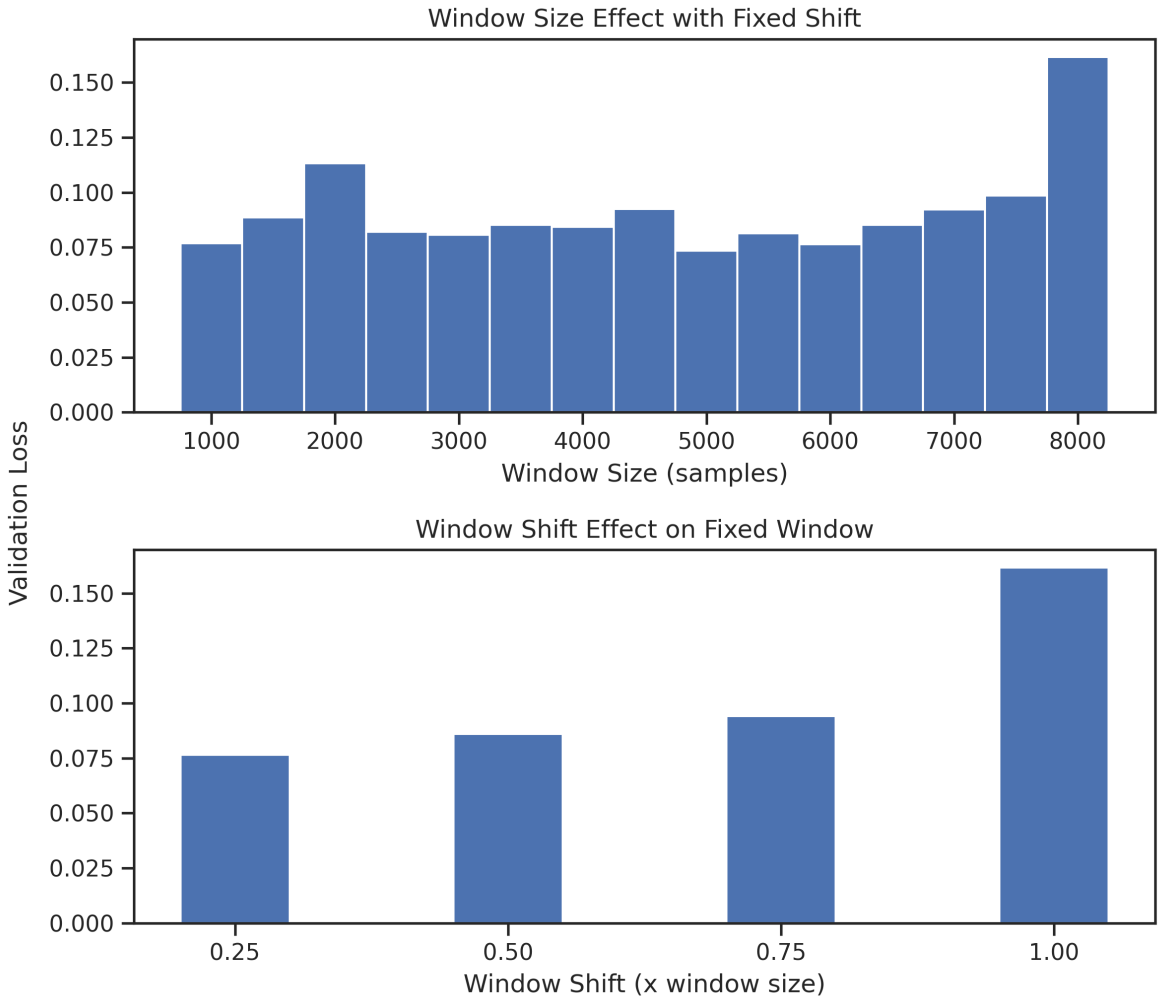

Figure 5.11: Sliding window size and shift results from the CNN2D-BiLSTM training experiment. Window shift analysis was performed with a fixed window size of 2000. Window size analysis was performed with fixed window shift of 0.5×window size.

activity, while CvT reported the opposite figs. 5.14 and 5.15. More specifically, ViT rejected false positives in left and right stepping and detected left stepping true positives more so than CvT. However, CvT had a higher rate of correctly labelling right stepping and standing true positives.

Comparing ViT with Xception, left step detection scores were near equal, with Xception improving over ViT in the recall metric by 0.02. ViT rejected false positives more accurately during right-step labelling, although the Xception model detected more true

Table 5.7: Macro evaluation of deep learning models using the entire test data set.

Model	Precision	Recall	F1-score
CNN2D-BiLSTM	0.40	0.84	0.52
ResNet50	0.55	0.81	0.65
ResNet101	0.50	0.72	0.59
ResNet152	0.45	0.70	0.54
Inception	0.43	0.67	0.50
Xception	0.57	0.83	0.66
ViT	0.61	0.65	0.59
CvT	0.51	0.75	0.59
XCiT	0.47	0.40	0.39
Xception-DANN	0.46	0.83	0.56

Table 5.8: Macro evaluation of deep learning models using only time windowed periods of activity.

Model	Precision	Recall	F1-score
CNN2D-BiLSTM	0.60	0.84	0.68
ResNet50	0.64	0.81	0.71
ResNet101	0.62	0.72	0.66
ResNet152	0.60	0.70	0.63
Inception	0.64	0.67	0.65
Xception	0.67	0.83	0.73
ViT	0.73	0.65	0.65
CvT	0.68	0.75	0.69
XCiT	0.65	0.40	0.46
Xception-DANN	0.59	0.83	0.66

positives. Within these differences, the F1-score reported a higher result for ViT over Xception in the scope of right-step labelling. In contrast, Xception stand event true positive detection was near double that of ViT outputs, see figs. 5.16 to 5.18.

Xception-DANN fine-tuned classification results did not improve over the Xception-only model. Xception-DANN managed to improve left and right step recall but to the detriment of rejecting false positives for all events and recalling stand events fig. 5.19.

Table 5.9: Left stepping evaluation of deep learning models using only time windowed periods of activity.

Model	Precision	Recall	F1-score
CNN2D-BiLSTM	0.47	0.79	0.59
ResNet50	0.54	0.74	0.63
ResNet101	0.54	0.67	0.60
ResNet152	0.53	0.70	0.60
Inception	0.52	0.58	0.55
Xception	0.56	0.81	0.66
ViT	0.58	0.79	0.67
CvT	0.56	0.73	0.63
XCiT	0.54	0.53	0.53
Xception-DANN	0.49	0.88	0.63

Table 5.10: Right stepping evaluation of deep learning models using only time windowed periods of activity.

Model	Precision	Recall	F1-score
CNN2D-BiLSTM	0.46	0.89	0.60
ResNet50	0.58	0.83	0.69
ResNet101	0.56	0.78	0.65
ResNet152	0.54	0.79	0.64
Inception	0.48	0.66	0.55
Xception	0.55	0.88	0.68
ViT	0.70	0.75	0.73
CvT	0.53	0.85	0.65
XCiT	0.57	0.47	0.51
Xception-DANN	0.41	0.92	0.57

5.5 Discussion

This study investigates the performance of deep learning methods towards pathological gait classification of spinally transected rats undergoing different neuromodulatory therapies with sparse EMG channel measurements. I use CWT pre-processing to leverage the image classification successes found in ResNet, Inception, and Xception architectures. I compare these results against emerging vision transformer models, including ViT, XCiT and CvT. Finally, I use DIAL to train a domain-invariant feature extractor before

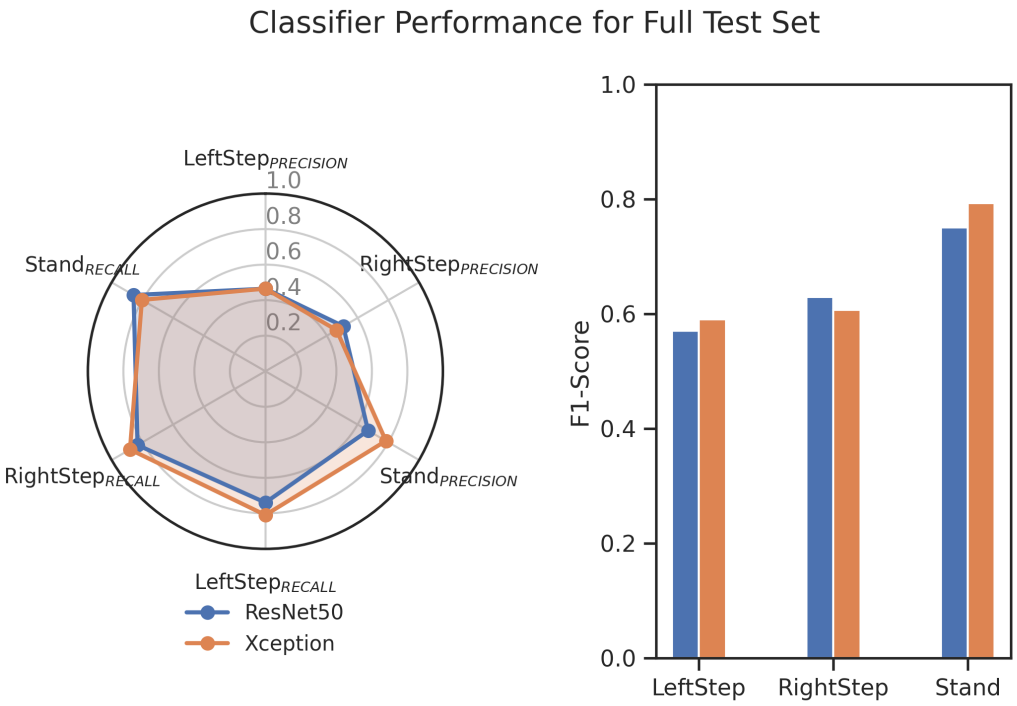

Figure 5.12: A spider and bar graph to illustrate the differences between the performance of convolutional models. The left shows the spider plot of different labels and their precision and recall. The right displays the F1-scores for different labels and models.

fine-tuning it with an MLP classifier. As far as I know, this is the first time SOTA deep learning methods have been performed to classify sparse EMG signals of pathological gait.

All models tested report evaluation metrics greater than those of previous works towards EMG locomotor classification, tested in chapter 4. This was especially highlighted in the time-windowed sampling. Deep learning models improved across the board, whereas all machine learning and digital signal processing methods with handcrafted features saw a drop in evaluation metrics. While XGBoost managed to record an F1-score >0.5 by correctly classifying imbalanced standing events, all tested deep learning models managed to perform >0.5 in stepping alone during time-windowed analysis tables 5.9 and 5.10. Similar results were reflected in other pathological lower limb activity classifications with spectrogram transforms (Issa and Khaled, 2022).

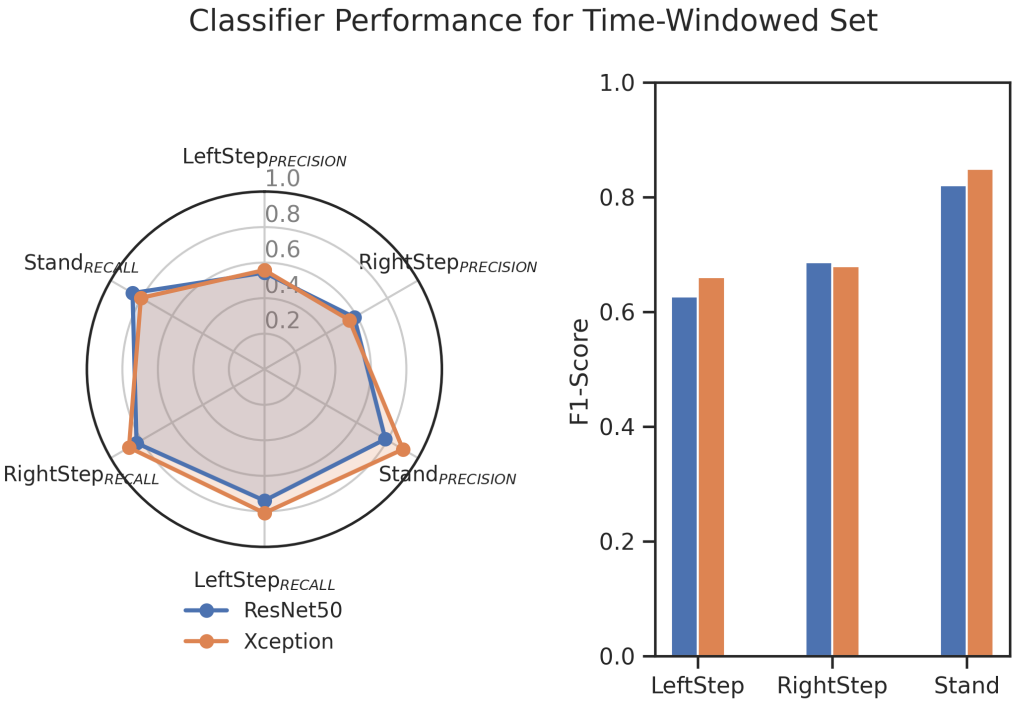

Figure 5.13: A spider and bar graph depicting CNN classifications for time windowed periods of activity.

Xception model networks outperform the other CNN and transformer models, thus rejecting the hypothesis of CvT local to global mapping of depthwise information as the better alternative. This was due to the Xception model's ability to encode depthwise information with local mapping. The arrangement of the input data (embedded EMG channel information across the third dimension) required the models to extract the relationship across each channel in a spatiotemporal fashion.

Given that CvT used depthwise separable convolutions to project inputs to attention operations, one could expect to develop patch-wise local-to-global relationships across channels for each relevant label better. However, CvT did not produce the same stepping classification results as ViT, nor did it predict standing activity and Xception. The CvT model reduced classification accuracy when including the CLS token, resulting in a macro F1-score of 0.52 and 0.62 for the full and time-windowed data set, respectively.

While fig. 5.10 suggests no discernible relationship between window size and shift

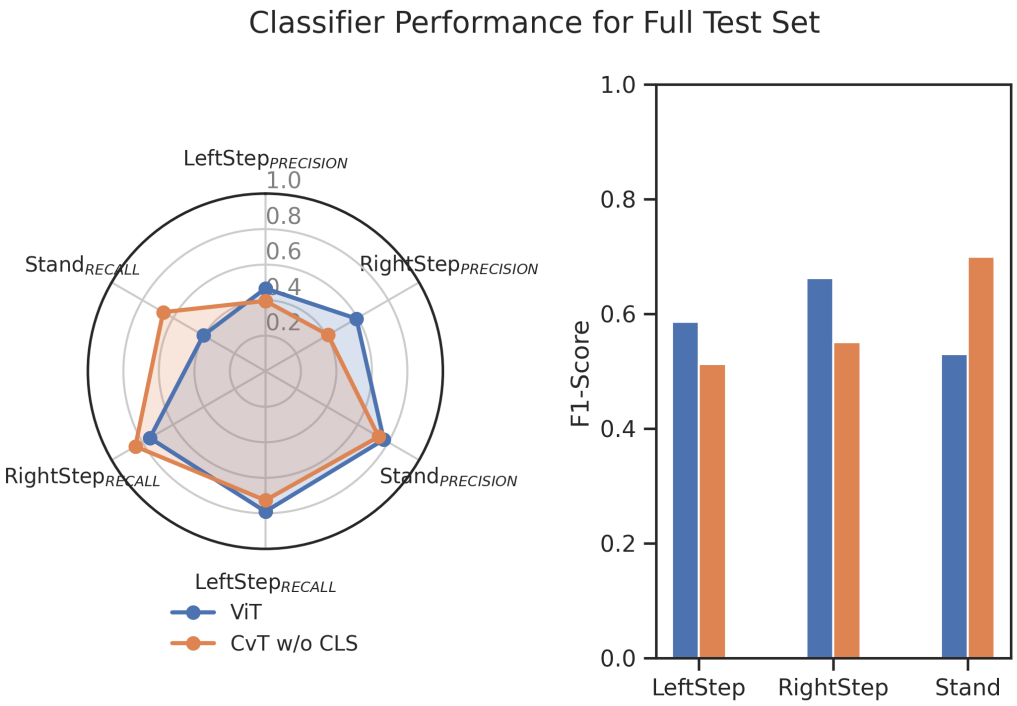

Figure 5.14: A spider and bar graph to illustrate the differences between the performance of vision transformer models. All CvT results were reported without using the class token (CLS).

for CNN models, this may not be true for transformers. Reducing the size of the CvT network and tuning the patch size may provide the appropriate space for CvT to converge better (fig. 5.29). To determine if the window size affected vision transformer outputs, a brief analysis of the effect of window sizing was completed for the ViT model. Repeating the same method described in section 5.3 for window sizes 0.15, 0.25, 0.35, and 0.45-sec showed no discernible difference in validation loss fig. 5.26.

The results from this study suggest that depthwise separable convolutions and feature-based attention operations were insufficient to represent the spatiotemporal dependencies for each channel across stepping and standing. A local depthwise separable mapping was more effective in developing the latent representation of locomotion and standing across EMG channels fig. 5.17. Each EMG channel could be considered a multi-modal information stream to represent more robust cross-channel activity. Heesoo

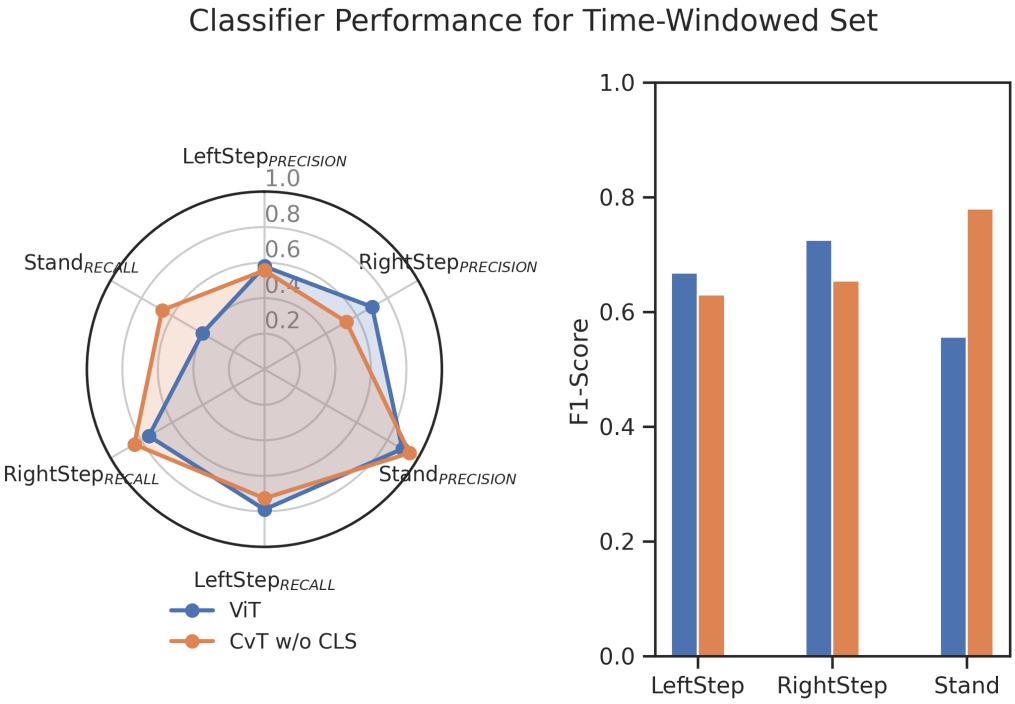

Figure 5.15: A spider and bar graph depicting vision transformer classifications for time windowed periods of activity.

et al. (2022) incorporated transformers for multi-modal biosignal classification by simultaneously completing cross-attention operations over the sensor modality and feature space. Such a strategy could embed stronger cross-channel representation than CvT or XCiT approaches.

XCiT performed least favourably out of all the models. The original paper reported strong depthwise perception for image segmentation, object detection, and image classification (El-Nouby et al., 2021). These results may suggest strong feature representation of relevant information where different heads learn different semantically coherent representations. It seemed intuitive to consider cross-covariance attention, attending over channels, to capture inter-channel relationships. XCiT implements patch interaction with the local patch interaction block, consisting of two depthwise 3x3 convolutional layers with batch normalisation and GeLu activation in between. This step was completed after cross-covariance attention, thus creating local maps. The training plots in fig. 5.30

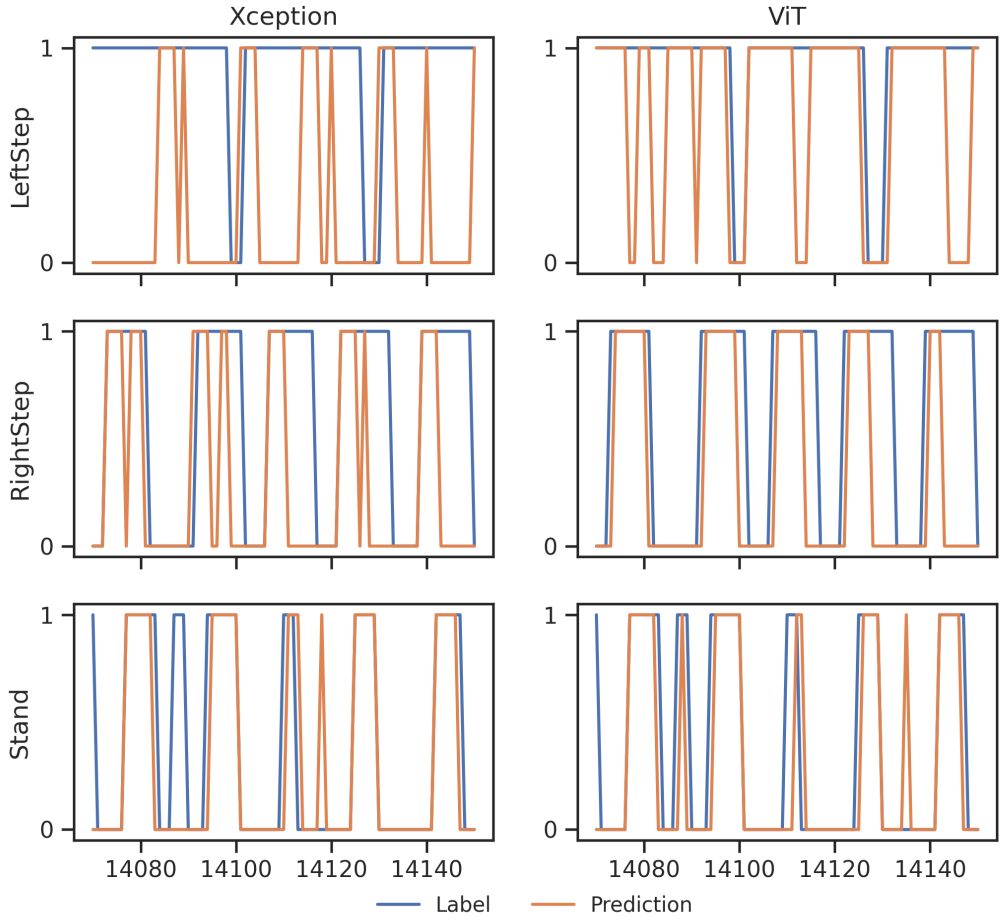

Figure 5.16: Plotted are the predictions after label smoothening and applying a prediction threshold of 0.5. The Xception model better represents the standing activity and struggles to maintain a robust prediction for stepping. ViT manages to perform all operations relatively well in this example. Note the long time-period for LeftStep labelling. This was due to the labelling method of extracting the median from large window sizes. The negative label time-gap between each step was smaller than the window size and label population.

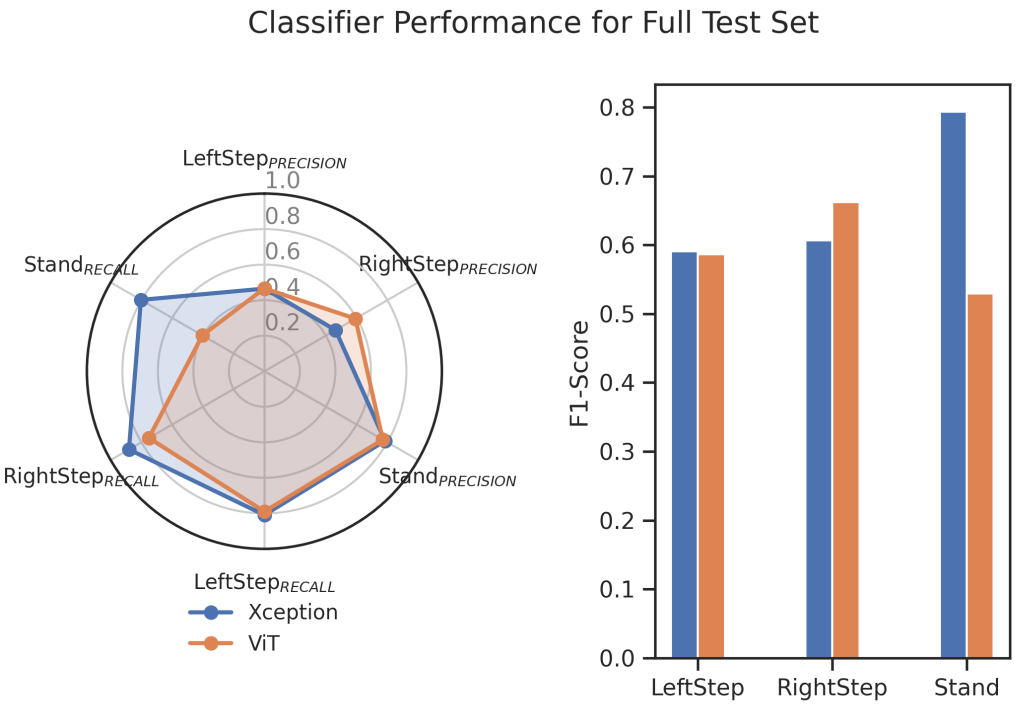

Figure 5.17: A spider and bar graph for more granular comparison of Xception and ViT results.

suggested a substantial degree of overfitting, which may explain most of the difficulty towards classifying event labels, an effect not seen in the ViT model (fig. 5.28). Reducing XCiT model size may help with performance, similar to results shown in ResNet50 – 152, see table 5.8. Thus, EMG CWT representations that fail to capture cross-channel dependencies may require shallower networks to reduce the effects of vanishing gradients. By applying convolutional patch embeddings of size 16x16, the XCiT may have more difficulty in mapping semantic representations compared to the 50x50 ViT patch size, see figs. 5.21 and 5.31.

ViT correctly classified more stepping windows than any other model. This could be due to the linear patch embedding performed earlier, with no convolutional layers or overlapping. This method of patch embedding could have led to more robust step-related spatiotemporal representations of the CWT. To investigate these results, a heatmap of Xception and ViT layers and attention heads are plotted fig. 5.20. The Xception heatmap

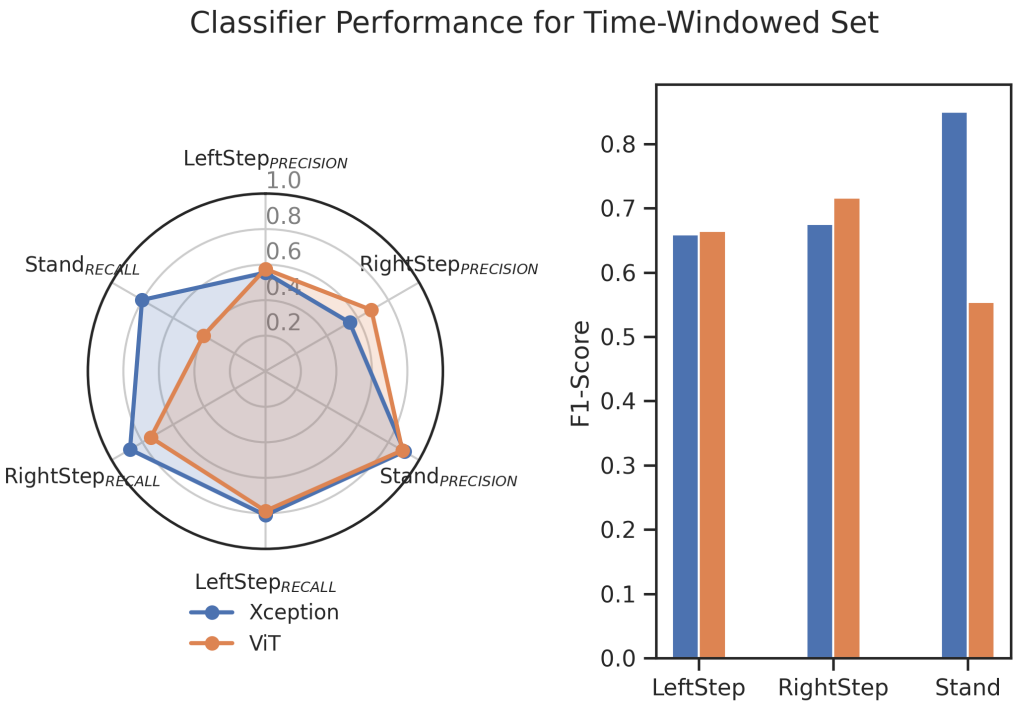

Figure 5.18: A spider and bar graph comparing Xception and ViT classifications for time windowed periods of activity.

showed a distinct activation on the right-hand side section of the CWT image. The RTA had a quiet period, while RSOL had an active, variable period. The area with high activations appears to have bimodal peaks, activating for both the oscillatory bursts between the TA and SOL, but only if there was adequate activity in the SOL, as no other areas showed activations. The Xception model has a robust discriminative effect on variability in the soleus. Thus, the Xception model represents the magnitude and coordination of the EMG signal within feature-stacked CWT.

Comparably, ViT heads each learnt different semantic representations of the 3D input fig. 5.21. Similar information on the right-hand side of fig. 5.20 can be seen multiple times in different heads fig. 5.21. ViT models encoded latent semantic representations of sparse multi-channel EMG CWT data in a spatiotemporal manner, partially confirming the initial hypothesis. Different maps included different representations for standing and left stepping. An example of standing between the Xception activation and ViT attention

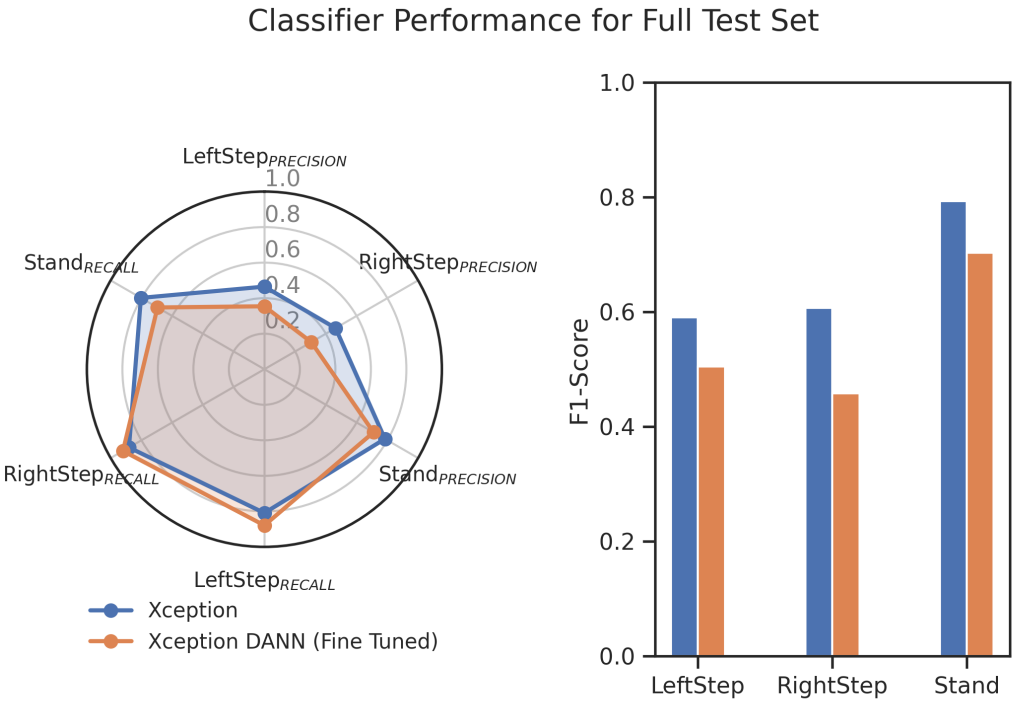

Figure 5.19: A spider and bar graph for more granular comparison of Xception and Xception-DANN results.

heat maps is seen in figs. 5.22 and 5.23. Each attention head displayed different attention weights when comparing standing and stepping attention maps in figs. 5.21 and 5.23. Combined with the results in table 5.7, these plots suggest ViT models could better discriminate between standing and stepping events with attention mechanisms. Further evidence of feature representations can be seen in fig. 5.25.

The Xception model was selected to be trained as a DIAL feature extractor using the DANN model, explained in fig. 5.5 and eq. (5.5). To see a label and domain training history of the domain invariant learning phase between source and target domains, refer to fig. 5.32. While the domain loss initially starts high, the classifier managed to reduce the domain loss despite applying a gradient reversal. This implies poor adversarial mapping between the source and target domains. Similarly, the label classifier had begun to overfit around the 20-epoch mark. This may have been due to the limited number of manually labelled data. By splitting the data into groups with and without quipazine, the model

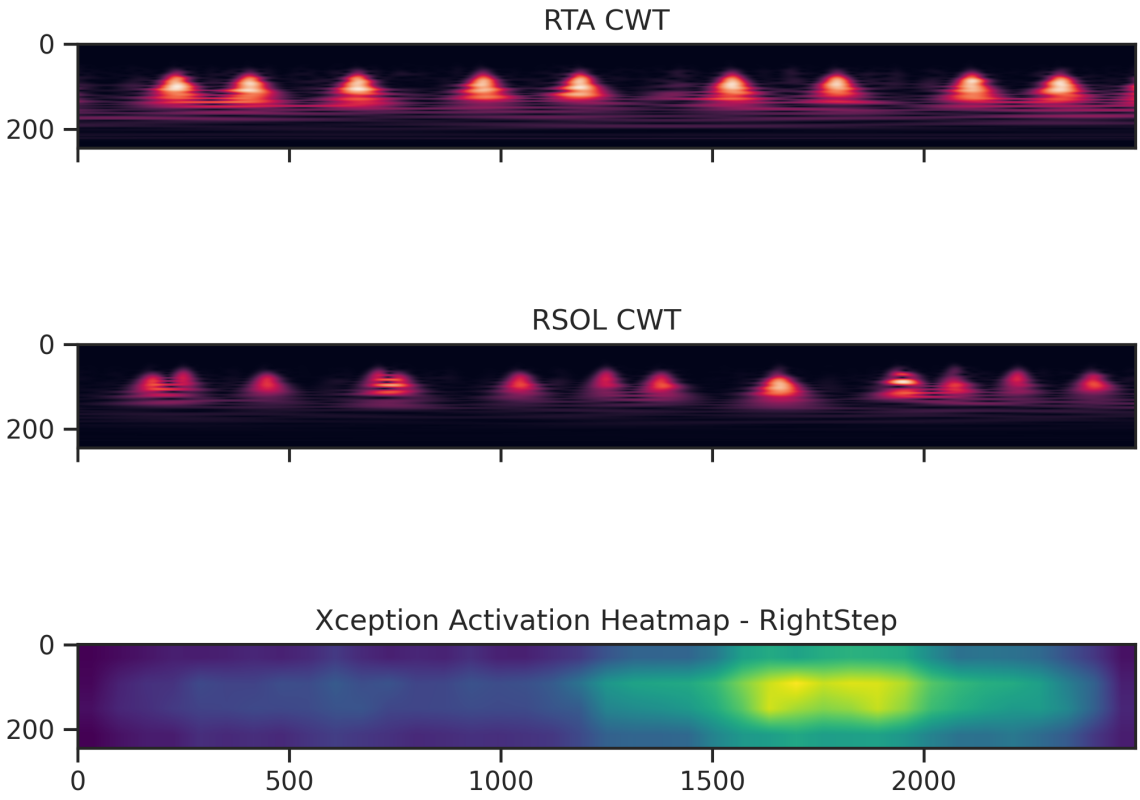

Figure 5.20: Grad-CAM heatmap of Xception activation layers for right step activity (Selvaraju et al., 2019). Note the variations in soleus activity in the bottom right during a quiet period in the tibialis anterior activity.

could become prone to overfitting issues, even with gradient-reversal layers. Attempting to repeat the training process with an 'r' value of 2 trained the feature extractor to register periods of low and high activity, but it did not improve. A straightforward method to overcome this is to initialise with a larger 'r' scale and slowly increase it over time. Another approach may be to split the source and target domain across different subjects, similar to (Côté-Allard et al., 2021).

Research in time-series data analysis has grown towards augmentation techniques (Ismail Fawaz et al., 2019). Incorporating augmentation strategies could introduce to

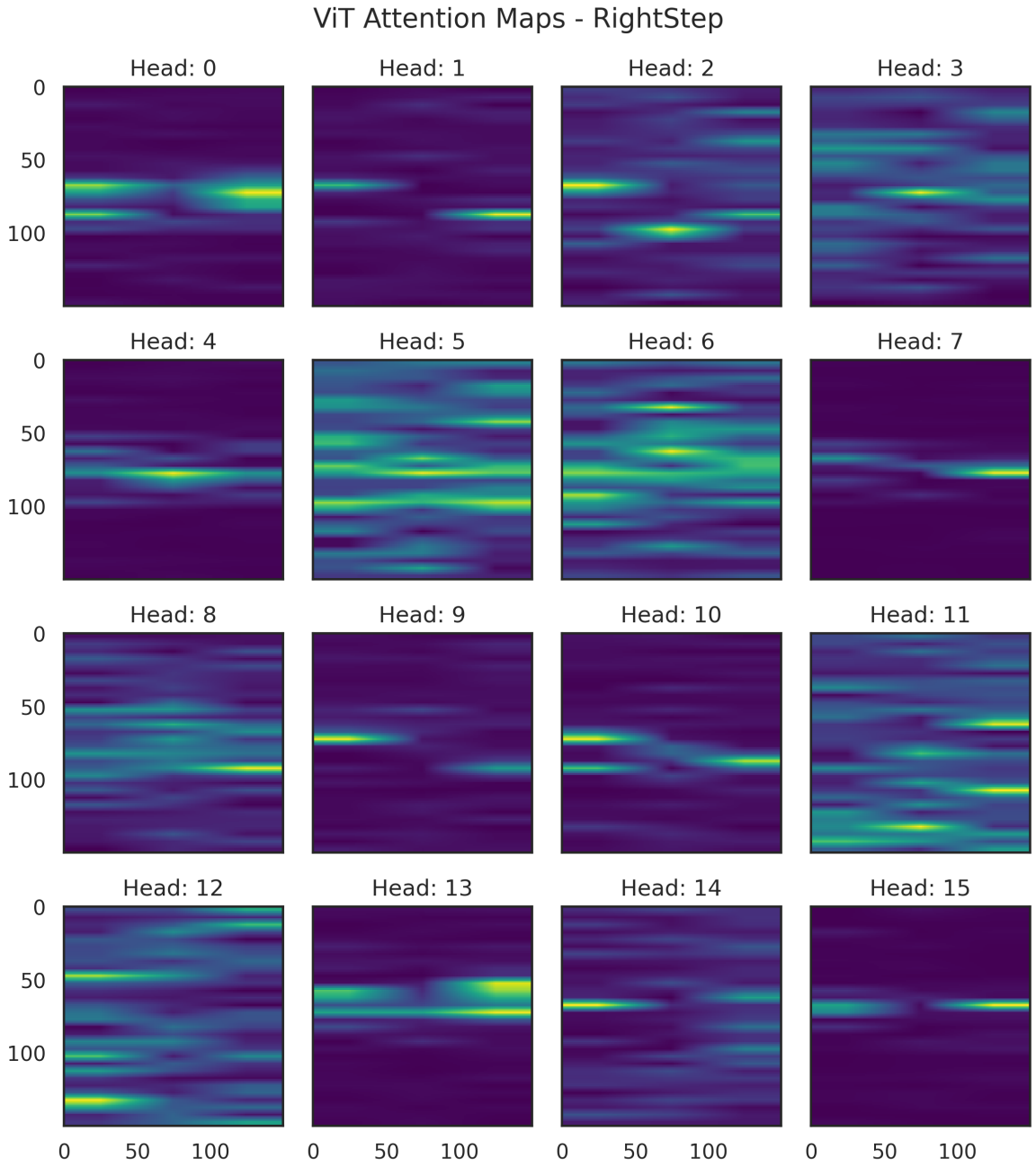

Figure 5.21: Heatmap of ViT attention heads for right step activity. Note the different semantic representations encoded in different heads, spread across the maps. The images have been resized for easier viewing.

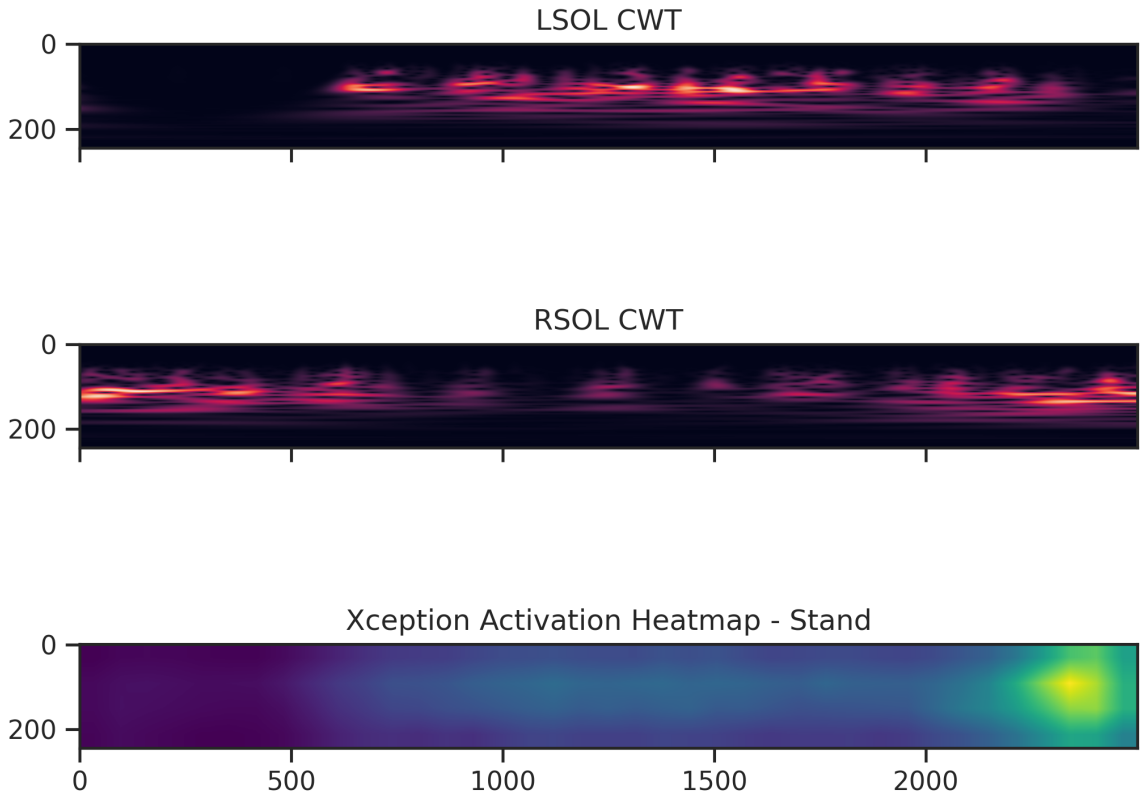

Figure 5.22: Xception activation heatmap of standing event within a window discussed in section 5.5.

better 'confuse' the feature extractor. Developing more robust feature representation and avoiding early collapse. The feature extractor was concatenated to the classifier head, and fine-tuning was performed. This reduced the validation loss much more than the history in the Xception model fig. 5.27. However, the DANN fine-tuned model struggled with rejecting false positives in all events and recall for standing events figs. 5.19 and 5.36. Intuitively, the Xception-DANN model became better at predicting true positive stepping events, likely because of heightened step label sensitivity, evidenced by the decrease in bilateral step precision. The adversarial training process seemed to have encoded new

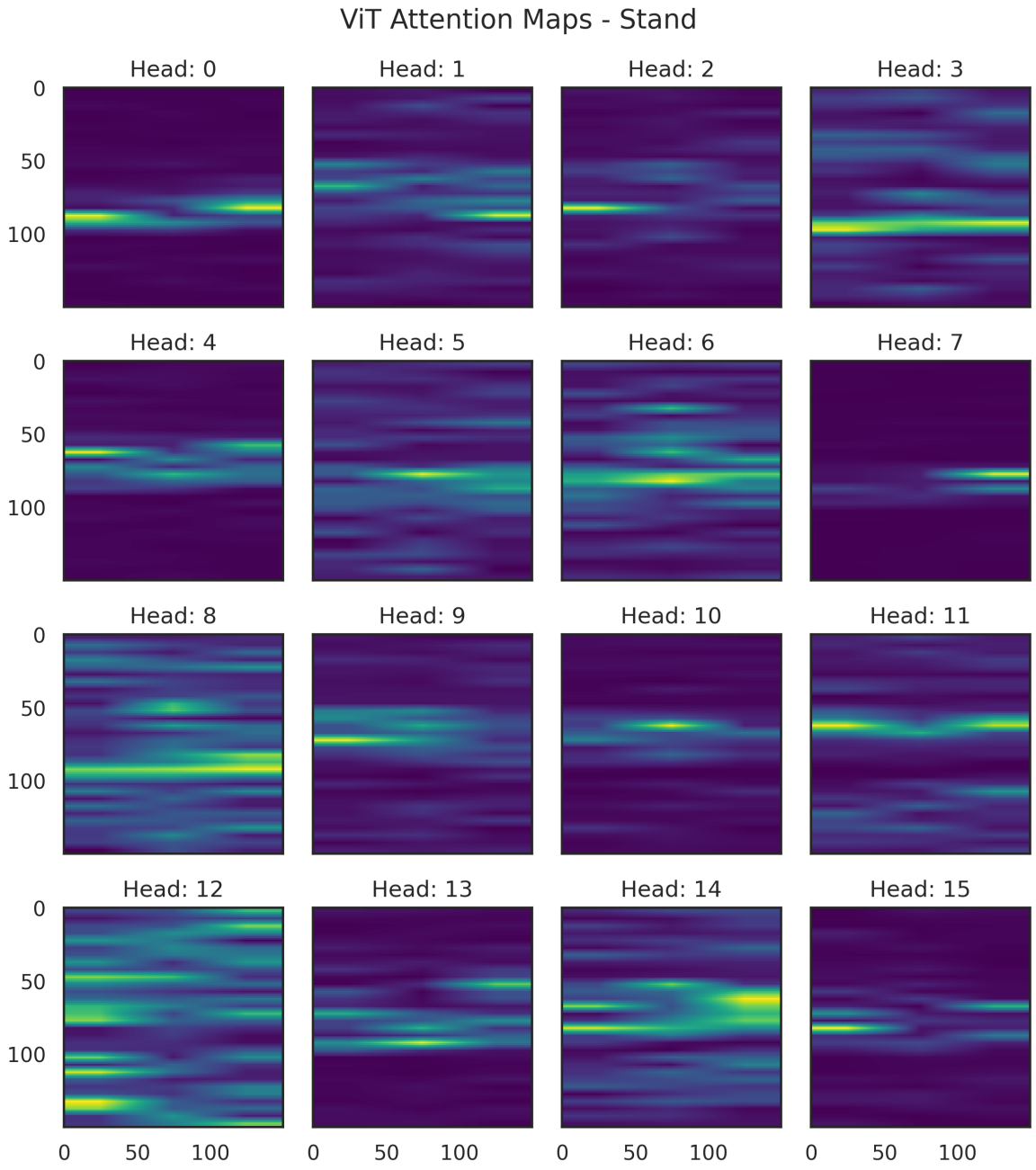

Figure 5.23: ViT attention heatmap of standing event within a window discussed in section 5.5. The images have been resized for easier viewing.

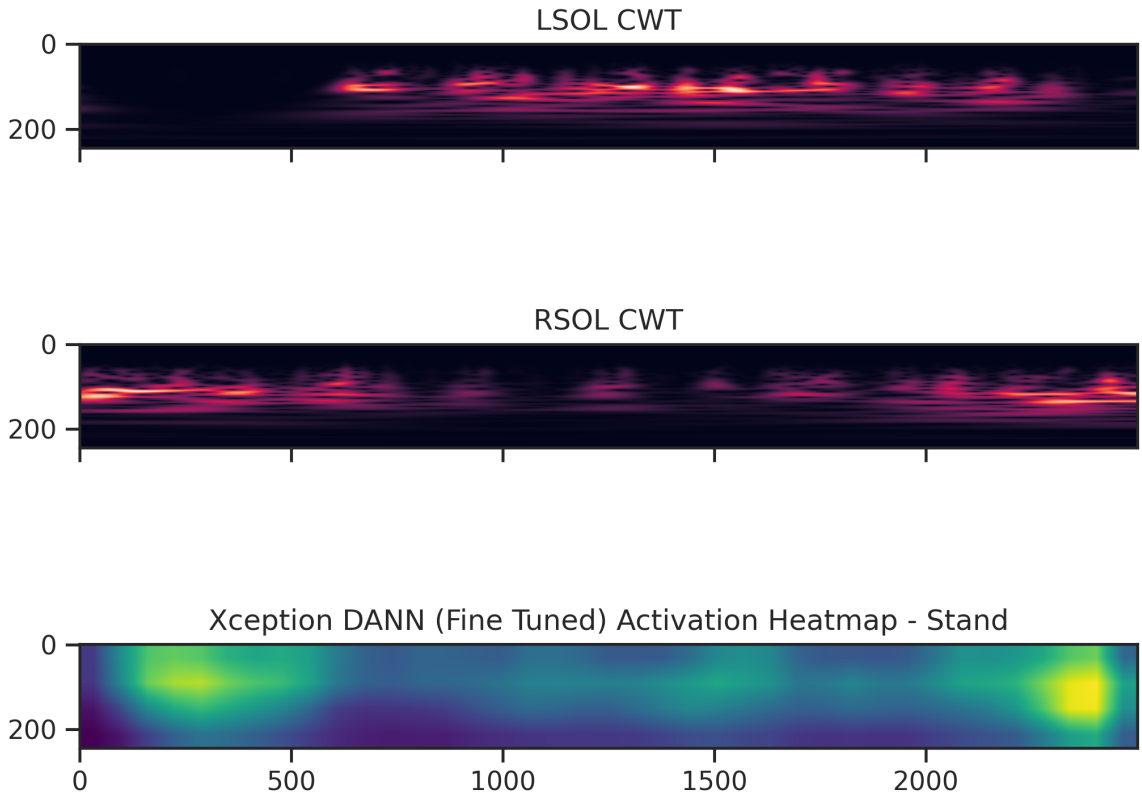

Figure 5.24: Xception-DANN activation heatmap of standing event within a window discussed in section 5.5.

representations in the Xception model that were not seen without DIAL, as verified in fig. 5.20 and fig. 5.35. Further experimentation with each domain adversarial parameter and their effects on data augmentation and synthetic data generation are suggested in Berrar and Dubitzky (2021); Li et al. (2021b); Iwana and Uchida (2021); Li et al. (2022b). The next set of experiments may include tuning the 'r' value increase domain confusion and introducing augmentation techniques towards more robust feature representation across domains.

The literature has few studies analysing the efficacy of domain adaptation techniques

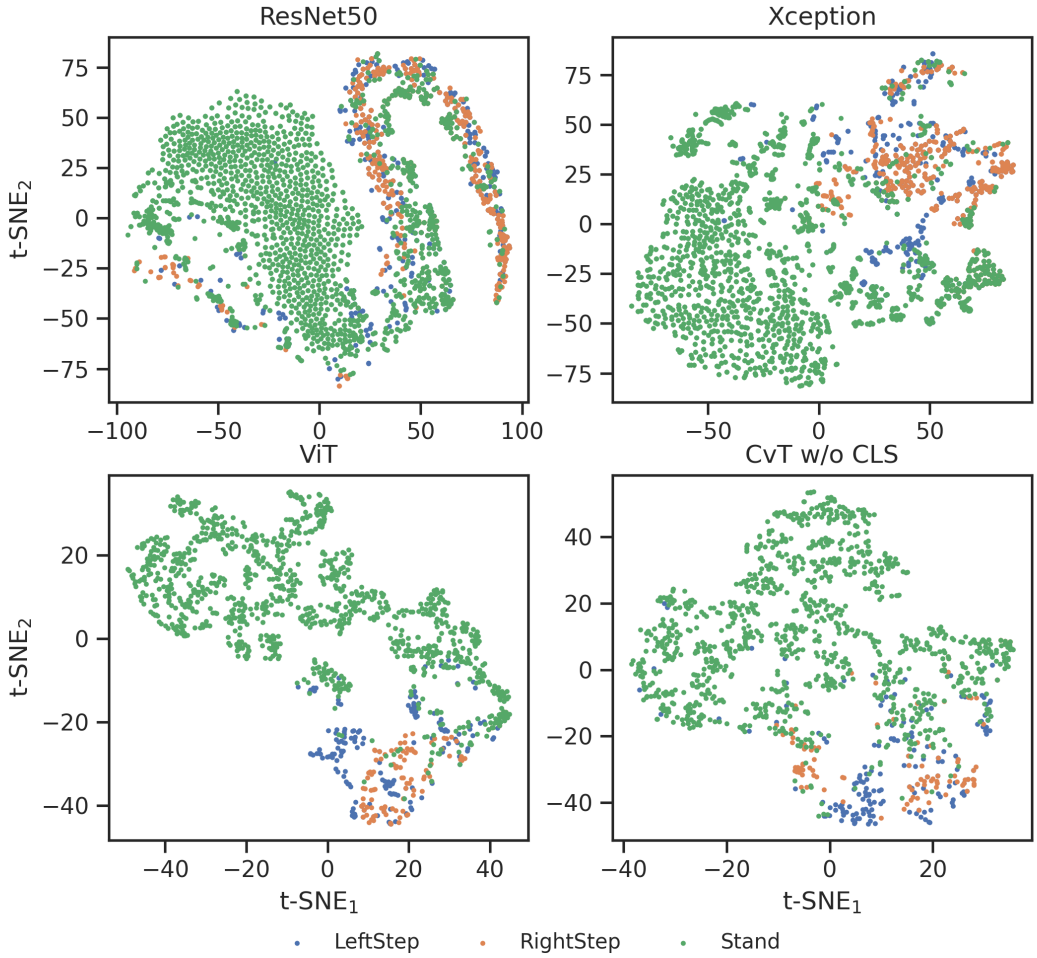

Figure 5.25: t-SNE feature representation of the penultimate layer outputs across each model.

in EMG classification, and the ones that do only look at hand gesture recognition (Côté-Allard et al., 2021; Du et al., 2017; Zhang et al., 2023). Applications of domain adaption for EMG hand gesture recognition primarily dealt with subject-to-subject variability, an effort to develop subject agnostic deep learning classification models or chronic recording activity, reducing entropic variability introduced with biosignal acquisition over time (Zhang et al., 2023; Côté-Allard et al., 2021). In this study, we apply domain adaptation techniques towards neurotherapy invariant representation of locomotion detection. The problems in the time dependency of previous frames and underlying physiological states

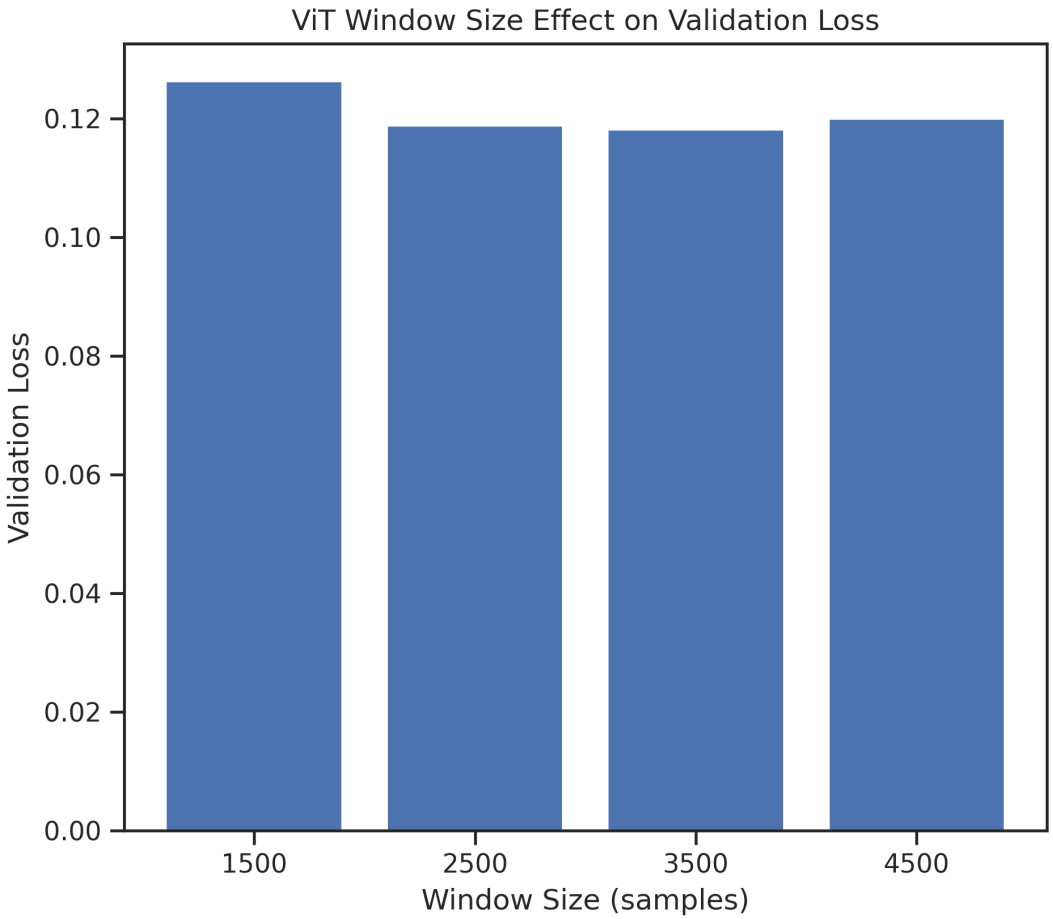

Figure 5.26: Brief study on the effect of different window sizes with 75% overlap using ViT model classification.

were not addressed in previous EMG domain adaptation papers. As far as I know, this work offers the first look into how these techniques perform in time-dependent, physiologically varying conditions.

Morbidoni et al. (2019) trained a 5-layer fully connected neural network and also applied a similar strategy to Huang et al. (2009) but limited their analysis to sEMG activity in healthy adults while overground walking in a figure-8 shaped path in a laboratory setting. Morbidoni et al. (2019) state their study as the first to classify stance and swing phases in a binary fashion. However, this process assumes locomotion is

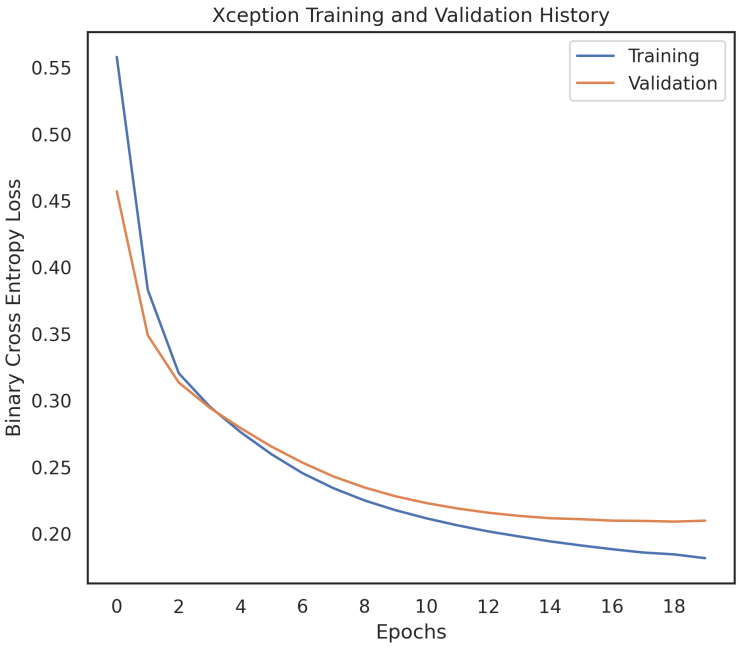

Figure 5.27: Training and validation loss for Xception.

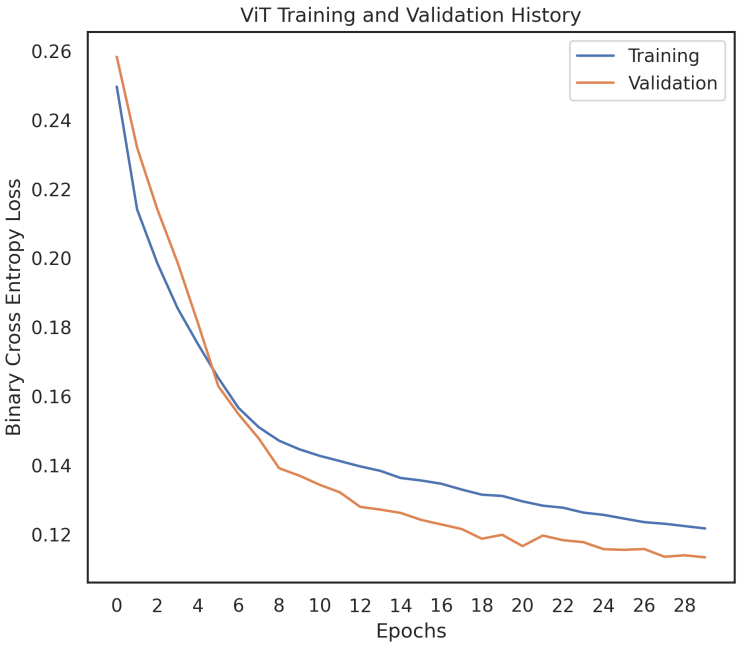

Figure 5.28: Training and validation loss for ViT.

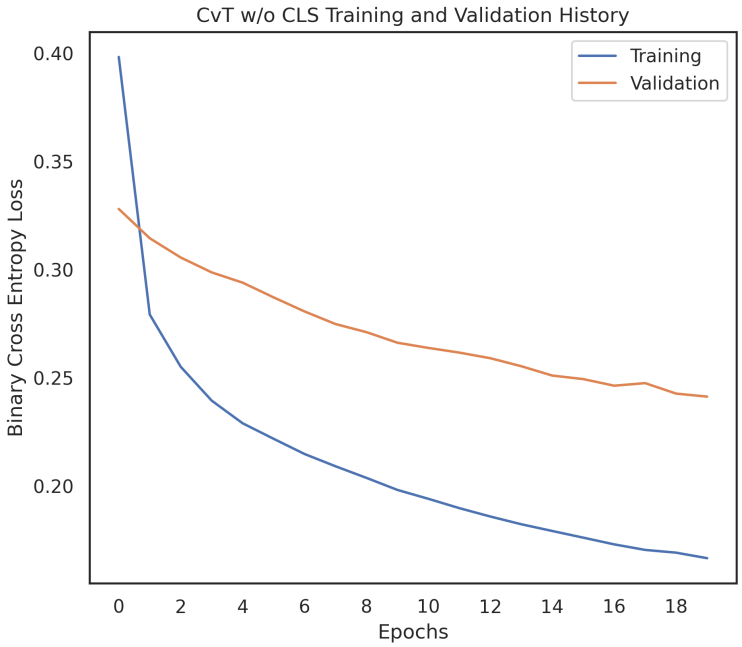

Figure 5.29: Training and validation loss for CvT without class token.

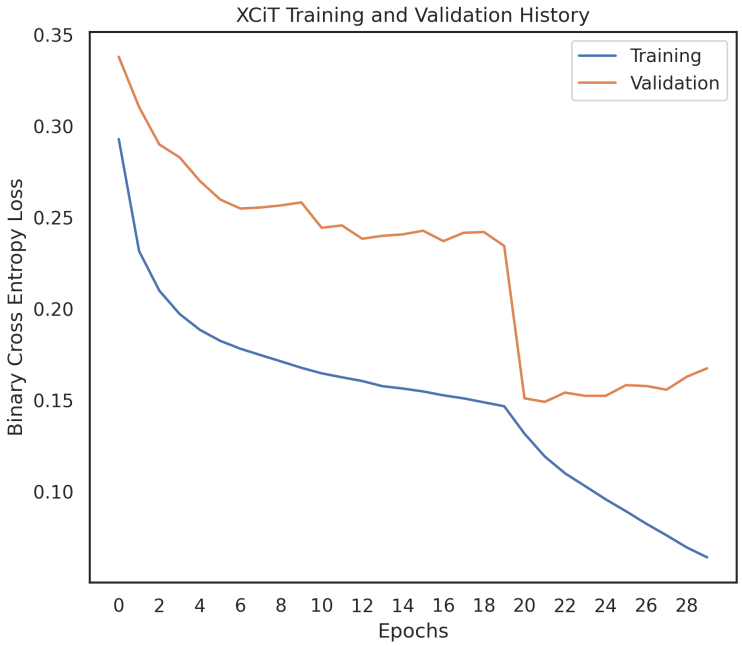

Figure 5.30: Training and validation loss for XCiT.

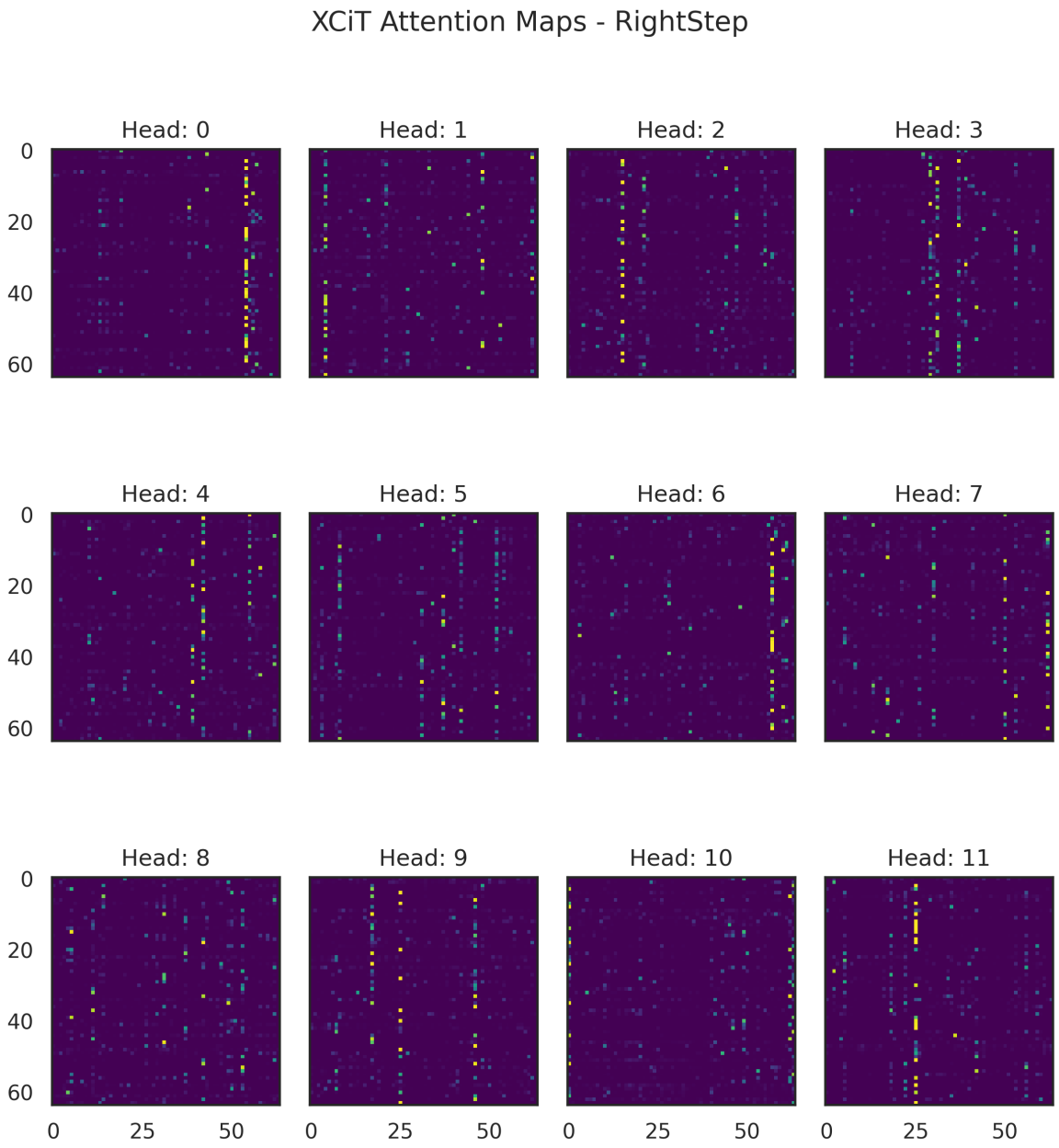

Figure 5.31: Attention mapping of the same right step window discussed in section 5.5.

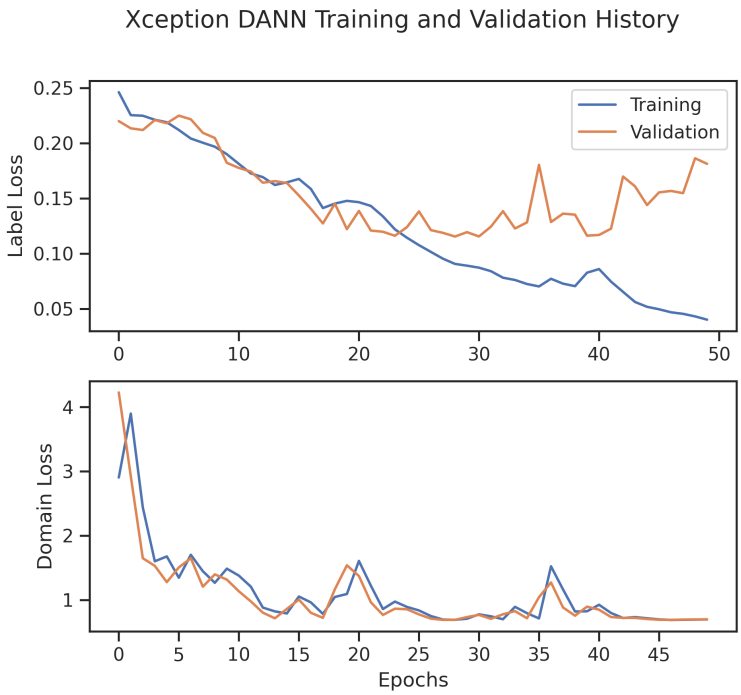

Figure 5.32: Label and domain loss history for Xception-DANN.

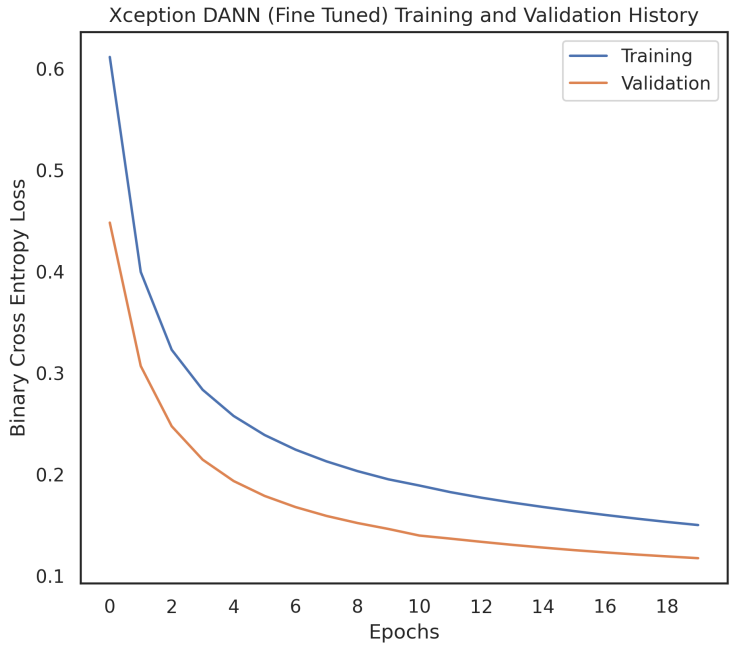

Figure 5.33: Label and domain loss history for Xception-DANN fine tuning. See fig. 5.34 for the loss history with $r = 2$.

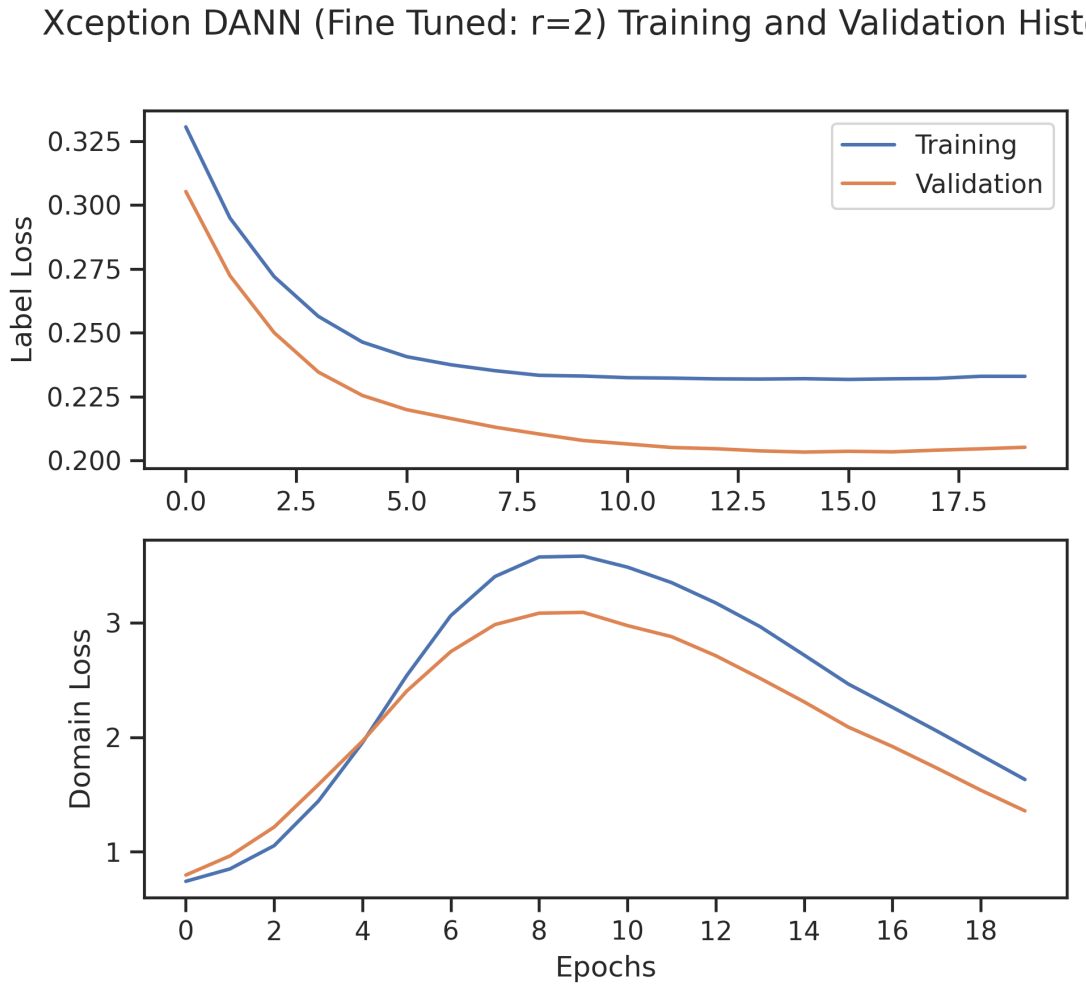

Figure 5.34: Training and validation loss history for Xception-DANN with domain scaling factor $r = 2$.

already in motion. A large pool of stride samples doubles the channel information on each leg and does not differentiate between rest and active states. In the extension of the work towards cerebral-palsy hemiplegic children, their results suggest high accuracy with F1 scores > 0.9 (Morbidoni et al., 2021). In later experiments, researchers applieda sliding window to post-process the signal and label accordingly. This process was unique because the label was defined as the last x% of the signal while taking the mean of overlapping frame labels. This effectively creates a buffer for each window that only predicts the final x% of the frame in question. This suggests a post-processing labelling

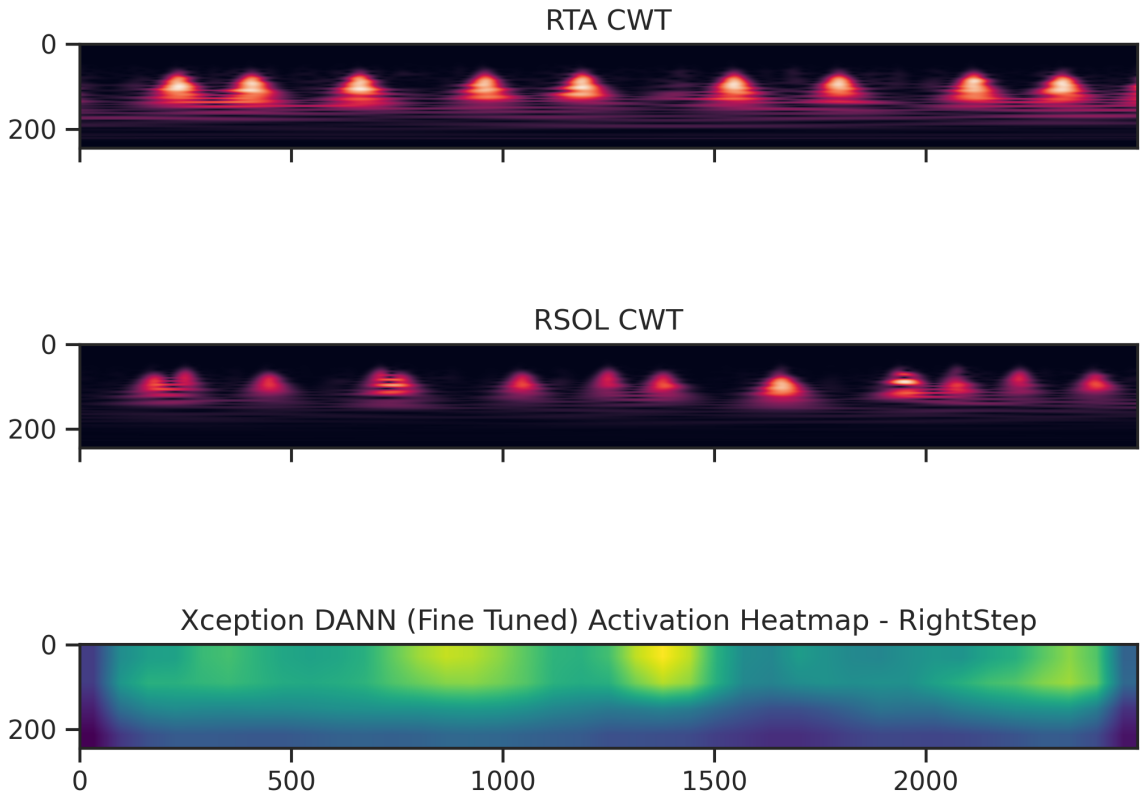

Figure 5.35: Xception-DANN activation map of a detected right step after fine-tuning.

method allowed the MLP to more reliably predict the stance and swing phase by using the past information only to predict the most recent sub-window. This transforms the problem towards something closer to binary forecasting. Applying similar methodologies may improve the deep learning result reported in this chapter.

Several limitations lie in blocking the deployment of deep learning models for clinical use. Major ones include the lack of interpretability, and 'black box' nature of deep learning models, and the enormous volumes of labelled data necessary to train robust models (Berrar and Dubitzky, 2021). A method to combat these limitations is the better understanding and development of biologically constrained models (Hole and Ahmad,

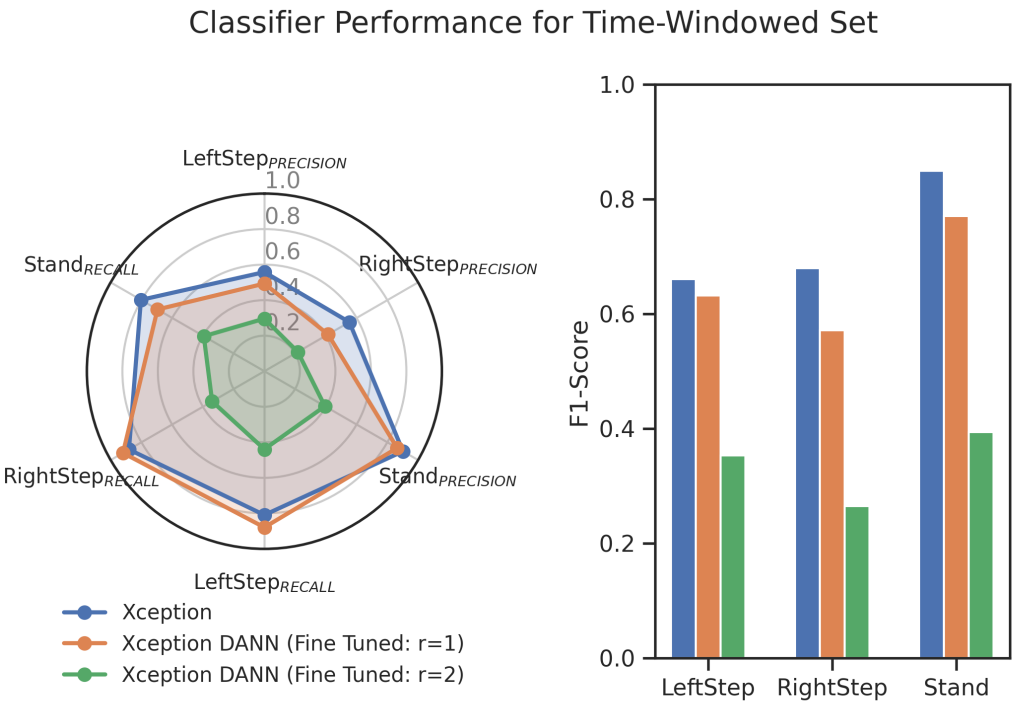

Figure 5.36: A spider and bar graph comparing Xception and DANN fine tuned classifications with different 'r' scale values for time windowed periods of activity.

2021; Pulvermüller et al., 2021). These models could contain the neurological structure required to perform the task at hand, thus filling the gap of interpretability. Fitting generative models with data can enable clinically relevant representations of subject data. Some studies have suggested using the encoder from autoencoder models as a feature extractor for discriminative tasks (Li et al., 2023).

A second limitation lies in the difficulty of generalising deep learning models in unseen domains and contexts (Chaki and Woźniak, 2023). Neurological injury and neurodegenerative disease datasets are often sparse and heterogeneous in disease expression and data collection methodologies (Young et al., 2018; Endo et al., 2024). Moreover, transformer architecture outperforms CNNs with heterogenous data, improving generalisability across domains in neurodegenerative datasets (Aguayo et al., 2023). While transformer architectures have become more popular for their short and long-term pattern detection capabilities, CNNs outperform ViTs for medical imaging classification

with random weight initialisation (Matsoukas et al., 2021). ViTs reap the benefits of the transformer architecture only after pre-training or self-supervised techniques. However, self-supervised pre-training with CNNs has been shown to improve the generalisation performance across shifted medical dataset domains (Azizi et al., 2021). New deep learning techniques such as pre-training, few-shot learning, domain adaptation, and self-supervised training may pave the way towards more robust deep learning models to address the heterogenous and sparse nature of neurological disease datasets (Ditthapron et al., 2021; Li et al., 2021a).

5.6 Conclusion

Several approaches have been applied towards the EMG classification of pathological gait. Many incorporate handcrafted feature generation and a 'divide-and-conquer' strategy to identify locomotion events. In this study, I aimed to exploit the latent representational power of deep learning models, reducing the need for complex and domain-sensitive feature generation. I tested several local CNN mapping deep learning models and discovered Xception to best discriminate relevant information in CWT channel stacked input data. I used this model to perform unsupervised domain-invariant adversarial learning and supervised fine-tuning. The Xception-DANN struggled to develop invariant representations between quipazine and non-quipaine therapy domains. Vision transformers performing depthwise attention operations did not successfully map local to global semantic information of cross-channel data as hypothesised. I show explanatory graphs and suggest future works to consider performing cross-attention operations over each EMG channel data rather than multi-head self-attention encoding. Future improvements may incorporate data augmentation and autoencoder methodologies.

CHAPTER 6

CURRICULUM LEARNING AIDED INTER-SUBJECT DOMAIN ADAPTATION

Existing time series datasets lack cohesion, labelling, and poor generalisability. These limitations impose challenges in the development of high-dimensional time series modelling. Thus, new deep-learning techniques to leverage the available information have been developed to work around these challenges. This chapter tests SOTA representation learning techniques such as contrastive learning, domain adaptation, and curriculum learning. Previous domain adversarial learning across therapy domains resulted in poor classification, here I applied domain adaptation across subjects. I hypothesise that subject-specific variability provides greater disruption to the feature extraction layers, thus developing more generalisable representations. I also tested curriculum learning techniques by segmenting the stepping labels into the swing and stance phases of gait. These new segmentations were used to train feature-extracting layers before fine-tuning and linear training on the more complex multi-label tasks of stepping and standing classification. My results show that incorporating curriculum

learning into our locomotion dataset yields comparable classification performance with existing SOTA methods. Curriculum learning gains were extended by incorporating inter-subject domain adaptation. Applying linear training after pre-training with curriculum learning improved class and subject bias while fine-tuning re-introduced these biases. Presented are techniques to perform subject-invariant robust classification of pathological gait from sparse EMG signals.

6.1 Introduction

Wearable technology has promised to provide users with insightful data for health monitoring, healthcare cost reduction, clinician and patient burden reduction, and improved patient assessment (Bruce and Andrew, 2011; De Fazio et al., 2023; Johansson et al., 2018). Wearable systems must be robust, timely, and meet privacy and data security standards to deliver on these outputs (Rodgers et al., 2019). Algorithm performance and generalisability have hinged on access to a wide distribution of data for both development and assessment (Wenig et al., 2022; Liew et al., 2022). However, well-annotated and high-quality data in life sciences has historically been inaccessible, expensive to record, and difficult to compile (Lathe, 2023; Nagaraj et al., 2020). Reduced volume of accessible data, time-series classification and deep learning in the life-sciences field has progressed slower than other sciences domains (Fawaz et al., 2018). Thus, to achieve improved benchmark performance and provide more robust classifiers, alternative methodologies have been suggested, including contrastive learning (Eldele et al., 2021; Yue et al., 2022), masked auto-encoding (Nie et al., 2023), and transfer learning (Fawaz et al., 2018; Ragab et al., 2023).

Contrastive learning is a self-supervised learning (SSL) algorithm first introduced in the computer vision domain (Chen et al., 2020). Intuitively, the same label instance can be measured with varying environment noise, equipment, and artefact; thus, developing

a model to recognise the same instance in its many forms is a valid method to provide more robust representations. By introducing variable augmentations to the sample, a base encoder extracts representation vectors before a small projection head maps the representations to the space where contrastive loss is applied. Simply put, the contrastive loss function calculates the temperature normalised cross-entropy loss of the cosine similarity between the two vectors **u** and **v**, see eq. (6.1) and eq. (6.2). Note (i,j) are indexes of augmented representations in a mini-batch given a set (k). By assuming the cluster hypothesis, contrastive learning populates clusters with different augmentations, leading to greater accuracy and generalisability, see fig. 6.1 for illustrated example (HaoChen et al., 2022).

I believe only one paper has been published that utilises contrastive learning for gait prediction (Fu and Guan, 2023). EMG signals provided positive examples of gait activity to guide EEG signal representation similarity, as per eq. (6.2). This problem differs from the classification problem in this thesis, which is the sparse EMG channel gait classification in neurologically impaired rodents receiving different neuromodulation therapies. The long-time course and electrophysiological dynamics introduced by the neuromodulation will intrinsically change the measured EMG signal over time. However, the paper raises interesting options for sensor-fusion techniques towards more robust sparse electrode wearables.

$$sim_{u,v} = \frac{u \cdot v}{\|u\|\|v\|} \tag{6.1}$$

$$L_{i,j} = -\log \frac{\exp\left(\text{sim}\left(\mathbf{z}_i, \mathbf{z}_j\right)/\tau\right)}{\sum_{k=1}^{2N} 1_{[k \neq i]} \exp\left(\text{sim}\left(\mathbf{z}_i, \mathbf{z}_k\right)/\tau\right)} \tag{6.2}$$

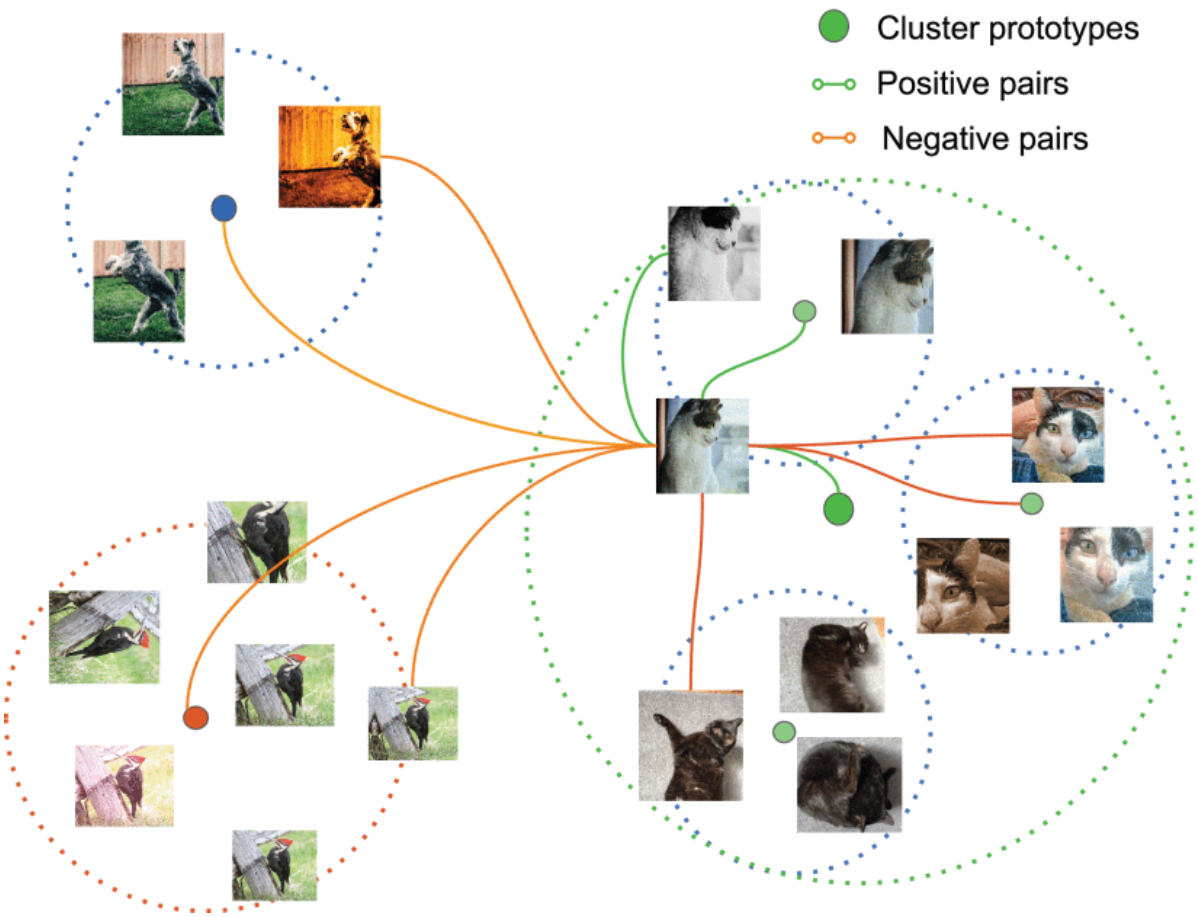

Figure 6.1: Illustration of the intuition behind contrastive learning, taken from Le-Khac et al. (2020). Representations of the same sample (e.g., cat) populate the cluster space with different augmentations. Similar samples cluster together while non-matching samples become separate clusters, embedding the manifold from the bottom up. Licensed under Creative Commons Attribution 4.0 International License.

Transfer learning aims to transfer knowledge from the source domain towards the target domain, typically related to the source domain data but inherently different (Zhuang et al., 2021; Hosna et al., 2022). This method of knowledge transfer addresses several problems in traditional machine learning: (1) insufficient labelled data, (2) mismatched source and target distributions, and (3) insufficient computational power (Niu et al., 2020). See fig. 6.2 for an illustration of the transfer learning process. Common approaches train a deep neural network model on data from well-annotated and trustworthy datasets before fine-tuning or linear probing the feature extraction layers (Fawaz et al., 2018; Ye

and Dai, 2021).

Transfer learning for EMG classification has mainly been explored in hand gesture recognition with techniques to leverage the impressive volume of large generic image datasets (Demir et al., 2019; Li et al., 2021c), temporally transferable feature representation (Côté-Allard et al., 2017, 2021), inter-subject transfer learning (Côté-Allard et al., 2019), and electrode shift (Ameri et al., 2020). Note that none of these methods apply any domain adaptation (DA) techniques. Methods applying non-EMG or activity-related pre-trained models appear unintuitive towards human activity recognition. This 'black-box' behaviour has been the source of users' hesitancy in adopting deep learning models in practice (Adler-Milstein et al., 2022).

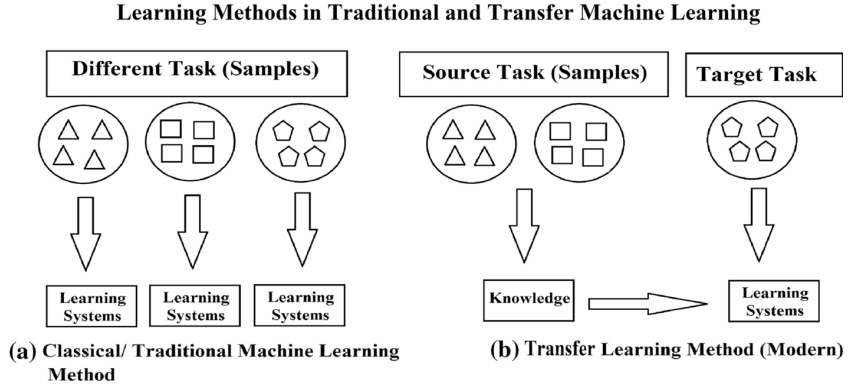

Figure 6.2: Illustration of the intuition behind transfer learning, taken from Hosna et al. (2022). (a) Develops several models, each specifically trained on the domain dataset with limited generalisability. (b) Developing representations from training on the source dataset before transferring knowledge to train on the target dataset. Licensed under Creative Commons Attribution 4.0 International License.

Finally, inspired by natural learning mechanisms, curriculum learning (CL) exposes a model to a sequence of tasks that gradually increase in complexity (Bengio et al., 2009). This method of training has been adopted across multiple tasks where complexity could range between increasing signal-to-noise ratio, increasing spatial and temporal resolution, increased artefact presence, and weakly labelled data (Soviany et al., 2022). To my knowledge, no work on CL for EMG signal classification has been published.

A clear question now emerges: Does applying representation transfer learning techniques in combination with curriculum learning strategies improve the classification performance of multi-domain EMG signal data? I hypothesise that a more robust classifier can be trained by localising weights and biases at a better parameter space.

6.2 Methods

Further manual labelling was performed to extend the dataset to include at least 5 minutes of activity across all rodents. Each rodent was identified by a single letter and digit, namely A3, A5, A7, and A8. Several transfer learning strategies were incorporated to assess the effectiveness of curriculum learning in unstable locomotor EMG signals. These include self-supervised contrastive learning, domain adaptation, and pre-training. Step labels were split into swing and stance phases for the right and left sides. This was completed by iterating through each pre-labelled step event and manually choosing the phase split, see fig. 6.4.

Three CL pipelines were applied, see fig. 6.3. (1) Pretrain a locomotion phase feature extractor then fine-tune or linear train on step and stand data. (2) Contrastive learning pretraining from the target dataset and open source datasets before fine-tuning or linear training on step and stand data. (3) Domain adaptation phase pretraining between subjects followed by linear training on step and stand data.

Inter-subject domain adaptation methods with phase CL were performed using the AdaTime benchmark repository (Ragab et al., 2023). The code was adapted to include a new temporally aware adversarial domain adaptation (TADA) methodology (Yi et al., 2024) and support multi-label learning. TADA has been shown to adversarially bridge the domain gap in long- and short-term information and fine granularity for patient outcome forecasting. This method was incorporated to capture short bursting EMG activations and longer phasic relationships in locomotion. Loss functions were set according to the

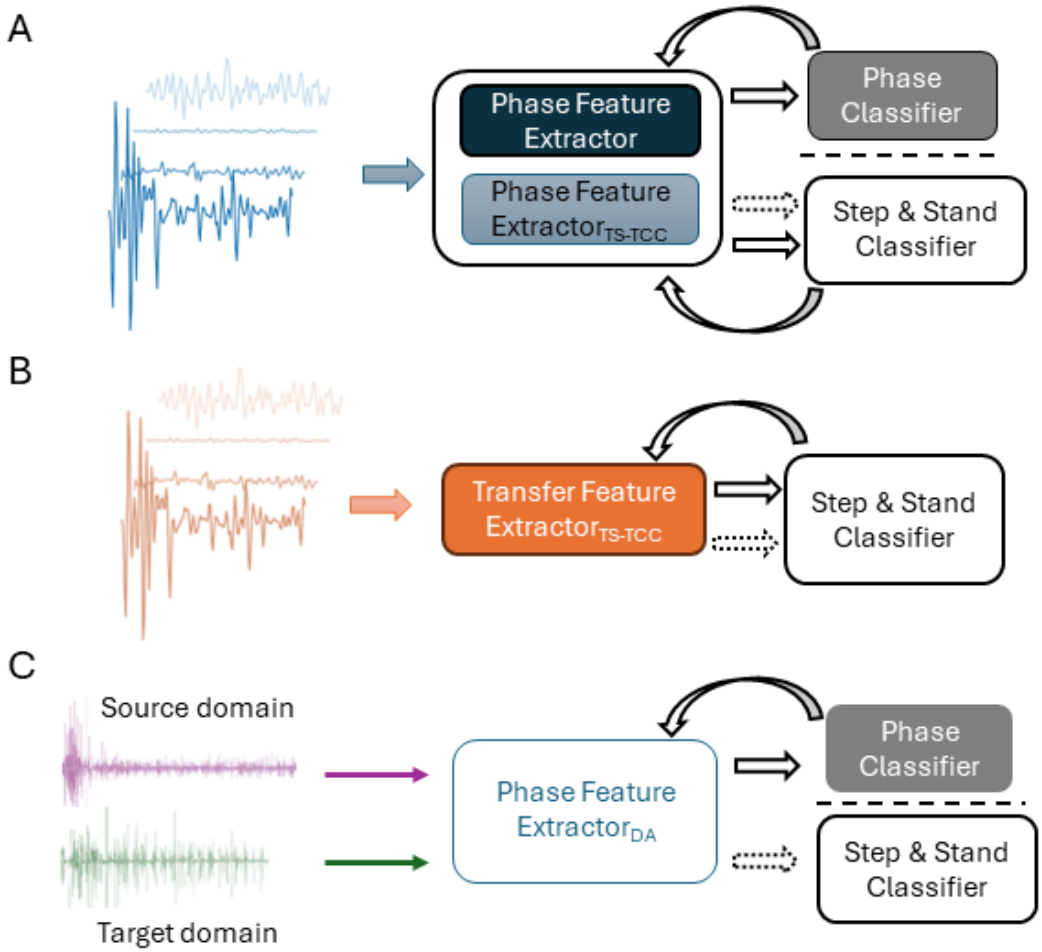

Figure 6.3: The general framework of the proposed curriculum and transfer learning approach. Arrows with dotted lines represent linear training with frozen feature extraction layers while hard line arrows represent fine-tuning. (**A**) Rodent hindlimb dataset was input to a self-supervised TS-TCC contrastive learner or a supervised CNN1D to extract embeddings for phase labels before linear training or fine-tuning for step and stand labels. (**B**) Open source datasets were preprocessed and used to train the TS-TCC contrastive learner. The TS-TCC trained CNN1D was used to linearly train or fine-tune step and stand labels. (**C**) Source and target domain refers to different rodents. Source and target inputs were fed into a CNN1D to extract domain adaptation embeddings for phase classification. The pretrained CNN1D domain adapted feature extractor was used to linear train step and stand labels in the target domain.

original paper specifications (Ragab et al., 2023; Yi et al., 2024).

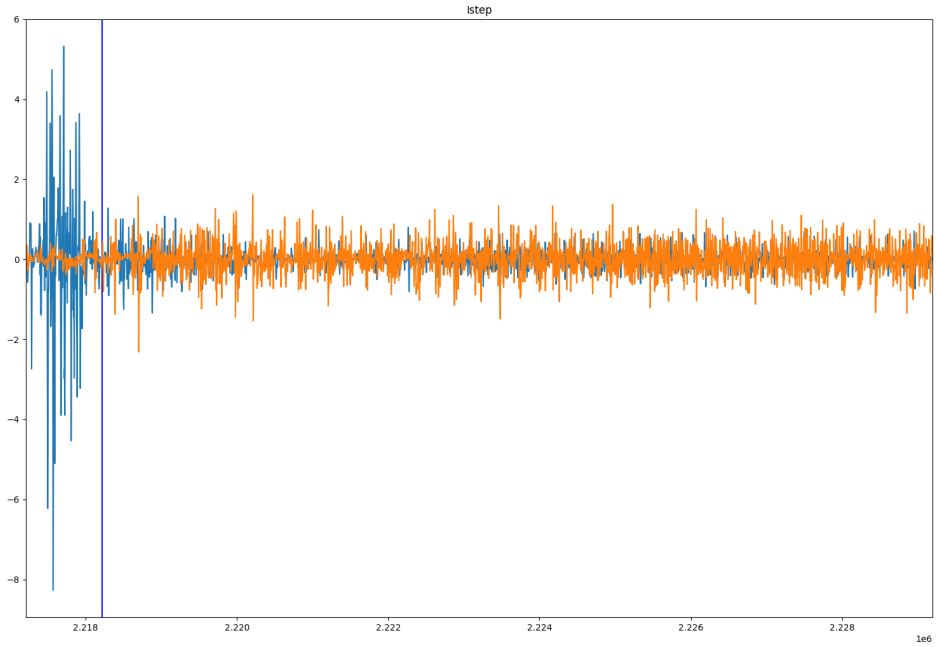

Figure 6.4: A simple custom software GUI to separate each phase of left and right stepping. X-axis and y-axis details the sample index and EMG voltage (mV) respectively. The vertical blue line separates the swing from the stance phase. Ipsilateral tibialis anterior and soleus muscle activity are represented in the muted bue and orange signal.

6.2.1 Deep Learning Models

Single dimension convolutional neural networks (CNN1D) have ranked as a top performer in multivariate time series classification tasks (Ismail Fawaz et al., 2019). A three-layered CNN1D network was selected as the feature extractor for contrastive learning, curriculum learning, and all domain adaptation experiments, excluding TADA. Specification of the CNN1D and LSTM TADA network can be found in table 6.1 and table 6.2, respectively. Preliminary experimentation to determine the most suitable penultimate layer was performed with supervised training using a dense fully connected, LSTM, and multi-head attention layers. While LSTM provided the highest accuracy, the results were prone to single subject bias and class imbalance effects, see tables A.1 and A.2. All feature extractors were connected to a single fully connected network before the final output layer.

Time-Series Representation Learning via Temporal and Contextual Contrasting

(TS-TCC) was selected as the contrastive learning algorithm to develop self-supervised representations (Eldele et al., 2021). This decision was based on the higher-performing biosignal classification evaluation metrics compared to ts2vec (Yue et al., 2022). Other methodologies were also considered, but attempts to replicate the results from the paper were not successful and highly sensitive to hyperparameter tuning (Zhang et al., 2022), or not suited for multi-labelling tasks (Liu et al., 2023).

Deep learning models were trained using NVIDIA Quadro RTX 6000 Passive graphics cards for 40 epochs with a batch size of 128 and learning rate of 3×10^{-4} with Adam optimizer (Kingma and Ba, 2017). All models were written using the PyTorch v2.1.1 framework (Paszke et al., 2019).

6.2.2 Open Source Datasets

The TaichiDB, SEMG, and GrabMYO datasets from goldberger2000 were selected based on the relevance to the task and overall quality of annotation (Goldberger et al., 2000). TaichiDB consists of longitudinal data of 27 Tai Chi experts and 60 healthy, Tai Chi, naïve elderly (50 - 70 years) subjects (Wayne et al., 2021, 2013). Data was labelled with force-sensitive footswitches and EMG electrodes placed on TA and lateral gastrocnemius muscles. EMG and footswitch data were collected at 1500Hz. Footswitch data detected heel strike and toe-off events. Subjects were requested to perform single- or dual-task walking at the preferred speed for 10m and 90s respectively.

The SEMG dataset consists of surface EMG data collected from 5 leg muscles; in this study, only the lateral gastrocnemius and TA were selected (Di Nardo et al., 2021, 2024). Footswitch data was used to determine the swing and stance phases. Both EMG and foot switch samples were collected at a 2kHz rate. 31 young able-bodied subjects between the ages of 20 and 30 were selected to perform 5-minute ground walking.

The GrabMYO dataset consists of gesture data from 43 healthy participants who

Layer Name	CNN1D
$conv_1$	3×1, 32, stride 2
batch normalisation	
ReLu	
maxpooling 1d	2×1, stride 1
dropout	0.35
$conv_2$	8×1, 64, stride 1
batch normalisation	
ReLu	
maxpooling 1d	2×1, stride 1
dropout	0.35
$conv_3$	8×1, 128, stride 1
batch normalisation	
ReLu	
maxpooling 1d	2×1, stride 1
dropout	0.35
flatten	b c t → b (c t)

Table 6.1: 3-layer CNN1D model. The notation follows as batch size 'b', channel 'c', timestep 't', 'd' stands for variable dimension and 'fc' stands for fully connected.

repeatedly performed 17 hand and wrist gestures 7 times, with each trial lasting 5s (Jiang et al., 2022; Pradhan et al., 2022). Participants were requested to repeat the same experiment on 3 separate days, presenting an impressive volume of multi-session hand and wrist gesture data. Data was preprocessed to use pairs of antagonistic forearm muscle groups based on the location of the 8 x 8 electrode array.

Layer Name	LSTM
lstm	128-d

Table 6.2: 1-layer LSTM model. The notation follows as variable dimension 'd', 'fc' for fully connected.

Layer Name	CNN1D
$conv_1$	5×1, 64, stride 1
batch normalisation	
ReLu	
maxpooling 1d	2×1, stride 2
dropout	0.5
$conv_2$	8×1, 128, stride 1
batch normalisation	
ReLu	
maxpooling 1d	2×1, stride 2
$conv_3$	8×1, 128, stride 1
batch normalisation	
ReLu	
maxpooling 1d	2×1, stride 1
adaptiveavgpool 1d	b c t → b c 1

Table 6.3: 3-layer CNN1D model. The notation follows as batch size 'b', channel 'c', timestep 't', 'd' stands for variable dimension, and 'fc' stands for fully connected.

6.2.3 Signal Procesing

All signal channels were filtered using a 5-th order bandpass filter with cut-off frequencies between 10 and 500Hz. To capture phasic information, window size was reduced to 75ms and window shift was set to 75% of window size length (Leblond et al., 2003).

To reduce memory requirements and expedite training speed, all data was linearly resampled to 2kHz. The same filtering procedures were repeated for TaichiDB open soure dataset. The remaining open source datasets were already preprocessed using the same filtering procedure. TaichiDB was upsampled to 2kHz from 1.5kHz and GrabMYO was downsampled to 2kHz from 2048Hz. SEMG was already sampled at 2kHz.

All datasets were split as 60%/20%/20% training, validation, and test sets. To statistically measure the performance of each classifier, precision eq. (3.4), recall eq. (3.5), and F1-Score with weighted averaging eq. (3.2) to capture multi-labelling imbalance. An ROC curve (receiver operating characteristic curve) was used to graphically illustrate the performance of classifiers against baseline random prediction (Hoo et al., 2017). Linear correlations were tested with Pearson Correlation Coefficient.

Predictions were smoothened using the Savitzky-Golay filter with a width of 3-samples. Thresholds for predictions were made using the sum of the mean and standard deviation of each label with a tuning gain applied to the standard deviation variable, dependent on the subject. All outputs for step predictions were set to a maximum and minimum duration threshold of 0.3 and 1.2s, respectively. All stand predictions were set to a minimum duration threshold of 0.3s.

Data was assumed to be dependent, and the Shapiro-Wilk test was used to determine normality ($p > 0.05$). Normal distributions were tested with the Tukey Honestly Significant (HSD) test, and non-normal distributions were tested with the Wilcoxon signed-rank test. Where relevant, results are reported as mean $\pm$ standard deviation.

6.3 Results

Supervised training yielded a weighted F1 score of 0.37 ± 0.20 across all subjects with a heavy bias in the rodent with the most amount of collected labels, A7, see table 6.4. Notably A3 and A5 reported low weighted F1 scores. These were mainly caused by poor

right step in A5 and standing prediction for both A3 and A5.

Table 6.4: Supervised step and stand training using CNN1D only.

	Accuracy	Precision	Recall	F1-Score (weighted)
A3	0.20	0.80	0.11	0.18
A5	0.82	0.12	0.55	0.19
A7	0.80	0.73	0.62	0.64
A8	0.61	0.65	0.37	0.46
Mean	0.61	0.57	0.41	0.37
SD	0.25	0.27	0.20	0.20

6.3.1 Phase Classification

The phase classifiers successfully detected right and left stance and swing phases greater than baseline. Pretraining the feature extractor using TS-TCC contrastive learning followed by fine-tuning yielded the greatest F1-score, 0.60, without separating by subject, see table 6.5. However, after calculating the F1-score per subject, the average performance drops considerably; see table A.4.

The top-4 grand mean values from domain adaptation experiments were calculated as 0.43, 0.42, 0.41, and 0.41 from Higher-order Moment Matching (HoMM) (Chen et al., 2019), Adversarial Spectral Kernal Matching (AdvSKM) (Liu and Xue, 2021), Conditional Domain Adversarial Networks (CDAN) (Long et al., 2018), and TADA respectively, see table 6.11. Comparing domain adaptation algorithms to inter-subject transfer learning for feature extraction, the top domain adaptation strategies, HoMM and TADA, outperformed the inter-subject self-supervised contrastive learning approach by 0.12 and 0.10, respectively. HoMM and TADA domain adaptation predictions were equivalent to subject-specific supervised training classifiers in all phases ($p > 0.1$); see table A.3.

Table 6.5: Performance of phase classification during pretraining transfer learning stage. These metrics are for phase labels only.

	Accuracy	Precision	Recall	F1-Score (weighted)
$CL_{fine-tune}$	0.77	0.63	0.56	0.58
CL_{linear}	0.74	0.52	0.56	0.53
TS-TCC + $CL_{fine-tune}$	0.78	0.63	0.59	0.60
TS-TCC + CL_{linear}	0.75	0.53	0.57	0.54

Table 6.6: Average phase label classification F1-score (binary) performance for TADA after 3 runs set at different random seeds.

	Right Swing	Right Stance	Left Swing	Left Stance
A3 → A7	0.27	0.29	0.27	0.08
A5 → A7	0.42	0.27	0.25	0.31
A7 → A3	0.61	0.37	0.64	0.39
A7 → A5	0.54	0.46	0.69	0.54
A7 → A8	0.52	0.54	0.44	0.52
A8 → A7	0.52	0.53	0.43	0.54
Mean	0.48	0.41	0.45	0.40
SD	0.11	0.11	0.17	0.17

6.3.2 Step and Stand Classification

Pretraining CNN1D feature extractors on open source datasets yielded a range of evaluation metrics, differing between each dataset, (table 6.7). Interestingly, the worst feature extraction model, $SSL_{TaichiDB,fine-tune}$, resulted in the top F1-score after fine-tuning. SSL+CL pretraining using only rodent training data and SLL pretraining using all open-source data report the same weighted F1-score. While $SSL_{All,linear}$ detected more true positives than SSL+CL pretraining, SSL+CL more successfully rejected false positives. Fine-tuning after CL reduced subject-specific variability in left step detection compared to non-CL approaches, seen in figs. 6.5 and 6.6. The subject-specific results in non-DA methods show large variation, suggesting poor inter-subject classification performance. No statistically significant outcomes were found between top-performing SSL, CL, and DA models ($p > 0.05$).

Table 6.7: Transfer and curriculum learning classification performance for step and stand labels. SSL specifies TS-TCC self-supervised contrastive learning using rodent or open source data. Unless specified by GrabMYO, Taichidb, SEMG, or All, each model was trained using the training set from the rodent data. 'All' represents a feature extractor pretrained across all open source datasets, excluding the rodent data. The best values for each metric are in bold.

	Accuracy	Precision	Recall	F1-Score (weighted)
$SSL_{fine-tune}$	0.77	0.60	0.60	0.60
SSL_{linear}	0.76	0.57	0.29	0.38
$SSL_{GrabMYO,fine-tune}$	**0.79**	0.68	0.52	0.58
$SSL_{GrabMYO,linear}$	0.77	0.68	0.43	0.51
$SSL_{SEMG,fine-tune}$	0.76	0.57	0.54	0.55
$SSL_{SEMG,linear}$	0.72	0.49	0.40	0.44
$SSL_{TaichiDB,fine-tune}$	0.76	0.63	**0.62**	**0.61**
$SSL_{TaichiDB,linear}$	0.75	0.68	0.17	0.23
$SSL_{All,fine-tune}$	**0.79**	0.69	0.56	0.60
$SSL_{All,linear}$	0.77	**0.73**	0.43	0.50
$CL_{fine-tune}$	0.77	0.63	0.56	0.58
CL_{linear}	0.74	0.52	0.56	0.53
SSL + $CL_{fine-tune}$	0.78	0.63	0.59	0.60
SSL + CL_{linear}	0.75	0.53	0.57	0.54

Analysing weighted F1-score only, $SSL_{TaichiDB,fine-tune}$ ranked the top classifier out of all the transfer and curriculum learning models. A subject-specific breakdown of the results shows that only A7 and A8 achieve high performance table 6.8. Moreover, the TaichiDB pretrained linearly trained model did not effectively map relevant features between the source and target dataset (table A.10 and fig. 6.6). Fine-tuning on All and GrabMYO datasets did not classify standing data as well as TaichiDB (fig. 6.5). Although, linearly trained All and GrabMYO datasets performed better for standing than after fine-tuning (fig. 6.6.

SSL+CL approaches did not have any access to open-source datasets but report competitive classification results in stepping and standing. However, still suffer from the effects of poor inter-subject mapping. Linearly trained SSL and CL models reduce subject variability but the effects of class and subject bias return when fine-tuning is

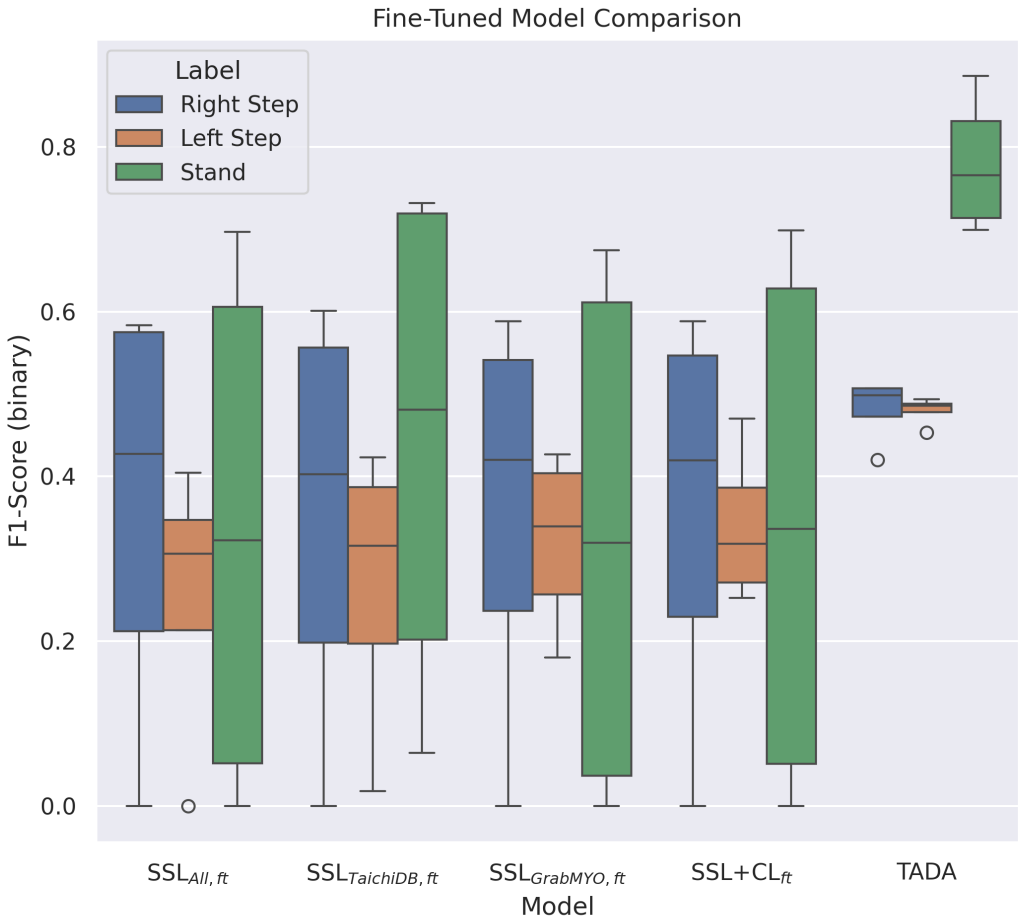

Figure 6.5: Box plot comparison of fine-tuned models and the top performing linearly trained curriculum training + domain adaptation model, TADA. Subject bias in TADA is lower than non-domain adaptation models. No significance was detected between models.

performed figs. 6.5 and 6.6.

In contrast, domain adaptation CL performance achieved high classification evaluation across all subjects, with TADA marginally outperforming HoMM, see tables 6.9 and 6.10. Adapting from different source domains (A3, A5, and A8) to the singular subject (A7) yielded varying evaluation metrics, see tables 6.9 and 6.10. For HoMM, choosing A3 resulted in a greater F1-score than A5 or A8. In contrast, for TADA, choosing A8 resulted in a better F1-score. Domain adaptation reduces the inter-subject bias previ-

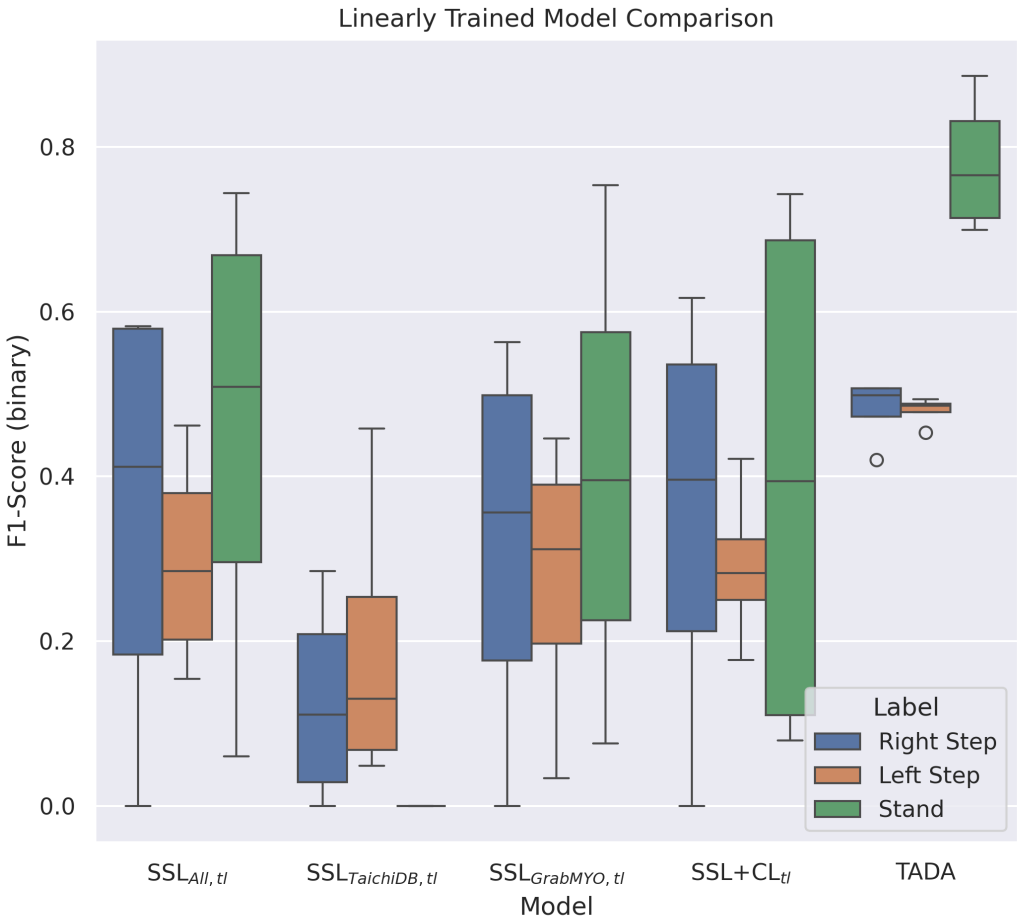

Figure 6.6: Box plot comparison of linearly trained models and the top performing curriculum training + domain adaptation model, TADA.

ously observed after fine-tuning in SSL feature extractors; refer to tables 6.8 and A.9 and tables 6.9 and 6.10.

Unlike non-DA pretraining methods that could not detect A5 right stepping, TADA and HoMM successfully classify A5 right side locomotion activity fig. 6.7. Top-2 domain adaptation approaches outperformed all models specified in table 6.7 in both step and stand events. Inter-subject variability was reduced with an area under ROC curve (AUC) range of 0.25 and 0.18 for HoMM right and left step prediction, compared to $\text{SSL}_{TaichiDB,fine-tune}$ which resulted in unsuccessful A5 right step classification and

Table 6.8: Step and stand label results after fine-tuning from a TS-TCC pretrained feature extractor using TaichiDB open source dataset.

	Accuracy	Precision	Recall	F1-Score (weighted)
A3	0.27	0.81	0.17	0.27
A5	0.81	0.03	0.18	0.05
A7	0.79	0.73	0.63	0.64
A8	0.63	0.69	0.47	0.56
Mean	0.63	0.56	0.36	0.38
SD	0.22	0.31	0.20	0.24

Table 6.9: HoMM domain adaptation curriculum learning classification performance for step and stand labels.

	Accuracy	Precision	Recall	F1-Score (weighted)
A3 $\rightarrow A7$	0.79 ± 0.00	0.62 ± 0.02	0.62 ± 0.03	0.61 ± 0.01
A5 $\rightarrow A7$	0.78 ± 0.05	0.62 ± 0.12	0.57 ± 0.05	0.58 ± 0.08
A7 $\rightarrow A3$	0.48 ± 0.03	0.69 ± 0.03	0.62 ± 0.03	0.64 ± 0.03
A7 $\rightarrow A5$	0.80 ± 0.01	0.69 ± 0.03	0.63 ± 0.08	0.65 ± 0.06
A7 $\rightarrow A8$	0.76 ± 0.01	0.58 ± 0.02	0.56 ± 0.02	0.57 ± 0.00
A8 $\rightarrow A7$	0.77 ± 0.00	0.58 ± 0.02	0.56 ± 0.07	0.56 ± 0.04

Table 6.10: TADA domain adaptation curriculum learning classification performance for step and stand labels.

	Accuracy	Precision	Recall	F1-Score (weighted)
A3 $\rightarrow A7$	0.77 ± 0.01	0.57 ± 0.03	0.46 ± 0.08	0.49 ± 0.06
A5 $\rightarrow A7$	0.79 ± 0.02	0.60 ± 0.04	0.55 ± 0.10	0.56 ± 0.06
A7 $\rightarrow A3$	0.41 ± 0.03	0.65 ± 0.02	0.62 ± 0.03	0.63 ± 0.02
A7 $\rightarrow A5$	0.82 ± 0.01	0.72 ± 0.04	0.63 ± 0.03	0.66 ± 0.04
A7 $\rightarrow A8$	0.79 ± 0.01	0.64 ± 0.03	0.59 ± 0.04	0.61 ± 0.02
A8 $\rightarrow A7$	0.80 ± 0.01	0.64 ± 0.02	0.63 ± 0.02	0.63 ± 0.02

0.31 inter-subject AUC range for left step classification. TADA outperformed HoMM, achieving higher inter-subject AUC values.

TADA more accurately classified A3 (AUC = 0.61) and A5 (AUC = 0.67) right stepping compared to HoMM A3 (AUC = 0.52) and A5 (AUC = 0.52) results that were marginally above chance. Left stepping for all subject's results was better detected in TADA over HoMM. However, the stand-label HoMM AUC surpassed TADA evaluations in A3 and

A8 subjects. Rodent A7 classification using domain adaptation presented lower AUC values compared to SSL models. Conversely, A3, A5, and A8 subject domain adaptation AUC results were greater than all non-domain adaptation model AUC results.

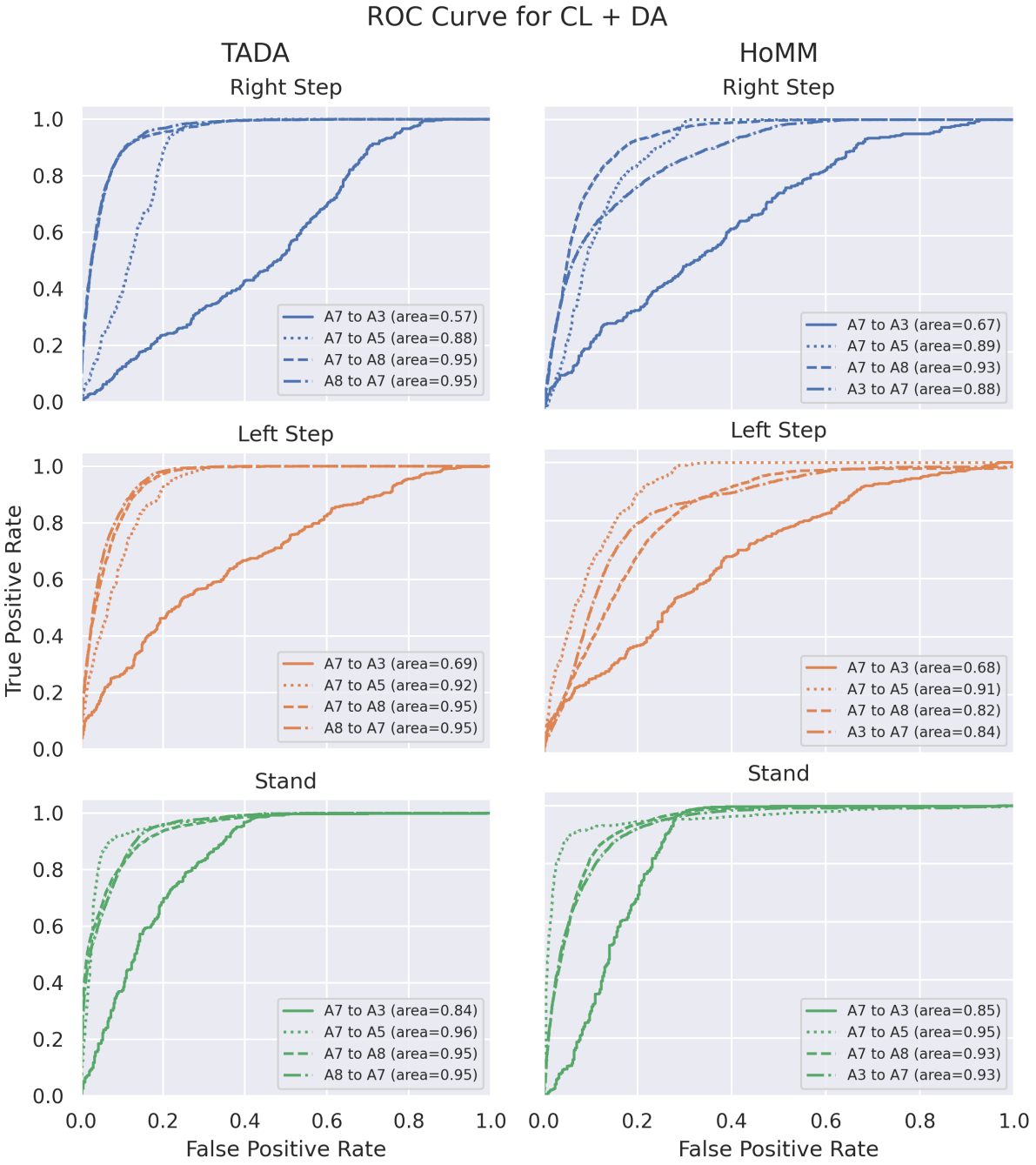

Figure 6.7: ROC curve of the each subject and each stepping and standing label for TADA$_{linear}$ (left) and HoMM$_{linear}$ (right). Both TADA and HoMM successfully detected right steps for A3 and A5 though TADA was more accurate. The best A7 source dataset for each method was selected based on the F1-score.

Table 6.11: Average and standard deviation F1-score metric after domain adaptation classification weighted for phase labels only after 3 runs using different random seeds.

	A3 → *A*7	A5 → *A*7	A7 → *A*3	A7 → *A*5	A7 → *A*8	A8 → *A*7
NO ADAPT	0.40 ± 0.01	0.34 ± 0.05	0.43 ± 0.06	0.30 ± 0.10	0.31 ± 0.07	0.37 ± 0.04
Deep Coral	0.35 ± 0.03	0.33 ± 0.03	0.48 ± 0.01	0.45 ± 0.03	0.39 ± 0.01	0.41 ± 0.01
MMDA	0.37 ± 0.03	0.36 ± 0.02	0.47 ± 0.01	0.41 ± 0.10	0.37 ± 0.02	0.42 ± 0.02
DANN	0.33 ± 0.04	0.37 ± 0.01	0.46 ± 0.03	0.48 ± 0.04	0.38 ± 0.03	0.43 ± 0.01
CDAN	0.42 ± 0.02	0.35 ± 0.01	0.41 ± 0.01	0.49 ± 0.01	0.38 ± 0.04	0.43 ± 0.02
DIRT	0.37 ± 0.02	0.28 ± 0.02	0.44 ± 0.04	0.42 ± 0.03	0.29 ± 0.10	0.32 ± 0.04
DSAN	0.32 ± 0.05	0.34 ± 0.02	0.41 ± 0.02	0.42 ± 0.01	0.37 ± 0.00	0.37 ± 0.02
HoMM	0.39 ± 0.02	0.35 ± 0.03	0.49 ± 0.02	0.48 ± 0.02	0.42 ± 0.01	0.43 ± 0.00
CoDATS	0.28 ± 0.04	0.35 ± 0.02	0.44 ± 0.06	0.50 ± 0.02	0.40 ± 0.01	0.39 ± 0.00
AdvSKM	0.39 ± 0.01	0.36 ± 0.04	0.50 ± 0.01	0.48 ± 0.00	0.34 ± 0.06	0.43 ± 0.00
SASA	0.26 ± 0.09	0.21 ± 0.06	0.08 ± 0.11	0.00 ± 0.00	0.00 ± 0.00	0.00 ± 0.00
CoTMix	0.09 ± 0.02	0.14 ± 0.01	0.28 ± 0.03	0.17 ± 0.02	0.21 ± 0.03	0.23 ± 0.07
TADA	0.19 ± 0.07	0.30 ± 0.01	0.41 ± 0.01	0.52 ± 0.01	0.52 ± 0.00	0.53 ± 0.01

6.4 Discussion

Domain adaptation in conjunction with curriculum learning improved subject generalisability, and linear training reduced class bias compared to fine-tuning. High classification performance was achieved using these techniques, outperforming transfer learning models pretrained from larger open-source datasets.

Previous attempts to use phasic information for locomotion classification applied phase-only classifiers to pre-process raw signals and segment them into temporally relevant sections (Negi et al., 2020; Morbidoni et al., 2019; Huang et al., 2009). Such ensemble approaches do not take advantage of transfer learning but add additional complexity to the process of locomotion prediction. In the presented application, curriculum learning was used to transfer knowledge from smaller temporal scales of phase-relevant information to macro-temporal scales for locomotion classification. To my knowledge, this was the first demonstration of how CL can be used for activity recognition. Evaluation metrics from curriculum trainer models were plotted in fig. 6.8 to determine if phase classification performance was predictive of locomotion classification performance. The positive and significant relationship between phase and locomotion classification suggests that phase-related information encoding benefits scaling across time scales. This experiment shows that CL provides a general strategy for global optimization function through contextual knowledge transfer. Interestingly, these benefits were observable in small sub-100ms time windows where a reduced window size often inhibits the effectiveness of machine learning algorithms to extract salient features (Smith et al., 2011).

Allowing gradients to flow back through feature extraction layers is an intuitive method for refining a neural network's biases and weights to optimise classification performance. However, in this study, fine-tuning reintroduces class and subject-relevant bias; see tables 6.8 and A.9 and tables 6.9 and 6.10. If contextually relevant informa-

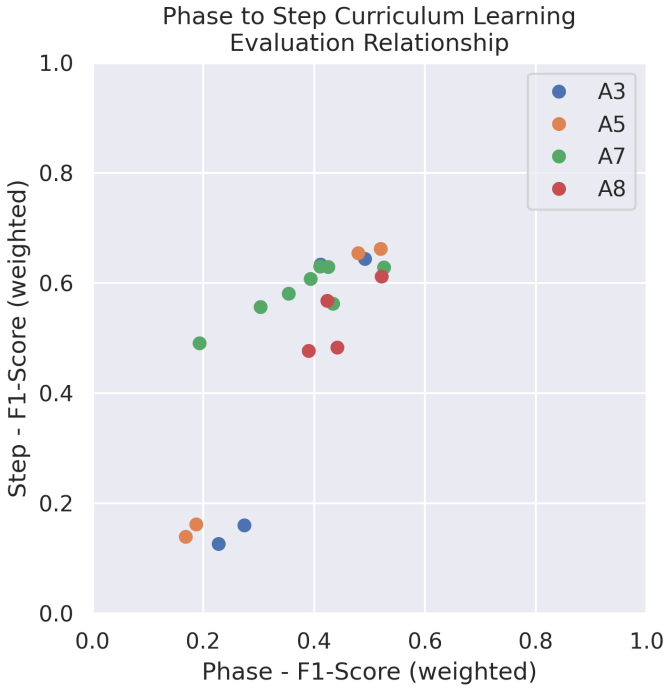

Figure 6.8: Phase and step F1-score classification metrics for curriculum trained deep learning models. High quality phase classification linearly correlated with locomotion prediction ($r = 0.82$, $p < 0.001$).

tion is learned by the feature extraction layers, simply freezing the feature extractor and linearly tuning the final classification layer can reduce the effects of bias. As an additional advantage, the feature extraction layers provide a dual use for both ends of the curriculum structure, phase and locomotion activity. However, the feature extractor must be exposed to the appropriate information to work. Simply applying a brute force approach by exposing a model to much information is insufficient to develop a strong classifier; see figs. 6.5 and 6.6.

During transfer learning, no skip connections were used, and only the final layer was used to extract features. This may reduce the generalisability of the feature extractions by being more susceptible to vanishing gradients (He et al., 2015). However, a three-layer CNN1D model is small compared to other CNN1D models (e.g. InceptionTime (Ismail Fawaz et al., 2020)), reducing the likelihood of vanishing gradients. The transfer

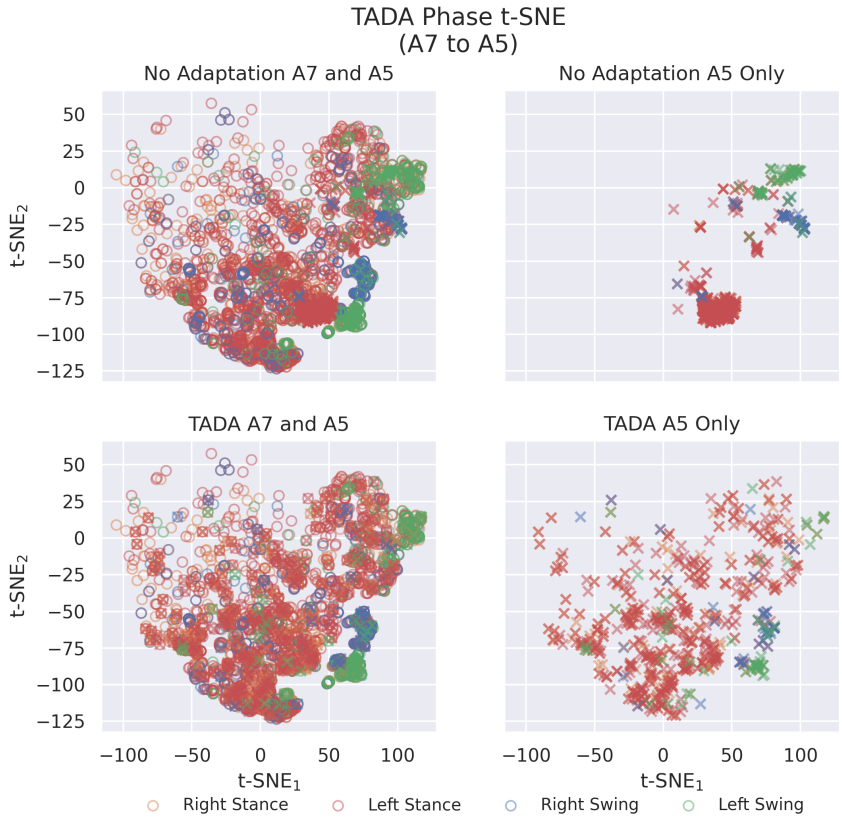

Figure 6.9: Phase related t-SNE feature representation for domain adaptation between A7 to A5. After domain adaptation, a spread across all labels can be observed. Notably, the swing phases for right and left labels are closer together and more closely resemble A7 clusters.

learning feature extraction layers may have benefitted from using residual blocks to reduce vanishing gradient effects and combine higher and lower level features (Neyshabur et al., 2020).

While data augmentation methods used in self-supervised contrastive learning were insufficient to reduce inter-subject bias, a successful method emerged in domain adaptation. This experiment's results support the hypothesis that inter-subject variability could be bridged by adequate disruption to the feature extraction layers. Bridging the domain gap between subjects can be illustrated by the figs. 6.9 and 6.10.

From the CNN1D domain adaptation methods, the top performing algorithm, HoMM, incorporated distribution moment matching calculations in multiple orders to minimise

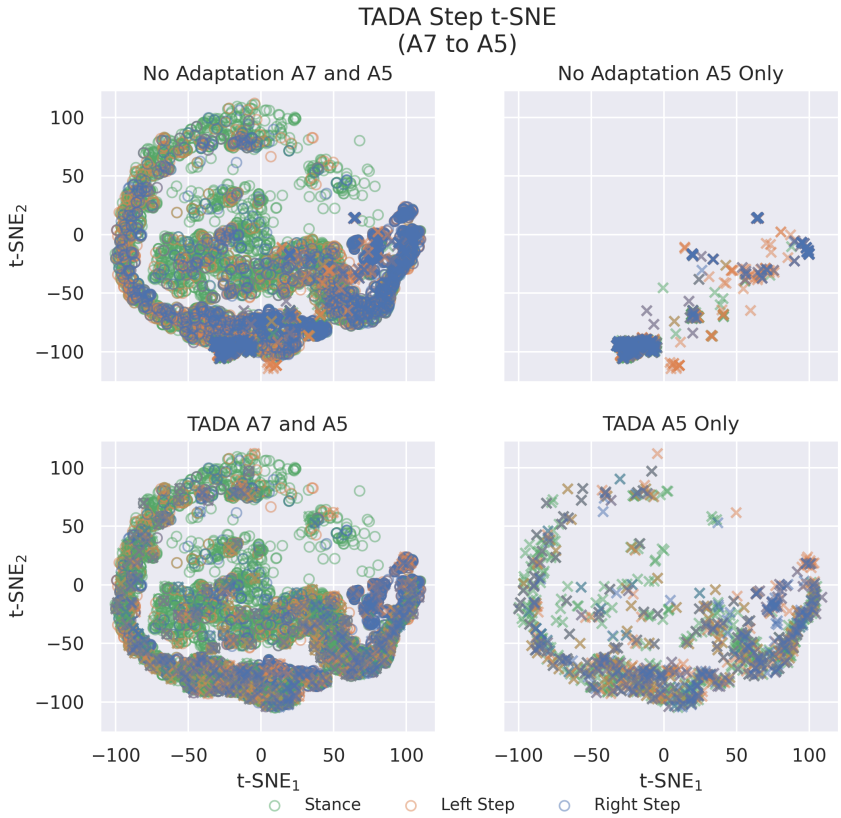

Figure 6.10: Step related t-SNE feature representation for domain adaptation between A7 to A5. After domain adaptation, a greater spread across labels can be observed with right step and stance labels more closely resembling A7 clusters.

the statistical distance between source and target distributions (Chen et al., 2019). Previous studies using mean-maximum discrepancy (MMD) have shown strong feature representation kernels for complex univariate multi-label problems (Chu et al., 2023). In this experiment, reducing the means in the third-order tensor product effectively reduced the domain gap between subjects. These results suggest that adversarially introducing randomisation during curriculum learning improves generalisation and enhances diversity (Neyshabur et al., 2020).

The highest performing strategy, TADA, operates on mapping short to long-term temporal information at a single sample point granularity (Yi et al., 2024). The loss function operates by training a domain discriminator with gradient-reversed domain loss for samples from 1 – N-1, where N is the number of time steps. A second loss function

classifies the final sample, N, with cross-entropy loss. Perhaps this method of temporal mapping creates better embeddings for feed-forward locomotion activity compared to CNN1D methodologies.

6.5 Conclusion

This study shows, for the first time, the effectiveness of curriculum learning in the scope of movement classification using multivariate EMG signals. To effectively capture stochastic multivariate biological signal activity, the feature extraction layers must be exposed to a suitable set of inputs. Curriculum learning with domain adaptation was able to sufficiently select a better set of parameters than pretraining on large volumes of datasets. Inter-subject variability can be bridged using inter-subject domain adaptation techniques.

CHAPTER 7

ELECTROPHYSIOLOGICAL BIO-MARKER OF THE FUNCTIONAL STATE OF SPINAL CIRCUITRY

A mid-thoracic SCI severely impairs activation of the lower limb sensorimotor spinal networks, leading to paralysis. Various neuromodulatory techniques, including electrical and pharmacological activation of the spinal networks, have restored locomotor function after SCI. I hypothesised that combining self-training in a natural environment with ES, quipazine, and strychnine would result in greater activity in a cage environment after paralysis than either intervention alone. To assess this, I evaluated the relationship between the change in recorded activity over time and motor-evoked potentials (MEPs) in animals receiving treatments. The combination of ES, quipazine, and strychnine (sqES) generated the most significant level of recovery, followed by ES + quipazine (qES). In contrast, ES + strychnine (sES) and ES alone showed the slightest improvement in recorded activity. Further, I observed an exponential relationship between the late response (LR) component of the MEPs and spontaneously generated step-like activity. Data demonstrated the feasibility and

potential importance of quantitatively monitoring mechanistic factors linked to activity dependence in response to combinatorial interventions compared to individual therapies after SCI.

7.1 Introduction

The instrumental works of Cajal and Golgi developed our understanding of the CNS today under the 'Neuron Doctrine' hypothesis. At the time of inception, the 'Neuron Doctrine' pushed the idea of discrete neurons acting in concert to output complex patterns and behaviour, challenging the 'Reticular Theory', that being the CNS consisting of and behaving as a singular continuous network (Burke, 2007). The debate was settled in favour of the 'Neuron Doctrine' after Sir Charles Sherrington presented a set of lectures summarising his work on reflex and sensorimotor coordination, including the reciprocal inhibition, in decerebrate cats (Stuart and Hultborn, 2008). Sherrington's work showed the impact of sensory integration and how the 'integrative action' of external stimulus can express coordinated rhythmic activity. While evidence of the CPG has been clearly expressed in quadrupeds and fish, only recently have we begun to see evidence of synthetic activation of the locomotor CPG and persistence in SCI neural circuitry in humans (Grillner, 2011; Grillner and El Manira, 2020; Minassian et al., 2023). Descending supraspinal and ascending afferent sensory information integrate at spinal locomotor centres, but the interactions of critical supraspinal and sensory inputs after spinal cord injury still need to be fully understood (Capogrosso et al., 2016; Tolmacheva et al., 2017). Even today, with the advances in optical, genetic, and electrical recording techniques, the architecture and precise mechanisms behind the CPG remain elusive (Burke, 2007).

The locomotor CPG has been hypothesised as a persistent neural substrate across bony vertebrates, visible through biological evolution. The current research landscape

conveys uncertainty behind why the CPG exists in the first place. First, one must appreciate the complex high dimensionality of vertebrate neurological architecture and the built-in anatomical redundancies towards function movement. Upon doing so, questions about why similarities between intra-and inter-subject subject neural outputs and behavioural expression arise (Whiting and Bernshtein, 1984; Latash et al., 2010). These mysteries have remained unanswered. Recent works have suggested an 'optimality principle' as reasoning for how spinal reflexive circuitry integrate and form locomotion pattern (Ryu and Kuo, 2021). A summary of the above information is illustrated in fig. 2.8.

It is intuitive to consider off-loading repetitive operations to local circuitry, reducing the energy load of higher operating neural centres for other activities (Bizzi et al., 1991; Giszter and Hart, 2013; Giszter, 2015; Hart and Giszter, 2010; Flash and Hochner, 2005; Grau, 2014; Edgerton et al., 2004; Mussa-Ivaldi and Bizzi, 2000). Moreover, the sensorimotor networks have been shown to operate on a feedforward paradigm (Wagner and Smith, 2008; Giboin et al., 2020; Hosseini et al., 2017; Prochazka et al., 2017; Gerasimenko et al., 2018). In the healthy spinal cord, sensory feedback information has predominantly understood to play a tone and reflex role (Dzeladini et al., 2014; Rossignol and Frigon, 2011). However, the significance and modulatory effect of the sensory information entering spinal locomotor circuitry dominates when no supraspinal or trans-lesional activity enters (Edgerton and Roy, 2009a; Rossignol and Frigon, 2011).

Modelling work by Ryu and Kuo (2021) showed that motor commands could be executed in feedforward or feedback-only operands. Although best when incorporated together, each had its pitfalls. Feedforward, or endogenous time-based rhythm only, were susceptible to falling due to process noise. Rhythm generation in a noisy environment can disrupt the desired gait pattern, developing a mismatch. Thus, executing based on sensory feedback is better under noisy conditions. Although, using feedback only had

similar problems when introducing noise from sensory inputs.

Now understanding the significance of the exchange between the feedforward neural substrate and feedback, essential questions regarding the role of sensory integration arise. How do different sensory inputs integrate into the CPG, and what is the neurological environment necessary to drive coordinated sensorimotor expression?

In a healthy animal, descending activity from the brain activates locomotor centres with tonic input, allowing the local spinal networks to modulate sensory information and achieve a balanced excitation-inhibition environment to propagate forward stepping (Capelli et al., 2017). After SCI, the excitatory connection becomes mute, and the locomotor networks, although capable of generating the relevant activity, do not have the adequate environment to drive coordinated motor outputs (Taccola et al., 2018). However, task-dependent sensory activation alongside neuromodulatory therapies of the spinal circuitry has shown to reorganise and enable some activity recovery after SCI.

The reorganisation of the transected spinal cord has been thought to be due to the task-dependent sensory inputs exposed during specific training protocols (Gerasimenko et al., 2007; Edgerton et al., 1997a). The CPG has specifically seen reinforcement of activity during load-bearing activity, expressing switched Ib-reflex modes and facilitating stance and swing phase transition (Pearson, 1993). Thus, load-bearing activity appears critical to exploiting CPG mechanisms for locomotor recovery. In conjunction, cutaneous afferent inputs can inhibit flexion generation during the swing phase, facilitating extensor activity during loading (Jankowska et al., 1967). Given the long phase stance period, it makes sense for locomotor centres to contain robust neural mechanisms for maintaining kinematic balance. Additionally, hip flexor proprioceptive activity and contralateral step cycle phases are critical for swing (flexion activity) initiation (Grillner and Rossignol, 1978; Lam and Pearson, 2001).

Extensive animal model evidence has supported the hypothesis of task-dependent

sensorimotor recovery in the injured spinal cord (Kobayakawa et al., 2019; Hodgson et al., 1994; Edgerton and Roy, 2009a). Notable examples describe the effect of standing vs. stepping activity training in rodents (Hodgson et al., 1994). Spinally transected cats trained to stand had difficulty generating hindlimb locomotion, and vice versa; cats trained to step could not maintain standing. Similar results were reported in the forelimb activities; rats saw improvements in skilled reaching after training but poor performance during ladder walking (Jin et al., 2021). Investigations with neuromodulation synergies paralleled activity-dependent results (Fong et al., 2005; Cai et al., 2006). The sensory-dominant neurological environment requires sensory information to benefit from neuromodulation therapies.

Task-specific recovery shows the adaptive and learning behaviours of the spinal cord. Spinally transected neonatal rats learned to walk on a treadmill in multiple directions, including forward, sideward, and backward orientations (Shah et al., 2012). Spinally transected rats could also adapt to external trip perturbation by increasing flexor activity (Zhong et al., 2012), which means that before initiating the swing phase, the spinal neural circuits reprogrammed the swing trajectory to overcome the obstacle and maintain stability while propagating forward momentum (Ryu and Kuo, 2021). Similarly, the sensorimotor circuitry requires some variability in the kinematic trajectory to elicit favourable learning (Ziegler et al., 2010). Current hypotheses behind this mechanism incorporate some feedforward-feedback mismatch in forward propulsion, thus adapting relevant circuits to deal with perturbations. The feedforward system adjusted the neural activity to adjust the kinematic projection of the limb, using information from the sensory feedback system.

Research conducted on complete spinal transected cats challenged the hypothesis of task-specific recovery reorganising lumbosacral locomotor centres towards functional recovery (Harnie et al., 2019). After surgery and recovery, cats were separated into a

group receiving manual therapy, a group receiving locomotor treadmill training, and a group that received no treatment. All cats, regardless of receiving interventional therapy, recovered hindlimb locomotion. Standing activity also spontaneously recovered. The authors concluded that the return of sufficient excitability within spinal sensorimotor circuits was more likely the cause of hindlimb locomotor recovery than the rearrangement of neural circuitry trained by ensembles of task-specific sensory inputs. Although sensory information was necessary to entrain locomotion, recovery was not dependent on task-specific training (Alluin et al., 2015). The kinematic displacement range was no different between trained and untrained rats, but the expression of locomotor patterns in trained rats was significantly more coordinated than in untrained rats. Though requiring a considerable number of repetitions of weight-bearing locomotor training may be contentious, the neural adaptations occurring in the spinal cord due to sensory afferent inputs are evident.

Genetic labelling work has unravelled some insights on the necessary neurological components towards locomotor recovery after SCI. Bui et al. (2016) studied the nature of dI3 interneurons during locomotion. dI3 INs are excitatory neurons, receiving monosynaptic input from low threshold sensory afferents and proprioceptive afferents (Tuan et al., 2013; Bui et al., 2016). Projections synapse to ipsilateral MNs rostrocaudally via ventrolateral and dorsal funiculus (Lu et al., 2015; Stepien et al., 2010; Avraham et al., 2010). Genetic ablation studies showed that dI3 INs were not necessary for locomotion in healthy rats but for training-induced recovery following spinal transection, (Bui et al., 2016). Similarly, V2a INs, glutamatergic INs receiving serotonergic projections from the brainstem, primary afferents, and other INs, have been identified as crucial restorative IN for locomotion recovery during epidural stimulation therapies in mice (Heng and de Leon, 2007).

Neuromodulation therapies have brought about new protocols and scientific studies

about their dose-response, mechanisms of action, and clinical relevance (Guan et al., 2018; Taccola et al., 2018; Zheng et al., 2020; Cote et al., 2017; Micera et al., 2020; Courtine and Sofroniew, 2019). Some methods have offered 'inducing' the desired kinematically expressive outcome by surpassing the motor activity threshold either electrically or pharmacologically. Induced activity evokes activity in the hypothesised targets, dorsal roots (Bonizzato et al., 2018; Wenger et al., 2016; Capogrosso et al., 2013). However, this method floods ortho- and antidromic pathways into hyperpolarisation, limiting the ability of sensory receptive spinal INs to access sensory afferent inputs and bidirectionally transmit IN activity (Formento et al., 2018).

As discussed, primary afferent proprioceptive and cutaneous in synergistic agonist muscle groups have significantly benefited mammalian locomotor recovery. Yet, subjects receiving these forms of therapy appear to achieve incredible success in achieving sensorimotor recovery. Some methods to circumvent the muting of sensory activity involved engineering specific stimulation patterns to allow propagation of sensory activity (Formento et al., 2018; Moraud et al., 2016). Maintaining such granular precision in stimulation accuracy towards coordinated gait patterns has been impressive.

While the results from neuromodulatory therapies have been promising, I suggest thoroughly investigating combinatorial approaches and understanding the effects of each pharmacological agent in conjunction with electrical stimulation and task-specific physical therapies. Understanding the underlying mechanisms allows full exploitation of the CPG and natural sensorimotor pathways that lay dormant in SCI neural circuits.

7.2 Background

Numerous studies of different animal models of spinal cord injury have demonstrated that modulating the physiological states of spinal networks, pharmacologically and electrically and in combination with motor training enables improved motor performance

(Edgerton et al., 2004; Ichiyama et al., 2005; Gerasimenko et al., 2008; Lavrov et al., 2008b; Courtine et al., 2009).

Several works have investigated the locomotor capacity of the spinal cord across animals and humans (Edgerton et al., 1976, 1991; Harkema et al., 2011). Taccola et al. (2018) put forward a hypothesis where ES does not 'induce' movement via dorsal root activation but rather 'enables' movement by elevating relevant spinal networks towards a more excitable state. By doing so, appropriate sensory commands can initiate coordinated movement via the feedforward-feedback mechanisms discussed above (Angeli et al., 2014; Danner et al., 2015; Rath et al., 2018; Gill et al., 2020b).

Quipazine, a serotonin agonist, has been regularly proven to significantly improve stepping performance in spinally transected animals and humans (Gad et al., 2015; Courtine et al., 2009; Radhakrishna et al., 2017). Reasons for this may be due to the innate connectivity of the CNS. Serotonergic pathways from the brainstem descend into lumbosacral networks to apply some tonic signal and signal locomotor activity (Jacobs and Fornal, 1993; Cabaj et al., 2017). Serotonin receptor subtypes contribute towards locomotor rhythm generation and assist in recovering locomotor activity (Kim et al., 2001; Landry et al., 2006). Moreover, these receptors differentiate from other subtypes in their ability to activate locomotor relevant pathways (Barbeau and Rossignol, 1990). Serotonin agonists have been shown to increase flexor and extensor amplitude, facilitating weight support and step length with increased sensitivity to cutaneous reflex excitation (Gackière and Vinay, 2014). These effects have been recorded in a sub-threshold manner, without triggering fictive locomotion in animal preparations (Barbeau and Rossignol, 1987).

Strychnine, a glycinergic antagonist, has improved the stepping ability of poor step-performing cats (Edgerton et al., 2004; de Leon et al., 1999; De Leon et al., 1998b). Glycine receptors represent some of the densest populations in the deep dorsal horn (Gradwell

et al., 2023). The critical reciprocal inhibitory pathways express dense populations of glycinergic activity, implying coordination reliance on the appropriate timing of inhibitory activity (Zhang et al., 2014; Lu et al., 2015). Over expression of glycinergic activity may lead to an overly inhibited network, reducing the likelihood of locomotor initiation and progression. Strychnine restores the ability to step after some step training period in spinal transected cats, but the same was not achieved after administration to stand-trained cats (de Leon et al., 1999). These results imply selective glycinergic gating or adaptations according to the task trained.

Several studies have investigated the synergistic effects of neuromodulation Edgerton et al. (2008). These ideas were first explored in Gerasimenko et al. (2007), quipazine and ES were combined and shown to differentially modulate flexor and extensor networks, facilitating locomotion activity in spinally transected rats. These therapies have a summing effect on their efficacy, and individually they could not positively impact locomotion (Ichiyama et al., 2008b; Courtine et al., 2009).

Studies performed on humans with serotonin agonists and ES showed mixed results where some populations had no difference (Freyvert et al., 2018) whilst others had synergistic (Gad et al., 2017) or differential (Lavrov et al., 2008b, 2006) effects. Moreover, these studies found polysynaptic activity in motor-evoked potentials (MEPs) correlated with improved locomotor performance. These polysynaptic drives could indirectly provide compensatory excitation to local spinal networks and endogenously rebalance excitation-inhibition (Musienko et al., 2013; Gad et al., 2015).

In this study, I aim to answer the following questions. Do spinally transected rats in an enriched cage environment express differences to synergistic neuromodulatory therapies? Secondly, do late-response MEPs correlate with the spinal functional state during identified events? I hypothesise that multiple neuromodulatory modalities can transform non-functional spinal networks into more excitable physiological states to

enable 'self-training' in freely moving spinally transected rats. Additionally, MEPs could present a functional biomarker towards the mentioned physiological states (Gad et al., 2015; Lavrov et al., 2008b).

7.3 Methods

A select number of therapies were considered for analysis. Included were the baseline data without any therapy (Pre), electrical stimulation (ES), strychnine and ES (sES), quipazine and ES (qES), and the combination of strychnine, quipazine, and ES (sqES).

The Rule-Based algorithm described in chapter 4 was used to classify the data set specified from chapter 3. The better rejection of false positive stepping data and rapid result turn-around was deemed more appropriate when considering time-cost.

Individual bursting activity within each step was sorted into the swing phase of the stance phase accordingly. Signal statistics and features for each unilateral step identified were calculated to gain insight into the effect of each therapy. IEMG of each burst and phase of gait was calculated per table 4.2. The stance period was considered the active time of bursting soleus activity during stepping.

Within each identified step, MEPs were extracted from the bandpass-filtered EMG data for each channel. Using a recording of the stimulation pulses, the end of each 40Hz stimulation pulse was used to separate the EMG signal into 25ms MEPs. The early response (ER), middle response (MR) and late response (LR) time windows were defined as 1–4ms, 4–7ms and 7–25ms, respectively fig. 7.1. A second-order differential threshold was used to detect the peaks and troughs of the MEP signal successfully. Each MEP was upsampled to find the local maxima and local minima. The minimum separation of 0.6ms and minimum prominence of 0.2 were used to filter through a second-order differential threshold of 1.5×10^6 such that only peaks and troughs that met the threshold criteria were accepted fig. 7.1. This was used to calculate the total number of peaks in each MEP.

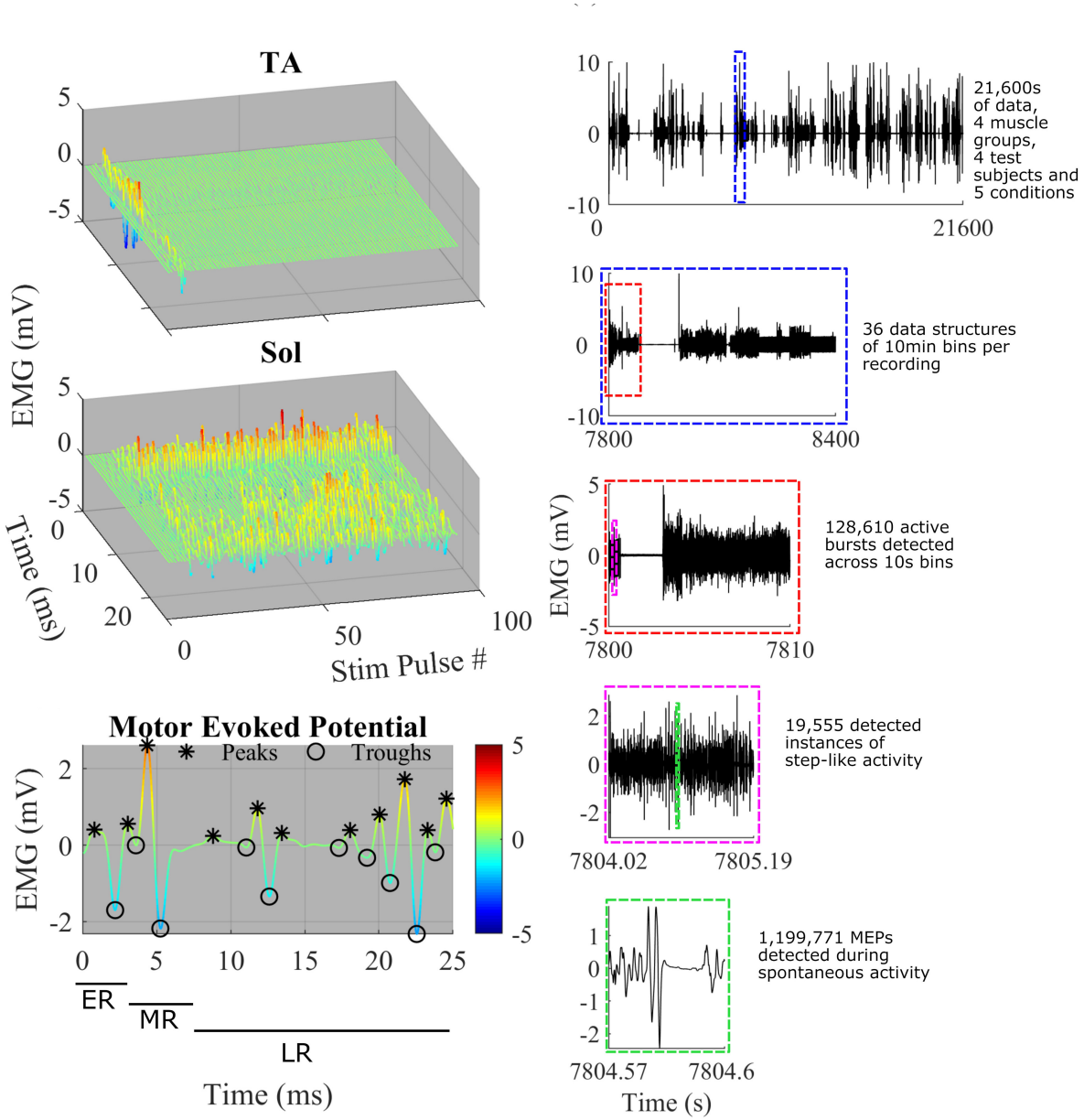

Figure 7.1: The left column details a singularly identified step using the TOKEDA method as summarised in chapter 4. This plot illustrates motor evoked potentials (MEPs) over time for the Tibialis Anterior (TA) and Soleus (Sol) respectively. The bottom left illustrates a representative MEP from the TA recording shown in the example step. Colour scaling reflects amplitude in mV. Note the windows marking the early, middle and late responses and peaks (*) and troughs (o). On the right side is a breakdown of the volume of data involved within the experiments and the process of data structure and analysis.

All data reported as means ± standard error (SE). Statistically significant differences were determined using a one-way ANOVA with the Tukey-Kramer posthoc test, and correlation coefficients were calculated using Pearson's linear coefficient. All statistical difference was set at $p < 0.05$. All results reporting step-like activity were normalised to no intervention (Pre) measurements.

7.4 Results

7.4.1 Electropharmacological treatmenets modulate functional state of spinal circuitry

All interventional conditions increased the number of spontaneous step-like activities compared to baseline (Pre) fig. 7.2. Quipazine or strychnine significantly increased recorded step-like activity in all animals tested. A significant level of variability was observed amongst rats, especially in the qES and sqES experiments. However, the sqES treatment generated the highest number of steps recorded compared to Pre and ES ($p < 0.05$).

Since a single bolus dose of a pharmacological treatment was administered at the start of the experiment, a time-depended phenomenon in the number of steps detected was observed. The greatest counts of activity were seen in the first 120 min fig. 7.3. These observations were specific to the rapid registration of step-like activity for sqES and qES treatments figs. 7.3 and 7.4. This time-dependent phenomenon was not observed in Pre or ES cases. The stepping activity occurred stochastically throughout the 6 hrs figs. 7.3 and 7.4. Spontaneous step-like activity during the first 120 min occurred with longer, more consistent step lengths and increased muscle activity during sqES and qES. During continuous stepping activity, an average stance period of ~2 sec was observed fig. 7.3. Both the step activity and stance period across the population had lower variability

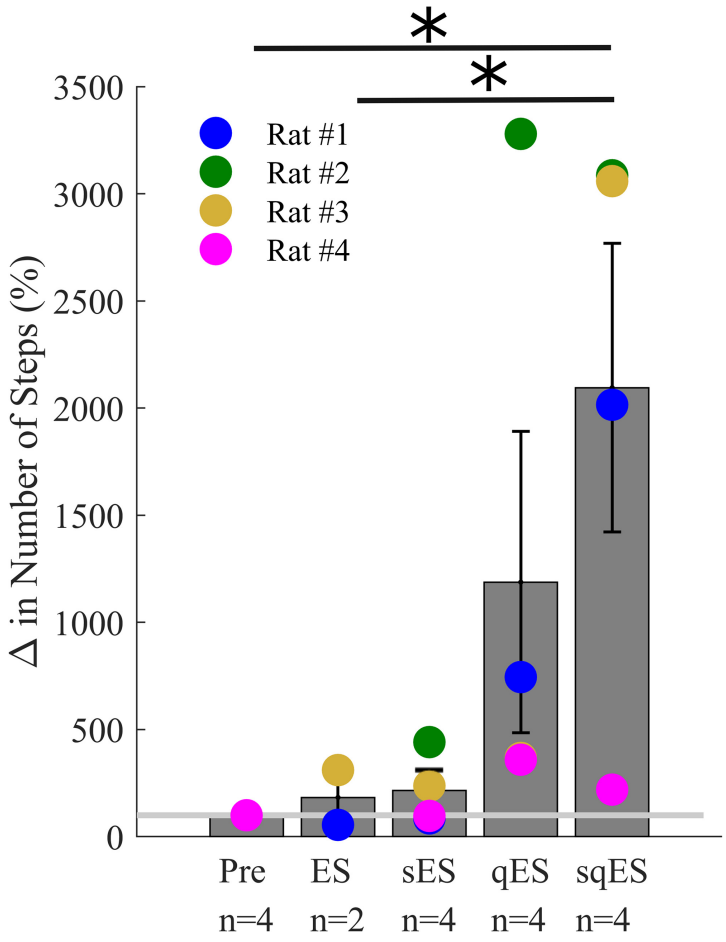

Figure 7.2: Mean % change in step-like events for each rat over the 6-hr period for each treatment (*). The light gray line is set at 100%, normalised to pre-treatment for each rat. Results for sqES were significantly different compared to Pre and ES ($p < 0.05$).

during sqES compared to other conditions tested. A smaller variance was present in the sqES stance period compared to qES within the first 2 hrs. In addition, during the entire 6-hr period, overall left-right symmetry was maintained suggesting a bipedal response fig. 7.3.

Including multiple pharmacological agents in the presence of ES they resulted in a more consistent and greater IEMG response fig. 7.4. While sES reduced the variability across both extensor and flexor muscles in the hindlimbs, the inclusion of quipazine significantly increased IEMG magnitude compared to Pre ($p < 0.05$) figs. 7.4 and 7.5. For the ES and Pre treatments, the IEMG of TA differed in shape compared to Sol with

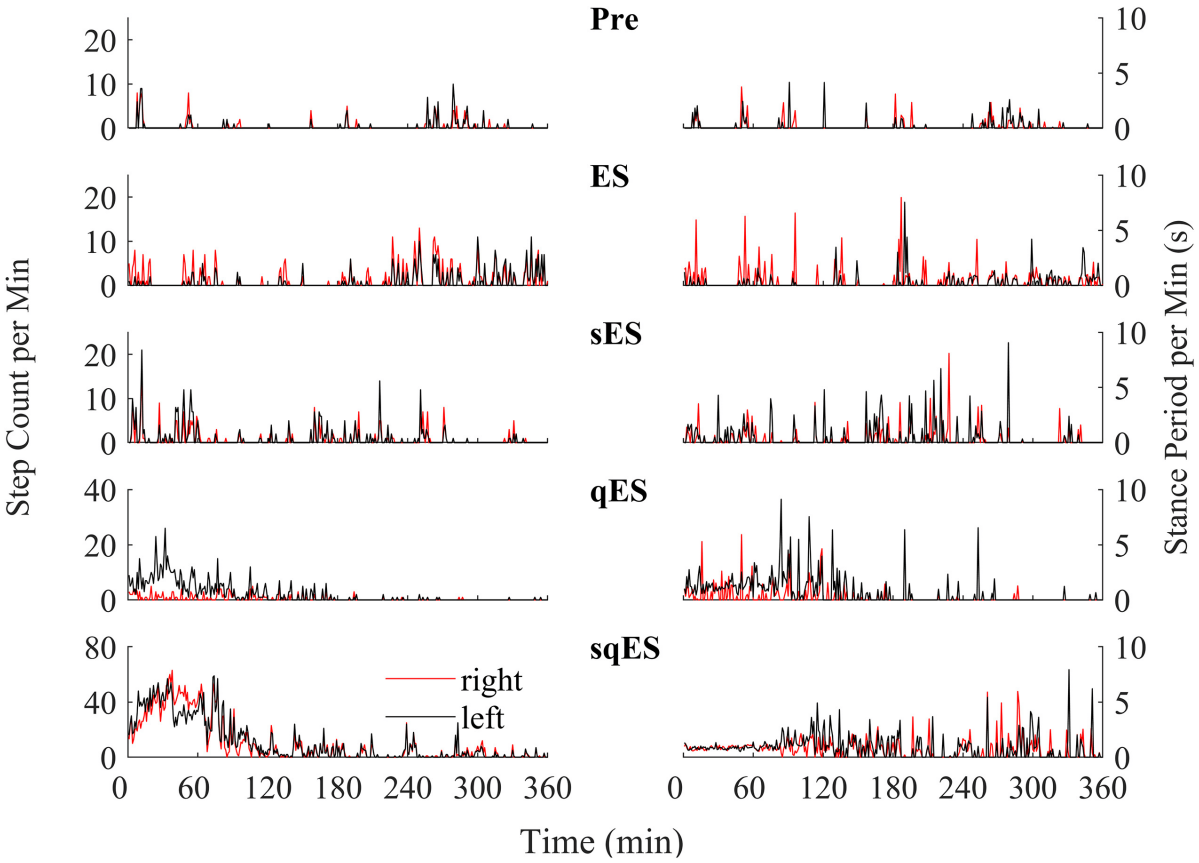

Figure 7.3: An example of the step-like activity across interventions plotted as number of steps per minute and mean stance periods for the left (black) and right (red) hindlimb for rat #3. For other subjects see figs. A.11 to A.13.

wider error bands while the sES, qES and sqES relatively coordinated activity in the TA and Sol muscles with narrower error bands were observed fig. 7.4. Differences between TA and Sol may be explained by the higher occurrence of co-contractions and organised coordinated activity during the pharmacological interventions. The steep gradient was only observed during the first 2 hrs of sqES and qES and became more linear during hours 2 to 6, possibly indicating the effective half-life of the drug.

A significant correlation was observed between the overall muscle activity (IEMG) and the steps registered across both right hind-limb muscles (fig. 7.5, $p < 0.05$). The Sol channel for sqES and qES significantly differed from Pre ($p < 0.05$). There was an increasing mean and standard error trend in IEMG in both TA and Sol as more

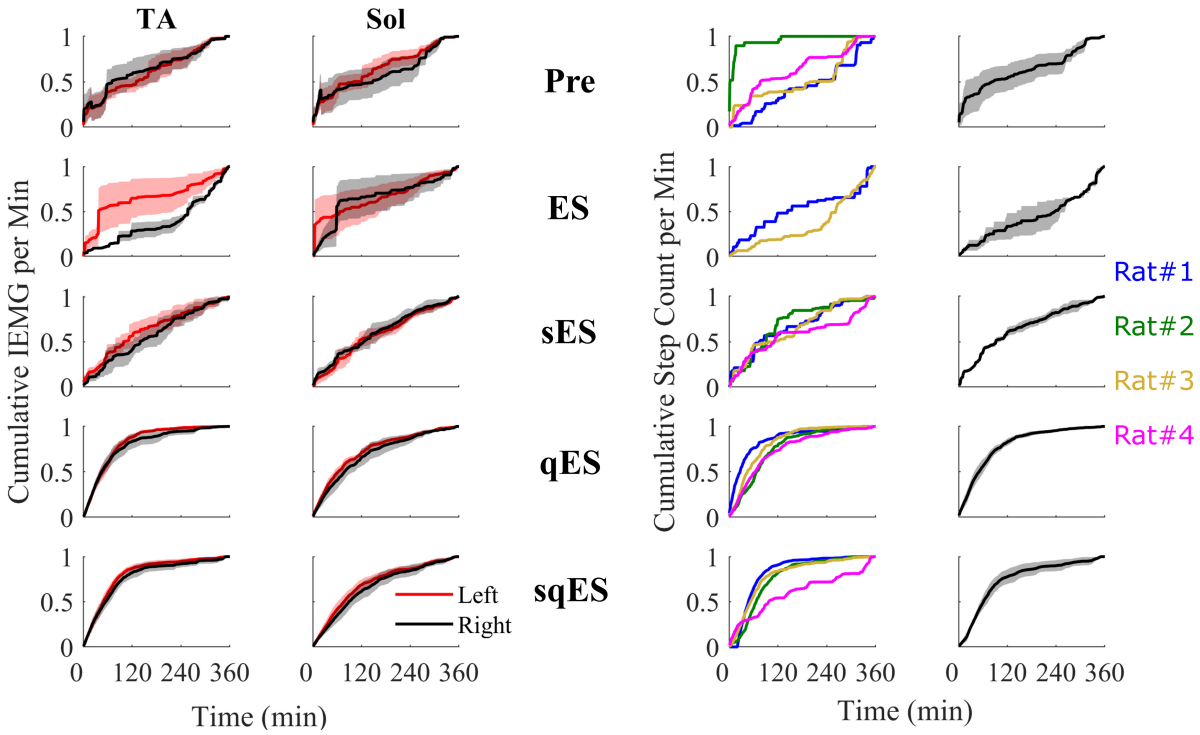

Figure 7.4: All cumulative sum plots are normalised per animal from 0 to 1. On the left is the cumulative sum of IEMG in the left and right TA and Sol. The third column from the left is the cumulative sum plot of step-like events occurring over time for each treatment and each rat. The final column shows the averaged cumulative sum plot, shaded is the standard error.

interventions were introduced on top of ES. Both sqES and qES have an exponential relationship between IEMG and step-like activity, whilst sES, ES and Pre reflect a linear correlation, see fig. 7.5. sqES intervention had the largest standard error across the x and y axes of fig. 7.5 whereas sES and Pre have a minimally discernible spread amongst the sampled population. Increased baseline tone in Sol during rest correlates ($R = 0.6943$, $p < 0.05$) with the increased step-like activity across all conditions and rats and is consistent with the overall summed IEMG across the 6-hrs (fig. 7.5). The inclusion of pharmacology and ES increases the ln(Sol) threshold. Only qES and sqES have a drastic change in detected step-like events.

Given the logarithmic response in the basal tone in Sol represented fig. 7.5, there appears to be a breakaway condition. A Pearson's linear correlation coefficient reveals

a significant positive correlation in all interventions for both hind-limbs ($p < 0.05$ in all cases). While the sES, ES and Pre interventions are linearly correlated, the qES and sqES have an exponential relationship between the natural log of the Total IEMG / 10-min and the step-like events / 10-min. Note that sqES, qES and ES have a distinct y-axis error bound while the x-axis error bound is less notable. This is especially notable in the RSol graph fig. 7.5.

7.4.2 Evoked reponses correlate with spontaneous step-like activity

MEPs were analysed across the soleus during spontaneous step-like activity as these signals more accurately reflect the state of the neural networks associated with the trained task. The detected peaks in the middle and late responses (MRs and LRs) of the soleus during spontaneous step-like activity in their home cages were exponentially correlated (fig. 7.6). Due to the sub-threshold nature of spinal stimulation, the evoked responses appeared non-time linked to the stimulation pulses compared to suprathreshold stimulation on a treadmill (Gad et al., 2013c). Each treatment had linear regression applied to both the LRs and MRs. ES and sES display a negative gradient associative with decreasing change in step-like activity compared with Pre, whilst qES and sqES have a steep positive slope. Combining all data points was fitted to an exponential equation where the LRs and MRs have a similar relationship with step-like activity. The MR trend has a lower first-order coefficient when compared to the LR. As anticipated, the sqES and qES evoked the highest number of LRs and MRs, corresponding to a greater number of detected spontaneous step-like activities.

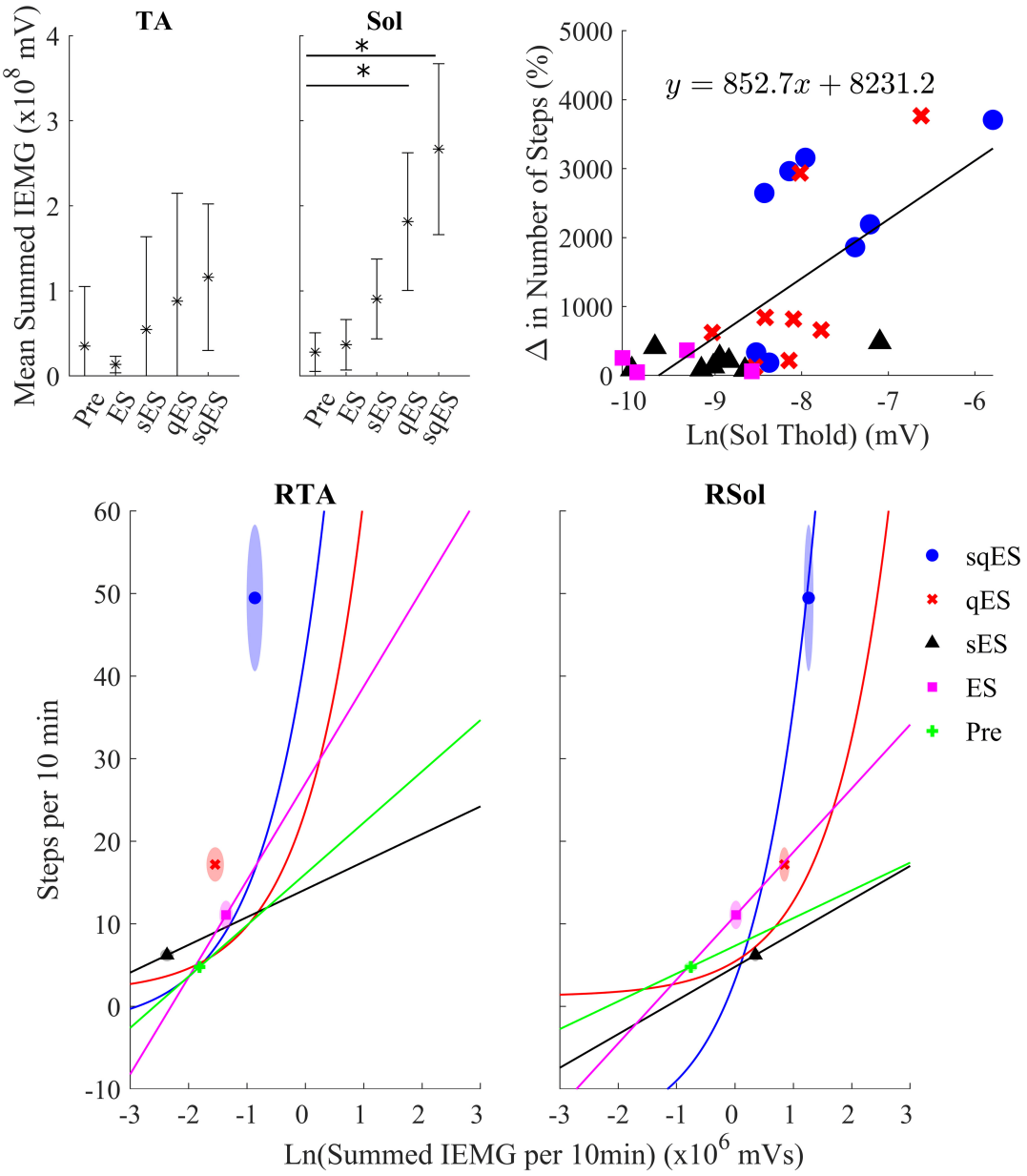

Figure 7.5: Top left shows the average sum of IEMG across all the animals in each treatment in the TA and Sol channels for both sides and the 95% confidence interval. Top right figure depicts the relationship of the calculated EMG amplitude threshold required to determine burst activity of the neural networks in the Sol and the change in step-like activity normalised to pre intervention for all rat subjects in both hindlimbs. Bottom left and right plots Ln(Total IEMG / 10min) against step-like events / 10min across 6 hrs for sqES, qES, sES, ES and Pre in the right hind-limb. In the corresponding shaded area is the standard error for the x and y axis represented in an ellipse.

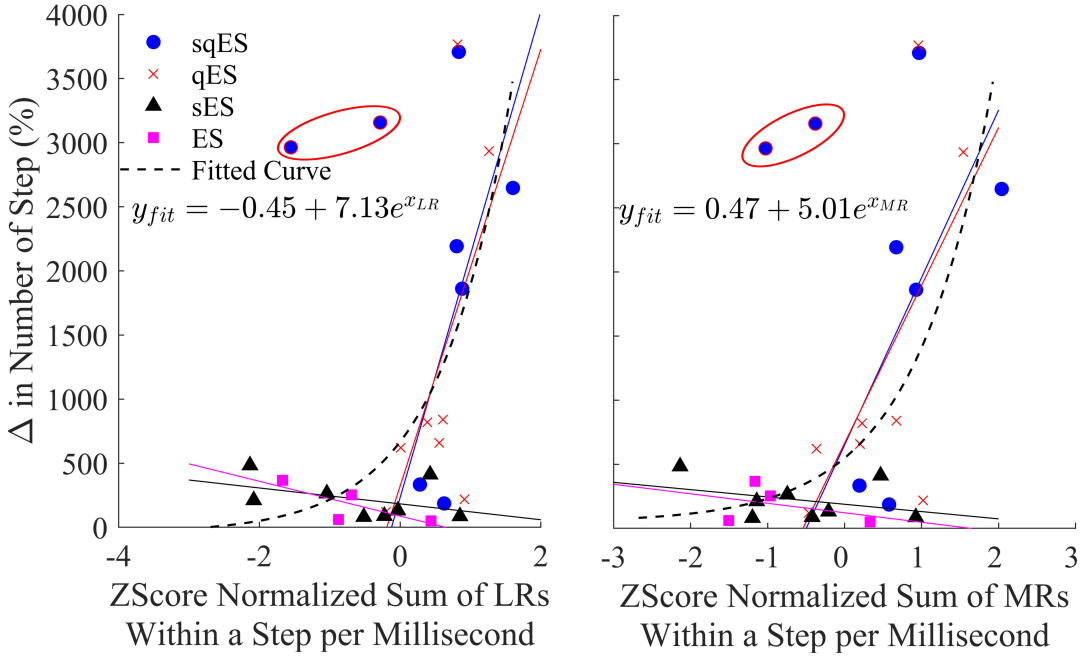

Figure 7.6: Left shows the change in number of late and on the right, middle peaks responses (normalised to pre values) for each rat, treatment, left and right hind-limb of the Sol MEPs. Circled in red are two outliers identified as rat number 3 during the sqES treatment. Additionally, linear regressions for each of the respective treatments in their corresponding color are plotted. An exponential curve (dashed line) encompasses all treatments.

7.5 Discussion

In this study, I have demonstrated the effects of different neuromodulation therapies in synergy across 4 spinally transected rats by monitoring step-like activity in chronic EMG recordings. Results from the study suggest serotonergic activity is a key contributor towards elevating levels of excitability in the isolated spinal cord and balancing. For the first time, I demonstrated the time-dependent expression of enabled behaviour in rats receiving synergistic neuromodulatory therapies. Analysis of electrophysiological activity during registered time windows of step-like events indicated activity in the soleus to be critical towards self-training. Finally, I provide evidence of polysynaptic activity in spinal MEPs as a biomarker of the functional state of the isolated spinal cord.

Access to neuromuscular activity synchronised with stimulation pulses directly linked to behaviours provides a direct and realistic measurement of reorganising neural networks throughout a chronic period as the nervous system becomes more functional (Edgerton et al., 2008). As the MEPs and associated behaviour are directly linked from an 'input-output' relationship, I hypothesise that a biomarker for the reorganisation may be discernible from the presented data. This notion has been reflected in past research papers (Lavrov et al., 2006, 2008b; Gad et al., 2015; Alam et al., 2017). Unfortunately, without using kinematic recordings, information such as locomotion speed, step quality, step length and other metrics remain rare, given the availability of the appropriate technologies.

Long-term recordings of electrophysiological data in laboratory animals and humans before and after treatment for a dysfunction have been performed previously (Alaimo et al., 1984). The existing hypothesis regarding the possibility of electrophysiological biomarkers is the emergence of MRs and LRs in MEPs during activity-driven training (Lavrov et al., 2006, 2008b; Gad et al., 2015). Underlying neurological mechanisms are involved in time-related modulation in MEPs during treadmill activities. Re-emergence in LR and reduced MR changes in flexor extensor motor pool modulation reflect the neural network's plasticity (Gad et al., 2015; Lavrov et al., 2006). In the present study, we explore the characteristics of the same signals during spontaneous in vivo step-like activity within an enriched caged environment. Paralleled between these findings, fig. 7.6 presents an exponentially increasing trend between the emergence of LRs and the functional response to hind-limb step training. In contrast to past research, no distinct differences were detected between LRs and MRs fig. 7.6 (Gad et al., 2015). These differences may be due to the small sample size or difference in an experimental environment. The difference in locomotive setting (treadmill vs. free-roaming) may introduce disruptions to the reorganisation of neural networks due to the loss of highly

organised and predictable sensory input patterns typically generated with step training on a treadmill (Taccola et al., 2018; Edgerton and Roy, 2009a).

Additionally, note that the highlighted outliers in fig. 7.6 were not included in the regression calculations. These data points suggest that high activity levels can occur at below-average low MEP peak counts. These outliers were measured from the same rat within the same experiment. During video data analysis, an unusual frequency of induced air-stepping was observed. The fact that some number of these counted step-like events were not enabled but instead induced by ES may result in minimal polysynaptic pathways being activated during air-stepping, i.e. when the proprioceptive and tactile afferents typically associated in over-ground, weight-bearing hind-limb locomotion were not present Grillner and Zangger (1979).

The exponential trend visible in fig. 7.6 alongside the data in fig. 7.5, present the possibility of a 'breakaway' point where the minimum level of neuronal activity and polysynaptic mechanisms are required for significant functional improvement. Only when quipazine was introduced was a significant improvement in spontaneous step-like activity observed. Given the extensive research provided with training under the influence of strychnine, one would expect that strychnine experiments would provide equal benefit when compared with quipazine (de Leon et al., 1999; Gad et al., 2015, 2013c).

Polysynaptic MEP activity may be a valuable biomarker for predicting therapy efficacy after SCI. The recovery of stochastic late-response activity coincides with the return of weight-bearing locomotion (Lavrov et al., 2006; Gad et al., 2015). Stochastic late-responses, not synchronised with ES pulse onset, indicate involvement of complex polysynaptic networks. In the transected spinal cord, these can only be excited from exogenous afferent stimuli of long lasting recurrent activations in pre-motor networks (Taccola et al., 2018). The prolongued late-responses may be explained by the longer

stance period, supplying additional afferent inputs from weight-bearing activity (Edgerton et al., 2008; Hubli and Dietz, 2013). Interestingly, the reemergence of late-response activity in sensorimotor recovery has also been observed in upper-limb MEP experiments in humans, indicating a task indepedent, common adaptation strategy across spinal sensorimotor pools (Inanici et al., 2018).

Albeit a small sample size, these data extend the hypothesis of the existence of electrophysiological biomarkers and warrant the extension of further investigation into longer-term longitudinal studies and the involvement of more robust algorithms and in vivo sensing technologies. These observations, alongside the previously discussed representation of plastic mechanisms in MEPs, agree with our initial hypothesis of multiple neuromodulatory modalities transforming non-functional spinal networks to a more excitable state to enable 'self-training'.

Presented here is a novel result of identifying step-like activity while recording electrophysiological biomarkers of stepping in chronic, cage-roaming environments. The present data provide an example of a 'proof of concept' approach to examine the level of activity dependence present when testing an intervention's efficacy. It is technically becoming more feasible to chronically record EMG from many muscles to detect how the reorganisation of neuronal networks that control locomotion can be focused on the patterns of coordination of flexion/extension, abduction/adduction and non-repetitive tasks such as grip and pinch manoeuvres as well as repetitive tasks such as cycling etc. Moreover, the ability to measure the state of the locomotive neural circuitry to determine the direct relationship between the treatment provided and the underlying neuronal mechanics serves as detailed insight as the subject undergoes training, providing the opportunity to adjust treatments to maintain an enabling effect, maximising activity-dependent recovery (Curt et al., 1998; Petersen et al., 2012).

Precise mechanisms behind these observations are currently unknown. Some expla-

nation can come from modelling the circuitry within the lumbosacral locomotor networks. Pre-motor glutamatergic dI3 INs, receiving proprioceptive afferent inputs, projecting in bilateral rostrocaudal directions via ventrolateral and dorsal funiculus, easily accessible by ES activity (Lu et al., 2015; Stepien et al., 2010; Avraham et al., 2010; Parker et al., 2020; Capogrosso et al., 2016). V2a neurons have been elucidated as key recovery INs during neuromodulatory recovery paradigms (Kathe et al., 2022). Precisely, greater extension activity seen in this study can be paralleled to the longer and stronger stance phases of serotonin-facilitated stepping during treadmill locomotion (Fong et al., 2005; Antri et al., 2003). At least for spinal transected adult rats, LRs could be considered partly due to the involvement of serotonergic neurons. Moreover, GABAergic INs in direct contact with CSF along the central canal of the spinal cord in the mouse project to what authors assume as axial pre-motor V2a INs (Nakamura et al., 2023).

Disrupting the excitation-inhibition balance led to aberrant neural states (Musienko et al., 2015). Maintaining a balance of excitation and inhibition, especially during load-bearing activity, while regulating inputs from multisensory sources appears critical to recovery and locomotion expression (Gad et al., 2015). These complex inhibitory pathways are readily positioned to adapt to incoming sensory information. Perhaps, ES and quipazine assist in returning the balance of excitation and inhibition, though the mechanisms are uncertain.

Further work may consider the following. The first steps may include replicating these results in a larger sample size. Secondly, a longitudinal study analysing the relationship between LRs, MRs, and functional kinematic expression of locomotor activity in larger complex mammals, such as non-human primates or humans. Finally, an investigation into the origins of these potential polysynaptic pathways through genetic labelling experiments or computational modelling.

7.6 Conclusion

I successfully demonstrated algorithms to detect specific functional hind-limb spontaneous locomotion using minimal biosignals while monitoring biomarkers representing a polysynaptic neurophysiological system input-output response of the spinal circuitry that controls locomotive activity. In addition, I discuss the correlation between these biomarkers and the functional responses to spinally evoked potentials.

CHAPTER 8

BALANCING EXCITATION AND INHIBITION IN THE LOCOMOTOR SPINAL CIRCUITS

Pre-synaptic inhibition after SCI has been hypothesised to disproportionately affect flexion reflex loops in locomotor spinal circuitry. Reducing GABAergic inhibition activity increased the excitation of flexion circuits, restoring muscle activation, and stepping ability. Conversely, nociceptive sensitisation and spasticity can emerge from insufficient GABAergic inhibition. To investigate the effects of neuromodulation and proprioceptive sensory afferents in the spinal cord, a biologically constrained spiking neural network (SNN) was developed. The network describes the flexor motoneuron reflex loop with inputs from ipsilateral Ia- and II-fibres and tonically firing interneurons. The model was tuned to a baseline level of locomotive activity before simulating an inhibitory-dominant and body-weight supported (BWS) SCI state. ES and serotonergic agonists were simulated by the excitation of dorsal fibres and reduced conductance in excitatory neurons. ES was applied across all afferent fibres without phase- or muscle-specific protocols. Results suggest serotonin effectively increased MN

excitability while ES tuned the excitation towards stable sensory-driven flexor activation.

8.1 Introduction

Flexor activity is critical for step progression during locomotion, acting as shock absorbers before foot strike (Akazawa et al., 1982), adapting step-height to continue locomotion progression (Zhong et al., 2012), and resetting locomotion (Schomburg et al., 1998). Conversely, having too much flexion activity can result in spastic muscle expression, leading to poor balance and coordination (Schmit et al., 2000; Little et al., 1989). Maintaining an excitation-inhibition balance of excitability emerges as an intuitive solution to enabling robust locomotor expression.

SCI interrupts normal bidirectional signalling, leading to dysfunctional neural circuitry (Beauparlant et al., 2013). Lack of descending activity keeps MNs at a predominantly inhibited state (Ghosh and Pearse, 2014) while inhibitory populations in the dorsal and intermediate zone become over-reactive (Edgerton et al., 2004). A large percentage of the SCI population experience spastic muscle activity, likely due to an uninhibited activation of GABA receptors (Bellardita et al., 2017; Dimitrijevic et al., 1986; Pinter et al., 2000; Cowley and Schmidt, 1995; McKay et al., 2011). Nevertheless, even with an overly excited or inhibited environment and detached from brain inputs, the locomotor spinal circuit can continue to express coordinated motor function given sufficient excitation and contextually relevant sensory information (Edgerton et al., 2006; Capelli et al., 2017; Taccola et al., 2018).

Proprioception is a critical sensory input to entrain and recover locomotion after SCI (Takeoka et al., 2014; Takeoka and Arber, 2019; Akay et al., 2014). Proprioceptive afferent innervation is widespread and diverse, projecting to MNs (Lavrov et al., 2006; Flynn et al., 2011; Cote et al., 2018), GABAergic (Tillakaratne et al., 2014; Liu et al., 2021), and serotonergic (Nakamura et al., 2023; Zagoraiou et al., 2009; Lu et al., 2015;

Nascimento et al., 2020) INs in the dorsal and intermediate zone of the spinal cord. Long and short axons spread across multiple segments and organised spatially and by modality (Niu et al., 2013; Cote et al., 2018; Brownstone et al., 2015; Laliberte et al., 2019). Proprioceptive interneurons (PINs) are mainly excitatory, with most inhibitory populations projecting ipsilaterally (Flynn et al., 2017). Due to their complex and integratory nature, PINs have been suggested to be a possible neural detour around spinal lesions, recovering voluntary sensorimotor control after SCI (Eisdorfer et al., 2020; Filli et al., 2014; Taccola et al., 2018; Gerasimenko et al., 2009; Laliberte et al., 2019). For further reading on the anatomy of propriospinal afferents, see appendix A.3.

There remains uncertainty on how neuromodulatory inputs regulate sensorimotor control via propriospinal connections (Edgerton and Harkema, 2011). After losing excitable input, it is natural to seek methods to return that excitation to sub-lesional networks. Most ES techniques have sought to excite and entrain locomotion by activating dorsal roots in the epidural space (Capogrosso et al., 2013; Moraud et al., 2016; Formento et al., 2018; Angeli et al., 2014; Danner et al., 2015). However, ES, in a very similar anatomical space, using similar stimulation protocols, can equally evoke inhibition and restore an overly excited network (Caylor et al., 2019; Dimitrijevic et al., 1986; Pinter et al., 2000). A more in-depth and nuanced view of ES therapy is required to fully appreciate the complexity of modulating the neural environments. A key question remains: How do neuromodulation therapies integrate with sensory information?

This study analyses a biologically constrained flexor MN spiking neural network receiving heterogeneous excitatory and inhibitory synapses, including GABAergic presynaptic inhibition. A combination of ES and serotonin agonist neuromodulators are simulated in an SCI and SCI with a body-weight support (BWS) locomotion setting. The hypothesis is this: Spinal cord locomotor circuits require balanced excitation and inhibition to coordinate flexor activity.

8.2 Methods

A biologically constrained SNN was developed to investigate the effect of neuromodulation on sensory-driven spinal locomotor circuits. Simulations were run on an Intel Xeon Gold 6238R 2.2GHz Processor. The software was developed in Python 3.10.0 using the Brian2 neural simulator module (v2.6.0) (Stimberg et al., 2019; Van Rossum and Drake, 2009). The simulation time step was set to 5 µs and run for 8-step cycles using Euler approximations for ordinary differential equation solving. A total of 8 steps were simulated, and gait stance and swing phases were split at 65% of the gait cycle (Leblond et al., 2003). This study simulated three different neurological environments, including a baseline, SCI, and SCI with a BWS state. Each neurological state was modulated with inputs from ES and serotonergic agonists (Quip).

The simulated data was considered dependent and tested using the Shapiro-Wilk method, where $p > 0.05$ was considered a normal distribution. Normal distributions were tested for significance using Tukey Honestly Significant Difference (HSD), and non-normal distributions were tested using the Wilcoxon signed-rank test. The significance between distributions was set to a p-value of 0.05. Population firing rates were averaged with a 75 ms Gaussian window. Experiment code can be found at appendix A.4.

8.2.1 Afferent Signal Inputs

Ia and II TA and gastrocnemius medialis (GM) muscle afferent signals were calculated by using musculoskeletal and muscle spindle models during locomotion, previously described in Formento et al. (2018). To emulate BWS afferent signals, both TA and GM Ia and II data were offset by a scalar amount using values from Kristiansen et al. (2019). The new BWS equations were set to eqs. (8.1) and (8.2) where $K_{TA} = -0.676$ and $K_{GM} = -0.221$, reducing the EMG effect by 32.4% and 77.9% respectively. The equations refer to x as stretch, v as stretch velocity, and EMG_{env} as the normalised EMG envelope

(Prochazka, 1999). Afferent signals were set as timed array poisson distributed inputs with a sampling frequency of 200 Hz and connected to leaky integrate and fire (LIF) axon models, see eq. (8.3). Parameters were set according to Capogrosso et al. (2013) and tuned to replicate the input firing rate, see table 8.1. Tuning was validated with Pearson correlation coefficient and mean absolute error, refer to table A.15.

$$\text{Ia firing rate} = 50 + 2 \cdot x + 4.3 \cdot sign(v) \cdot |v|^{0.6} + K \cdot 50 \cdot EMG_{env} \tag{8.1}$$

$$\text{II firing rate} = 80 + 13.5 \cdot x + K \cdot 20 \cdot EMG_{env} \tag{8.2}$$

$$\frac{dv}{dt} = \frac{E_l - v}{\tau} \tag{8.3}$$

Table 8.1: Axon parameters for LIF model.

Parameter	Value
N	60
τ	30 ms
$\tau_{refractory}$	1.6 ms
E_l	−80 mV
V_{th}	−60 mV
V_{rest}	−70 mV

8.2.2 Spiking Neural Network

The SNN models the ankle flexor's mono- and di-synaptic stretch and stretch velocity afferent reflexes. Proprioceptive afferents innervated the TA MN, GABA, IaIN, and V2a neurons (Cowley et al., 2010; Baek et al., 2017). IaINs receiving Ia and II afferent inputs

of the flexor and extensor muscles were reciprocally inhibited (Adolfo et al., 2011). GABA INs applied presynaptic inhibition to excitatory inputs of the TA MN (Mazzone et al., 2021; Khristy et al., 2009). V2a INs received flexor II afferent inputs and applied tonic excitation to TA MNs (Li et al., 2022a). TA MNs received monosynaptic excitation from flexor Ia afferents (Tuan et al., 2013; Bui et al., 2016). Refer to fig. 8.1 for an illustration of the entire network.

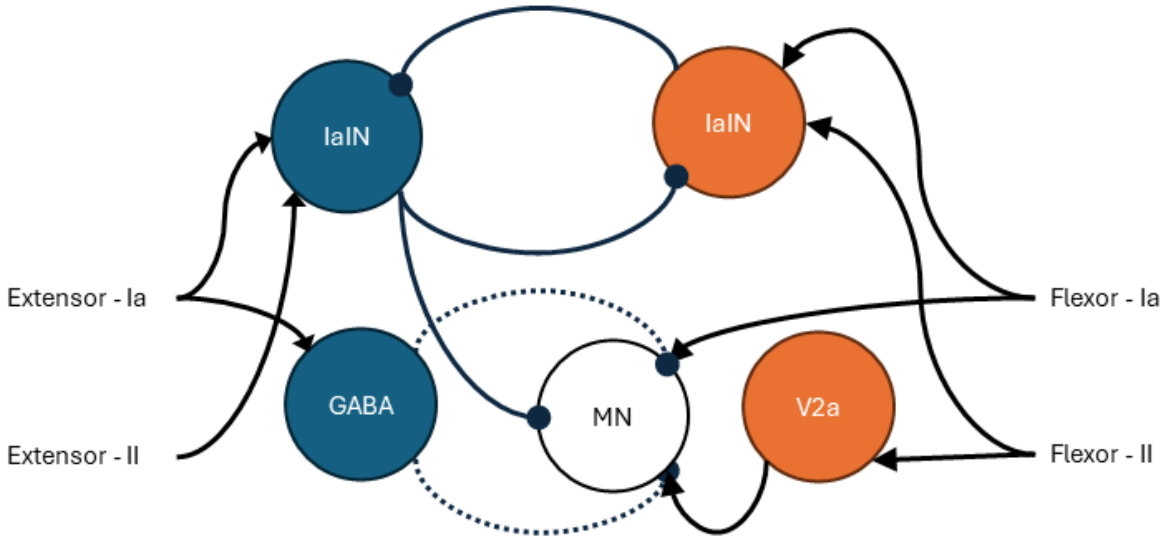

Figure 8.1: The flexor network with GM extensor and TA flexor proprioceptive Ia and II inputs. Arrow ends indicate excitation, circle ends indicate inhibition, and dotted line with circle ends indicate presynaptic inhibition connections.

Ia inhibitory interneurons (IaINs) were modelled as conductance-based LIF neurons receiving excitation from Ia and II afferent fibres and inhibition from opposing IaINs, see eq. (8.4). I_{syn} is the cumulative synaptic current from excitatory and inhibitory components. IaIN parameters in table 8.2 were set to match experimental results (Bui et al., 2003; Formento et al., 2018).

$$\frac{dv}{dt} = \frac{g_L(E_L - v) + I_{syn}}{C_m} \tag{8.4}$$

Table 8.2: Ia inhibitory IN parameters.

Parameter	Value
N	196
C_m	31.13 pF
E_L	−70 mV
V_{th}	−50 mV
V_{rest}	−65 mV
g_L	5 nS

GABA presynaptic inhibitory INs and V2a INs were modelled as conductance-based adaptive exponential (AdEx) LIFs (Naud et al., 2008). GABA parameters (Fink et al., 2014; MacDonald, 2006) and V2a parameters (Dougherty and Kiehn, 2010; Dougherty et al., 2013; Zhong et al., 2010) were set as per experimental results. AdEx equation was defined per eq. (8.5). GABA and V2a IN parameters were set per table 8.3 and table 8.4. V2a IN g_L was reduced by 15% to emulate serotonin agonist response (Husch et al., 2014).

$$\frac{dv}{dt} = \frac{g_L(E_L - v) + g_L(\Delta_v \exp\frac{v - v_{th}}{\Delta_v}) + I_{syn} - w}{C_m} \tag{8.5}$$

$$\frac{dw}{dt} = \frac{a(v - E_L) - w}{\tau_w} \tag{8.6}$$

TA flexor MNs were modelled as AdEx LIFs receiving excitation from TA Ia fibres, V2a INs, inhibition from GM originating IaINs and presynaptic inhibition from GABA

Table 8.3: GABA IN parameters.

Parameter	Value
N	196
C_m	100 pF
E_L	−70 mV
V_{th}	−50 mV
V_{rest}	−62.3 mV
g_L	1.2 nS
Δ_v	2 mV
a	2 nS
τ_w	20 ms

Table 8.4: V2a IN parameters.

Parameter	Value
N	196
C_m	45 pF
E_L	−53 mV
V_{th}	−42 mV
V_{rest}	−47 mV
g_L	1.2 nS
Δ_v	0.5 mV
a	2 nS
τ_w	55 ms

Table 8.5: TA MN parameters.

Parameter	Value
N	169
C_m	162 pF
E_L	−70 mV
V_{th}	−50 mV
V_{rest}	−65 mV
g_L	27 nS
Δ_v	0.05 mV

INs (Formento et al., 2018; Tillakaratne et al., 2014; Li et al., 2022a). The AdEx equation for TA MNs was the same as eq. (8.5) but set the parameter, w, to 0. Parameters in table 8.5 were set to best estimate experimental results (Özyurt et al., 2022; Caillet et al., 2022; Bui et al., 2003). To simulate serotonin agonist response, MN g_L was reduced

by 40% during SCI experiments and 15% during BWS experiments (Formento et al., 2018; Husch et al., 2014; Booth et al., 1997). See figs. 8.2 and 8.3 for MN responses with varying stimulation pulse widths.

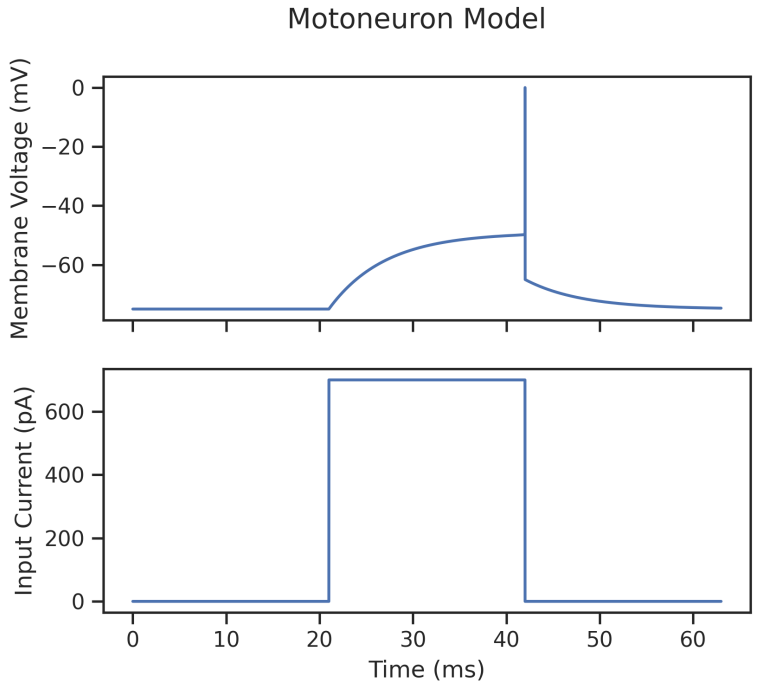

Figure 8.2: Simulated AdEx LIF TA MN single spike response after receiving a 20 ms stimulation pulse at 670 pA.

8.2.3 Synapses

Alpha and exponential conductance synapses were used to describe inhibitory and excitatory synapses, respectively, see table 8.6 and figs. 8.4 and 8.5. The reversal potential of excitatory synapses was set to 0 mV, while inhibitory synapses were set to the target neuron reverse potential. II-fibre synapse weights were scaled by a factor of 0.33 to simulate the effect of smaller axon size (Formento et al., 2018). Synaptic connections, with the exclusion of GABA, were determined by probabilities specified in table 8.7. GABA connections were predetermined by index rules dependent on the experiment condition; see fig. 8.6. GABA connections were tuned to match previous baseline responses

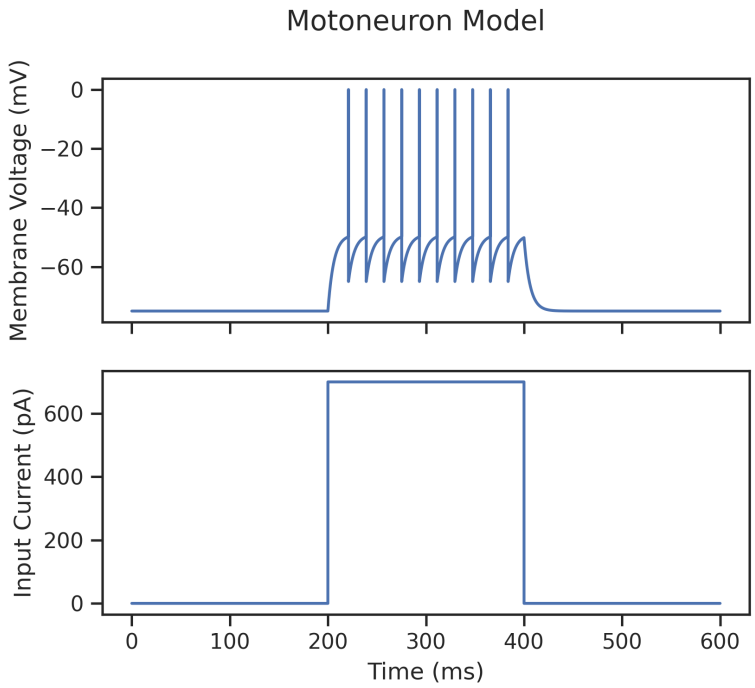

Figure 8.3: Simulated AdEx LIF TA MN tonic burst response after receiving a 200 ms stimulation pulse at 670 pA.

(Formento et al., 2018; Moraud et al., 2016). SCI condition GABA connections were increased by 150% as seen in flexor MNs after SCI transection (Khristy et al., 2009).

Table 8.6: Alpha and exponential synapse and GABA spillover parameters. Alpha synapses were used for inhibitory connections while exponential synapses were used for excitatory connections.

Parameter	Value
τ_{exc}	0.25 ms
$\tau_{inh,rise}$	2 ms
$\tau_{inh,decay}$	4.5 ms
τ_p	20 ms

Presynaptic inhibition was a multiplicative gain, scaling synaptic weights of each excitatory connection to the TA MN population (Fink et al., 2014; Hochman et al., 2010; Lalonde and Bui, 2021; Rudomin, 1990). GABA spillover was modelled as a linear decrease in release factor, p, see eq. (8.7). β determined the strength of the inhibition, τ_p determined the decay rate, and C was considered a unitless value for local GABA

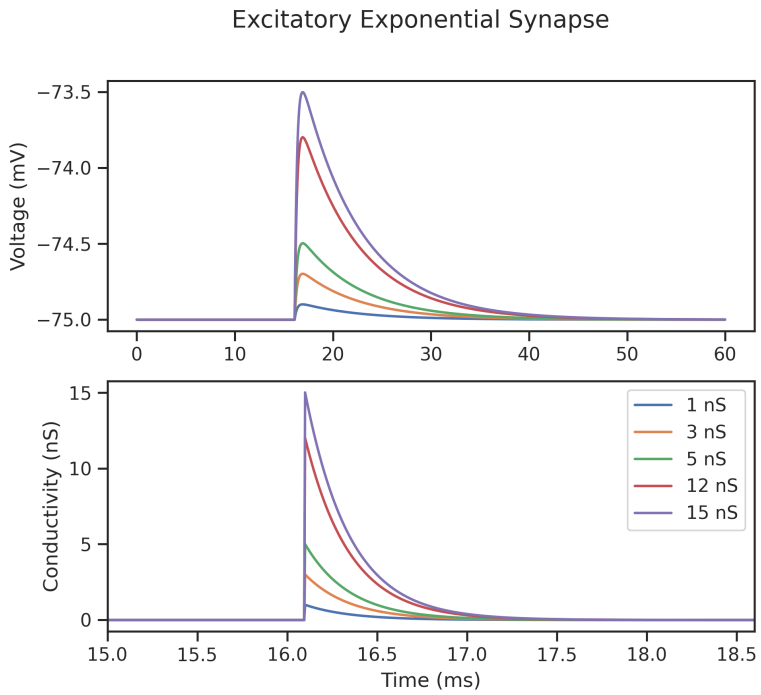

Figure 8.4: Excitatory exponential synapse with different synaptic condunctance values for the simulated flexor motoneuron.

Table 8.7: Synapse connection probabilities and synaptic conductance by source and target neurons. Excitatory (exc.) and inhibitory (inh.) synaptic conductance apply to target neurons.

Source	Target	Probability	Exc. Conductance	Inh. Conductance
Axon	IaIN	0.3	3 nS	–
Axon	GABA	0.3	12 nS	–
Axon	V2a	0.6	1 nS	–
$\text{IaIN}_{TA/GM}$	$\text{IaIN}_{TA/GM}$	0.1	–	1 nS
Axon, V2a, IaIN	MN	0.3	12 nS	5 nS

concentration (Naumann and Sprekeler, 2020).

$$\tau_p \frac{dp}{dt} = -p + (1 - \beta \cdot C_{GABA}) \tag{8.7}$$

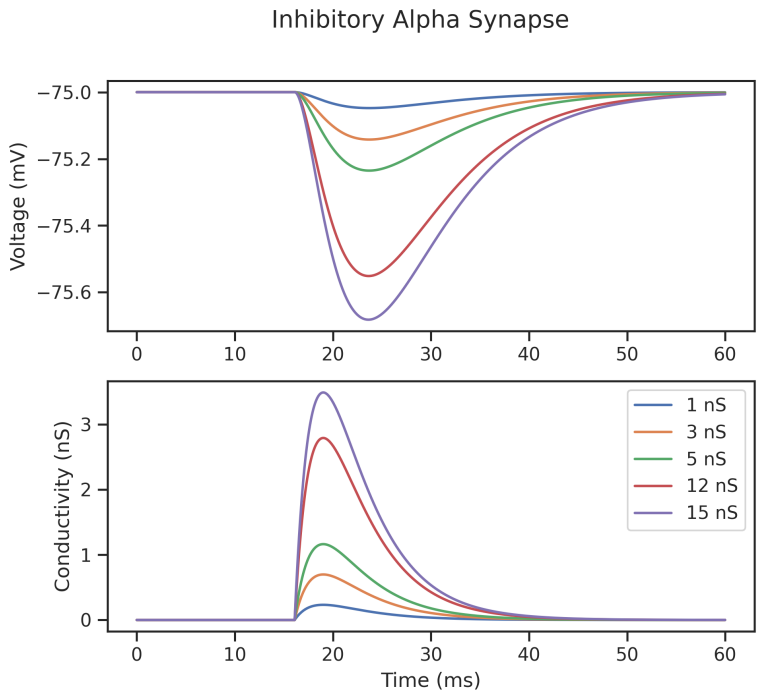

Figure 8.5: Inhibitory alpha synapse with different synaptic condunctance values for the simulated flexor motoneuron.

8.3 Results

Statistical analysis on flexor activity after outlier removal (SCI, SCI_{qES}) during each phase presented a normal distribution in the swing and stance phases ($p > 0.05$). Swing phase flexor activity significantly differed between all simulated conditions with the exclusion of baseline – BWS_{ES}, BWS_{ES} – BWS_{Quip}, and BWS_{Quip} – BWS_{qES} pairs. Stance phase flexor activity was significantly different in all simulated conditions except baseline – BWS_{ES}, baseline – BWS_{Quip}, baseline – SCI_{Quip}, and BWS_{Quip} – BWS_{qES} pairs. See fig. 8.7 for TA MN activity distributions in both swing and stance phases. Box-and-whisker plots for GABA INs and V2a INs can be found in figs. A.15 and A.16.

Simulated TA MN expression during baseline step cycles was unaffected by stimulation amplitudes but minorly affected by frequencies, refer to figs. 8.8 and 8.9. Though, GABA and V2a INs firing rates were scaled according to stimulation frequency. Note 20 Hz and 40 Hz at 10 mV stimulation intensities resulted in the same firing patterns.

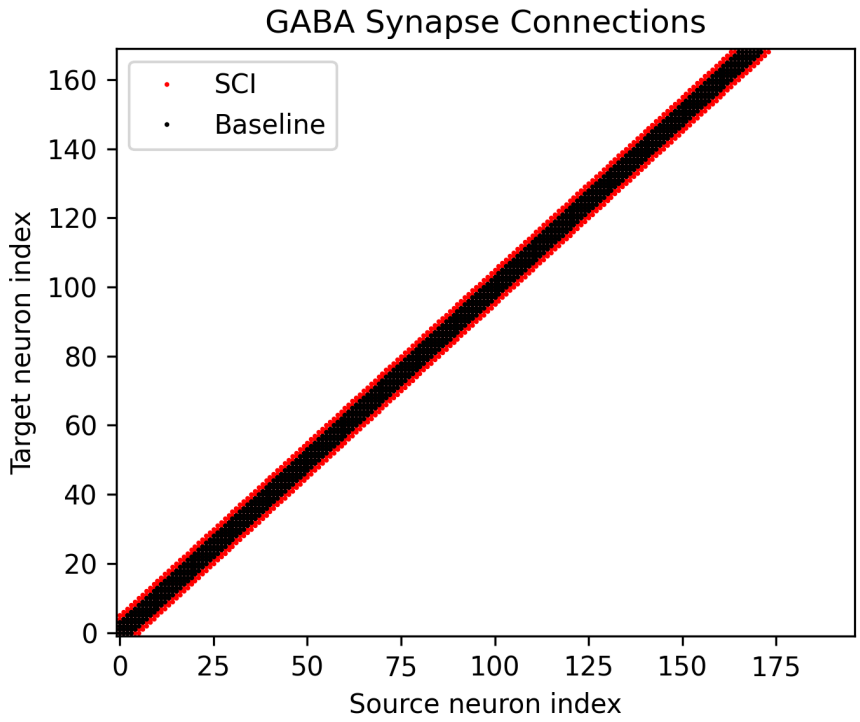

Figure 8.6: Comparison of synaptic connection between GABA and TA MN neurons with and without SCI (Khristy et al., 2009). The red points indicate extra synaptic connections between GABA and TA MN populations. All other synapse variables were kept the same.

During baseline stepping, most variation occurred within the swing stages and transition between the swing and stance phases of the gait cycle, see fig. 8.10. The TA MN population firing rates between baseline and SCI conditions were significantly different. Deterministically scaling the GABAergic connectivity to flexor MNs by 1.5 reduced mean firing rates by 16 Hz and increased mean standard deviation by a factor of 4.

Simulating SCI settings by increasing GABAergic connections resulted in greater frequency of presynaptic inhibition activity (fig. 8.7). GABA IN firing rates were increased while receiving ES inputs. V2a IN firing rates were equal between baseline and SCI since it did not receive GABA IN synapses. Simulating serotonergic agonist activity by reducing the membrane conductance of V2a INs and MNs increased firing rates in MNs, bringing MN firing rates closer towards the baseline. This effect was abolished when

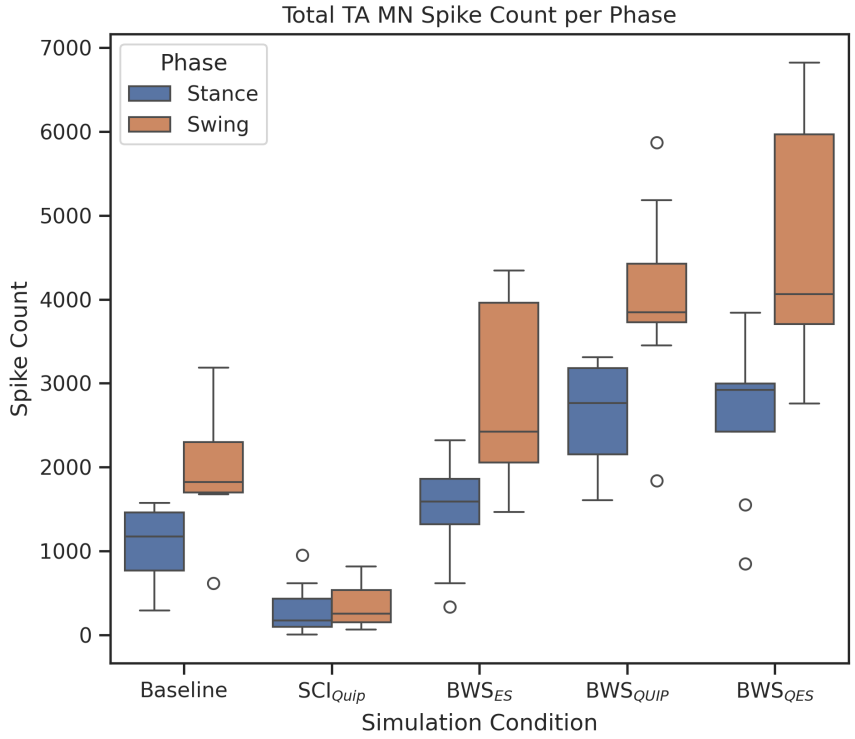

Figure 8.7: Box-and-whisker plots of 8-steps during baseline and simulated conditions. All stance flexor activity was significantly different with the exception of Baseline – SCI$_{Quip}$, Baseline – BWS$_{ES}$, and BWS$_{Quip}$ – BWS$_{qES}$. All swing flexor activity was significantly different with the exception of Baseline – BWS$_{ES}$, BWS$_{ES}$ – BWS$_{Quip}$, and BWS$_{Quip}$ – BWS$_{qES}$.

combined with ES, see figs. 8.7 and 8.11. Applying qES increased V2a IN and GABA IN activation, reducing the MN excitation to below SCI. In combination with the SCI condition, ES resulted in the same MN firing rate expression as qES.

BWS locomotion with SCI increased overall flexor activity to averages greater than the baseline condition. This was further amplified with the introduction of Quip. Applying ES without Quip smoothened the output of MN activity, returning MN activations to baseline. Combining Quip and ES further increased peak activity during the swing phase and reduced activations during stance phases, see figs. 8.7 and 8.12.

The reduction in flexor afferents from BWS reduced the Quip-modulated V2a IN activity towards SCI levels; these effects were reversed with ES modulation. GABA

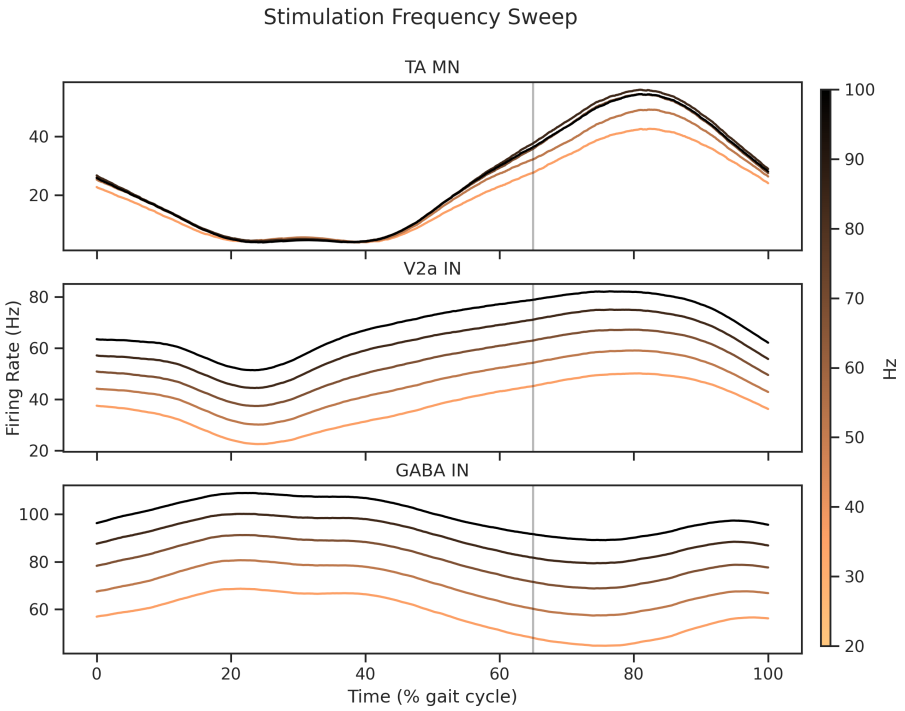

Figure 8.8: Stimulation frequency sweep applied at 20, 40, 60, 80, and 100 Hz at 10 mV amplitude using poisson inputs to flexor and extensor axons.

IN activity was reduced due to BWS simulated stance EMG reduction. Introducing ES returned GABA IN activity closer to the baseline. GABA activity was equivalent when comparing BWS_{ES} and BWS_{qES} since no modulation was applied from serotonin, refer to figs. 8.7 and 8.12.

8.4 Discussion

A biologically constrained SNN model of the flexor reflex circuit was designed to investigate the integration mechanisms between sensory and neuromodulation inputs to the spinal cord. Analysis of the stance and swing phases of 8 steps during simulated SCI activity reveal serotonergic agonists as a method to excite V2a INs and TA MNs after SCI. Applying unspecific ES to proprioceptive afferent axons amplified the effects of reciprocal inhibition, further accentuating excitatory peaks and inhibitory valleys. More-

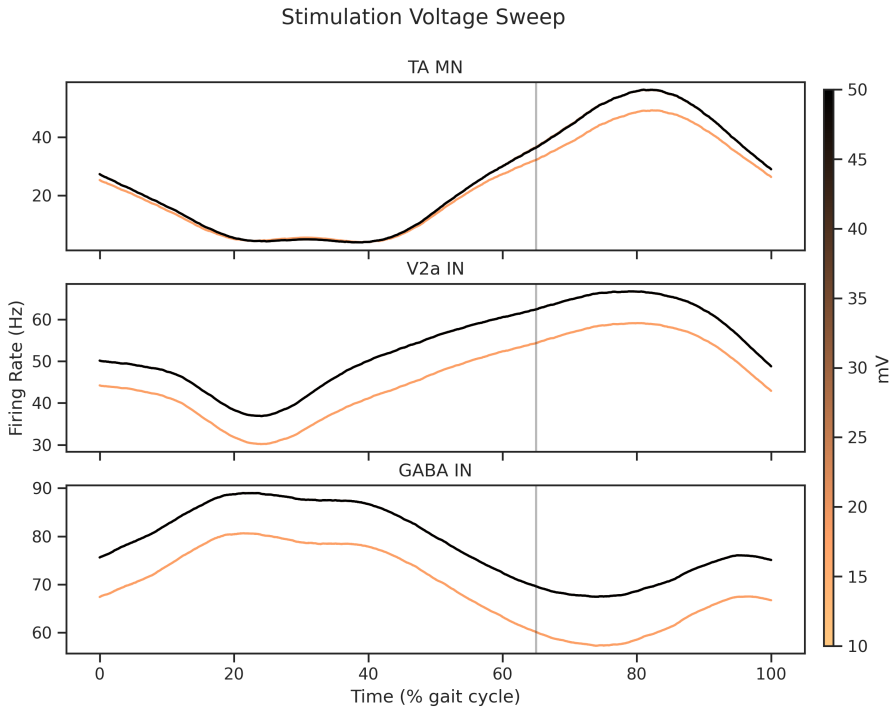

Figure 8.9: Stimulation intensity sweep applied at 10, 20, 30, 40, and 50 mV and 40 Hz frequency using poisson inputs to flexor and extensor axons.

over, simulating BWS locomotion decreased presynaptic inhibition, which reestablished TA MN firing rates. Applying ES during BWS locomotion resulted in a smoother MN activation profile, returning swing and stance firing rates to the baseline level.

Historically, ES has been applied for chronic pain management and spasticity reduction (Stewart et al., 1991; Edgerton and Roy, 2010; Caylor et al., 2019). The activation pathways of spinal cord stimulation for pain management are understood to be via large-diameter dorsal column and root fibres that carry propriosensory, mechanosensory, and nociceptive information (Guan et al., 2018). GABA INs activate and depress afferent nociceptive signals by antidromic activation of the dorsal column at frequencies, electrode positions, and stimulation amplitudes similar to that of ES for sensorimotor recovery (Meuwissen et al., 2020; Wenger et al., 2016). Similarly, ES applied for spasticity reduces the excitatory inputs to MNs through the proprioceptive inhibitory pathways (Alashram et al., 2023; Mahrous et al., 2024). Yet, literature in SCI motor recovery places an intense

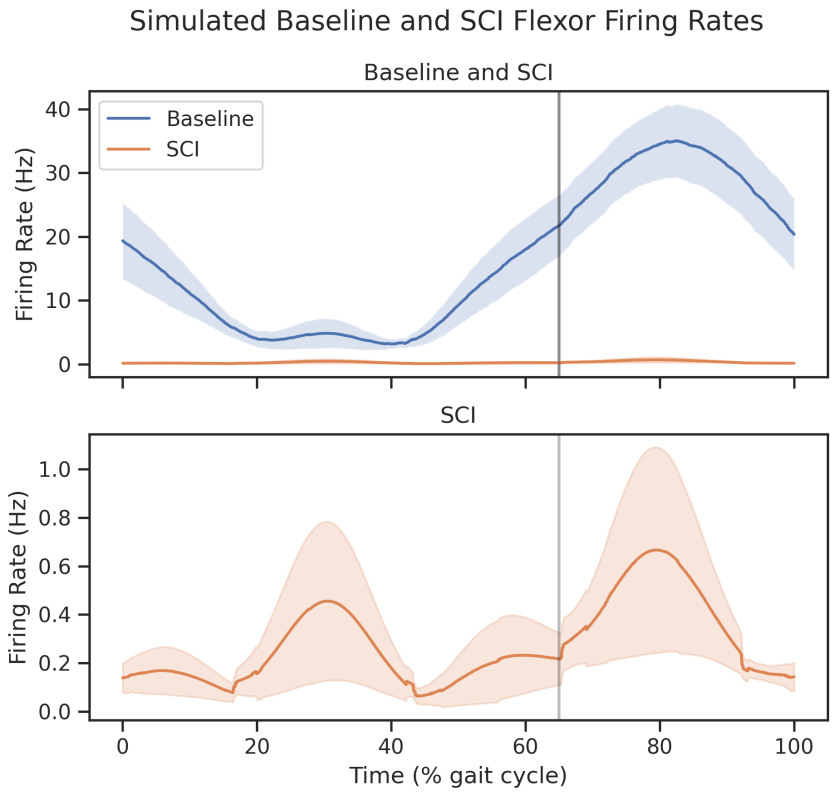

Figure 8.10: Average and standard deviation plots of 8-steps during baseline and simulated SCI conditions. The vertical grey line separates the stance (left of the grey line) and the swing (right of the grey line) phases, estimated at 65% of the gait cycle (Leblond et al., 2003).

focus on excitation (Alluin et al., 2015; Lorach et al., 2023; Minassian and Hofstoetter, 2016).

Given the heightened inhibitory state of the injured spinal cord, it seems intuitive to return excitation to depressed neurons. However, results from this study suggest activating the spinal cord with the same proposed mechanisms as pain and spasticity modulation equally activate inhibitory pathways, strengthening an already maladapted inhibition dominant circuit (Edgerton et al., 2001a; Khristy et al., 2009). A more refined and nuanced approach needs to be considered in order to return the required balance of excitation and inhibition to allow phasic activity to propagate. Results in this study suggest that appropriate sensory information must be provided to drive flexor network

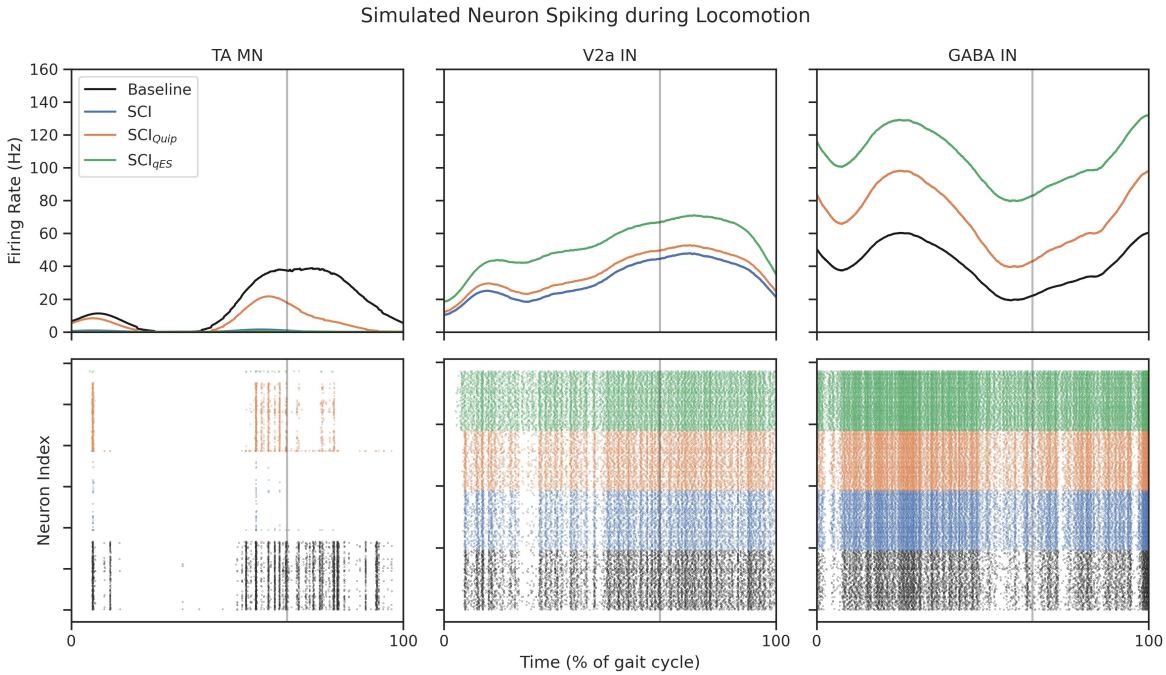

Figure 8.11: MN, V2a IN, and GABA IN spiking activity during an example step. The effect of SCI and SCI while receiving serotonergic agonists, (Quip), and the combination of Quip and ES (qES) were compared. The top row illustrates the population firing rates and the bottom row shows the individual neuron spiking activity during the gait cycle.

plastic adaptation towards a less inhibited and more task-specific tuned state. Tonically depressing or exciting, the spinal circuits do not provide the necessary sensory information to provide that plastic tuning (Fong et al., 2005; Cai et al., 2006). This explains the requirement of propriosensory information for locomotor recovery after SCI (Takeoka et al., 2014; Takeoka and Arber, 2019; Akay et al., 2014).

The normal sensory processing occurring within the injured spinal cord becomes more stochastic and lacks the necessary bias required to perform the task (Gad et al., 2015). As a result, pre-motor polysynaptic connections play a more active role in the expression of muscle tone and activity (Sakurai et al., 2016). By establishing an appropriate balance in excitation and inhibition, repetitive sensory information can reinforce appropriate synaptic adaptations towards a more functional spinal state (Rossignol et al., 2006; Edgerton et al., 2008; Ichiyama et al., 2008b). Results in this study show, for the first

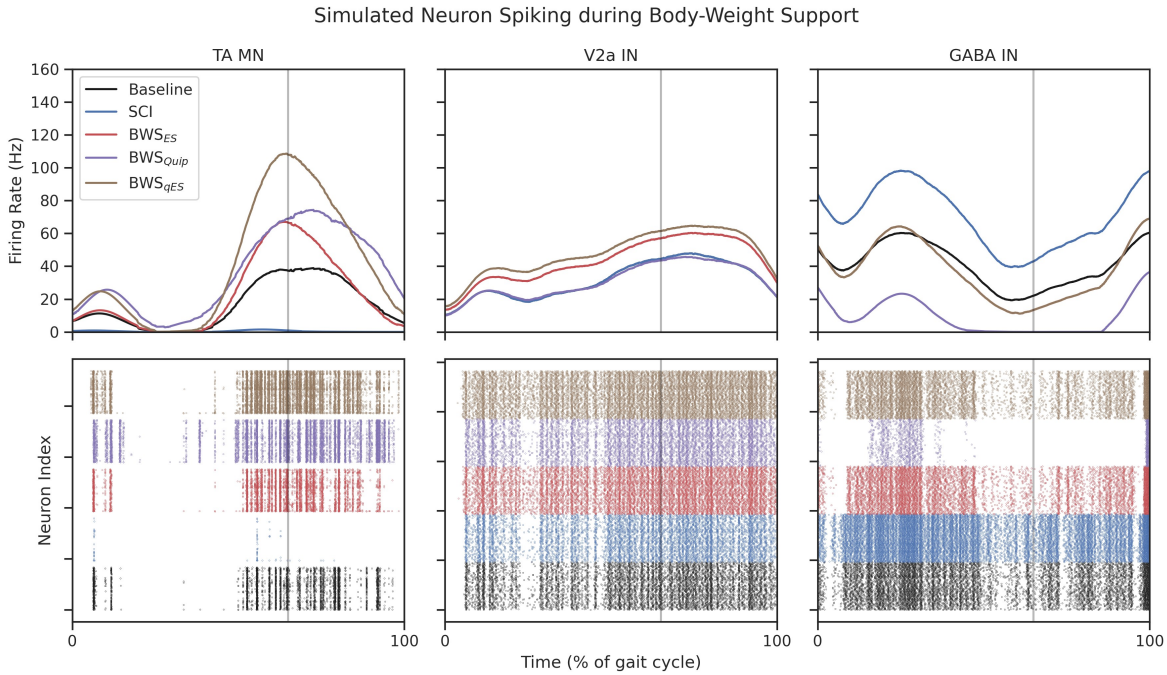

Figure 8.12: MN, V2a IN, and GABA IN spiking activity during an example step during simulated BWS locomotion. The effect of BWs while receiving serotonergic agonists (Quip) and the combination of Quip and ES (qES) were compared. The top row illustrates the population firing rates and the bottom row shows the individual neuron spiking activity during the gait cycle. Descreased firing rates from extensor afferents increased excitation in V2a INs and MNs by reducing the effect of inhibition.

time, the synaptic mechanisms at which this can be accomplished and provide an understanding of why BWS treadmill training works (Hicks and Ginis, 2008; Nam et al., 2017; Feldman et al., 2021).

The greater deviation in normalised firing rate indicates greater variation in neuronal populations after SCI (figs. 8.10 and 8.13). This may be due to the lack of necessary excitation required to inhibit and excite in phase with the incoming sensory signals (Gad et al., 2015). Thus, increasing the excitability of MNs and premotor excitatory neurons and reducing the effect of stance phase inhibition by BWS can assist with reducing inhibitory effects on flexors (de Leon et al., 2002; Cantoria et al., 2011; Pizzolato et al., 2021; Cabaj et al., 2017). After reaching a suitably excitable state where phasic step information can propagate in a timely manner, sub-threshold ES could provide the

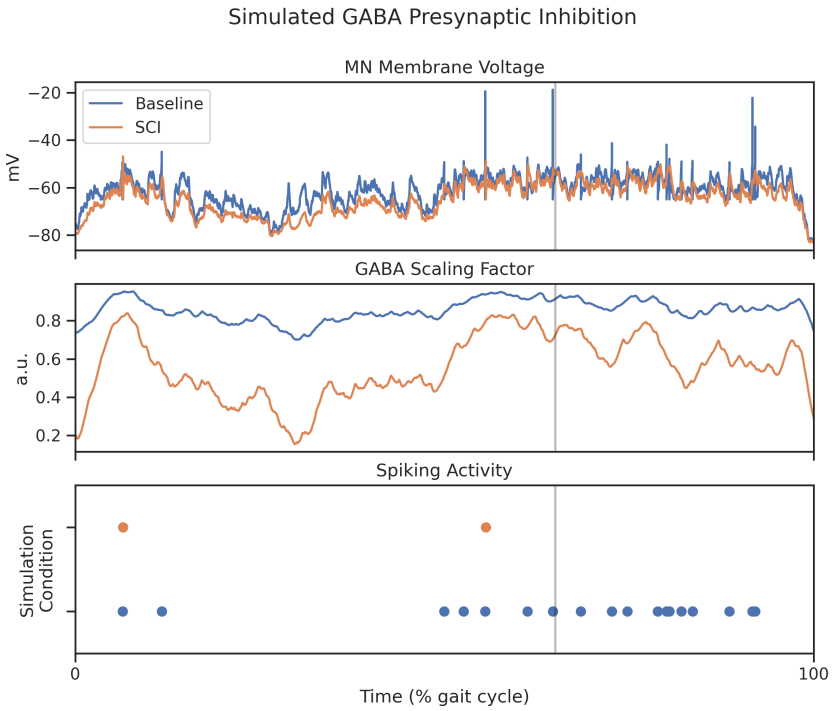

Figure 8.13: SCI simulation of a single motoneuron receiving presynaptic inhibition by local concentration of GABA transmitters during a single step. Note the reduced number of spike events due to GABA inhibition.

necessary smoothening process to synergistically reinforce relevant pathways without too much inhibition or excitation (Formento et al., 2018; Gerasimenko et al., 2007; Ichiyama et al., 2008b).

Computational studies such as this are limited in their ability to generalise due to the estimates and tuning that are required to generate the model itself. The simulated flexor reflex loop's SNN architecture is simplistic compared to the complex bidirectional information exchange between the contralateral sides (Danner et al., 2019; Rybak et al., 2015). Though the cells were modelled from experimental data, there are errors and missing variables within experiments that have a carry-on effect on computational models. This study utilised LIF and AdEx equations to reduce computational burden and improve simulation runtime speeds. Though previous efforts have incorporated the same approach (Moraud et al., 2016; Formento et al., 2018), mathematical approximations

of firing patterns limit the generalisability (Feng, 2001; Merzon et al., 2019). However, even with simple estimations, a computational model could provide new hypotheses to the inner workings of neurological systems and unlock novel recovery protocols (Wenger et al., 2016; Edlund, 2019).

Future studies could include the investigation of previous electrophysiological results that uncovered correlations between the appearance of long-latency polysynaptic potentials and recovery of locomotion in spinal rats (Lavrov et al., 2008a; Gerasimenko et al., 2007, 2006; Lavrov et al., 2008b, 2006; Gad et al., 2013c). Re-emergence of uninterrupted late-response polysynaptic potentials may be the expression of increased excitability in local spinal networks, re-balancing the inhibitory dominant pre-motor circuity (Gad et al., 2015; Sakurai et al., 2016). Functional recovery may be mediated by increased magnitude in polysynaptic activity, compensating for the loss in direct excitation (Edgerton et al., 2008). Finally, extending the computational model to include neuroplastic dynamics could uncover the relationship between neuromodulation and neuroplastic adaptations (Brzosko et al., 2019; Naumann and Sprekeler, 2020). Investigating these effects within an extended biologically constrained computational model would be worthwhile.

8.5 Conclusion

The development of a biologically constrained SNN has provided insights into the mechanistic basis of sensory and neuromodulatory integration after SCI. Simulations suggest that BWS locomotion in conjunction with ES returns phasic flexor coordination in an inhibition-dominant environment. Without BWS, serotonergic agonists increased excitation to enable sensory-driven flexor rhythmic activation. The spinal cord requires a balance of excitation and inhibition to enable the correct phasic modulation of sensorimotor pathways. The work described in this chapter provides a potential explanation for why BWS locomotor training works with neuromodulation.

CHAPTER 9

FUTURE DIRECTIONS

This thesis has described methods for pathological gait monitoring during longitudinal studies of neuromodulation effects in SCI populations. The developed rule-based algorithms and machine learning models with curated features, per standard in the literature, from chapter 4 could not reliably capture event labels. Deep learning models from chapters 5 and 6 successfully classified windows of locomotor and standing activity with state-of-the-art methods without requiring significant post-processing. Using the abovementioned methods, chapter 7 analysed the effect of different combinatorial neuromodulation therapies on spinally transected rats during chronic recording sessions in cage-roaming environments. The MEPs extracted from each locomotion event suggest LRs as a potential biomarker to indicate the functional state of the local spinal circuitry. Mechanisms for this have yet to be investigated. Thus, the below section performs an in-depth review of the biological architecture of locomotor CPG known thus far to extend the SNN model design from chapter 8 for hypothesis generation.

9.1 Human Studies

Wearable technologies have become less intrusive and easily accessible to daily use (Zhao et al., 2021; Lymberis, 2003). This thesis has focused on why this data is essential when monitoring and adjusting the effects of neuromodulation therapies and protocols. By enabling out-of-lab recordings of event-related activity, new options for treatments are presented. Such include understanding dose-response and flexibly changing the complex parameter list of stimulation waveforms and location (Edgerton and Harkema, 2011). The first step to deploying such an intertwined environment is aggregating EMG lower-limb data with wearable sensors in an out-of-lab context. There already exists plenty of activity recordings on the treadmill and within-lab.

If the above steps are successful, one may decide to expand the model to include pathological gait and non-pathological gait domains, developing a domain-invariant representation of locomotor activity across populations. Sensor-fusion techniques may also be appropriate to reliable classification, including previously studied IMU incorporation in table 4.1. Data augmentation strategies offer methods to improve robustness and invariance in time-series classification. Further investigations of these transfer learning and augmentation techniques enable the measurement of neural recovery in the final common pathway of the MN in neuropathological gait subjects.

Another opportunity is to address the engineering problem of regular tuning of stimulation parameters. For example, participant-specific spatiotemporal tuning of electrode position and stimulation parameters to reach an optimised stimulation protocol (Angeli et al., 2014; Wagner et al., 2018). To combat such issues, an active machine learning algorithm utilising a structured Gaussian process optimised stimulation parameters in four spinal rats with multi-electrode implant arrays (Desautels et al., 2015). Unpublished data from Kachuee et al. (2018) used machine learning models to predict the grip force of a patient with chronic SCI based on different epidural stimulation parameters.

These studies illustrate the high complexity of electrical neuromodulation in catering to subject, spatiotemporal, and parametric-specific stimulation protocols for optimised rehabilitative outcomes.

The electrode configuration and stimulation parameters significantly affect the CNS. Even within the same stimulation site, changing the applied frequency can recruit spinal sensorimotor pathways relevant to a different task. Interleaved stimulation even affects multiple spinal premotor circuit recruitment (Cheng et al., 2019; Wenger et al., 2016). Electrical neuromodulation strategies to facilitate motor recovery are still in their infancy. Its effects on the CNS concerning the requirements for patient specificity still need to be fully understood. A large body of research has been conducted on how the spinal cord integrates sensory information after introducing an electric field (Edgerton et al., 2001a, 2004, 2008; Edgerton and Roy, 2009a).

Applying ongoing monitoring of MEP activity could off-load the frequency of recalibration, reducing the cost and complexity of ES-related therapy options. In advanced modelling, it may be possible to consider the predicted adjustment of stimulation parameters for more optimised usage based on forecasting.

9.2 SNN Modelling

There have been many advancements in the clinical application of electrical stimulation. However, the gaps in understanding the mechanisms of action, especially how endogenous and exogenous signals coordinate to produce polysynaptic responses in MEPs remain unsolved. The observations in chapter 7 complement previous literature (Lavrov et al., 2006, 2008b; Gad et al., 2015). Some have considered LRs an endogenous compensatory excitation to local spinal networks to rebalance excitation-inhibition (Musienko et al., 2013; Gad et al., 2015). Genetic labelling works have also suggested dI3 and V2a INs as key contributors to locomotor recovery, though they are not previously required

during healthy locomotion (Bui et al., 2016; Kathe et al., 2022). While scientists have speculated the reasoning behind the above observations, further investigation is required to describe why or how empirically.

Electrically stimulated polysynaptic activity evoked more complex behaviour in spinal circuits but the threshold to reach polysynaptic activity was not constant (Vargas Luna et al., 2021). The work suggests a level of modulation in central excitability, facilitating the activation of polysynaptic activity. A recently submitted thesis also investigates the mechanics behind facilitation during sub-threshold stimulation (Edlund, 2019). This study documents an in-depth biophysical computational methodology to show the activation of dorsal interneurons and the idea of the 'facilitation window'. Perhaps this explains why we see neuromodulatory facilitation via low-intensity stimulation in sensory-driven training protocols. Polysynaptic activity expression may reflect the central state of excitability in local spinal cord neural networks. Electrical stimulation recruiting superficial dorsal interneurons, dorsal column, and dorsal root pathways could facilitate endogenous afferent activity towards sensorimotor recovery.

Depolarisation of dorsal root fibres may lead to activation of more extensive interneuron connections (Bannatyne et al., 2009; Cote et al., 2018; Vargas Luna et al., 2021). Further evidence for this hypothesis was suggested in experiments using simple repetitive neurostimulation to sufficiently activate locomotor CPGs (Grillner and El Manira, 2020). Computational modelling has shown that the electrical energy injected into the epidural space is likely recruiting large diameter dorsal root fibres rather than interneuron spinal networks (Mahrous et al., 2019; Capogrosso et al., 2013). These models were developed mainly by assuming that other spinal neurons and axons are not activated via epidural stimulation. A recent paper (Greiner et al., 2021) uses computational methods to investigate the effect of electrode positioning and cervical motoneuron recruitment in monkeys. Neuronal activation was achieved in the dorsal column, spinocerebellar tract,

corticospinal tract, and primary afferent fibres. Current evidence is too rudimentary to confidently accept dorsal root activation via ES as the direct pathway for sensorimotor recovery after SCI.

The original reasoning postulated MEPs were deemed suitable estimates to define activation sites via electrical stimulation (Rattay et al., 2000; Murg et al., 2000). While the excitation of posterior roots activates α – MNs via reflex pathways, how do researchers know if the dorsal column is unaffected? Rattay et al. (2000) ignores its effect in the dorsal column because sufficient α – MN activation is > 10V, outside of the stimulation amplitude range of interest. This assumption discounts the possibility of interneuron activation via short or long propriospinal and mechanosensory dorsal column structures. Spinal cord stimulation was originally used for neuromodulating chronic pain via activation of dorsal column axons (Guan et al., 2018; Parker et al., 2020; Jensen and Brownstone, 2019; Prager, 2010). The role of electrically activated axons in the dorsal column and root and neurons of the dorsal horn in sensorimotor recovery is not obvious. How these structures and neuromodulatory interventions couple together warrant further investigation.

Identifying key contributors in electrically modulated complex spinal interneuron circuitry (Niu et al., 2013; Cote et al., 2018; Wu et al., 2021a; Hagglund et al., 2013; Jankowska, 2013b) and unravelling why these networks are necessary for spinal sensorimotor recovery (Gill et al., 2020b; Eisdorfer et al., 2020; Takeoka, 2020; Takeoka and Arber, 2019; Laliberte et al., 2019; Taccola et al., 2018; Flynn et al., 2011; Etlin et al., 2010; Gerasimenko et al., 2009; Edgerton et al., 2008) is a worthy research pursuit.

Spinal cord electrical stimulation has shown differential effects in supra-spinal and sub-cortical networks (Benavides et al., 2020; Knikou et al., 2015; Gerasimenko et al., 2018). (Mahrous et al., 2019) investigated how sensory feedback may synergise with descending neural firing. They had recorded short-term facilitation in descending inputs

but short-term depression in sensory inputs. The concurrent activation of descending and sensory inputs produced supra-linear facilitation in ventral root compound action potentials but a sub-linear summation in intracellular EPSPs. This study gives insight into the spinal cord's integrative actions but does not answer how ES affects these networks.

Facilitatory effects of epidural and transcutaneous dorsal ES were investigated in (Guiho et al., 2021). Similar results to (Mahrous et al., 2019) were reported in vivo in neurologically intact monkeys while delivering timed primary motor cortex and epidural or transcutaneous dorsal ES. It was noted that facilitatory interactions likely occurred at the spinal level as similar activity was observed when only stimulating the pyramidal tract, an area unaffected by cortical excitability modulation. Additionally, authors report longer facilitation windows in transcutaneous than in epidural ES. It may be possible that transcutaneous ES recruit additional spinal networks, providing support for activity-dependent plasticity (Benavides et al., 2020). Guiho et al. (2021) results suggest an increased net excitatory synaptic influence on motoneurons via Ia afferent pathways and slower presynaptic inhibition of subsequent afferent input via primary afferent depolarisation (see fig. 9.1). The paper needs to investigate the interactions between sensory afferents, ES, and descending input.

To further our understanding of the net effects and interplay of ES with voluntary descending input, recent studies were performed to investigate the modulation of spinal circuitry in healthy and SCI humans (Steele et al., 2021; Calvert et al., 2021). Steele et al. (2021) explored the multi-segmental convergence of descending drive to spinal motor pools in healthy subjects using a double-trigger stimulus protocol during both preparatory and execution stages. Authors reported increased excitability in primary agonists and antagonists before movement and evidence of ongoing descending drive decreasing presynaptic inhibition of Ia fibres acting on spinal MNs. There was greater

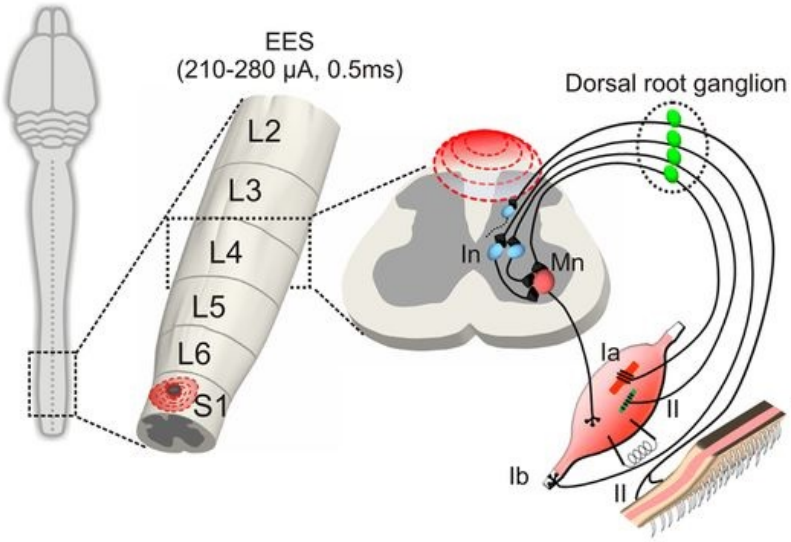

Figure 9.1: Hypothesised pathway of epidural electrical stimulation via axon depolarisation of primary afferent fibres, entering through the dorsal roots, exciting MNs and pre-motor INs (Capogrosso et al., 2013). Licensed under Creative Commons Attribution-Noncommercial-Share Alike 3.0 Unported License (CC-BY-NC-SA).

complexity expressed during voluntary isometric contraction. The authors observed task-specific facilitation in agonists and antagonists. Knee extension and ankle dorsiflexion saw expected facilitation in agonists and inhibition in antagonists. Whereas knee flexion and ankle plantarflexion saw both agonists and antagonists facilitated. Furthermore, the contralateral muscle recordings facilitated most muscles during isometric knee flexion, plantarflexion, and dorsiflexion. While isometric knee extension resulted in inhibition in responses of all recorded contralateral muscles. These task-specific differences reflect feedforward mechanisms between cortical and spinal networks. The switching between preparatory and execution states may be critical to delivering spinal stimulation for sensorimotor recovery.

Calvert et al. (2021) investigates the effect of voluntary control and low-frequency spinal cord stimulation at the motor threshold, using transcutaneous and epidural, in SCI individuals under relaxed and MVC flexion of lower extremities. Spinally evoked motor potentials were used to unravel the descending information through a lesion in

concert with spinal cord stimulation. When instructed to contract lower limb muscles voluntarily, spinally evoked motor potentials saw inhibited activity. Furthermore, joint-specific contractions saw inhibition in all recorded muscles bilaterally. This is in direct contact with the previously discussed paper from (Steele et al., 2021). This cohort of SCI participants may have increased inhibitory responses due to neural reorganisation post-injury. However, other studies on SCI participants using TMS-paired transcutaneous spinal stimulation saw bilateral facilitation (Knikou et al., 2015; Roy et al., 2014). Perhaps at higher rates of stimulation, a dominant excitatory effect takes place. If the participants were in a more active position with greater afferent input, perhaps a greater facilitatory effect could be generated. The reasons why the study saw inhibition instead of facilitation remain unanswered.

The mechanistic basis of electrically neuromodulated sensorimotor networks is in question. Eisdorfer et al. (2020) discusses the mechanisms of epidural electrical stimulation in SCI participants, highlighting its utility in enhancing motor activation. The author acknowledges the gap in knowledge surrounding electrical neuromodulatory mechanisms driving improvements in sensorimotor function. The review suggests epidural stimulation promotes recovery via changes in local lumbar circuitry, specifically through propriospinal interneurons. Recent work from Courtine's lab shines a light on the role of V2a interneurons in locomotor recovery after SCI (Kathe et al., 2022). Their paper reveals activity-dependent V2a interneurons responsible for transforming information projecting from brainstem locomotor regions and large diameter afferents into executive commands innervating ventral neurons. However, descending input transforms after injury cannot be the sole mechanism behind recovery. Bui et al. (2016) showed dI3 interneurons as critical neurons for motor recovery only after spinal transection.

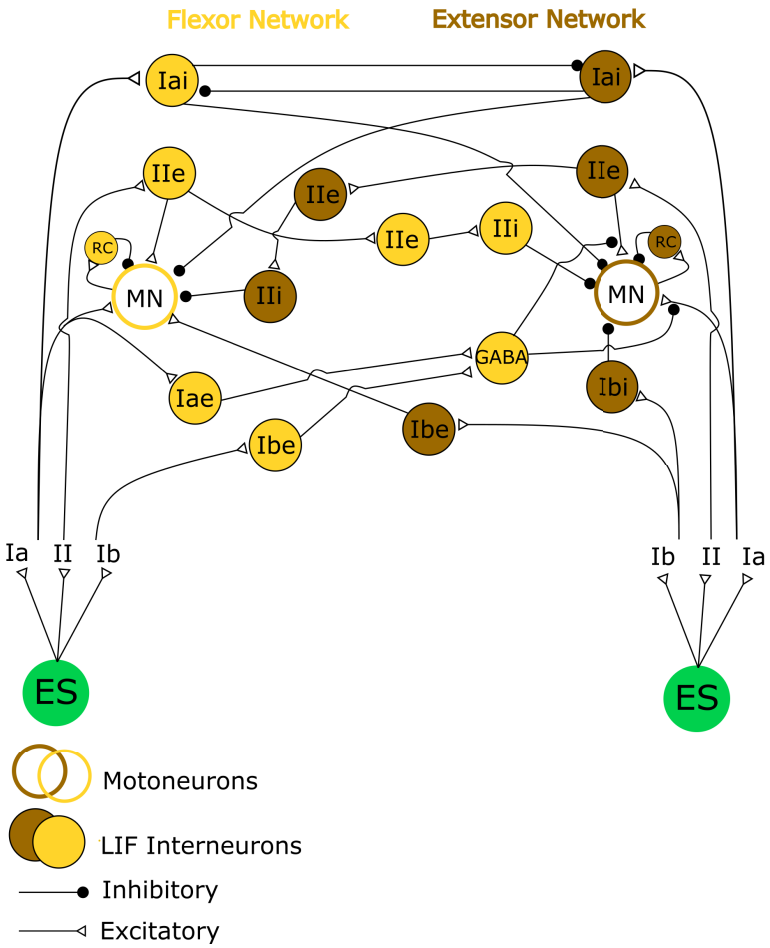

Figure 9.2: Detailed biologically constrained SNN model, designed based on electrophysiological and genetic labelling studies from appendix A.3.

9.2.1 Model Design

With the architecture now laid out, an SNN design is proposed in fig. 9.2. Using the event labels from chapter 7, an SNN model may be trained to uncover the sensory activity and generate the EMG and MEPs discovered in chapter 7. The roles, inputs, and projections of these neurons are reviewed in appendix A.3.

This work builds upon the model from chapter 8 but adds the extensor portion of the ipsilateral reflex circuit (Capogrosso et al., 2013; Formento et al., 2018; Moraud et al., 2016; Wenger et al., 2016; Edlund, 2019).

CHAPTER 10

CONCLUSIONS

This dissertation aimed to address two main gaps in the literature. The first gap was the need for robust methods towards monitoring neurological, task-dependent activity in an out-of-lab setting. The second was the need for mechanistic explanations of synergistic neuromodulatory therapies involving electrical stimulation and pharmacological treatment. Several machine learning and deep learning techniques were utilised to classify locomotor and standing-related activity in spinally transected rodents receiving multimodal therapy over a 6-hr period. Identified unilateral stepping-like events were analysed over 5 different therapies. The late and middle responses produced from motor-evoked potentials during identified events appear to reflect the functional state of the spinal cord while undergoing therapy. Finally, a biologically constrained SNN was developed to investigate the effects of sensory integration with neuromodulation for flexor activity. Balancing the excitation and inhibition levels produced robust stepping activations by the flexor network. Future works include scaling the developed deep learning models towards humans with pathological gait in out-of-lab settings. A biologically constrained spiking neural network generative model was de-

signed and suggested as a possible means of explaining where the late responses appear and the effect of electrical stimulation on specific neural cell types.

Chapter 4 sets out to perform a comparative study on the existing methodologies towards lower-limb activity classification, including unilateral stepping and bilateral standing events. Many approaches today break down the problem into smaller phases to classify. The data set available does not have this luxury. A digital signal processing pipeline and rule-based algorithm were designed to identify activity instances in rodent hindlimb pathological stepping and standing. The development of the adaptive burst thresholding technique allowed flexible burst detection in dynamic neurological environments. The first stage creates a signal envelope and breaks down windowed data into sub-windows before identifying the index with the lowest magnitude. A threshold on the first-order differential was applied to determine the periods of activity and inactivity. The in-active segments were concatenated and used as the 'resting' period for that activity window. The adaptive filter allowed robust false positive rejection in the following processes. However, the rule-based method did not successfully classify relevant labels and returned poor evaluation metrics. Other machine learning options performed better, though they returned an F1 score < 0.5. Existing methodologies towards lower-limb activity recognition did not extract events during pathological gait in spinally transected rodents receiving multimodal neuromodulatory therapy.

Chapter 5 aimed to investigate the state-of-the-art deep learning models towards latent representations of the locomotor and standing events in the same data set. The hypothesis was two-fold. Firstly, convolution vision transformers can develop spatiotemporal relationships in CWT signals via depthwise separable projections and attention operations. Secondly, unsupervised domain-invariant adversarial learning and fine-tuning can aid with classification across therapies. The experiment included several deep convolutional neural networks and vision transformers. Results from this study

suggest that ViT was able to capture the locomotor-specific semantic information behind locomotor CWT. However, despite the disproportionate imbalance between standing and stepping labels, it struggled with standing events. The Xception model captured standing events best out of all the tested methods. Finally, the DIAL strategy did not successfully develop robust representations between therapies. Results from this experiment far outperformed existing approaches.

Chapter 6 applied curriculum learning, transferring knowledge from locomotion phase classification to whole step cycle and standing classification. This study was the first time curriculum learning was applied in activity detection using physiological signals. This new method was then improved by using domain adaptation techniques to bridge inter-subject domains. Combining curriculum learning with domain adaptation outperformed transfer learning after self-supervised contrastive learning and supervised one-dimensional convolutional neural network models.

Chapter 7 performed an in-depth analysis of the effect of 5 different neuromodulatory therapies over 6 hours in spinally transected rats. The extracted stepping-like events were summed and compared between therapies. Additionally, MEPs from event-labelled sections of time were extracted. This study provided the first chronic study of multimodal neuromodulation therapies. Results suggest the inclusion of serotonin as a pivotal contributor to enabling sensory-driven locomotion activity in the isolated rat spinal cord. The excitability in the soleus was directly linked to the number of steps completed throughout the recording. Finally, a potential electrophysiological biomarker of the functional state of the isolated spinal cord was identified in the late and middle responses of the MEPs during sensory-driven activity. Implications of these results include the monitoring of activity and excitability during rehabilitation in SCI subjects.

Chapter 8 investigated the effects of stance-specific presynaptic inhibition on flexor networks. A biologically constrained SNN model was developed and fed proprioceptive

afferent signals from ankle flexors and extensors. Simulating a SCI environment uncovered a significant reduction in motoneuron excitation and increased variability in motoneuron activation. The reduced excitation was reversed with simulated body-weight support and serotonergic agonists. The application of ES smoothened the expression of flexor activity.

Future directions suggest scaling the developed deep learning models towards human subjects suffering from pathological gait during overground out-of-lab locomotion with sparse EMG channels. Furthermore, extending the biologically constrained spiking neural network with extensor circuits may uncover the origins of the assumed polysynaptic activity in the MEP late-response window.

APPENDIX A

APPENDIX

A.1 Supplementary Tables

Table A.1: Evaluation of penultimate layers during supervised step and stand training.

	Accuracy	Precision	Recall	F1-Score (weighted)
Dense	0.78	0.59	0.58	0.58
LSTM	0.78	0.59	0.62	0.60
ATTN	0.77	0.58	0.46	0.50

Table A.2: Evaluation of a LSTM penultimate layer during supervised step and stand training per subject.

	Accuracy	Precision	Recall	F1-Score (weighted)
A3	0.18	0.31	0.09	0.14
A5	0.72	0.01	0.16	0.03
A7	0.81	0.72	0.60	0.63
A8	0.64	0.66	0.39	0.49
Mean	0.59	0.42	0.31	0.32
SD	0.24	0.28	0.20	0.25

Table A.3: Evaluation of a Target Only classification of phases using CNN1D.

	Right Swing	Right Stance	Left Swing	Left Stance
A3 → A7	0.41	0.46	0.24	0.38
A5 → A7	0.41	0.46	0.24	0.38
A7 → A3	0.56	0.44	0.62	0.52
A7 → A5	0.56	0.45	0.69	0.52
A7 → A8	0.47	0.44	0.33	0.38
A8 → A7	0.41	0.46	0.24	0.38
Mean	0.47	0.45	0.39	0.42
SD	0.07	0.01	0.19	0.07

Table A.4: TS-TCC self-supervised training followed by phase label fine-tuning classification performance per subject. Detailed are

	Accuracy	Precision	Recall	F1-Score (weighted)
A3	0.44	0.35	0.23	0.25
A5	0.83	0.10	0.77	0.17
A7	0.81	0.31	0.72	0.42
A8	0.61	0.35	0.39	0.36
Mean	0.67	0.27	0.53	0.30
SD	0.16	0.10	0.23	0.10

Table A.5: Average phase label classification F1-score (binary) performance for HoMM after 3 runs set at different random seeds.

	Right Swing	Right Stance	Left Swing	Left Stance
A3 → A7	0.45	0.38	0.29	0.42
A5 → A7	0.52	0.28	0.40	0.37
A7 → A3	0.53	0.45	0.69	0.49
A7 → A5	0.44	0.43	0.71	0.49
A7 → A8	0.47	0.48	0.37	0.38
A8 → A7	0.50	0.49	0.29	0.41
Mean	0.49	0.42	0.46	0.43
SD	0.03	0.07	0.18	0.05

Table A.6: Evaluation of a rodent step classification after TS-TCC pretraining on SEMG open source dataset and linear training on hindlimb rodent data.

	Accuracy	Precision	Recall	F1-Score (weighted)
A3	0.25	0.71	0.12	0.21
A5	0.91	0.13	0.49	0.21
A7	0.81	0.66	0.67	0.65
A8	0.67	0.74	0.50	0.59
Mean	0.66	0.56	0.44	0.41
SD	0.25	0.25	0.20	0.21

Table A.7: Evaluation of a rodent step classification after TS-TCC pretraining on SEMG open source dataset and fine-tuning on hindlimb rodent data.

	Accuracy	Precision	Recall	F1-Score (weighted)
A3	0.18	0.32	0.10	0.15
A5	0.78	0.02	0.14	0.03
A7	0.81	0.72	0.60	0.63
A8	0.66	0.74	0.44	0.55
Mean	0.61	0.45	0.32	0.34
SD	0.25	0.30	0.21	0.26

Table A.8: Step and stand label results after linear training from a TS-TCC + curriculum pretrained feature extractor.

	Accuracy	Precision	Recall	F1-Score (weighted)
A3	0.22	0.74	0.12	0.19
A5	0.84	0.02	0.14	0.04
A7	0.80	0.65	0.67	0.65
A8	0.63	0.63	0.46	0.52
Mean	0.62	0.51	0.35	0.35
SD	0.25	0.29	0.23	0.25

Table A.9: Step and stand label results after fine-tuning from a TS-TCC + curriculum pretrained feature extractor.

	Accuracy	Precision	Recall	F1-Score (weighted)
A3	0.21	0.82	0.11	0.17
A5	0.81	0.08	0.53	0.14
A7	0.79	0.72	0.61	0.63
A8	0.65	0.70	0.39	0.50
Mean	0.62	0.58	0.41	0.36
SD	0.24	0.29	0.19	0.21

Table A.10: Step and stand label results after linear training from a TS-TCC pretrained feature extractor using TaichiDB open source dataset.

	Accuracy	Precision	Recall	F1-Score (weighted)
A3	0.18	0.33	0.03	0.06
A5	0.96	0.30	0.22	0.25
A7	0.76	0.15	0.07	0.09
A8	0.56	0.14	0.03	0.04
Mean	0.61	0.23	0.08	0.11
SD	0.29	0.09	0.08	0.08

Table A.11: Step and stand label results after fine-tuning from a TS-TCC pretrained feature extractor using GrabMYO open source dataset.

	Accuracy	Precision	Recall	F1-Score (weighted)
A3	0.19	0.29	0.09	0.13
A5	0.81	0.02	0.16	0.03
A7	0.80	0.73	0.56	0.61
A8	0.65	0.70	0.41	0.51
Mean	0.61	0.44	0.30	0.32
SD	0.25	0.30	0.19	0.24

Table A.12: Step and stand label results after linear training from a TS-TCC pretrained feature extractor using GrabMYO open source dataset.

	Accuracy	Precision	Recall	F1-Score (weighted)
A3	0.22	0.70	0.16	0.25
A5	0.83	0.03	0.20	0.05
A7	0.81	0.71	0.60	0.64
A8	0.63	0.78	0.37	0.49
Mean	0.62	0.56	0.33	0.36
SD	0.24	0.30	0.17	0.23

Table A.13: Step and stand label results after fine-tuning from a TS-TCC pretrained feature extractor using all pre-processed open source datasets.

	Accuracy	Precision	Recall	F1-Score (weighted)
A3	0.20	0.33	0.11	0.16
A5	0.80	0.03	0.24	0.05
A7	0.81	0.73	0.56	0.61
A8	0.63	0.68	0.42	0.51
Mean	0.61	0.44	0.33	0.33
SD	0.25	0.29	0.17	0.24

Table A.14: Step and stand label results after linear training from a TS-TCC pretrained feature extractor using all pre-processed open source datasets.

	Accuracy	Precision	Recall	F1-Score (weighted)
A3	0.28	0.78	0.18	0.30
A5	0.81	0.05	0.20	0.06
A7	0.83	0.75	0.61	0.66
A8	0.64	0.72	0.41	0.52
Mean	0.64	0.58	0.35	0.38
SD	0.22	0.30	0.18	0.23

Table A.15: TA and GM afferent axon tuning performance measured by Pearson correlation coefficient (CC) and mean absolute error (MAE). All correlations were significant ($p < 0.05$).

Afferent	CC	MAE (Hz)
TA Ia	0.99	1.97
TA II	1.00	1.57
GM Ia	1.00	2.25
GM II	1.00	1.86

A.2 Supplementary Figures

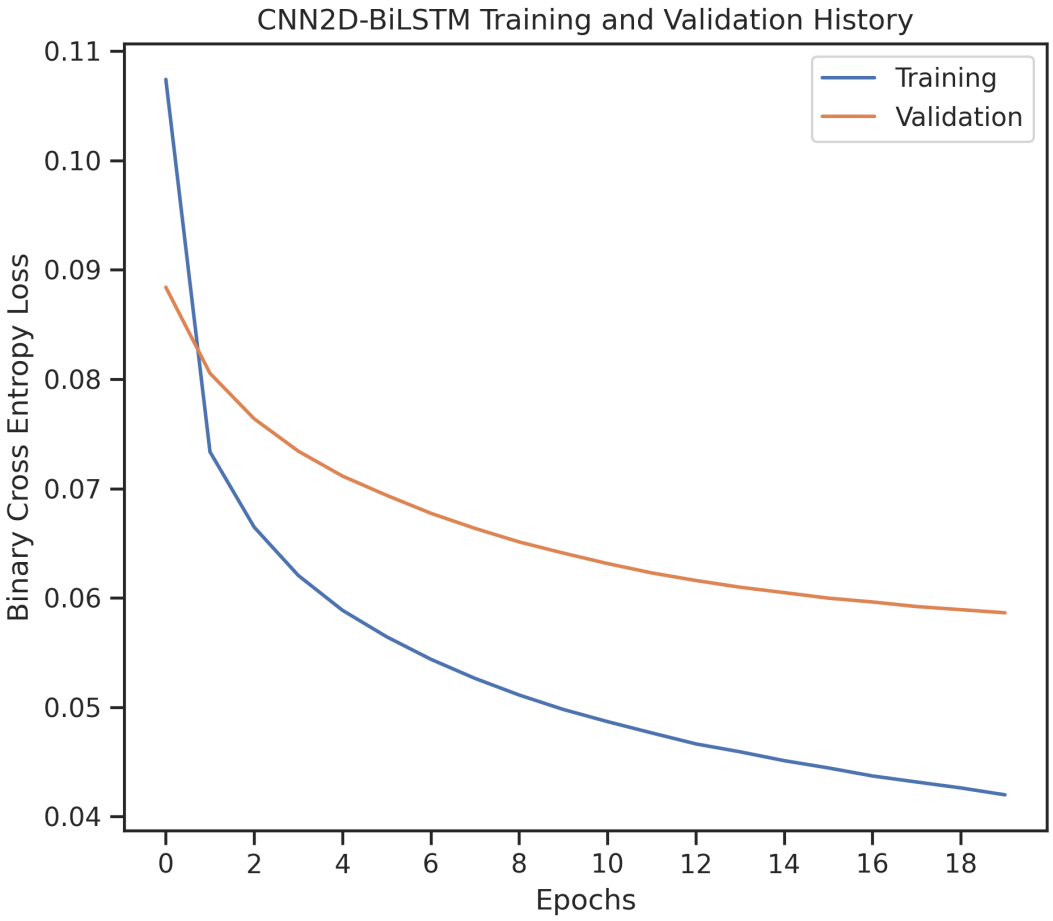

Figure A.1: Training and validation loss history of CNN2D-BiLSTM hybrid model.

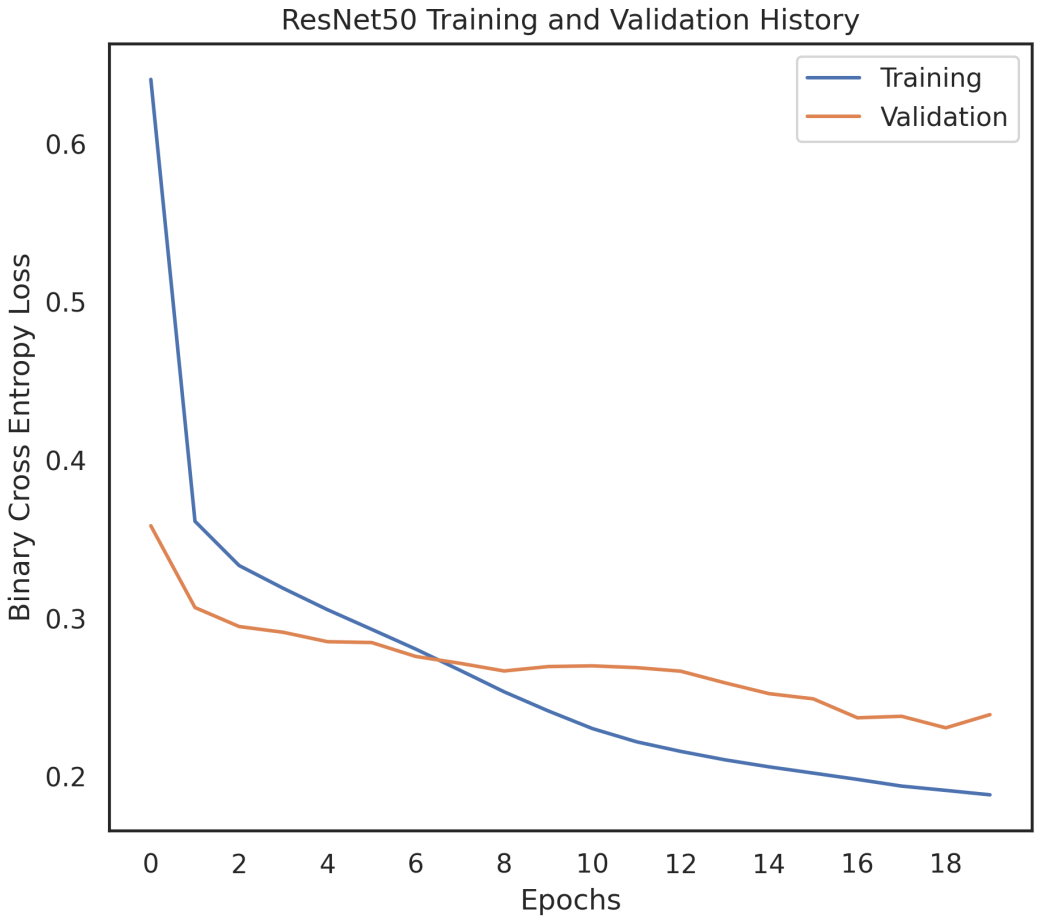

Figure A.2: Training and validation loss history of ResNet50 model.

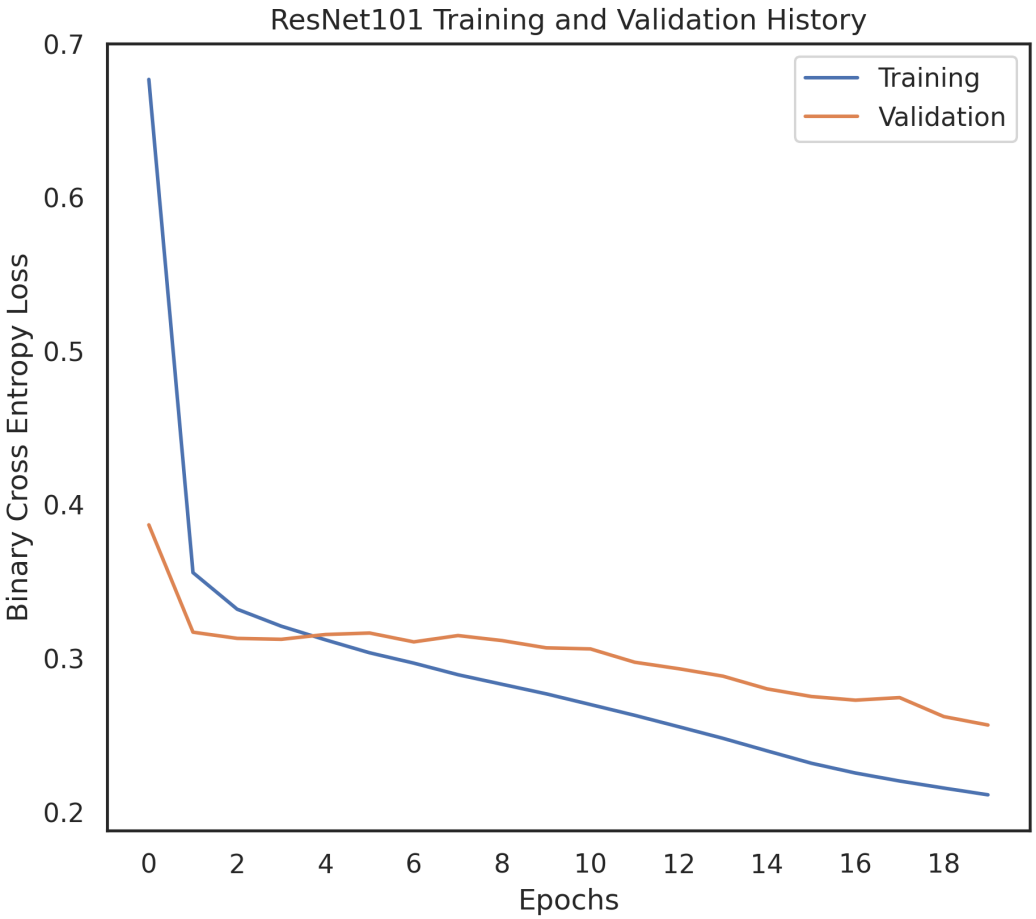

Figure A.3: Training and validation loss history of ResNet101 model.

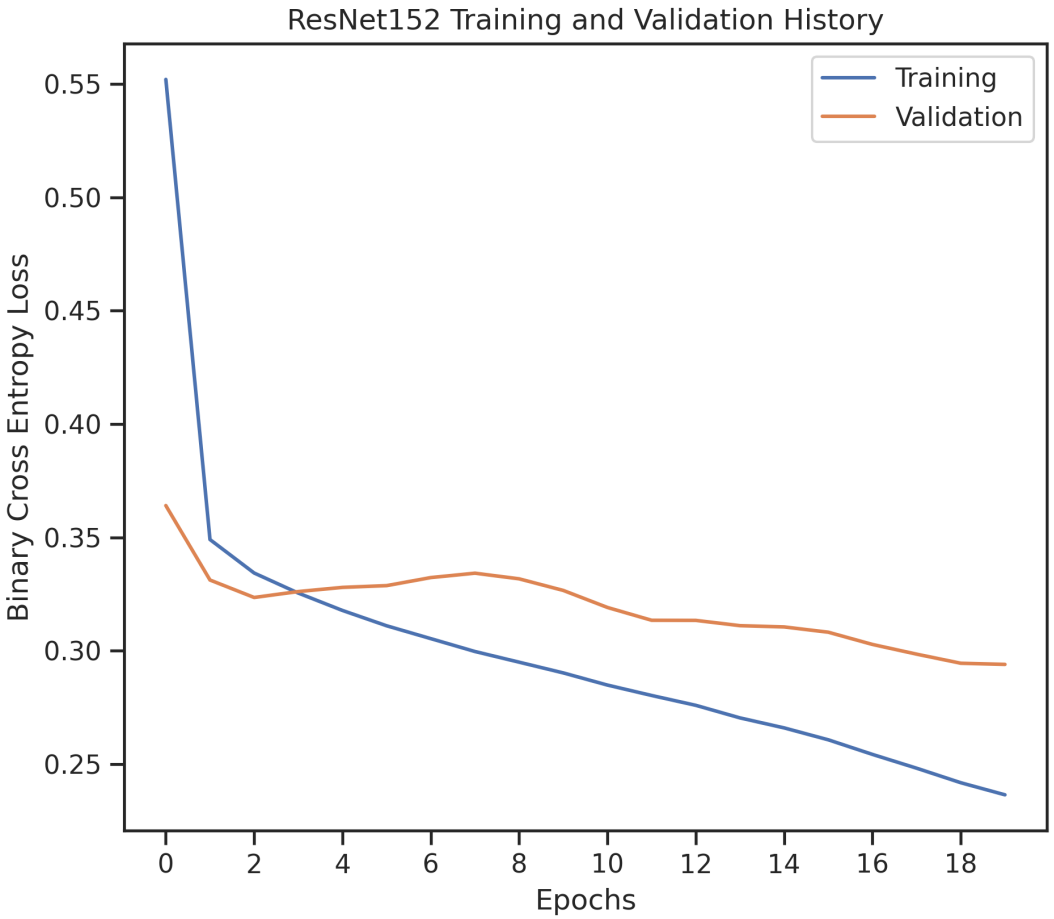

Figure A.4: Training and validation loss history of ResNet152 model.

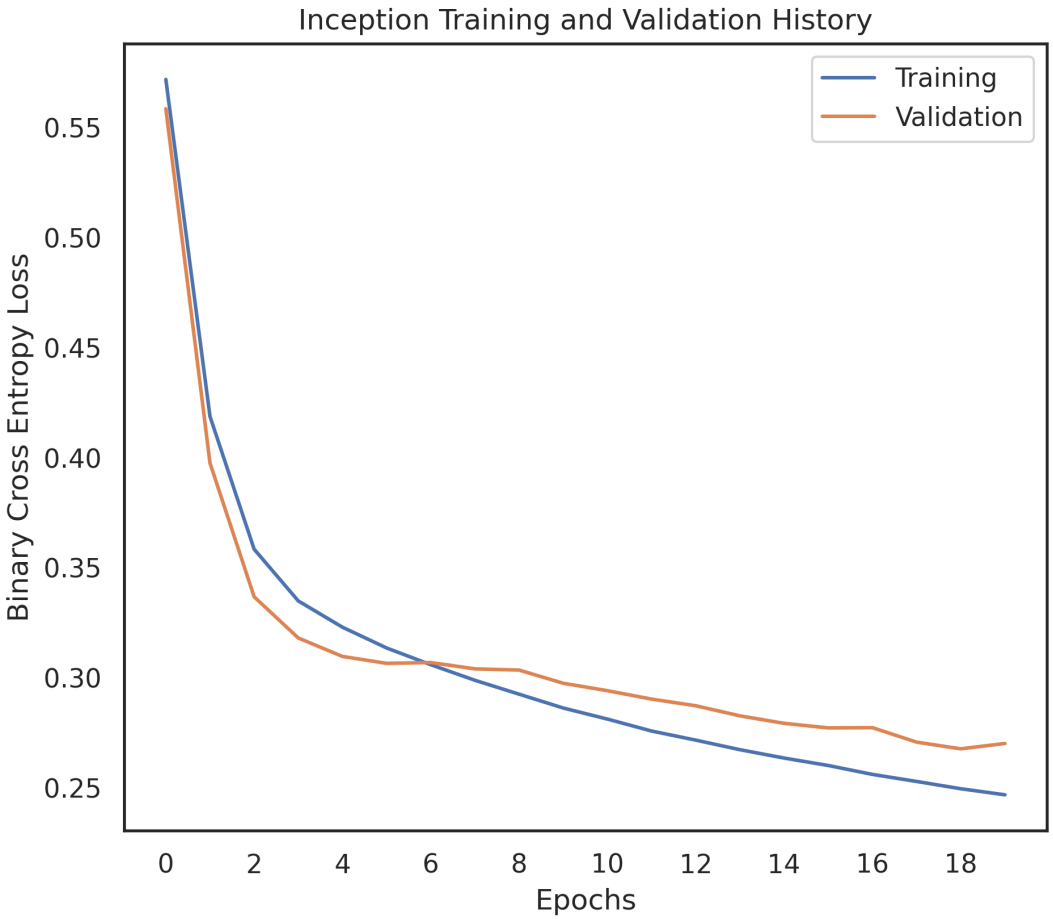

Figure A.5: Training and validation loss history of Inception model.

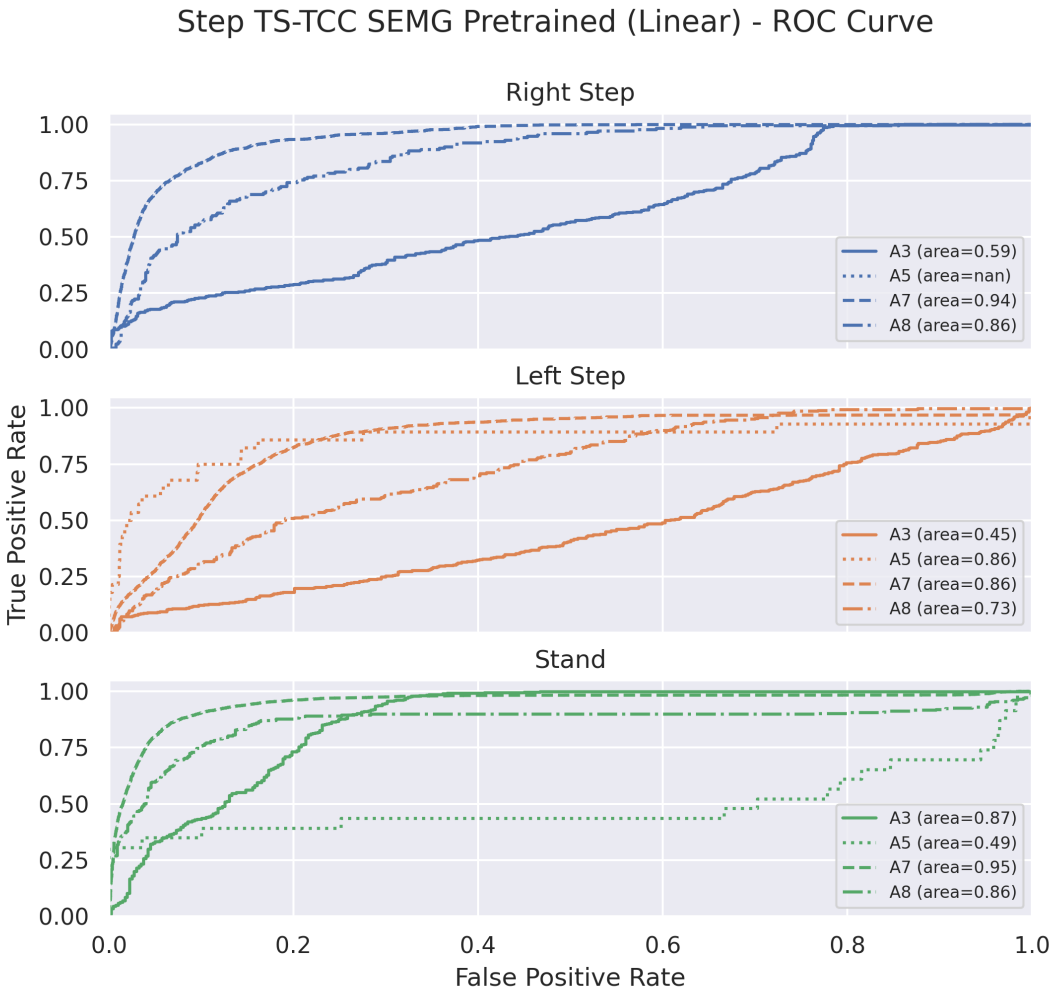

Figure A.6: ROC curve of the each subject and each stepping and standing label for $\text{SSL}_{SEMG,linear}$. No right steps were successfully detected for A5.

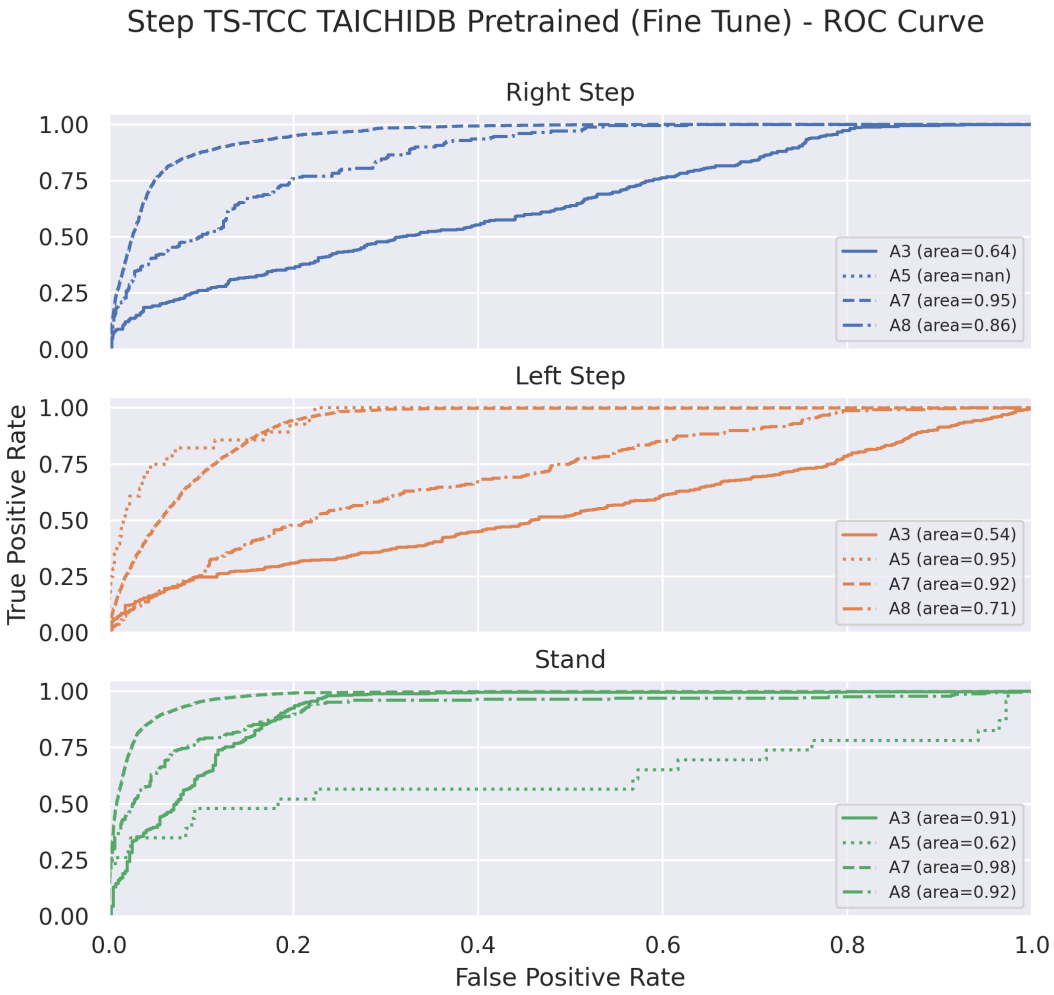

Figure A.7: ROC curve of the each subject and each stepping and standing label for $\text{SSL}_{TaichiDB,fine-tune}$. No right steps were successfully detected for A5.

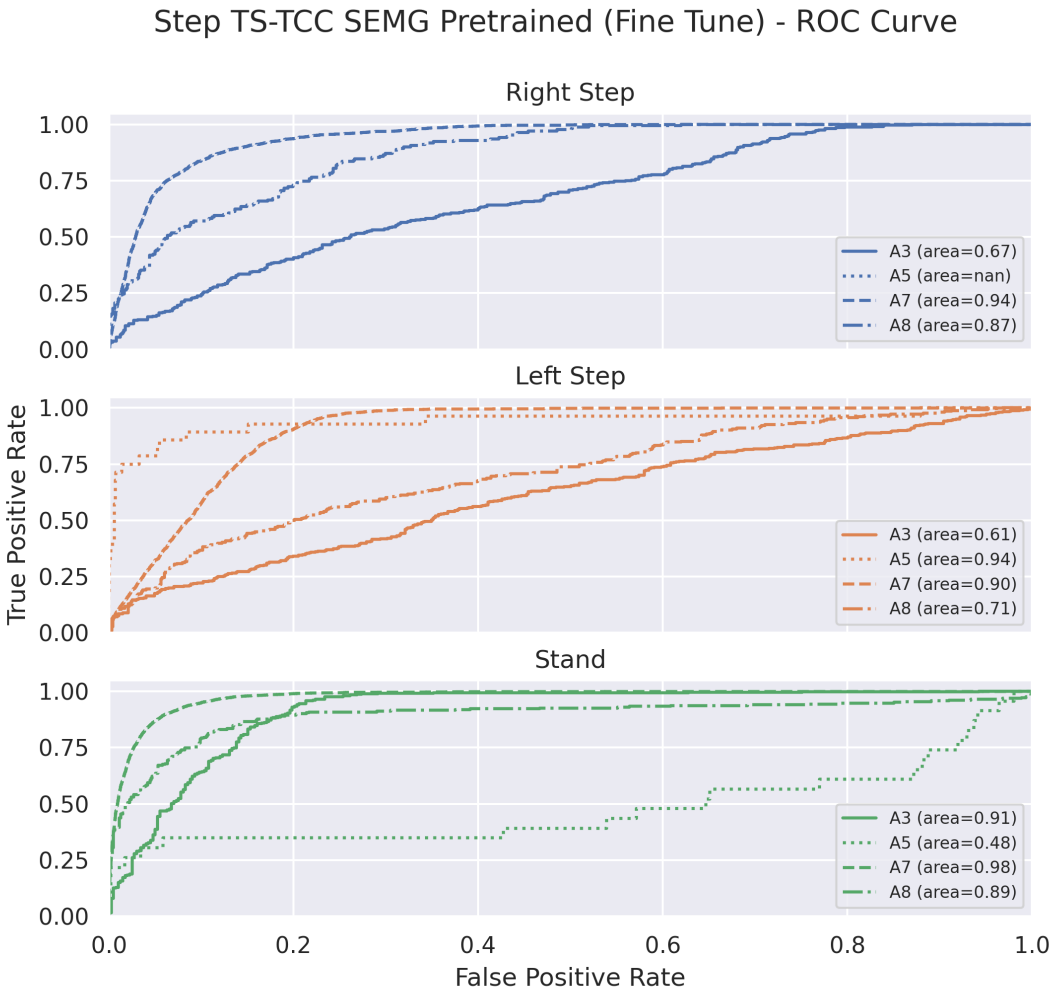

Figure A.8: ROC curve of the each subject and each stepping and standing label for $\text{SSL}_{SEMG,fine-tune}$. No right steps were successfully detected for A5.

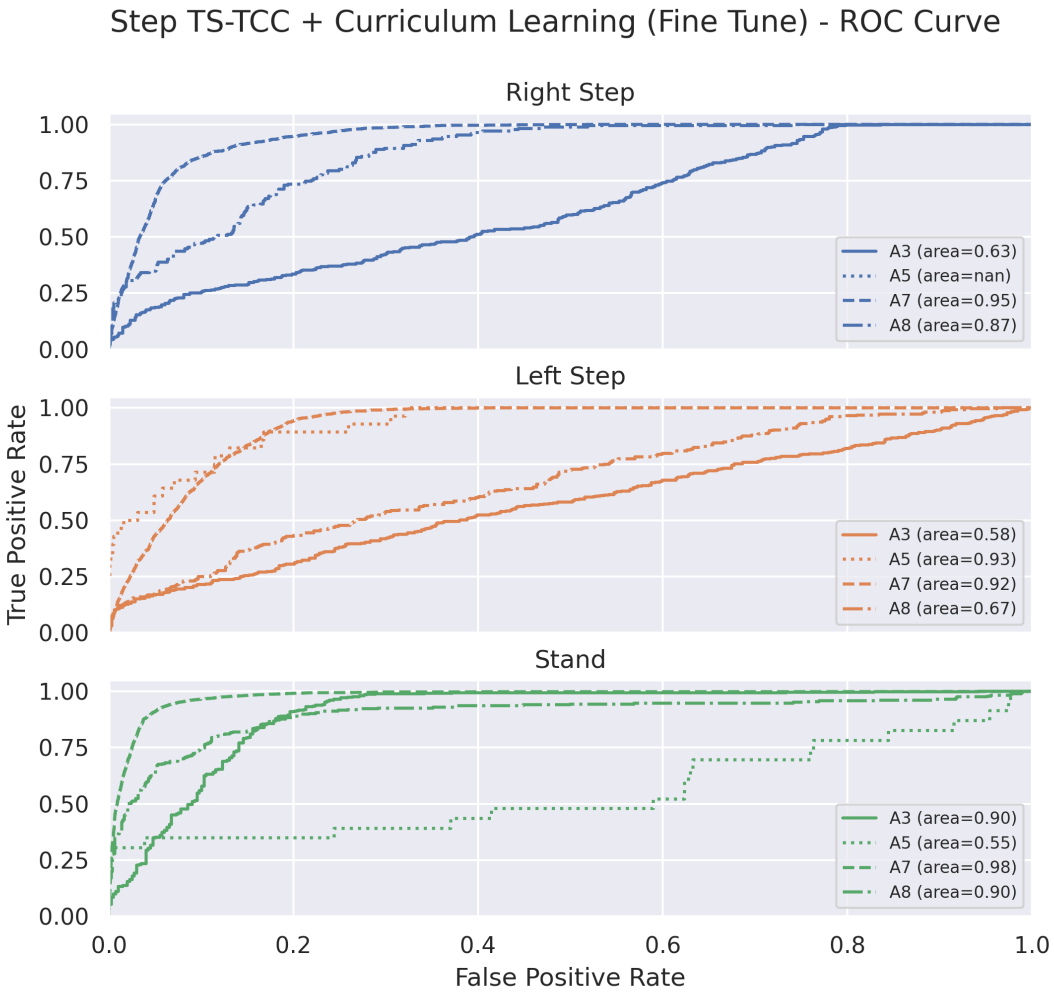

Figure A.9: ROC curve of the each subject and each stepping and standing label for SSL+CL$_{fine-tune}$. No right steps were successfully detected for A5.

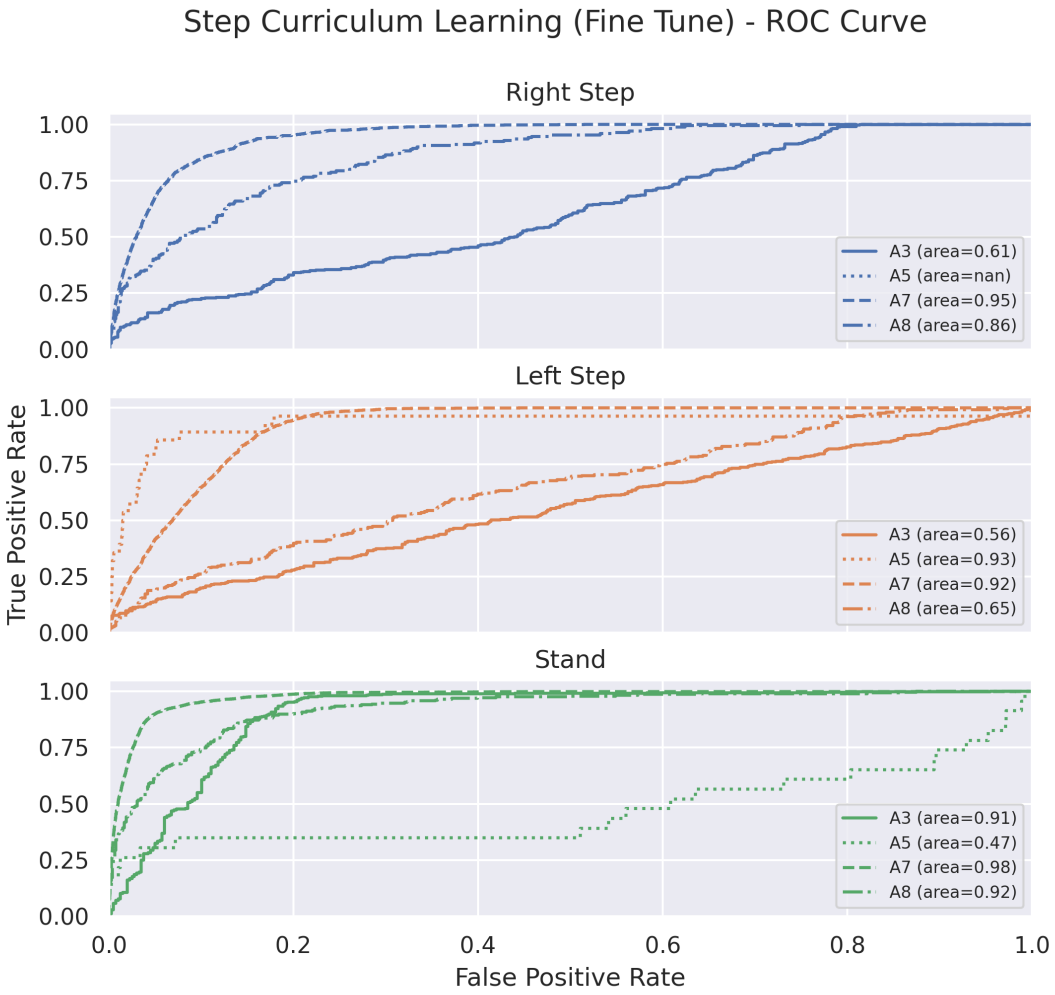

Figure A.10: ROC curve of the each subject and each stepping and standing label for $\mathrm{CL}_{fine-tune}$. No right steps were successfully detected for A5.

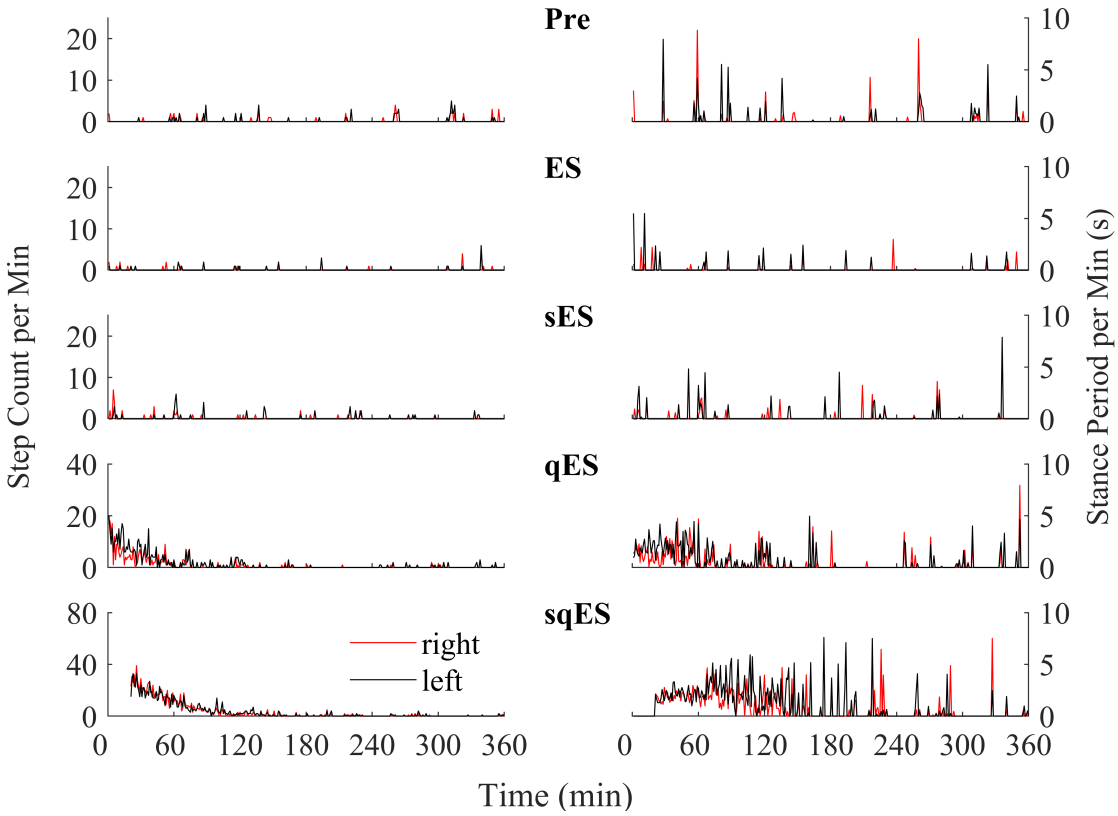

Figure A.11: Example plot of number of detected step-like activity over the course of 6-hr recording across different therapies for rat number 1.

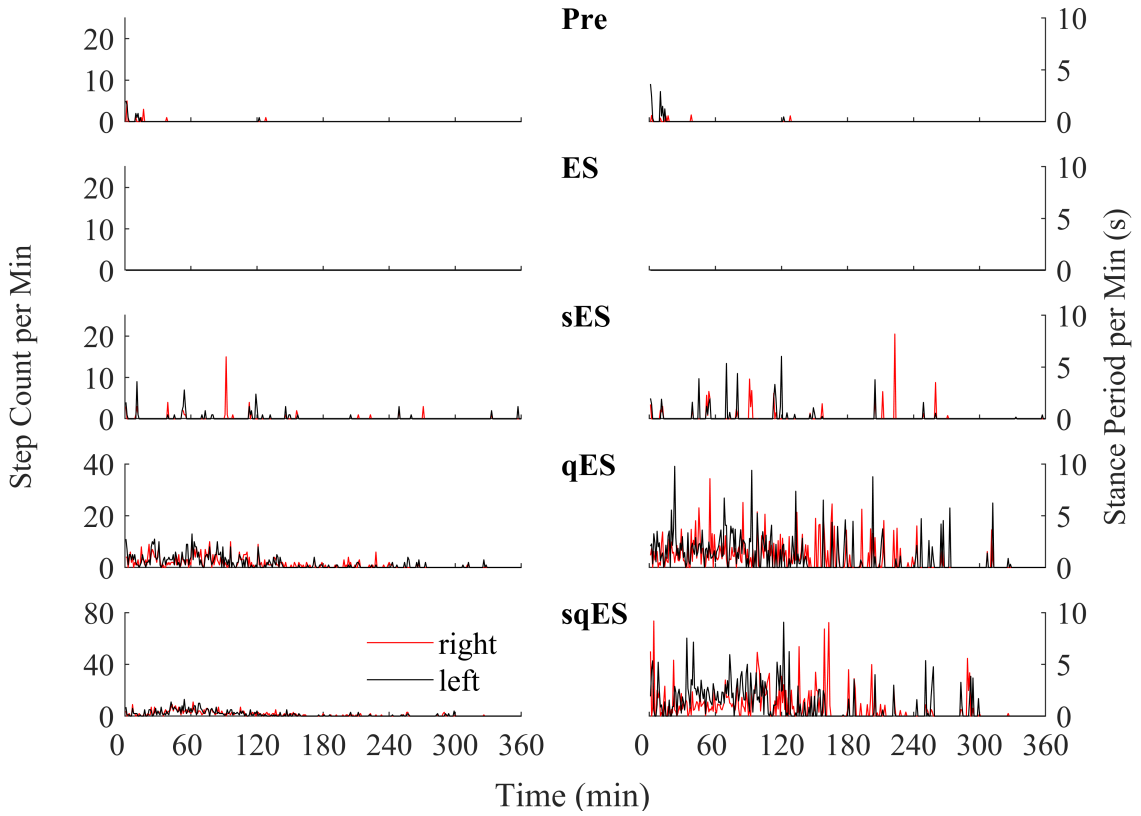

Figure A.12: Example plot of number of detected step-like activity over the course of 6-hr recording across different therapies for rat number 2.

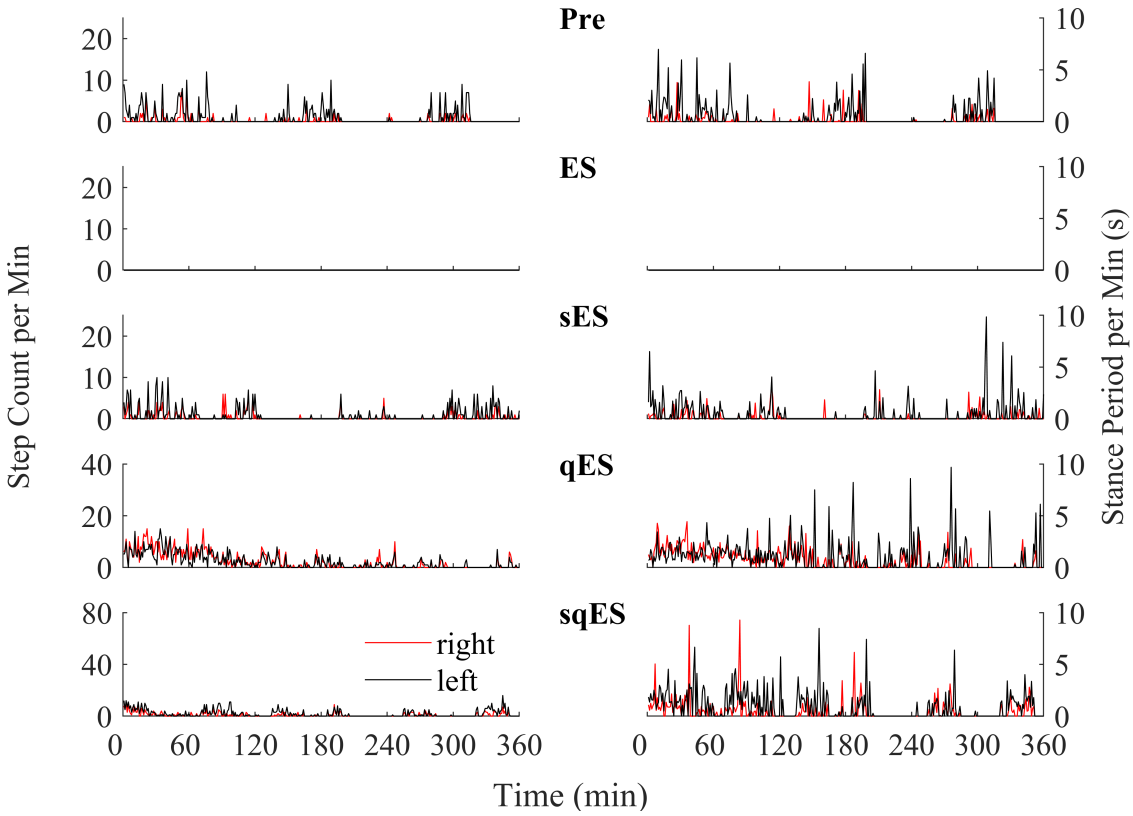

Figure A.13: Example plot of number of detected step-like activity over the course of 6-hr recording across different therapies for rat number 4.

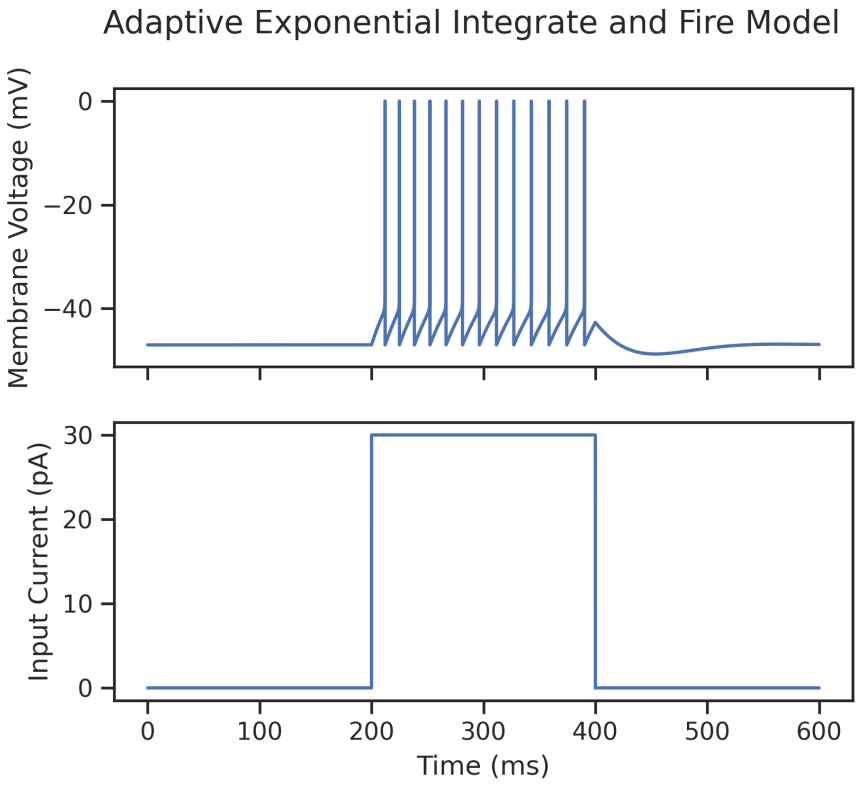

Figure A.14: Simulated AdEx LIF V2a IN tonic spiking response after receiving a 200 ms stimulation pulse at 30 pA.

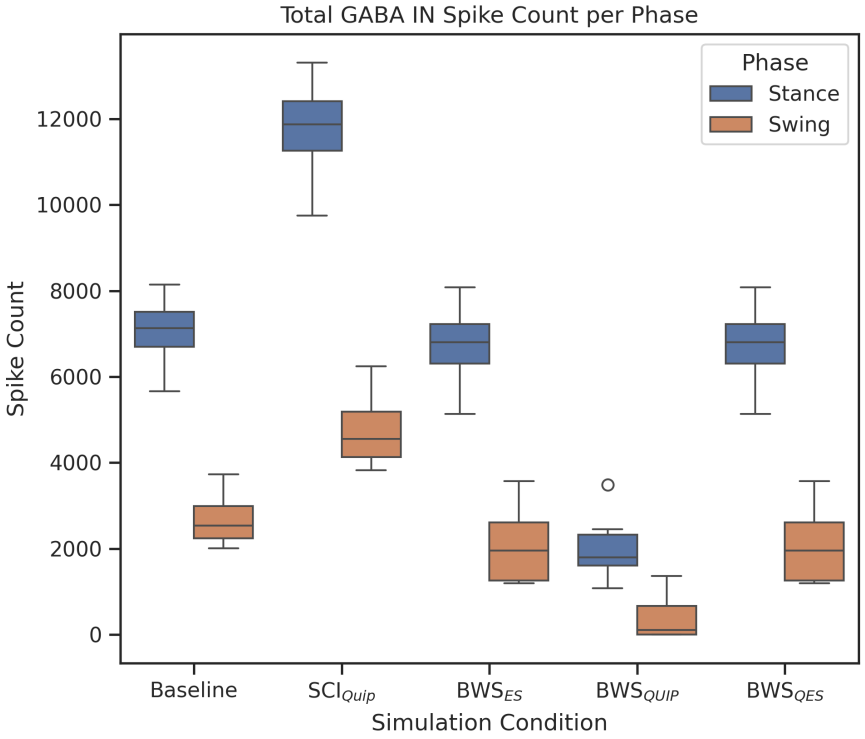

Figure A.15: Box-and-whisker plots of GABA IN spiking activity for 8-steps during baseline and simulated conditions. Shapiro-Wilk test returned a normal distribution for swing phase only. All stance flexor activity was significantly different after Wilcoxon signed-rank test with the exclusion of BWS$_{ES}$ – BWS$_{qES}$. Swing flexor activity was significantly different after Tukey HSD test with the exclusion of Baseline – BWS$_{ES}$, Baseline – BWS$_{qES}$, and BWS$_{ES}$ – BWS$_{qES}$.

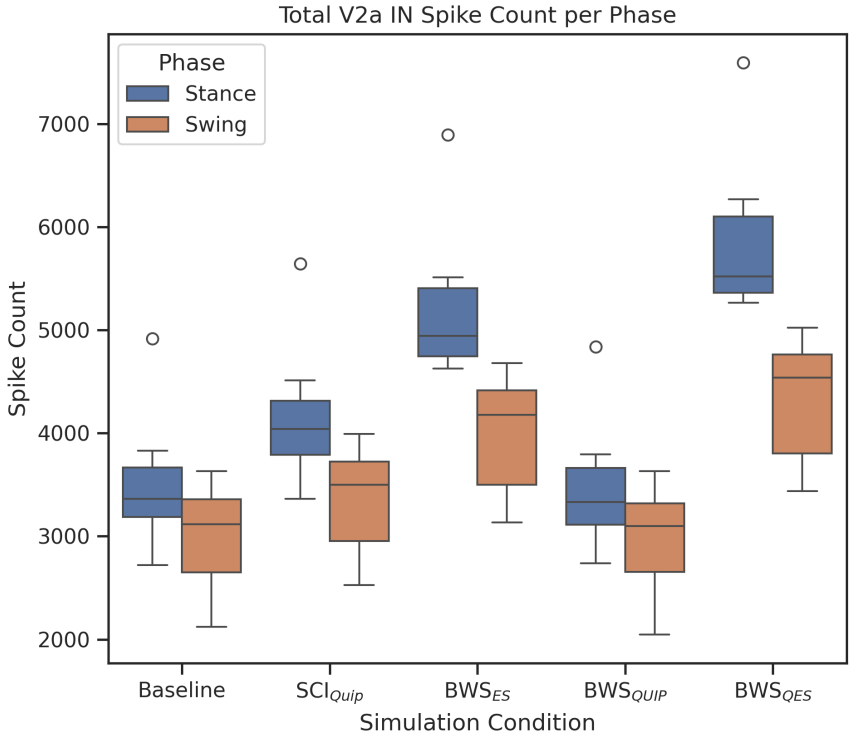

Figure A.16: Box-and-whisker plots of V2a IN spiking activity for 8-steps during baseline and simulated conditions. Shapiro-Wilk test returned a normal distribution for both phases. All stance flexor activity was significantly different after Tukey HSD test with the exclusion of Baseline – SCI$_{Quip}$, Baseline – BWS$_{Quip}$, SCI$_{Quip}$ – BWS$_{Quip}$, and BWS$_{ES}$ – BWS$_{qES}$. Swing flexor activity was only significantly different between Baseline – BWS$_{ES}$, Baseline – BWS$_{qES}$, SCI$_{Quip}$ – BWS$_{qES}$, BWS$_{ES}$ – BWS$_{Quip}$, and BWS$_{Quip}$ – BWS$_{qES}$ after Tukey HSD test.

A.3 Spinal Circuit Architecture

A.3.1 Commissural INs

Commissural INs (CINs) are spinal synapses that cross the midline of the spinal cord to the contralateral side with long or short segmental range. CINs are located in laminae IV – VIII, and X within the cervical and lumbar spinal cord segments (Jankowska et al., 2009; Soteropoulos, 2018; Bannatyne et al., 2003). These connections are thought to contribute to left-right coordination during locomotion via glutamatergic and glycinergic/GABAergic

inputs (Quinlan and Kiehn, 2007). CINs are observed in crossed reflex actions from group I, II and cutaneous afferents, projecting onto MNs (Edgley and Jankowska, 1987; Jankowska et al., 2009). Crossed inhibitory responses are likely to be spinally mediated in humans and shine some light on potential CPG networks in the human spinal cord (Stubbs et al., 2011a,b).

A.3.2 Propriospinal INs

Propriospinal INs (PINs) originate and terminate within the spinal cord through intra-segmental connections across multiple spinal segments (Cowley et al., 2010). Short PINs extend 1 – 6 spinal segments in most laminae, except IX (see fig. 2.4) (Flynn et al., 2011). These short networks involve upper- and lower-limb commands during movement, conveying descending information to MN pools. Cell bodies of short PINs are densely populated in lamina VII, the intermediate zone. Axons of short PINs surround deep layers of the white matter, bordering the grey matter and the dorsal column (Flynn et al., 2011; Niu et al., 2013; Baek et al., 2017). Short PINs medially located often project contralaterally, and laterally located PINs often project ipsilaterally (Flynn et al., 2011). Most long PINs are located in lamina VIII and medial lamina VII. Still, they also exist in lamina I, IV – VI, and X. Axons of long PINs project bilaterally and rostrocaudal towards the superficial white matter tracts of the spinal cord, more ventrolaterally (Flynn et al., 2011). Long PINs terminate in laminae V – VIII and sparsely in IX (Flynn et al., 2011). Some of these long PINs synapse between cervical and lumbar enlargements are hypothesised to contribute to forelimb-hindlimb interlimb coordination and trunk stabilisation (Brockett et al., 2013; Eisdorfer et al., 2020; Etlin et al., 2010; Flynn et al., 2017; Ni et al., 2014; Niu et al., 2013; Laliberte et al., 2019; Pocratsky et al., 2020). Long PINs are mainly excitatory, but most inhibitory populations project ipsilaterally (Flynn et al., 2017). PINs receive both supraspinal and sensory inputs and project to other INs,

MNs, and cortical structures (Cote et al., 2018; Brownstone et al., 2015; Laliberte et al., 2019; Niu et al., 2013). Due to their complex and integratory nature, PINs have been suggested to be a possible neural detour around spinal lesions, recovering voluntary sensorimotor control after SCI (Eisdorfer et al., 2020; Filli et al., 2014; Taccola et al., 2018; Gerasimenko et al., 2009; Laliberte et al., 2019).

A.3.3 Presynaptic Inhibition

Classically, presynaptic inhibition has been thought to contribute to movement smoothening by filtering noisy sensory feedback from the periphery (Eccles et al., 1962; Willis, 2006; Fink et al., 2014). This mechanism, caused by primary afferent depolarization, involves GABAA receptor release at Ia-MN synapses. During activation of GABAA receptors, an outward movement of Cl^- ions leads to depolarization (Rudomin, 1990). Presynaptic inhibition exhibits strong graded inhibitive control over spike amplitude and has an 'all-or-nothing' effect at the release site (Segev, 1990).

GABAergic synapses have inputs from brainstem reticular formation, expressing inhibitory connections with GABA INs synapsing directly to Ia fibres, see fig. A.17. Group Ib fibres are depolarized by other group Ib afferents and reticulospinal, rubrospinal, corticospinal, and vestibulospinal fibres (Rudomin, 1990). Studies have also shown GABAB receptors producing presynaptic inhibition behaviour between interneurons and Ia afferent fibres in the mammalian spinal cord (Rudomin, 1990). GABAA actions appear to be short lasting and more suited to block conduction at branch points. However, GABAB receptors could be involved in long-term modulation of synaptic efficacy in afferent fibres (Rudomin, 1990).

Observations of presynaptic inhibition have also been noted in Ib, II, cutaneous mechanoreceptors, and nociceptor afferents (Goulding et al., 2014). In the article (Jankowska et al., 1981), stimulation of group I flexor fibres produced primary afferent depolarization

in group Ia fibres of both flexors and extensors via pathways of at least 2 interneurons. Driven by proprioceptive input, these neural circuits are highly selective and are not distributed equally, affecting specific MN pools differentially. The existence of neural asymmetries allows for selective control of converging Ia and Ib afferents. Examples of presynaptic inhibition differentially controlling sensory integration during locomotion have been documented in the following papers (Rossignol et al., 2006; Courtine et al., 2007b; Lamy et al., 2010; Gerasimenko et al., 2016a,b) and reviewed in (Rudomin and Schmidt, 1999; Rudomin, 2009; Knikou, 2008).

Motor outputs of an isolated lumbosacral rodent spinal cord modulate according to the phase of the step cycle (Gad et al., 2015, 2013c; Shah et al., 2013). In these studies, exogenous neuromodulatory inputs were tonic. Thus, these modulations were hypothesised to be an effect of sensory-dependent mechanisms. See (Stein, 1995; Dy et al., 2010; Hultborn et al., 1987) for descriptions of how potential presynaptic inhibition pathways control the onset of movement and aid selective muscle activation.

Mazzone published a recent article discussing the GABAergic mechanisms as therapeutic targets in damaged spinal cord networks (Mazzone et al., 2021). The authors hypothesise an imbalance of GABA activity in the early stages of spinal cord injury gate sensory inputs, disabling afferent sensory network activity. These ideas were paralleled in a review by Bui and Lalonde (Lalonde and Bui, 2021). In contrast, deficits in GABAergic mechanisms contribute to spasticity. The presynaptic inhibition networks inhibiting sensory inflow may be downregulated from supraspinal centres. Notably, anodal trans-spinal direct current stimulation plus bumetanide (antagonist of NKCC1, or $NA^{+}-K^{+}-2Cl^{-}$ cotransporter 1, expression, important for synaptic actions of GABA and glycine), downregulated NKCC1 after spinal contusion (Mekhail et al., 2018). This attenuated spasticity and reduced abnormal locomotor muscle tone in rodent models. Further evidence behind the excitation/inhibition homeostasis for an improved, coordi-

nated locomotor function was recently published in (Gong et al., 2021), highlighting the therapeutic potential of GABA neurons after SCI. In the zebrafish, GABAergic spinal neurons, in contact with CSF, directly project onto glutamatergic premotor interneurons ($V0_v$). Activation of these GABAergic neurons at rest induced delayed slow fictive locomotion. Selective activation of the rostral neurons during ongoing activity disrupted rostrocaudal propagation and inhibited ongoing slow locomotion (Fidelin et al., 2015). Evidence to suggest GABAergic neurons in contact with CSF are conserved in bony vertebrate species was presented in (Djenoune et al., 2014).

Investigation towards the excitation/inhibition balance on sensory integration in the spinal cord is an area for further research. The reasons behind these observations and the mechanisms of action have yet to be fully understood. However, we can see collectively that these results provide evidence of local locomotor spinal circuitry capability in automatically integrating proprioceptive and mechanosensory information, with minimal input required from cortical centres. Indeed, presynaptic pathways play a significant role in coordinating locomotor and other rhythmic motor patterns.

A.3.4 Group Ia INs

Group Ia INs (IaIN) are located in lamina V, VI, dorsal VII, dorsal or dorsomedial to the associate motor nuclei (Jankowska, 1992). Group Ia afferents, carrying proprioceptive stretch velocity information, excite IaINs (Cote et al., 2018), mediating short-latency inhibition (glycinergic) on antagonist MNs and contralateral IaINs. IaINs may act as premotor multimodal integration neurons, receiving inputs from peripheral and supraspinal structures (fig. A.18). These INs affect MNs up to one or two segments away, projecting over several millimetres in white matter tracts surrounding the ventral horn. Axons then re-enter grey matter and inhibit the antagonist's muscles.

Excitation of IaINs is directly received from ipsilateral vestibulospinal and pro-

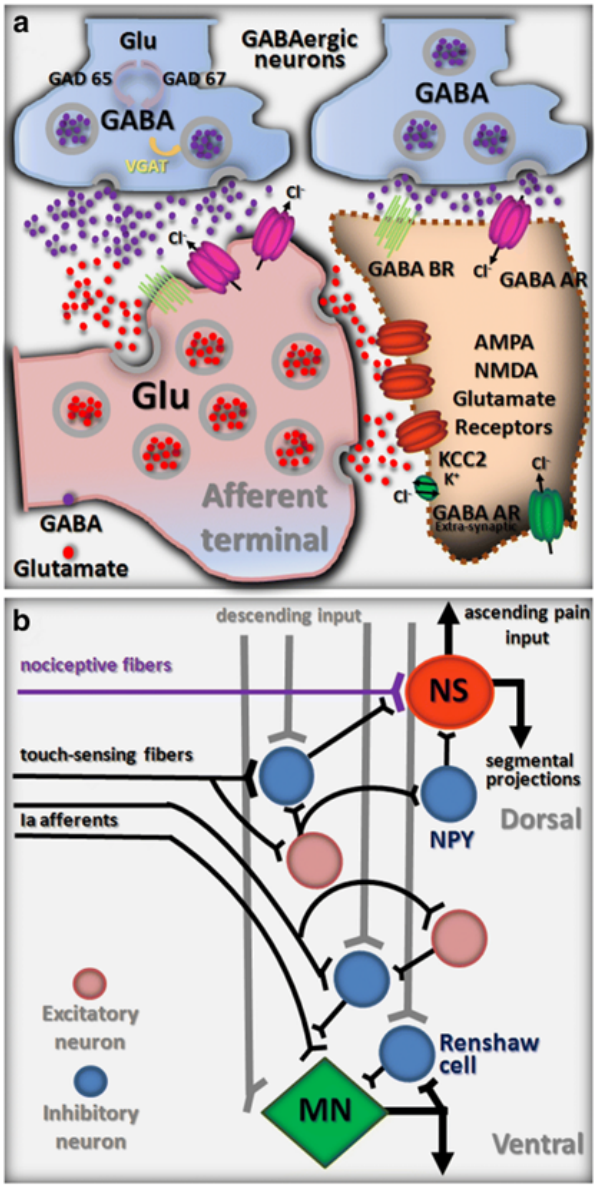

Figure A.17: Simplified illustration of GABAergic synapses and wiring in the spinal cord (Mazzone et al., 2021). **A** represents typical GABAergic synapse in pre (left) and post (right) synaptic inhibition, respectively. **B** is a simplified wiring diagram of basic GABAergic circuits in presynaptic inhibition of afferent input. NS, nociceptive-specific projection neuron; MN, motoneuron. Licensed under a Creative Commons Attribution 4.0 International License.

priospinal tracts. Indirect excitation occurs via ipsi- and contralateral flexor reflex afferents (FRAs), ipsilateral cutaneous afferents, and ipsilateral rubrospinal, corticospinal and contralateral vestibulospinal tracts. IaINs are inhibited by contralateral IaINs

and Renshaw Cells (RCs) of the homonymous MN pool. IaINs are also subject to flexor Ia afferent presynaptic inhibition. IaINs project monosynaptically to both MNs and contralateral IaINs (Jankowska, 2013a). Axons of IaINs may project over one or two segments away, entering deep white matter tracts before making synaptic contact with the antagonist MN (Jankowska, 2013a; Flynn et al., 2011).

As last-order glycinergic inhibitory INs, IaINs assist in ipsilateral coordination by reducing co-contraction. This is expressed by an amplitude-phase dependence with max amplitude for soleus during the extension phase and decreased reflex gain during the flexion phase (Stein and Capaday, 1988). (Adolfo et al., 2011) identifies Ia inhibitory INs as the primary contributor to reciprocal inhibition from muscle proprioceptors and antagonist motor neurons. Differentiating expressions of stretch amplitude modulation are attributed to α – MN excitability modulation produced by CPG via pre-motor networks. IaIN excitation can contribute to resetting locomotor rhythm during fictive locomotion, postulating a role in excitatory inputs to the CPG (Guertin et al., 1995). Recent genetic tracing work has shown that IaINs are one of the last spinal interneuron types to diversify during adulthood (Wu et al., 2021a). Compared to the control group, iaINs undergo site-specific differentiation during mouse free-running wheel exercise. These networks are suspected to contribute significantly towards spinal plastic change during task-specific training.

A.3.5 Renshaw Cells

Renshaw Cells (RCs) are locally recurrent inhibitory premotor INs, primarily found in lamina VII and occasionally lamina IX. RCs are predominantly glycinergic with a small GABAergic population (see fig. A.18) (Alvarez and Fyffe, 2007). The reflex response ranges from 1 – 1.2ms, suggesting direct inhibition, not mediated by dorsal root activation (Hultborn et al., 1971a). RCs receive excitatory inputs from any number of

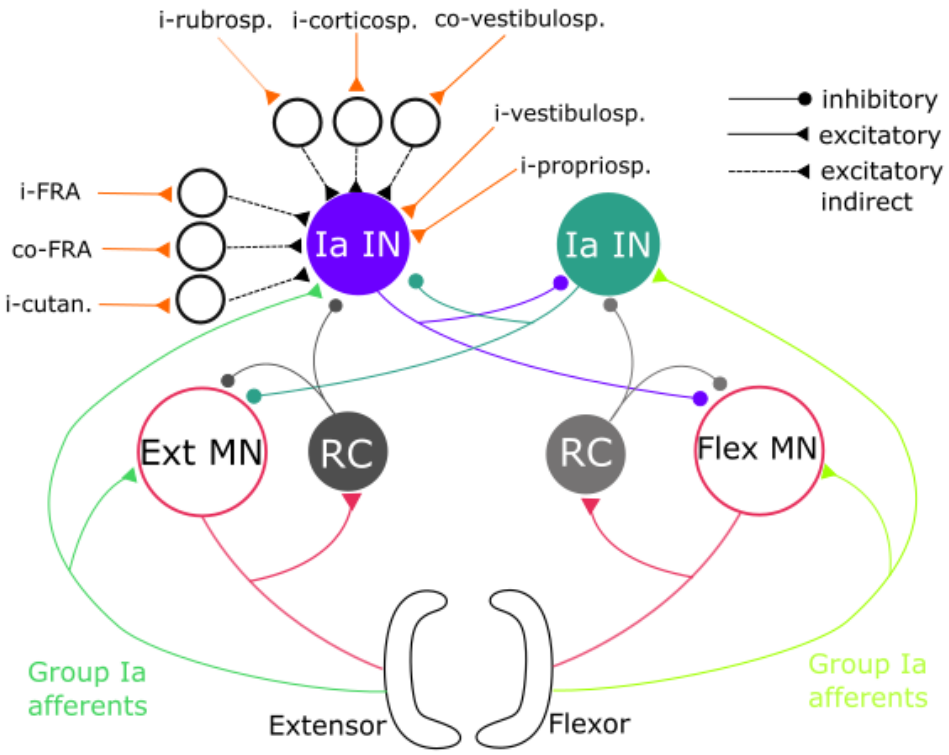

Figure A.18: Spinal network diagram of group Ia interneuron pathways, adapted from figure 30.5 (Jankowska, 2013a).

MNs and inhibitory inputs from other RCs. The inhibitory effects of RCs project onto neighbouring IaINs, coupled MNs, and MNs located one or two spinal segments away (Hultborn et al., 1971b). These inhibitory networks slow down rapidly firing contractions, synchronise MN discharge and prevent persistent inward currents (Hultborn et al., 2003). RC activation appears more prominent in stereotyped activity but absent when skilled motor activity is required (Cote et al., 2018). RC networks, alongside Group Ia activity, have been hypothesised to participate in reciprocal inhibition and locomotion CPG rhythm frequency.

A.3.6 Group Ib INs

Group Ib INs (IbINs) are located in laminae VI and dorsal VII of the spinal cord, characterised by the convergence of multimodal inputs from more than just Ib afferents (see

fig. A.19). Golgi tendon organ inputs, relaying active and passive muscle tension, travel through dorsal roots, synapsing to IbINs. Other inputs include corticospinal, rubrospinal, and reticulospinal tracts, propriospinal neurons via dorsomedial column, Ia/II spindle afferents, and cutaneous afferents (Jankowska and McCrea, 1983; Jankowska and Edgley, 2010). IbIN terminals are subject to presynaptic inhibition, which gates the autogenic inhibition exerted on coupled, homonymous MNs. IbINs project to ventral and dorsal spinocerebellar tract cells, α- and γ-MNs, and other IbINs. Historically, IbINs were thought to be solely responsible for autogenic gating. Studies have provided evidence for a more widespread function. The complex converging multimodal pathways suggest some role in information integration during muscle contraction and control of both onset and continuous contraction forces. This is expressed in the task-dependent 'switching' of inhibitory and excitatory effects in IbINs. Note that asymmetrical activation from extensor muscles predominantly activates IbINs. Excitation of IbINs can inhibit homonymous MNs or excitation of other MNs, mainly flexors. Group I extensor afferents can reverse from inhibitory to excitatory via excitatory pathways during locomotion (Guertin et al., 1995; Rossignol et al., 2006). These pathways contribute to coordinated movement and locomotion and participate in other segmental and descending inputs. IbINs appear critical for activating the isolated lumbosacral locomotor CPG (Markin et al., 2010; Conway et al., 1987; Rossignol et al., 2006; Van De Crommert et al., 1998).

A.3.7 Group II INs

Group II INs are varied in morphology, input sources, output projections, and function. These INs are in intermediate/ventral laminae VI – VIII and in dorsal laminae IV – V, receiving secondary muscle spindle afferents detailing muscle stretch (see fig. A.19). More ventral INs typically have larger somata and dendritic trees than those more dorsal. Dorsal INs receive group II afferent input and are co-excited by cutaneous afferents

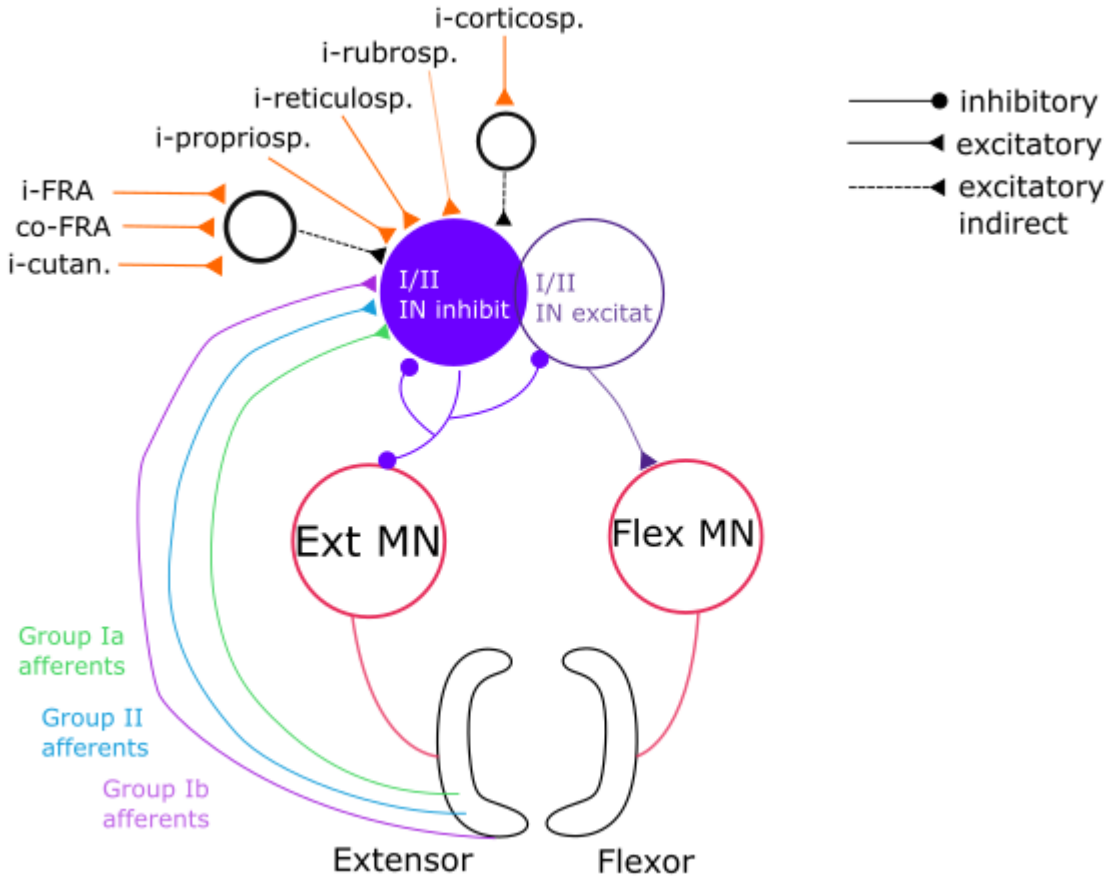

Figure A.19: A diagram of group Ib and II afferent interneuron circuits, adapted from figure 30.9 (Jankowska, 2013a).

(Edgley and Jankowska, 1987). INs across the L3 – 5 segments are not evenly distributed, with group II flexor afferents providing EPSPs to L3 – 5 INs and other muscles providing input to more caudal segments (Edgley and Jankowska, 1987; Lundberg et al., 1987). Dorsal INs with group II input are more likely part of polysynaptic pathways that target ascending cells, including the dorsal column, dorsolateral fasciculus (Bannatyne, 2006), and dorsal-spinocerebellar tract (Jankowska and Puczynska, 2008), or other INs in mixed excitatory and inhibitory pathways (Bannatyne, 2006; Bras et al., 1989). Intermediate excitatory INs are commonly last-order INs that synapse directly onto MNs after activation by muscle afferents or dorsal horn INs (Edgley and Jankowska, 1987). Group II INs in the intermediate zone also receive inputs from Ia, Ib, and II

sensory afferents (Edgley and Jankowska, 1987; Behrends et al., 1983). Group II INs exert di-synaptic excitatory and inhibitory actions on MNs (Cavallari et al., 1987), and tri- or polysynaptic actions of MNs via neurons located in the dorsal horn (Edgley and Jankowska, 1987; Jankowska, 1992). Excitatory group II INs, mainly in lamina IV (dorsal), projected predominantly to ipsilateral Group II INs also receive a low population of cutaneous and joint afferents with group activity subject to inhibition via IbINs and presynaptic inhibition. These pathways are responsible for coordinating contractions of stretch muscles but, given their widespread architecture, are likely involved in various reflex circuits.

A.3.8 Genetic Labelling

Genetic labelling has significantly increased the granularity of connectivity and functional studies in spinal cord neurons. By selectively stimulating or ablating populations of neurons, the architecture and evolutionary substrate of stereotyped movements begin to unravel. Advances in genetic labelling of developmental neurons across species have enabled scientists to establish cardinal spinal interneuron classes and observe their migration connectivity, and define their roles in sensorimotor networks (Goulding, 2009; Zholudeva et al., 2021; Kiehn, 2016; Lai et al., 2016; Lu et al., 2015; Grossmann et al., 2010). Below is a summary of key genetically identified spinal interneurons hypothesised to contribute towards spinal CPG networks.

Ventral interneurons, $V0_D$ and $V0_V$, have been identified in the VII – VIII laminae (Moran-Rivard et al., 2001; Pierani et al., 2001). These neurons receive excitatory glutamatergic input from V2a and primary afferents (Crone et al., 2009; Zhong et al., 2010; Pierani et al., 2001; Griener et al., 2015). $V0_D$ and $V0_V$ interneurons differentiate in their released neurotransmitter and projection targets. $V0_D$ inhibits mainly contralateral flexor MNs via GABAergic transmission, projecting 1 – 3 descending segments (Pierani

et al., 2001; Lanuza et al., 2004; Danner et al., 2016; Lu et al., 2015; Talpalar et al., 2013; Shimizu-Okabe et al., 2022). These neurons appear to have a role in low-speed left/right alternation (Talpalar et al., 2013). Conversely, glutamatergic $V0_V$ interneurons project to contralateral inhibitory populations that predominantly synapse to flexor MNs, across 1 – 3 descending segments (Pierani et al., 2001; Lanuza et al., 2004; Talpalar et al., 2013; Lu et al., 2015). $V0_V$ interneurons are suggested to be involved in high-speed left/right alternation (Talpalar et al., 2013).

$V0_C$ interneurons are in the same laminae as $V0_D$ and $V0_V$. However, they receive glutamate input from descending projections and serotonergic input from the brainstem (Zagoraiou et al., 2009). Presynaptic inhibition from oligosynaptic synaptic sensory inputs also projects onto $V0_C$ interneurons (Zagoraiou et al., 2009). These neurons excite ipsilateral MNs, across 1 – 3 descending segments and appear to modulate MNs in a task-specific manner (Zagoraiou et al., 2009; Lu et al., 2015; Nascimento et al., 2020). More specifically, activation of $V0_C$ neurons resulted in higher recruitment muscle activity, enabling spinal motor output to be matched variably to behaviour-specific demands (Nascimento et al., 2020). $V0_C$ neurons project to extensor MNs. The role of $V0_G$ (glutamate transmitters) in locomotion remains elusive (Zagoraiou et al., 2009; Nascimento et al., 2020).

V1 and V2b neurons reside in laminae VII and receive inputs from primary afferents (Saueressig et al., 1999; Alvarez et al., 2005; Sapir, 2004; Zhang et al., 2014; Stam et al., 2012; Lundfald et al., 2007; Sapir, 2004). V1 and V2b neurons, characterised as Renshaw Cells (RCs) and Ia inhibitory interneurons (IaINs), were mainly glycinergic, and a third were GABAergic (Zhang et al., 2014; Lu et al., 2015). V1 neurons project to descending ipsilateral flexor MNs while V2b neurons project rostrocaudally to ipsilateral extensor MNs (Zhang et al., 2014; Stam et al., 2012; Lundfald et al., 2007; Lu et al., 2015). Research suggests that the flexor-extensor system is organised around V1 and V2b cell

types. This architecture could be evidence of evolutionary substrates from swimming to movable bilateral appendages in overground vertebrates. Indeed, perhaps the locomotor CPG is a neuronal substrate of evolution (Edgerton et al., 2001b). In support, Stam et al. (2012) revealed RCs from V1 progenitors, demonstrating genetically hardwired programming, see appendix A.3.3.

V2a neurons reside in laminae VII and receive serotonergic, glutamatergic inputs from the brainstem and sensory inputs from dI5 INs and mechanosensory feedback (Zhong et al., 2010; Dougherty and Kiehn, 2010; Bourane et al., 2015; Al-Mosawie et al., 2007; Li et al., 2022a). These glutamatergic neurons project rostrocaudally across more than 2 segments to ipsilateral V0s and MNs (Crone et al., 2009; Lanuza et al., 2004; Dougherty and Kiehn, 2010; Lundfald et al., 2007; Stepien et al., 2010; Lu et al., 2015). V2a INs comprise ~30% of glutamatergic INs in the ventral horn and are involved in left/right coordination (Crone et al., 2008). Subclasses of these neurons activate at different locomotor speeds (Zhong et al., 2010; Ausborn et al., 2012). A recent study examined critical spinal interneurons involved in electrically stimulated locomotor recovery after SCI (Kathe et al., 2022). Although not necessary for walking in healthy subjects, ablating V2a neurons prevented spontaneous walking recovery. These results are not necessarily surprising upon appreciating the inputs for V2a activation. Moreover, V2a neurons project to many excitatory elements in the local circuitry. Turning off the activity after SCI significantly hindered locomotor recovery. Refer to fig. A.20 for visual representation.

$V3_D$ INs are found in laminae IV – V and VI – VII and receive inputs from primary, cutaneous, and group II afferents (Borowska et al., 2013; Jankowska, 2008; Jankowska and Edgley, 2010). These INs are excitatory and project bilaterally in rostral and caudal directions across more than 2 segments (Blacklaws et al., 2015; Danner et al., 2019; Borowska et al., 2013; Lu et al., 2015). Contralateral targets include extensor MNs and

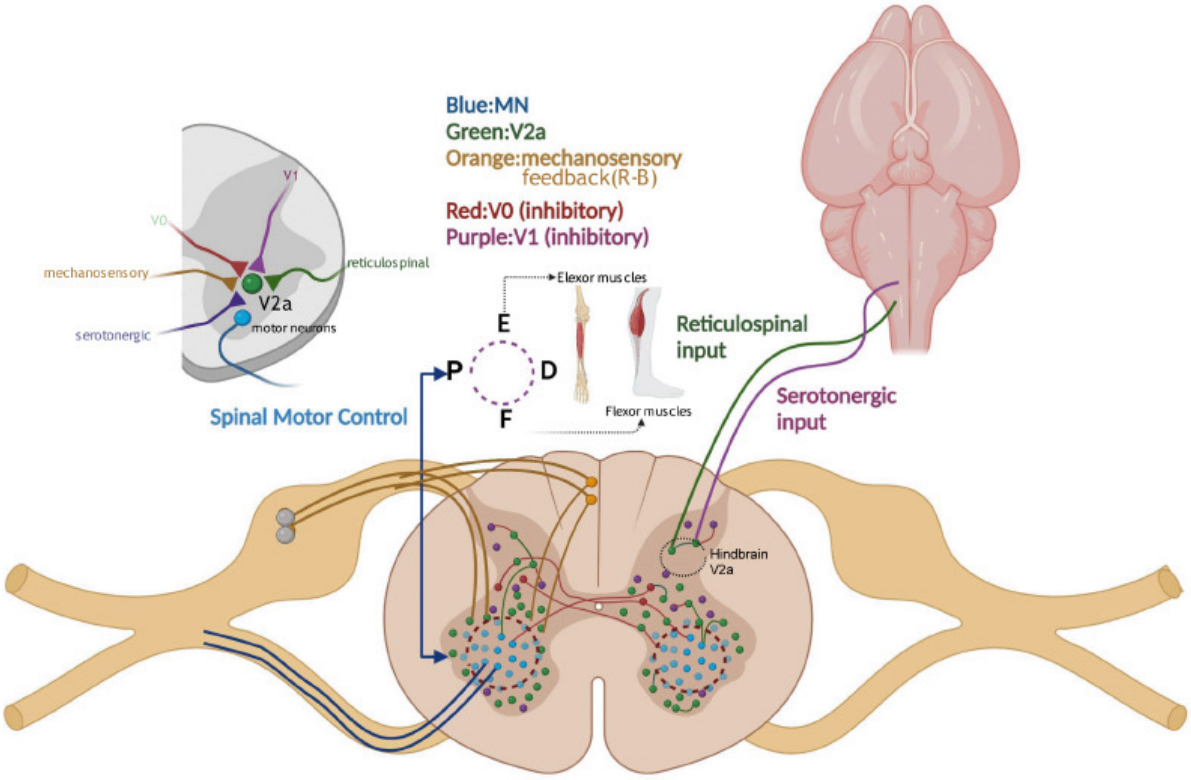

Figure A.20: V2a IN organisation in spinal motor networks to provide excitatory drive to proximal (P), distal (D), extensor (E), and flexor (F) muscles. V2a INs synapse to V0 CINs (Red), in turn provide inhibitory input to MNs. V1 INs (Purple) provide inhibitory drive to V2a INs. V2a INs receive hindbrain inputs, including reticulospinal neurons and serotonergic inputs. Taken from figure 3 (Li et al., 2022a) under Creative Commons Attribution-NonCommercial-ShareAlike 4.0 License.

IaINs/RCs (V1, V2b) (Blacklaws et al., 2015; Danner et al., 2019). These neurons are hypothesised to integrate sensory information, adjust left/right alternation, and actively only during running but not swimming (Borowska et al., 2013). Thus, $V3_D$ have some role in integrating or acting upon load bearing.

$V3_V$ INs are present in laminae VII/VIII and X and receive recurrent inputs from ipsilateral MNs (Borowska et al., 2013; Jankowska, 2001, 2008; Jankowska and Edgley, 2010). They also receive input from descending fibres and some group II afferents. $V3_V$ INs are glutamatergic and project ipsilaterally to MNs, contralaterally to extensor MNs, as well as other V3 INs (Zhang et al., 2008; Borowska et al., 2013; Danner et al., 2019; Chopek et al., 2018). These neurons project in rostral and caudal directions across

more than 2 segments (Lu et al., 2015). As indicated by their projection, they function as premotor excitatory commissural neurons and are hypothesised to be involved in left/right coordination, speed transition, and extensor burst duration (Borowska et al., 2013; Danner et al., 2017, 2019; Zhang et al., 2008; Danner et al., 2019). Conversely, to $V3_D$ INs, $V3_V$ neurons are active during swimming and running activity (Borowska et al., 2013).

dI3 are excitatory glutamatergic neurons residing in laminae V – VII, which receive monosynaptic input from low threshold sensory afferents from Aβ fibres, 'rhythmic locomotor circuit', and proprioceptive afferents (Tuan et al., 2013; Bui et al., 2016). dI3 INs project towards ipsilateral MNs in both rostral and caudal directions along the ventrolateral and dorsal funiculus (Lu et al., 2015; Stepien et al., 2010; Avraham et al., 2010). At the dorsal funiculus, the axons projecting from dI3 INs elongate at the dorsal root along the axons of the dorsal root ganglion neurons. The axons at the ventrolateral funiculus elongate towards the axons of MNs. Most dI3 INs are inhibited during the flexor phase in locomotion, perhaps suggesting an efference copy transmission to dI3 INs (Bui et al., 2016).

Interestingly, by genetically eliminating dI3 glutamate neurotransmission, Bui et al. (2016) showed that dI3 INs are not necessary for locomotion in healthy rats but are necessary during training-induced recovery following spinal transection. This stereotyped behaviour may be evidence in support of the evolutionarily derived neuronal substrate for locomotor patterns in the spinal cord. Recent research investigated the role of dI3 in palmar grasp reflex and uncovered the development of presynaptic inhibitory circuits attaching to dI3 INs during maturation, indicating the changes in sensorimotor integration from postnatal experiences (Laliberte et al., 2022).

dI4/dIL_A INs are GABAergic inhibitory neurons in laminae V – VI and I – IV, receiving proprioceptive afferents and low threshold mechanoreceptive sensory inputs

(Goulding et al., 2014; Fink et al., 2014; Betley et al., 2009; Goulding et al., 2014). These neurons project ipsilaterally towards proprioceptive sensory afferent terminals and ipsilateral MNs within less than 2 segments (Gross et al., 2002; Tripodi et al., 2011; Lu et al., 2015). Their inhibitory influence is suggested to reduce flexor muscle activity during the swing phase and promote smooth movement (Gross et al., 2002; Müller et al., 2002; Pillai et al., 2007; Koch et al., 2017; Betley et al., 2009; Fink et al., 2014).

dI5/dIL_B INs are glutamatergic excitatory neurons in laminae I – III and VII receiving low threshold mechanoreceptive afferents from Aβ, Aδ, and C fibres (Szabo et al., 2015; Bourane et al., 2015; Rabe et al., 2009). dI5 neurons project towards contralateral MNs, $V0_C$s, and V2 INs. They have also been reported to project towards ipsilateral neurons of the post-synaptic dorsal column in laminae III and IV in less than 2 segments (Gross et al., 2002; Müller et al., 2002; Bourane et al., 2015; Lu et al., 2015). The role of dI5 INs in locomotion is unknown. However, they have been suggested to be involved in transmitting pain, itch, and light touch (Lai et al., 2016).

dI6 INs are GABAergic and glycinergic inhibitory neurons residing in laminae VII – VIII (Griener et al., 2017; Dyck et al., 2012; Andersson et al., 2012; Goetz et al., 2015). Their inputs are currently unknown but are functionally active during locomotion. dI6 INs project in both rostral and caudal directions and towards contralateral and ipsilateral MNs, but are mainly commissural projections (Andersson et al., 2012; Goetz et al., 2015; Perry et al., 2019; Haque et al., 2018; Lu et al., 2015). Silencing dI6 activity has provided evidence of their involvement in left/right coordination and was shown to be rhythmically active during locomotion (Haque et al., 2018; Andersson et al., 2012; Goetz et al., 2015).

table A.16 summarises the connectivity and functions of the identified progenitor spinal cord INs. For a review of the identified spinal progenitor and cellular development of the spinal cord locomotor circuitry, including their neurotransmitters, projections, inputs, and functional roles see Lu et al. (2015).

Table A.16: Summary of genetically identified cardinal interneurons of the spinal cord.

IN	Lamina	Inputs	Projections	Function
$V0_D$	VII – VIII	V2a and primary afferents	Contralateral MNs. Projects across 1 – 3 descending segments	Inhibition of contralateral MNs
$V0_V$	VII – VIII	V2a and primary afferents	Contralateral inhibitory populations synapsing mainly flexor MNs. Projects across 1 – 3 descending segments.	Excitation of contralateral inhibitory INs. High speed left/right alternation.
$V0_C$	VII – VIII	Glutamatergic input from descending projections and surrounding glutamatergic INs. GABA input via oligosynaptic sensory afferents. Serotonin from brainstem output.	Ipsilateral MNs. Projecs across 1 – 3 descending segments.	Excitation of ipsilateral inhibitory MNs. Modulation of MNs in task-specific manner.
$V1$	VII – IX	Primary afferents	Ipsilateral flexor MNs. Projects across 1 – 3 segments.	Flexor inhibition

Continue on the next page

Table A.16: Summary of genetically identified cardinal interneurons of the spinal cord. (cont)

IN	Lamina	Inputs	Projections	Function
$V2a$	VII	Serotonergic brainstem output, dI5, and mechanosensory afferents	Ipsilateral $V0_C$s and MNs. Projects rostro-caudally acros > 2 segments.	Excitatory. Involved in left-/right alternation, subclasses of V2a activates at different locomotor speeds. Involved in locomotor recovery after SCI.
$V2b$	VII	Primary afferents	Ipsilateral extensor MNs. Projects rostro-caudally across > 2 segments.	Extensor inhibition
$V3_D$	IV – V and VI – VII	Primary, cutaneous, and group II afferents	Projects bilaterally (mainly contralateral) and rostro-caudally > 2 segments. Innervates contralateral IaINs/RCs.	Excitatory. Integrates sensory inromation and indirectly adjusts left/right alternation. Active only during running.

Continue on the next page

Table A.16: Summary of genetically identified cardinal interneurons of the spinal cord. (cont)

IN	Lamina	Inputs	Projections	Function
$V3_V$	VII, VIII and X	Ipsilateral MNs recurrently, descending fibres, some group II afferents	Projects contralaterally and rostro-caudally > 2 segments. Innervates contralateral extensor MNs. Ventromedial $V3_V$ INs synapse to other V3 INs. Ventrolateral $V3_V$s synapse with ipsilateral MNs.	Excitatory, premotor commissural neurons. Involved in left/right alternation and speed transition. Involved in extensor burst duration modulation and active during both swimming and running.
dI3	V – VII	Monosynaptic low threshold sensory afferents from Aβ fibres	Ipsilateral ascending and descending MNs. Entering via ventrolateral and dorsal funiculus	Excitatory. Majority inhibited during flexion phase. Necessary for locomotion recovery.
dI4/dIL_A	V – VI / I – IV	Proprioceptive afferents and low threshold sensory afferents	Ipsilateral MNs and proprioceptive sensory afferent terminals. Projects < 2 segments	Presynaptically inhibits flexor activity during swing. Muscle smoothening
dI4/dIL_A	V – VI / I – IV	Proprioceptive afferents and low threshold sensory afferents	Ipsilateral MNs and proprioceptive sensory afferent terminals. Projects < 2 segments	Presynaptically inhibits flexor activity during swing. Muscle smoothening

Continue on the next page

Table A.16: Summary of genetically identified cardinal interneurons of the spinal cord. (cont)

IN	Lamina	Inputs	Projections	Function
dI5/dIL_B	I – III and VII	low threshold sensory afferents	Contralateral MNs, $V0_C$, and V2. Ipsilateral neurons of post synaptic dorsal column (laminae III/IV). Projects < 2 segments	Excitatory, glutamatergic
dI6	VII – VIII	*Unknown*	Bilateral MNs (mainly commissural). Projects rostrocaudally.	Inhibitory (GABA/glycine). Involved in gait coordination, rhythmically active during locomotion.

Notably, V1s (IaINs) are positioned more medial dorsally and RCs more medial ventrally relative to target MNs (Bikoff et al., 2016). Similar spatial organisation appears in premotor INs (Tripodi et al., 2011). Flexor premotor INs were more lateral to extensor premotor INs, projecting mainly ipsilaterally. Evidence suggests spinal cord interneuron organisation to be biased towards their respective projection. For example, presynaptic inhibitors are more likely to be positioned near interneurons receiving primary afferent input and contralaterally projecting INs are more medial than non-contralateral projecting INs. Coupled with this, mechanosensory and propriosensory rostrocaudal projection depicts the somatotopically and modality-based organisation of the direct dorsal column (Niu et al., 2013). The spinal cord neuron morphology expresses bias towards efficient and functionally relevant architecture. The neuronal organisation will inform clinicians and engineers of the best methods to target the desired circuit.

A.4 Flexor Spiking Neural Network Code

```
from os import makedirs
from os.path import join
import matplotlib.pyplot as plt
import numpy as np

from argparse import ArgumentParser

from brian2 import *
from brian2cuda import *

from biophysical_parameters import *
from utils import *

import time

'''
------
 ARGS
------
'''
```

```
parser = ArgumentParser()
parser.add_argument('--run_id', type=int, default=0,
                    help='Unique number for run identification')
parser.add_argument('--stim_w', type=float, default=0,
                    help='Stim in mV for poisson input to axons')
parser.add_argument('--stim_freq', type=float, default=0,
                    help='Stim frequency for poisson input to axons')
parser.add_argument('--is_bws', type=int, default=0,
                    choices=[0, 1],
                    help='Offset variable for GM Ia and II afferent firing '\
                    'rates. Either 0 or 0.6. 0 being no offset and 0.6 being '\
                    'reduced EMG activity by 60%. (x - offset*K*EMGnorm)')
parser.add_argument('--use_quip', type=int, default=0,
                    choices=[0, 1],
                    help='Use quipazine or not')
parser.add_argument('--is_sci', type=int, default=0,
                    choices=[0, 1],
                    help='Activate SCI GABA settings')
parser.add_argument('--is_spastic', type=int, default=0,
                    choices=[0, 1],
                    help='Activate Spasticity GABA settings')
parser.add_argument('--debug', action='store_true',
                    help='save or not save run or make directories')

args = parser.parse_args()

t0 = time.time()

run_id = str(args.run_id).zfill(3)
is_sci = args.is_sci
is_spastic = args.is_spastic
debug = args.debug

# GM Ia Settings
is_bws = args.is_bws

# Quipazine Settings
use_quip = args.use_quip

"""
===============
 SYSTEM PARAMS
===============
"""
plt.close('all')
plt.rcParams.update({'axes.titlesize': 14,
```

```
                    'axes.labelsize': 12})

results_dir = '/data/rqchia/snn_results/experiment_log'
makedirs(results_dir, exist_ok=True)

output_dir = '/scratch/rqchia/brian2/output'
makedirs(output_dir, exist_ok=True)
set_device('cpp_standalone', directory=output_dir)

# output_dir = '/scratch/rqchia/brian2cuda/output'
# makedirs(output_dir, exist_ok=True)
# set_device('cuda_standalone', directory=output_dir)
defaultclock.dt = 0.005*ms
devices.device.seed(42)
np.random.seed(42)

"""
=======================
 Experiment Parameters
=======================
"""
duration = 1.12*second # gait cycle duration
n_cycles = 10
if debug:
    duration *= 2
    gauss_width = 1*ms
else:
    duration *= 8
    gauss_width = 75*ms

# PSI settings
if is_sci == 1:
    # Khristy W et al 2009
    psi_beta = 0.4

    # gaba inhibition populations
    ax_gaba_c = 0.45
    gaba_mn_k = 6
elif is_spastic == 1:
    raise NotImplementedError
    psi_beta = 0.4

    # gaba inhibition populations
    ax_gaba_c = 0.45
    gaba_mn_k = 3
else:
```

```
    psi_beta = 0.4

    # gaba inhibition populations
    ax_gaba_c = 0.3
    gaba_mn_k = 4

# multiplier to a normalised EMG component
if is_bws == 1:
    # extensors Kristiansen M et al 2019, 3.6km/h
    gm_offset = -0.676
    ta_offset = -0.221
else:
    gm_offset = 0
    ta_offset = 0

kappa = 5 # target rate
p_init = np.clip(1 - psi_beta*kappa, 0, 1)
gaba_w_gain = 1
gaba_mn_n = gaba_params['N']/((2*gaba_mn_k)-1)

# gain for gaba conductance (how much is released per spike)
gaba_g_gain = gaba_w_gain/gaba_mn_n

# Synaptic probabilities
p_ax_in   = 0.3 # axon to interneurons
p_ax_adex = p_ax_in*2 # axon to adex
p_iaIN    = 0.1 # recurrent iaIN
p_in_mn   = 0.3 # mn inputs

'''
------------
 STIM INPUT
------------
'''
stim_w = args.stim_w*mV # 5.0
stim_freqs = [0, 20, 40, 60, 80, 100]
stim_freq = args.stim_freq
poisson_stim = PoissonGroup(axon_params['N'], stim_freq*Hz)

I_ex = 0*pA

'''
---------
 CONFIGS
---------
'''
```

```
cfg_dict = {
    'duration'    : duration/second,
    'is_sci'      : is_sci,
    'is_bws'      : is_bws,
    'use_quip'    : use_quip,
    'beta'        : psi_beta,
    'kappa'       : kappa,
    'gaba_mn_n'   : gaba_mn_n,
    'ax_gaba_c'   : ax_gaba_c,
    'gaba_w_gain' : gaba_w_gain,
    'stim_w'      : args.stim_w,
    'stim_freq'   : stim_freq,
    'gauss_width' : gauss_width/ms,
    'p_ax_in'     : p_ax_in,
    'p_ax_adex'   : p_ax_adex,
    'p_iaIN'      : p_iaIN,
    'p_in_mn'     : p_in_mn,
}

"""
===============
 NeuronGroups
===============
"""

"""
------------
 AXON GROUP
------------
"""

# synapse delay of 2ms
ax_N       = axon_params['N']
ax_Vth     = axon_params['Vth']
ax_Vr      = axon_params['V_reset']
ax_tau_ref = axon_params['tau_ref']
ax_area    = np.pi*(ia_diameter_mu/2)**2

ax_v_mu = (ax_Vr + ax_Vth)/2
ax_v_sd = 10*mV
axon_init_v = ax_v_sd*np.random.randn(ax_N) + ax_v_mu

ax_eqn = '''
dv/dt = (El - v)/tau + i_stim/(Cm*ax_area) \
        : volt (unless refractory)
i_stim = I_ex*ax_stim : amp
```

```
ax_stim : 1
'''
ta_ia_axon = NeuronGroup(ax_N, ax_eqn, threshold='v>=ax_Vth',
                         reset='v=ax_Vr', method='euler',
                         refractory=ax_tau_ref,
                         namespace=axon_params)
ta_ia_axon.v = axon_init_v

gm_ia_axon = NeuronGroup(ax_N, ax_eqn, threshold='v>=ax_Vth',
                         reset='v=ax_Vr', method='euler',
                         refractory=ax_tau_ref,
                         namespace=axon_params)
gm_ia_axon.v = axon_init_v

ta_ii_axon = NeuronGroup(ax_N, ax_eqn, threshold='v>=ax_Vth',
                         reset='v=ax_Vr', method='euler',
                         refractory=ax_tau_ref, namespace=axon_params)
ta_ii_axon.v = axon_init_v

gm_ii_axon = NeuronGroup(ax_N, ax_eqn, threshold='v>=ax_Vth',
                         reset='v=ax_Vr', method='euler',
                         refractory=ax_tau_ref,
                         namespace=axon_params)
gm_ii_axon.v = axon_init_v

"""
-----------
 v2a GROUP
-----------
"""

## adex
# taken from Touboul_Brette_2008
adex_N = v2a_params['N']

# NOTE : change this for quip
if use_quip:
    adex_g_l = v2a_params['g_l_quip']
else:
    adex_g_l = v2a_params['g_l']

adex_v_mu = (v2a_params['v_t'] + v2a_params['v_r_mu'])/2
adex_v_sd = 10*mV
adex_init_v = adex_v_sd*np.random.randn(adex_N) + adex_v_mu

adex_eqn = """
```

```
dv/dt = (gL*(e_l - v) + gL*d_t*exp((v-v_t)/d_t) \
        + i_stim - w)/c_m + g_syn_e*(0*mV-v)/c_m : volt
dw/dt  = (a*(v - e_l) - w)/tau_w : amp
dg_syn_e/dt = -g_syn_e/exc_alpha_tau : siemens

i_stim : amp
gL : siemens (shared, constant)
"""

adex = NeuronGroup(
        adex_N,
        model=adex_eqn,
        threshold="v>0*mV",
        reset="v=v_r_mu; w+=b",
        method="euler",
        namespace=v2a_params,
)
adex.v = adex_init_v
adex.w = 0
adex.gL = adex_g_l

"""
------------
 IaIN GROUP
------------
"""

iaIN_N   = iaIN_params['N']
iaIN_Vth = iaIN_params['Vth']
iaIN_Vr  = iaIN_params['Vr']
iaIN_tau_ref = iaIN_params['tau_ref']

iaIN_v_mu = (iaIN_Vr + iaIN_Vth)/2
iaIN_v_sd = 5*mV
iaIN_init_v = iaIN_v_sd*np.random.randn(iaIN_N) + iaIN_v_mu
iaIN_eqn = '''
dv/dt = gL*(El - v)/Cm + (I_syn_e + I_syn_i)/Cm : volt

I_syn_e = g_syn_e * (0*mV - v) : amp
dg_syn_e/dt = -g_syn_e/exc_alpha_tau : siemens

I_syn_i = g_syn_i * (El - v) : amp
dg_syn_i/dt = (s_i - g_syn_i)/inh_alpha_tau2 : siemens
ds_i/dt = -s_i/inh_alpha_tau1  : siemens
'''
gm_iaIN = NeuronGroup(iaIN_N, iaIN_eqn, threshold='v>=iaIN_Vth',
```

```
                    reset='v=iaIN_Vr', refractory=iaIN_tau_ref,
                    method='euler', namespace=iaIN_params)
gm_iaIN.v = iaIN_init_v

ta_iaIN = NeuronGroup(iaIN_N, iaIN_eqn, threshold='v>=iaIN_Vth',
                    reset='v=iaIN_Vr', refractory=iaIN_tau_ref,
                    method='euler', namespace=iaIN_params)
ta_iaIN.v = iaIN_init_v

"""
------------
 GABA GROUP
------------
"""
gaba_N = gaba_params['N']
gaba_Vth = gaba_params['v_t']
gaba_Vr = gaba_params['v_r']
gaba_tau_ref = gaba_params['tau_ref']
gaba_gIE = gaba_params['gIE']

gaba_v_mu = (gaba_Vr + gaba_Vth)/2
gaba_v_sd = 10*mV
gaba_init_v = gaba_v_sd*np.random.randn(gaba_N) + gaba_v_mu

gaba_eqn = """
dv/dt = (g_l*(e_l - v) + g_l*d_t*exp((v-v_t)/d_t) + i_stim - w)/c_m \
        + g_syn_e*(0*mV-v)/c_m: volt
dw/dt  = (a*(v - e_l) - w)/tau_w : amp

dg_syn_e/dt = -g_syn_e/exc_alpha_tau : siemens

i_stim : amp
"""

gaba = NeuronGroup(
        gaba_params['N'],
        model=gaba_eqn,
        threshold="v>0*mV",
        reset="v=gaba_Vr; w+=b",
        method="euler",
        namespace=gaba_params,
)
gaba.w = 0
gaba.v = gaba_init_v

"""
```

```
----------
 MN GROUP
----------
"""

# Model as Leaky IntFire but also have alpha shape synapse for ipsp
mn_Vth     = mn_params['Vth']
mn_Vr      = mn_params['Vr']
mn_tau_ref = mn_params['tau_ref']

if use_quip and is_bws:
    mn_gL = mn_params['gL_quip_lo']
elif use_quip and not is_bws:
    mn_gL = mn_params['gL_quip_hi']
else:
    mn_gL = mn_params['gL']
print("using mn_gL: ", mn_gL)

mn_v_mu = (mn_Vr + mn_Vth)/2
mn_v_sd = 2*mV
mn_init_v = mn_v_sd*np.random.randn(N_mn) + mn_v_mu

# disable if PSI off
etap = 1
if psi_beta == 0:
    etap = 0
# taup = 200*ms
taup = 20*ms # approx from Fink et al 2015
taui = 10*ms

tau_gaba = mn_params['tau_GABA']

# exponential leaky int and fire
mn_conductance_exp_eqn = '''
I = mn_gL*(El - v + I_noise*R ) + mn_gL*deltaV*exp((v - mn_Vth)/deltaV) : amp

# dv/dt = (I + I_syn_GABA + I_syn_i) / Cm + g_syn_e*(-v)/Cm : volt
dv/dt = (I + I_syn_i) / Cm + g_syn_e*(-v)/Cm : volt

dg_syn_e/dt = -g_syn_e/exc_alpha_tau : siemens

I_syn_GABA = g_syn_GABA * (El-10*mV - v) : amp
dg_syn_GABA/dt = (s_GABA - g_syn_GABA) / tau_GABA : siemens
ds_GABA/dt = -s_GABA/taui : siemens

dp/dt = (-p + clip(1-beta*(s_GABA/nS), 0, 1))*etap/taup : 1
```

```
I_syn_i = g_syn_i * (El-10*mV - v) : amp
dg_syn_i/dt = (s_i - g_syn_i)/inh_alpha_tau2 : siemens
ds_i/dt = -s_i/inh_alpha_tau1  : siemens

I_noise : amp

beta : 1 (shared, constant)

'''

mn = NeuronGroup(N_mn, mn_conductance_exp_eqn, threshold='v>0*mV',
                 refractory='v>0*mV',
                 reset='v=mn_Vr', method='euler', namespace=mn_params)
mn.v = mn_init_v
mn.p = p_init
mn.beta = psi_beta

mn.run_regularly("I_noise = 0*nA", dt=1/fs)
# mn.run_regularly("I_noise = 1*randn()*nA", dt=1/fs)

"""
==========
 Afferent
==========
"""

ta_ia_data = get_afferent_signal('ta', 'ia') + ta_offset*50
ta_ia_data = np.clip(ta_ia_data, a_min=0, a_max=None)
ta_ia_signal = TimedArray(ta_ia_data*Hz, dt=1/fs)

ta_ii_data = get_afferent_signal('ta', 'ii') + ta_offset*20
ta_ii_data = np.clip(ta_ii_data, a_min=0, a_max=None)
ta_ii_signal = TimedArray(ta_ii_data*Hz, dt=1/fs)

gm_ia_data = get_afferent_signal('gm', 'ia') + gm_offset*50
gm_ia_data = np.clip(gm_ia_data, a_min=0, a_max=None)
gm_ia_signal = TimedArray(gm_ia_data*Hz, dt=1/fs)

gm_ii_data = get_afferent_signal('gm', 'ii') + gm_offset*20
gm_ii_data = np.clip(gm_ii_data, a_min=0, a_max=None)
gm_ii_signal = TimedArray(gm_ii_data*Hz, dt=1/fs)

# PoissonGroup
ta_ia_input = PoissonGroup(ax_N, rates='ta_ia_signal(t)')
gm_ia_input = PoissonGroup(ax_N, rates='gm_ia_signal(t)')
```

```
ta_ii_input = PoissonGroup(ax_N, rates='ta_ii_signal(t)')
gm_ii_input = PoissonGroup(ax_N, rates='gm_ii_signal(t)')

"""
==========
 Synapses
==========
"""
syn_ax_w = axon_params['w']

'''
--------------------
 Afferents to Axons
--------------------
'''

syn_ta_ia_ax = Synapses(ta_ia_input, ta_ia_axon, on_pre='v_post+=syn_ax_w')
syn_ta_ia_ax.connect(condition='abs(i-j)<2')

syn_gm_ia_ax = Synapses(gm_ia_input, gm_ia_axon, on_pre='v_post+=syn_ax_w')
syn_gm_ia_ax.connect(condition='abs(i-j)<2')

syn_ta_ii_ax = Synapses(ta_ii_input, ta_ii_axon, on_pre='v_post+=syn_ax_w')
syn_ta_ii_ax.connect(condition='abs(i-j)<2', p=0.9)

syn_gm_ii_ax = Synapses(gm_ii_input, gm_ii_axon, on_pre='v_post+=syn_ax_w')
syn_gm_ii_ax.connect(condition='abs(i-j)<2', p=0.9)

'''
--------------
 Axons to INs
--------------
'''
adex_g_e = v2a_params['g_e']
iaIN_g_e = iaIN_params['g_e']

# ta ia and ii
syn_ta_ax_ii = Synapses(ta_ii_axon, adex, on_pre='g_syn_e+=adex_g_e',
                        delay=2*ms)
syn_ta_ax_ii.connect(p=p_ax_adex)

syn_ta_ii_ia = Synapses(ta_ii_axon, ta_iaIN, on_pre='g_syn_e+=iaIN_g_e/3',
                        delay=2*ms)
syn_ta_ii_ia.connect(p=p_ax_in)

syn_ta_ax_ia = Synapses(ta_ia_axon, ta_iaIN, on_pre='g_syn_e+=iaIN_g_e',
```

```
                        delay=2*ms)
syn_ta_ax_ia.connect(p=p_ax_in)

# gm ia and ii
syn_gm_ax_ia = Synapses(gm_ia_axon, gm_iaIN, on_pre='g_syn_e+=iaIN_g_e',
                        delay=2*ms)
syn_gm_ax_ia.connect(p=p_ax_in)

syn_gm_ii_ia = Synapses(gm_ii_axon, gm_iaIN, on_pre='g_syn_e+=iaIN_g_e/3',
                        delay=2*ms)
syn_gm_ii_ia.connect(p=p_ax_in)


gaba_g_e = gaba_params['g_e']
syn_gm_ax_gaba = Synapses(gm_ia_axon, gaba, on_pre='g_syn_e+=gaba_g_e',
                          delay=2*ms)
syn_gm_ax_gaba.connect(p=ax_gaba_c)

'''
--------------
 INs to INs
--------------
'''
iaIN_g_i = iaIN_params['g_i']
syn_taIaIN_gmIaIN = Synapses(ta_iaIN, gm_iaIN, on_pre='g_syn_i+=iaIN_g_i')
syn_taIaIN_gmIaIN.connect(p=p_iaIN)
syn_gmIaIN_taIaIN = Synapses(gm_iaIN, ta_iaIN, on_pre='g_syn_i+=iaIN_g_i')
syn_gmIaIN_taIaIN.connect(p=p_iaIN)

'''
------------
 INs to MN
------------
'''

mn_g_e = mn_params['g_e']
mn_g_i = mn_params['g_i']
mn_syn_range = 10

syn_ta_ia_mn = Synapses(ta_ia_axon, mn,
                        on_pre='g_syn_e += p*mn_g_e',
                        delay=2*ms)
syn_ta_ia_mn.connect(p=p_in_mn)

syn_ta_ii_mn = Synapses(adex, mn, on_pre='g_syn_e += p*mn_g_e')
syn_ta_ii_mn.connect(p=p_in_mn) # 0.4
```

```
syn_gm_ia_mn = Synapses(gm_iaIN, mn, on_pre='g_syn_i+=mn_g_i')
syn_gm_ia_mn.connect(p=p_in_mn) # 0.8

syn_gm_gaba_mn = Synapses(gaba, mn,
                          on_pre='s_GABA+=mn_g_i*gaba_g_gain')
syn_gm_gaba_mn.connect(condition='abs(i-j)<gaba_mn_k', skip_if_invalid=True)

'''
--------------
 STIM CONNECT
--------------
'''
syn_stim_ta_ia_ax = Synapses(poisson_stim, ta_ia_axon, on_pre='v+=stim_w')
syn_stim_ta_ii_ax = Synapses(poisson_stim, ta_ii_axon, on_pre='v+=stim_w*0.8')
syn_stim_gm_ia_ax = Synapses(poisson_stim, gm_ia_axon, on_pre='v+=stim_w')
syn_stim_gm_ii_ax = Synapses(poisson_stim, gm_ii_axon, on_pre='v+=stim_w*0.8')

syn_stim_ta_ia_ax.connect(j='i')
syn_stim_ta_ii_ax.connect(j='i')
syn_stim_gm_ia_ax.connect(j='i')
syn_stim_gm_ii_ax.connect(j='i')

"""
==========
 Monitors
==========
"""
ax_monitor_vars = ['v']
in_monitor_vars = ['v', 'g_syn_e']
iaIN_monitor_vars = ['v', 'g_syn_e', 'g_syn_i']
mn_monitor_vars = ['v', 'g_syn_e', 'g_syn_i', 's_GABA', 'p']

monitor_units_dict = {
    'v'       : 'mV',
    'g_syn_e' : 'nS',
    'g_syn_i' : 'nS',
    's_GABA'  : 'nS',
    'p'       : 'a.u',
}

M_ta_ia_ax = StateMonitor(ta_ia_axon, ax_monitor_vars, record=[0])
P_ta_ia_in = PopulationRateMonitor(ta_ia_input)
P_ta_ia_ax = PopulationRateMonitor(ta_ia_axon)

M_gm_ia_ax = StateMonitor(gm_ia_axon, ax_monitor_vars, record=[0])
```

```
P_gm_ia_in = PopulationRateMonitor(gm_ia_input)
P_gm_ia_ax = PopulationRateMonitor(gm_ia_axon)

M_ta_ii_ax = StateMonitor(ta_ii_axon, ax_monitor_vars, record=[0])
P_ta_ii_in = PopulationRateMonitor(ta_ii_input)
P_ta_ii_ax = PopulationRateMonitor(ta_ii_axon)

M_gm_ii_ax = StateMonitor(gm_ii_axon, ax_monitor_vars, record=[0])
P_gm_ii_in = PopulationRateMonitor(gm_ii_input)
P_gm_ii_ax = PopulationRateMonitor(gm_ii_axon)

M_ta_adex  = StateMonitor(adex, in_monitor_vars, record=[0])
S_ta_adex  = SpikeMonitor(adex, record=True)
P_ta_adex  = PopulationRateMonitor(adex)

M_gm_iaIN  = StateMonitor(gm_iaIN, iaIN_monitor_vars, record=[0])
S_gm_iaIN  = SpikeMonitor(gm_iaIN, record=True)
P_gm_iaIN  = PopulationRateMonitor(gm_iaIN)

M_ta_iaIN  = StateMonitor(ta_iaIN, iaIN_monitor_vars, record=[0])
S_ta_iaIN  = SpikeMonitor(ta_iaIN, record=True)
P_ta_iaIN  = PopulationRateMonitor(ta_iaIN)

M_gm_gaba  = StateMonitor(gaba, in_monitor_vars, record=[0])
S_gaba     = SpikeMonitor(gaba, record=True)
P_gm_gaba  = PopulationRateMonitor(gaba)

M_mn       = StateMonitor(mn, mn_monitor_vars, record=[0])
S_mn       = SpikeMonitor(mn, record=True)
P_mn       = PopulationRateMonitor(mn)

run(duration)

"""
==========
 Outputs
==========
"""

run_dir = join(results_dir, run_id)
if not debug:
    makedirs(run_dir, exist_ok=True)

units_fname = join(results_dir, 'units.pkl')
cfg_fname   = join(run_dir, 'configs.json')
m_mn_fname  = join(run_dir, 'state_mn.pkl')
```

```
s_mn_fname  = join(run_dir, 'spike_mn.pkl')
p_mn_fname  = join(run_dir, 'prate_mn.pkl')

m_ta_ia_axon_fname = join(run_dir, 'state_ta_ia_axon.pkl')
p_ta_ia_axon_fname = join(run_dir, 'prate_ta_ia_axon.pkl')

m_gm_ia_axon_fname = join(run_dir, 'state_gm_ia_axon.pkl')
p_gm_ia_axon_fname = join(run_dir, 'prate_gm_ia_axon.pkl')

m_ta_ii_axon_fname = join(run_dir, 'state_ta_ii_axon.pkl')
p_ta_ii_axon_fname = join(run_dir, 'prate_ta_ii_axon.pkl')

m_gm_ii_axon_fname = join(run_dir, 'state_gm_ii_axon.pkl')
p_gm_ii_axon_fname = join(run_dir, 'prate_gm_ii_axon.pkl')

m_taIaIN_fname = join(run_dir, 'state_taIaIN.pkl')
s_taIaIN_fname = join(run_dir, 'spike_taIaIN.pkl')
p_taIaIN_fname = join(run_dir, 'prate_taIaIN.pkl')

m_gmIaIN_fname = join(run_dir, 'state_gmIaIN.pkl')
s_gmIaIN_fname = join(run_dir, 'spike_gmIaIN.pkl')
p_gmIaIN_fname = join(run_dir, 'prate_gmIaIN.pkl')

m_gaba_fname = join(run_dir, 'state_gaba.pkl')
s_gaba_fname = join(run_dir, 'spike_gaba.pkl')
p_gaba_fname = join(run_dir, 'prate_gaba.pkl')

m_adex_fname = join(run_dir, 'state_adex.pkl')
s_adex_fname = join(run_dir, 'spike_adex.pkl')
p_adex_fname = join(run_dir, 'prate_adex.pkl')

m_adex_fname = join(run_dir, 'state_adex.pkl')
s_adex_fname = join(run_dir, 'spike_adex.pkl')
p_adex_fname = join(run_dir, 'prate_adex.pkl')


'''
-------
 Plot
-------
'''

figsize = (14, 12)
def plot_afferent_to_axon():
    fig, axs = plt.subplots(4, 3, figsize=figsize)
```

```
axs[0,0].plot(P_ta_ia_in.t/ms, P_ta_ia_in.smooth_rate(window='gaussian',
                                                      width=gauss_width))
axs[0,0].set_title("ta ia poisson input (Hz)")

axs[0,1].plot(M_ta_ia_ax.t/ms, M_ta_ia_ax.v[0]/mV)
axs[0,1].set_title("ta ia axon0 (mV)")

axs[0,2].plot(P_ta_ia_ax.t/ms, P_ta_ia_ax.smooth_rate(window='gaussian',
                                                      width=gauss_width))
axs[0,2].set_title("ta ia axon (Hz)")

axs[1,0].plot(P_gm_ia_in.t/ms, P_gm_ia_in.smooth_rate(window='gaussian',
                                                      width=gauss_width))
axs[1,0].set_title("gm poisson input (Hz)")

axs[1,1].plot(M_gm_ia_ax.t/ms, M_gm_ia_ax.v[0]/mV)
axs[1,1].set_title("gm ia axon0 (mV)")

axs[1,2].plot(P_gm_ia_ax.t/ms, P_gm_ia_ax.smooth_rate(window='gaussian',
                                                      width=gauss_width))
axs[1,2].set_title("gm ia axon (Hz)")

axs[2,0].plot(P_gm_ii_in.t/ms, P_gm_ii_in.smooth_rate(window='gaussian',
                                                      width=gauss_width))
axs[2,0].set_title("gm poisson input (Hz)")

axs[2,1].plot(M_gm_ii_ax.t/ms, M_gm_ii_ax.v[0]/mV)
axs[2,1].set_title("gm ii axon0 (mV)")

axs[2,2].plot(P_gm_ii_ax.t/ms, P_gm_ii_ax.smooth_rate(window='gaussian',
                                                     width=gauss_width))
axs[2,2].set_title("gm ii axon (Hz)")

axs[3,0].plot(P_ta_ii_in.t/ms, P_ta_ii_in.smooth_rate(window='gaussian',
                                                      width=gauss_width))
axs[3,0].set_title("ta ii poisson input (Hz)")

axs[3,1].plot(M_ta_ii_ax.t/ms, M_ta_ii_ax.v[0]/mV)
axs[3,1].set_title("ta ii axon (mV)")

axs[3,2].plot(P_ta_ii_ax.t/ms, P_ta_ii_ax.smooth_rate(window='gaussian',
                                                      width=gauss_width))
axs[3,2].set_title("ta ii axon (Hz)")

if not debug:
    fig.savefig(join(run_dir, f"{run_id}_axon.png"))
```

```
def plot_axon_to_in():
    fig, axs = plt.subplots(4, 3, figsize=figsize)
    axs[0,0].plot(P_ta_ia_ax.t/ms, P_ta_ia_ax.smooth_rate(window='gaussian',
                                                          width=gauss_width))
    axs[0,0].set_title("ta axon poisson input (Hz)")

    ta_adex_vs = np.clip(M_ta_adex[0].v / mV, a_min=None, a_max=0)
    axs[0,1].plot(M_ta_adex.t/ms, ta_adex_vs)
    axs[0,1].set_title("ta adex_0 (mV)")

    axs[0,2].plot(P_ta_adex.t/ms, P_ta_adex.smooth_rate(window='gaussian',
                                                        width=gauss_width))
    axs[0,2].set_title("ta adex (Hz)")

    axs[1,0].plot(P_ta_ia_ax.t/ms, P_ta_ia_ax.smooth_rate(window='gaussian',
                                                          width=gauss_width))
    axs[1,0].set_title("ta ia axon (Hz)")

    axs[1,1].plot(M_ta_iaIN.t/ms, M_ta_iaIN.v[0]/mV)
    axs[1,1].set_title("ta iaIN_0 (mV)")

    axs[1,2].plot(P_ta_iaIN.t/ms, P_ta_iaIN.smooth_rate(window='gaussian',
                                                        width=gauss_width))
    axs[1,2].set_title("ta iaIN (Hz)")

    axs[2,0].plot(P_gm_ia_ax.t/ms, P_gm_ia_ax.smooth_rate(window='gaussian',
                                                          width=gauss_width))
    axs[2,0].set_title("gm ia axon (Hz)")

    axs[2,1].plot(M_gm_iaIN.t/ms, M_gm_iaIN.v[0]/mV)
    axs[2,1].set_title("gm iaIN_0 (mV)")

    axs[2,2].plot(P_gm_iaIN.t/ms, P_gm_iaIN.smooth_rate(window='gaussian',
                                                        width=gauss_width))
    axs[2,2].set_title("gm iaIN (Hz)")

    axs[3,0].plot(P_gm_ia_ax.t/ms, P_gm_ia_ax.smooth_rate(window='gaussian',
                                                          width=gauss_width))
    axs[3,0].set_title("gm ia axon (Hz)")

    axs[3,1].plot(M_gm_gaba.t/ms, M_gm_gaba.v[0]/mV)
    axs[3,1].set_title("gm gaba_0 (mV)")

    axs[3,2].plot(P_gm_gaba.t/ms, P_gm_gaba.smooth_rate(window='gaussian',
                                                        width=gauss_width))
```

```
    axs[3,2].set_title("gm gaba (Hz)")
    if not debug:
        fig.savefig(join(run_dir, f"{run_id}_IN.png"))

def plot_inputs_to_mn():
    fig = plt.figure(figsize=figsize)
    plt.subplot(321)
    plt.plot(M_mn.t/ms, M_mn.v[0]/mV)
    plt.title('mn_0 (mV)')
    plt.subplot(322)
    mn_freq = P_mn.smooth_rate(window='gaussian', width=gauss_width)
    plt.plot(P_mn.t/ms, mn_freq)

    mask = mn_freq > 5*Hz
    mask0 = mask[1:] ^ mask[:-1]
    mask0 = np.insert(mask0, 0, 0)
    idxs = np.arange(len(mask0))[mask0]
    start_idxs = idxs[::2]
    end_idxs = idxs[1::2]

    # dt = 5*1e-5
    dt = 1*1e-3
    f = 1/dt
    tmp = []
    for start, end in zip(start_idxs, end_idxs):
        if end - start < 0.01*f: continue
        if len(tmp) == 0:
            tmp = np.ravel(mn_freq[start:end])
        else:
            tmp = np.concatenate((tmp, np.ravel(mn_freq[start:end])), axis=0)
        print("{0} +- {1}".format(mn_freq[start:end].mean(),
                                  mn_freq[start:end].std())
              )
    print(np.mean(tmp))
    plt.title('mn pop. rate (Hz)')
    plt.subplot(323)
    plt.plot(S_mn.t/ms, S_mn.i, '.k')
    plt.title('Spikes')

    plt.subplot(324)
    plt.plot(M_mn.t/ms, M_mn.g_syn_e[0]/mV)
    plt.title('EPSP conductance mn_0 (nS)')
    plt.subplot(325)
    plt.plot(M_mn.t/ms, M_mn.g_syn_i[0]/mV)
    plt.title('IPSP conductance mn_0 (nS)')
```

```
    ax = plt.subplot(3,4,11)
    plt.plot(M_mn.t/ms, M_mn.s_GABA[0]/nS)
    plt.title("s_GABA (nS) and p scale")

    plt.subplot(3,4,12)
    plt.plot(M_mn.t/ms, M_mn.p[0])
    plt.title("p scale (a.u.)")
    if not debug:
        fig.savefig(join(run_dir, f"{run_id}_MN.png"))

plot_afferent_to_axon()
plot_axon_to_in()
plot_inputs_to_mn()

if debug:
    plt.show()

'''
-------
 WRITE
-------
'''

if not debug:
    save_dict(monitor_units_dict, units_fname)
    save_json(cfg_dict, cfg_fname)

    def write_monitor_data(statemon, state_fname, keys,
                           spikemon, spike_fname,
                           popmon, pop_fname):
        if statemon is not None:
            save_monitor_to_pickle(statemon, state_fname, keys=keys)
        if spikemon is not None:
            save_dict(spikemon.all_values(), spike_fname)
        if popmon is not None:
            save_dict(
                {'rate': popmon.smooth_rate(window='gaussian',width=gauss_width)},
                pop_fname
            )

    write_monitor_data(M_mn, m_mn_fname, mn_monitor_vars,
                       S_mn, s_mn_fname,
                       P_mn, p_mn_fname)

    write_monitor_data(M_ta_ia_ax, m_ta_ia_axon_fname, ax_monitor_vars,
                       None, None,
```

```
                    P_ta_ia_ax, p_ta_ia_axon_fname)

    write_monitor_data(M_ta_ii_ax, m_ta_ii_axon_fname, ax_monitor_vars,
                    None, None,
                    P_ta_ii_ax, p_ta_ii_axon_fname)

    write_monitor_data(M_gm_ia_ax, m_gm_ia_axon_fname, ax_monitor_vars,
                    None, None,
                    P_gm_ia_ax, p_gm_ia_axon_fname)

    write_monitor_data(M_gm_ii_ax, m_gm_ii_axon_fname, ax_monitor_vars,
                    None, None,
                    P_gm_ii_ax, p_gm_ii_axon_fname)

    write_monitor_data(M_ta_iaIN, m_taIaIN_fname, iaIN_monitor_vars,
                    S_ta_iaIN, s_taIaIN_fname,
                    P_ta_iaIN, p_taIaIN_fname)

    write_monitor_data(M_gm_iaIN, m_gmIaIN_fname, iaIN_monitor_vars,
                    S_gm_iaIN, s_gmIaIN_fname,
                    P_gm_ia_in, p_gmIaIN_fname)

    write_monitor_data(M_ta_adex, m_adex_fname, in_monitor_vars,
                    S_ta_adex, s_adex_fname,
                    P_ta_adex, p_adex_fname)

    write_monitor_data(M_gm_gaba, m_gaba_fname, in_monitor_vars,
                    S_gaba, s_gaba_fname,
                    P_gm_gaba, p_gaba_fname)

print("wall time: ", time.time()-t0)
```

BIBLIOGRAPHY

Abraham, L. D., Marks, W. B., and Loeb, G. E. (1985).
The distal hindlimb musculature of the cat.
Experimental Brain Research, 58(3):594–603.

Adler-Milstein, J., Aggarwal, N., Ahmed, M., Castner, J., Evans, B. J., Gonzalez, A. A., James, C. A., Lin, S., Mandl, K. D., Matheny, M. E., Sendak, M. P., Shachar, C., and Williams, a. A. (2022).
Meeting the Moment: Reducing Barriers and Facilitating Clinical Adoption of Artificial Intelligence in Medical Diagnosis.
NAM Perspectives.

Adolfo, Endo, T., Löw, P., Borgius, L., Hägglund, M., Kimberly, Ryge, J., Thomas, and Kiehn, O. (2011).
Identification of minimal neuronal networks involved in flexor-extensor alternation in the mammalian spinal cord.
Neuron, 71(6):1071–1084.

Aggarwal, R., Sounderajah, V., Martin, G., Ting, D. S. W., Karthikesalingam, A., King, D., Ashrafian, H., and Darzi, A. (2021).
Diagnostic accuracy of deep learning in medical imaging: A systematic review and meta-analysis.
npj Digital Medicine, 4(1):1–23.

Aguayo, G. A., Zhang, L., Vaillant, M., Ngari, M., Perquin, M., Moran, V., Huiart, L., Krüger, R., Azuaje, F., Ferdynus, C., and Fagherazzi, G. (2023).

Machine learning for predicting neurodegenerative diseases in the general older population: A cohort study.

BMC Medical Research Methodology, 23(1):8.

Ahissar, M. and Hochstein, S. (1997).

Task difficulty and the specificity of perceptual learning.

Nature, 387(6631):401–406.

Akay, T., Tourtellotte, W. G., Arber, S., and Jessell, T. M. (2014).

Degradation of mouse locomotor pattern in the absence of proprioceptive sensory feedback.

Proceedings of the National Academy of Sciences, 111(47):16877–16882.

Akazawa, K., Aldridge, J. W., Steeves, J. D., and Stein, R. B. (1982).

Modulation of stretch reflexes during locomotion in the mesencephalic cat.

The Journal of Physiology, 329(1):553–567.

Al-Chalabi, M., Reddy, V., and Alsalman, I. (2021).

Neuroanatomy, posterior column (dorsal column).

In *StatPearls*. StatPearls Publishing Copyright © 2021, StatPearls Publishing LLC., Treasure Island (FL).

Al-Mosawie, A., Wilson, J. M., and Brownstone, R. M. (2007).

Heterogeneity of V2-derived interneurons in the adult mouse spinal cord.

European Journal of Neuroscience, 26(11):3003–3015.

Alaimo, M. A., Smith, J. L., Roy, R. R., and Edgerton, V. R. (1984).

EMG activity of slow and fast ankle extensors following spinal cord transection.

Journal of applied physiology: respiratory, environmental and exercise physiology, 56(6):1608–13.

Alam, M., Garcia-Alias, G., Jin, B., Keyes, J., Zhong, H., Roy, R. R., Gerasimenko, Y., Lu, D. C., and Edgerton, V. R. (2017).
Electrical neuromodulation of the cervical spinal cord facilitates forelimb skilled function recovery in spinal cord injured rats.
Experimental neurology, 291:141–150.

Alam, M., Garcia-Alias, G., Shah, P. K., Gerasimenko, Y., Zhong, H., Roy, R. R., and Edgerton, V. R. (2015).
Evaluation of optimal electrode configurations for epidural spinal cord stimulation in cervical spinal cord injured rats.
Journal of neuroscience methods, 247:50–7.

Alam, M., Ling, Y. T., Wong, A. Y. L., Zhong, H., Edgerton, V. R., and Zheng, Y.-P. (2020).
Reversing 21 years of chronic paralysis via non-invasive spinal cord neuromodulation: A case study.
Annals of Clinical and Translational Neurology, 7(5):829–838.

Alashram, A. R., Padua, E., Raju, M., Romagnoli, C., and Annino, G. (2023).
Transcutaneous spinal cord stimulation effects on spasticity in patients with spinal cord injury: A systematic review.
The Journal of Spinal Cord Medicine, 46(4):582–589.

Albert, M. V., Azeze, Y., Courtois, M., and Jayaraman, A. (2017).
In-lab versus at-home activity recognition in ambulatory subjects with incomplete spinal cord injury.
Journal of NeuroEngineering and Rehabilitation, 14:10.

Albuquerque, I., Tiwari, A., Parent, M., Cassani, R., Gagnon, J.-F., Lafond, D., Tremblay, S., and Falk, T. H. (2020).

WAUC: A Multi-Modal Database for Mental Workload Assessment Under Physical Activity.

Frontiers in Neuroscience, 14.

Alian, A. A. and Shelley, K. H. (2014).

Photoplethysmography.

Best Practice & Research. Clinical Anaesthesiology, 28(4):395–406.

Al'joboori, Y. D., Edgerton, V. R., and Ichiyama, R. M. (2020).

Effects of rehabilitation on perineural nets and synaptic plasticity following spinal cord transection.

Brain sciences, 10(11).

Alluin, O., Delivet-Mongrain, H., and Rossignol, S. (2015).

Inducing hindlimb locomotor recovery in adult rat after complete thoracic spinal cord section using repeated treadmill training with perineal stimulation only.

Journal of Neurophysiology, 114(3):1931–1946.

Alvarez, F. J. and Fyffe, R. E. W. (2007).

The continuing case for the Renshaw cell.

The Journal of Physiology, 584(1):31–45.

Alvarez, F. J., Jonas, P. C., Sapir, T., Hartley, R., Berrocal, M. C., Geiman, E. J., Todd, A. J., and Goulding, M. (2005).

Postnatal phenotype and localization of spinal cord V1 derived interneurons.

The Journal of Comparative Neurology, 493(2):177–192.

Alvarez, F. J., Taylor-Blake, B., Fyffe, R. E., De Blas, A. L., and Light, A. R. (1996).

Distribution of immunoreactivity for the beta 2 and beta 3 subunits of the GABAA receptor in the mammalian spinal cord.

The Journal of comparative neurology, 365(3):392–412.

Alzubaidi, L., Zhang, J., Humaidi, A. J., Al-Dujaili, A., Duan, Y., Al-Shamma, O., Santamaría, J., Fadhel, M. A., Al-Amidie, M., and Farhan, L. (2021).

Review of deep learning: Concepts, CNN architectures, challenges, applications, future directions.

Journal of Big Data, 8(1):53.

Ameri, A., Akhaee, M. A., Scheme, E., and Englehart, K. (2020).

A Deep Transfer Learning Approach to Reducing the Effect of Electrode Shift in EMG Pattern Recognition-Based Control.

IEEE Transactions on Neural Systems and Rehabilitation Engineering, 28(2):370–379.

Anderson, K. D. (2004).

Targeting recovery: Priorities of the spinal cord-injured population.

Journal of Neurotrauma, 21(10):1371–1383.

Andersson, L. S., Larhammar, M., Memic, F., Wootz, H., Schwochow, D., Rubin, C.-J., Patra, K., Arnason, T., Wellbring, L., Hjälm, G., Imsland, F., Petersen, J. L., McCue, M. E., Mickelson, J. R., Cothran, G., Ahituv, N., Roepstorff, L., Mikko, S., Vallstedt, A., Lindgren, G., Andersson, L., and Kullander, K. (2012).

Mutations in DMRT3 affect locomotion in horses and spinal circuit function in mice.

Nature, 488(7413):642–646.

Andersson, O. and Grillner, S. (1981).

Peripheral control of the cat's step cycle I. Phase dependent effects of ramp-movements of the hip during "fictive locomotion".

Acta Physiologica Scandinavica, 113(1):89–101.

Andersson, O., Grillner, S., Lindquist, M., and Zomlefer, M. (1978).
Peripheral control of the spinal pattern generators for locomotion in cat.
Brain Research, 150(3):625–630.

Andrew (2016).
Movement: How the brain communicates with the world.
Cell, 164(6):1122–1135.

Angeli, C. A., Boakye, M., Morton, R. A., Vogt, J., Benton, K., Chen, Y., Ferreira, C. K., and Harkema, S. J. (2018).
Recovery of over-ground walking after chronic motor complete spinal cord injury.
The New England journal of medicine, 379(13):1244–1250.

Angeli, C. A., Edgerton, V. R., Gerasimenko, Y. P., and Harkema, S. J. (2014).
Altering spinal cord excitability enables voluntary movements after chronic complete paralysis in humans.
Brain : a journal of neurology, 137(Pt 5):1394–409.

Antri, M., Mouffle, C., Orsal, D., and Barthe, J. Y. (2003).
5-HT1A receptors are involved in short- and long-term processes responsible for 5-HT-induced locomotor function recovery in chronic spinal rat.
European Journal of Neuroscience, 18(7):1963–1972.

Aragao Rda, S., Rodrigues, M. A., de Barros, K. M., Silva, S. R., Toscano, A. E., de Souza, R. E., and Manhaes-de-Castro, R. (2011).
Automatic system for analysis of locomotor activity in rodents–a reproducibility study.
Journal of neuroscience methods, 195(2):216–21.

Arber, S. (2012).
Motor circuits in action: Specification, connectivity, and function.

Neuron, 74(6):975–989.

Arle, J. E., Iftimia, N., Shils, J. L., Mei, L., and Carlson, K. W. (2019).
Dynamic computational model of the human spinal cord connectome.
Neural computation, 31(2):388–416.

Asín Prieto, G., Ilzarbe Andrés, A., Venkatakrishnan, A., Malik, W. Q., Dietz, V., and Rymer, W. Z. (2016).
Rehabilitation technologies for spinal injury.
In Pons, J. L., Raya, R., and González, J., editors, *Emerging Therapies in Neurorehabilitation II*, pages 65–85. Springer International Publishing, Cham.

Atkinson, D. A., Sayenko, D. G., D'Amico, J. M., Mink, A., Lorenz, D. J., Gerasimenko, Y. P., and Harkema, S. (2020).
Interlimb conditioning of lumbosacral spinally evoked motor responses after spinal cord injury.
Clinical Neurophysiology.

Ausborn, J., Mahmood, R., and El Manira, A. (2012).
Decoding the rules of recruitment of excitatory interneurons in the adult zebrafish locomotor network.
Proceedings of the National Academy of Sciences, 109(52):E3631–E3639.

Australia, A. (2020).
Spinal Cord Injury in Australia Commissioned by Spinal Cure Australia and Insurance and Care NSW (iCare).
Technical report, Accenture, Sydney, Australia.

Australia, I. (2021).
Enabling digital health services for regional and remote Australia | Infrastructure Australia.

https://www.infrastructureaustralia.gov.au/map/enabling-digital-health-services-regional-and-remote-australia.

Australian Institute of Health and Welfare (2022).
Rural and remote health.
https://www.aihw.gov.au/reports/rural-remote-australians/rural-and-remote-health#Access.

Avraham, O., Hadas, Y., Vald, L., Hong, S., Song, M. R., and Klar, A. (2010).
Motor and dorsal root ganglion axons serve as choice points for the ipsilateral turning of dI3 axons.
Journal of Neuroscience, 30(46):15546–15557.

Azizi, S., Mustafa, B., Ryan, F., Beaver, Z., Freyberg, J., Deaton, J., Loh, A., Karthikesalingam, A., Kornblith, S., Chen, T., et al. (2021).
Big self-supervised models advance medical image classification.
In *Proceedings of the IEEE/CVF International Conference on Computer Vision*, pages 3478–3488.

Bacciu, D., Lisboa, P. J. G., Martín, J. D., Stoean, R., and Vellido, A. (2018).
Bioinformatics and medicine in the era of deep learning.

Baek, M., Pivetta, C., Liu, J.-P., Arber, S., and Dasen, J. S. (2017).
Columnar-intrinsic cues shape premotor input specificity in locomotor circuits.
Cell Reports, 21(4):867–877.

Bajaj, V. and Pachori, R. B. (2013).
Automatic classification of sleep stages based on the time-frequency image of EEG signals.
Computer Methods and Programs in Biomedicine, 112(3):320–328.

Baker, S. N. and Perez, M. A. (2017).

Reticulospinal contributions to gross hand function after human spinal cord injury.

The Journal of neuroscience : the official journal of the Society for Neuroscience, 37(40):9778–9784.

Balbinot, G., Li, G., Wiest, M. J., Pakosh, M., Furlan, J. C., Kalsi-Ryan, S., and Zariffa, J. (2021).

Properties of the surface electromyogram following traumatic spinal cord injury: A scoping review.

Journal of NeuroEngineering and Rehabilitation, 18:105.

Bannatyne, B. A. (2006).

Differential projections of excitatory and inhibitory dorsal horn interneurons relaying information from group II muscle afferents in the cat spinal cord.

Journal of Neuroscience, 26(11):2871–2880.

Bannatyne, B. A., Edgley, S. A., Hammar, I., Jankowska, E., and Maxwell, D. J. (2003).

Networks of inhibitory and excitatory commissural interneurons mediating crossed reticulospinal actions.

The European journal of neuroscience, 18(8):2273–2284.

Bannatyne, B. A., Liu, T. T., Hammar, I., Stecina, K., Jankowska, E., and Maxwell, D. J. (2009).

Excitatory and inhibitory intermediate zone interneurons in pathways from feline group I and II afferents: Differences in axonal projections and input.

The Journal of Physiology, 587(2):379–399.

Barbeau, H., McCrea, D. A., O'Donovan, M. J., Rossignol, S., Grill, W. M., and Lemay, M. A. (1999).

Tapping into spinal circuits to restore motor function.

Brain Research Reviews, 30(1):27–51.

Barbeau, H. and Rossignol, S. (1987).

Recovery of locomotion after chronic spinalization in the adult cat.

Brain Research, 412(1):84–95.

Barbeau, H. and Rossignol, S. (1990).

The effects of serotonergic drugs on the locomotor pattern and on cutaneous reflexes of the adult chronic spinal cat.

Brain Research, 514(1):55–67.

Barbeau, H. and Rossignol, S. (1991).

Initiation and modulation of the locomotor pattern in the adult chronic spinal cat by noradrenergic, serotonergic and dopaminergic drugs.

Brain Research, 546(2):250–260.

Barra, B., Roux, C., Kaeser, M., Schiavone, G., Lacour, S. P., Bloch, J., Courtine, G., Rouiller, E. M., Schmidlin, E., and Capogrosso, M. (2018).

Selective recruitment of arm motoneurons in nonhuman primates using epidural electrical stimulation of the cervical spinal cord.

In *2018 40th Annual International Conference of the IEEE Engineering in Medicine and Biology Society (EMBC)*, pages 1424–1427. IEEE.

Barshan, B. and Yurtman, A. (2016).

Investigating Inter-Subject and Inter-Activity Variations in Activity Recognition Using Wearable Motion Sensors.

The Computer Journal, 59(9):1345–1362.

Bayona, N. A., Bitensky, J., Salter, K., and Teasell, R. (2005).

The role of task-specific training in rehabilitation therapies.

Topics in stroke rehabilitation, 12(3):58–65.

Beauparlant, J., Van Den Brand, R., Barraud, Q., Friedli, L., Musienko, P., Dietz, V., and Courtine, G. (2013).

Undirected compensatory plasticity contributes to neuronal dysfunction after severe spinal cord injury.

Brain : a journal of neurology, 136(11):3347–3361.

Behrends, T., Schomburg, E. D., and Steffens, H. (1983).

Facilitatory interaction between cutaneous afferents from low threshold mechanoreceptors and nociceptors in segmental reflex pathways to α-motoneurons.

Brain Research, 260(1):131–134.

Belanger, M., Drew, T., Provencher, J., and Rossignol, S. (1996).

A comparison of treadmill locomotion in adult cats before and after spinal transection.

Journal of Neurophysiology, 76(1):471–491.

Bellardita, C., Caggiano, V., Leiras, R., Caldeira, V., Fuchs, A., Bouvier, J., Löw, P., and Kiehn, O. (2017).

Spatiotemporal correlation of spinal network dynamics underlying spasms in chronic spinalized mice.

eLife, 6.

Benavides, F. D., Jo, H. J., Lundell, H., Edgerton, V. R., Gerasimenko, Y., and Perez, M. A. (2020).

Cortical and subcortical effects of transcutaneous spinal cord stimulation in humans with tetraplegia.

The Journal of neuroscience : the official journal of the Society for Neuroscience, 40(13):2633–2643.

Bengio, Y., Louradour, J., Collobert, R., and Weston, J. (2009).

Curriculum learning.

In *Proceedings of the 26th Annual International Conference on Machine Learning*, ICML '09, pages 41–48, New York, NY, USA. Association for Computing Machinery.

Berkowitz, M., Kruse, D., O'Leary, P., and Harvey, C. (1998).

Spinal Cord Injury: An Analysis of Medical and Social Costs.

Demos Medical Publishing.

Bernstein, N. (1966).

The co-ordination and regulation of movements.

The co-ordination and regulation of movements.

Berrar, D. and Dubitzky, W. (2021).

Deep learning in bioinformatics and biomedicine.

Briefings in Bioinformatics, 22(2):1513–1514.

Betley, J. N., Wright, C. V. E., Kawaguchi, Y., Erdélyi, F., Szabó, G., Jessell, T. M., and Kaltschmidt, J. A. (2009).

Stringent specificity in the construction of a GABAergic presynaptic inhibitory circuit.

Cell, 139(1):161–174.

Bikoff, J. B., Gabitto, M. I., Rivard, A. F., Drobac, E., Machado, T. A., Miri, A., Brenner-Morton, S., Famojure, E., Diaz, C., Alvarez, F. J., Mentis, G. Z., and Jessell, T. M. (2016).

Spinal inhibitory interneuron diversity delineates variant motor microcircuits.

Cell, 165(1):207–219.

Bizzi, E., Mussa-Ivaldi, F., and Giszter, S. (1991).

Computations underlying the execution of movement: A biological perspective.

Science (New York, N.Y.), 253(5017):287–291.

Blacklaws, J., Deska-Gauthier, D., Jones, C. T., Petracca, Y. L., Liu, M., Zhang, H., Fawcett, J. P., Glover, J. C., Lanuza, G. M., and Zhang, Y. (2015).
Sim1is required for the migration and axonal projections of V3 interneurons in the developing mouse spinal cord.
Developmental Neurobiology, 75(9):1003–1017.

Bolton, D. A. E. and Misiaszek, J. E. (2009).
Contribution of hindpaw cutaneous inputs to the control of lateral stability during walking in the cat.
Journal of Neurophysiology, 102(3):1711–1724.

Bonato, P. (2010).
Wearable sensors and systems. From enabling technology to clinical applications.
IEEE engineering in medicine and biology magazine : the quarterly magazine of the Engineering in Medicine & Biology Society, 29(3):25–36.

Bonizzato, M., Pidpruzhnykova, G., DiGiovanna, J., Shkorbatova, P., Pavlova, N., Micera, S., and Courtine, G. (2018).
Brain-controlled modulation of spinal circuits improves recovery from spinal cord injury.
Nature communications, 9(1):3015.

Booth, V., Rinzel, J., and Kiehn, O. (1997).
Compartmental model of vertebrate motoneurons for Ca2+-dependent spiking and plateau potentials under pharmacological treatment.
Journal of Neurophysiology, 78(6):3371–3385.

Borowska, J., Jones, C. T., Zhang, H., Blacklaws, J., Goulding, M., and Zhang, Y. (2013).

Functional subpopulations of V3 interneurons in the mature mouse spinal cord. *Journal of Neuroscience*, 33(47):18553–18565.

Bourane, S., Grossmann, K. S., Britz, O., Dalet, A., Del Barrio, M. G., Stam, F. J., Garcia-Campmany, L., Koch, S., and Goulding, M. (2015).
Identification of a spinal circuit for light touch and fine motor control.
Cell, 160(3):503–15.

Bouyer, L. J. G. and Rossignol, S. (2003).
Contribution of cutaneous inputs from the hindpaw to the control of locomotion. I. Intact cats.
Journal of Neurophysiology, 90(6):3625–3639.

Bras, H., Cavallari, P., Jankowska, E., and Kubin, L. (1989).
Morphology of midlumbar interneurones relaying information from group II muscle afferents in the cat spinal cord.
The Journal of Comparative Neurology, 290(1):1–15.

Brockett, E. G., Seenan, P. G., Bannatyne, B. A., and Maxwell, D. J. (2013).
Ascending and descending propriospinal pathways between lumbar and cervical segments in the rat: Evidence for a substantial ascending excitatory pathway.
Neuroscience, 240:83–97.

Brogioli, M., Popp, W. L., Schneider, S., Albisser, U., Brust, A. K., Frotzler, A., Gassert, R., Curt, A., and Starkey, M. L. (2017).
Multi-day recordings of wearable sensors are valid and sensitive measures of function and independence in human spinal cord injury.
Journal of neurotrauma, 34(6):1141–1148.

Brooke, J. D., Cheng, J., Collins, D. F., McIlroy, W. E., Misiaszek, J. E., and Staines, W. R. (1997).

SENSORI-SENSORY AFFERENT CONDITIONING WITH LEG MOVEMENT: GAIN CONTROL IN SPINAL REFLEX AND ASCENDING PATHS.

Progress in Neurobiology, 51(4):393–421.

Brooker, C., Russo, M., Cousins, M. J., Taylor, N., Holford, L., Martin, R., Boesel, T., Sullivan, R., Hanson, E., Gmel, G. E., Shariati, N. H., Poree, L., and Parker, J. (2021). ECAP-Controlled Closed-Loop Spinal Cord Stimulation Efficacy and Opioid Reduction Over 24-Months: Final Results of the Prospective, Multicenter, Open-Label Avalon Study.

Pain Practice, 21(6):680–691.

Brown, T. G. (1911).

The intrinsic factors in the act of progression in the mammal.

Proceedings of the Royal Society of London. Series B, Containing Papers of a Biological Character, 84(572):308–319.

Brownstone, R. M. and Bui, T. V. (2010).

Spinal interneurons providing input to the final common path during locomotion.

In *Breathe, Walk and Chew: The Neural Challenge: Part I*, volume 187 of *Progress in Brain Research*, pages 81–95. Elsevier.

Brownstone, R. M., Bui, T. V., and Stifani, N. (2015).

Spinal circuits for motor learning.

Current Opinion in Neurobiology, 33:166–173.

Bruce, H. D. and Andrew, D. (2011).

The promise of mHealth: Daily activity monitoring and outcome assessments by wearable sensors.

Neurorehabilitation and Neural Repair, 25(9):788–798.

Brzosko, Z., Mierau, S. B., and Paulsen, O. (2019).
Neuromodulation of Spike-Timing-Dependent Plasticity: Past, Present, and Future.
Neuron, 103(4):563–581.

Buckley, C., Alcock, L., McArdle, R., Rehman, R. Z. U., Del Din, S., Mazzà, C., Yarnall, A. J., and Rochester, L. (2019).
The Role of Movement Analysis in Diagnosing and Monitoring Neurodegenerative Conditions: Insights from Gait and Postural Control.
Brain Sciences, 9(2):34.

Buffart, L. M., van den Berg-Emons, R. J., van Meeteren, J., Stam, H. J., and Roebroeck, M. E. (2009).
Lifestyle, participation, and health-related quality of life in adolescents and young adults with myelomeningocele.
Developmental medicine and child neurology, 51(11):886–94.

Bui, T. V., Cushing, S., Dewey, D., Fyffe, R. E., and Rose, P. K. (2003).
Comparison of the morphological and electrotonic properties of Renshaw cells, Ia inhibitory interneurons, and motoneurons in the cat.
Journal of Neurophysiology, 90(5):2900–2918.

Bui, T. V., Stifani, N., Akay, T., and Brownstone, R. M. (2016).
Spinal microcircuits comprising dI3 interneurons are necessary for motor functional recovery following spinal cord transection.
eLife, 5.

Bunday, K. L. and Perez, M. A. (2012).
Motor recovery after spinal cord injury enhanced by strengthening corticospinal synaptic transmission.
Current biology : CB, 22(24):2355–61.

Bunday, K. L., Urbin, M. A., and Perez, M. A. (2018).

Potentiating paired corticospinal-motoneuronal plasticity after spinal cord injury.

Brain stimulation, 11(5):1083–1092.

Burke, R. E. (2007).

Sir Charles Sherrington's The integrative action of the nervous system: A centenary appreciation.

Brain, 130(4):887–894.

Burns, A. and Adeli, H. (2017).

Wearable technology for patients with brain and spinal cord injuries.

Reviews in the Neurosciences, 28(8):913–920.

Cabaj, A. M., Majczyński, H., Couto, E., Gardiner, P. F., Stecina, K., Sławińska, U., and Jordan, L. M. (2017).

Serotonin controls initiation of locomotion and afferent modulation of coordination via 5-HT7receptors in adult rats.

The Journal of Physiology, 595(1):301–320.

Cadotte, D. W., Bosma, R., Mikulis, D., Nugaeva, N., Smith, K., Pokrupa, R., Islam, O., Stroman, P. W., and Fehlings, M. G. (2012).

Plasticity of the injured human spinal cord: Insights revealed by spinal cord functional MRI.

PLoS One, 7(9):e45560.

Cadotte, D. W. and Fehlings, M. G. (2011).

Spinal cord injury: A systematic review of current treatment options.

Clinical orthopaedics and related research, 469(3):732–41.

Cai, L. L., Fong, A. J., Otoshi, C. K., Liang, Y., Burdick, J. W., Roy, R. R., and Edgerton, V. R. (2006).

Implications of assist-as-needed robotic step training after a complete spinal cord injury on intrinsic strategies of motor learning.
Journal of Neuroscience, 26(41):10564–10568.

Caillet, A. H., Phillips, A. T. M., Farina, D., and Modenese, L. (2022).
Estimation of the firing behaviour of a complete motoneuron pool by combining electromyography signal decomposition and realistic motoneuron modelling.
PLOS Computational Biology, 18(9):e1010556.

Cakan, C. and Obermayer, K. (2020).
Biophysically grounded mean-field models of neural populations under electrical stimulation.
PLOS Computational Biology, 16(4):e1007822.

Calvert, J. S., Gill, M. L., Linde, M. B., Veith, D. D., Thoreson, A. R., Lopez, C., Lee, K. H., Gerasimenko, Y. P., Edgerton, V. R., Lavrov, I. A., Zhao, K. D., Grahn, P. J., and Sayenko, D. G. (2021).
Voluntary modulation of evoked responses generated by epidural and transcutaneous spinal stimulation in humans with spinal cord injury.
Journal of Clinical Medicine, 10(21):4898.

Calvert, J. S., Grahn, P. J., Zhao, K. D., and Lee, K. H. (2019).
Emergence of epidural electrical stimulation to facilitate sensorimotor network functionality after spinal cord injury.
Neuromodulation : journal of the International Neuromodulation Society, 22(3):244–252.

Cantoria, M. J., See, P. A., Singh, H., and De Leon, R. D. (2011).

Adaptations in glutamate and glycine content within the lumbar spinal cord are associated with the generation of novel gait patterns in rats following neonatal spinal cord transection.

Journal of Neuroscience, 31(50):18598–18605.

Cao, Z., Ding, W., Wang, Y.-K., Hussain, F. K., Al-Jumaily, A., and Lin, C.-T. (2020).

Effects of repetitive SSVEPs on EEG complexity using multiscale inherent fuzzy entropy.

Neurocomputing, 389:198–206.

Capelli, P., Pivetta, C., Soledad Esposito, M., and Arber, S. (2017).

Locomotor speed control circuits in the caudal brainstem.

Nature, 551(7680):373–377.

Capogrosso, M., Milekovic, T., Borton, D., Wagner, F., Moraud, E. M., Mignardot, J. B., Buse, N., Gandar, J., Barraud, Q., Xing, D., Rey, E., Duis, S., Jianzhong, Y., Ko, W. K., Li, Q., Detemple, P., Denison, T., Micera, S., Bezard, E., Bloch, J., and Courtine, G. (2016).

A brain-spine interface alleviating gait deficits after spinal cord injury in primates.

Nature, 539(7628):284–288.

Capogrosso, M., Wenger, N., Raspopovic, S., Musienko, P., Beauparlant, J., Bassi Luciani, L., Courtine, G., and Micera, S. (2013).

A computational model for epidural electrical stimulation of spinal sensorimotor circuits.

The Journal of neuroscience : the official journal of the Society for Neuroscience, 33(49):19326–40.

Caporale, N. and Dan, Y. (2008).

Spike timing-dependent plasticity: A Hebbian learning rule.

Annual Review of Neuroscience, 31:25–46.

Caron, G., Bilchak, J. N., and Côté, M.-P. (2020).

Direct evidence for decreased presynaptic inhibition evoked by PBSt group I muscle afferents after chronic SCI and recovery with step-training in rats.

The Journal of Physiology, 598(20):4621–4642.

Caron, M., Touvron, H., Misra, I., Jégou, H., Mairal, J., Bojanowski, P., and Joulin, A. (2021).

Emerging properties in self-supervised vision transformers.

In *Proceedings of the IEEE/CVF International Conference on Computer Vision*, pages 9650–9660.

Catala, M. and Kubis, N. (2013).

Gross anatomy and development of the peripheral nervous system.

In *Peripheral Nerve Disorders*, volume 115 of *Handbook of Clinical Neurology*, pages 29–41. Elsevier Health Sciences.

Catalfamo, P., Ghoussayni, S., and Ewins, D. (2010).

Gait Event Detection on Level Ground and Incline Walking Using a Rate Gyroscope.

Sensors (Basel, Switzerland), 10(6):5683–5702.

Cavallari, P., Edgley, S. A., and Jankowska, E. (1987).

Post-synaptic actions of midlumbar interneurones on motoneurones of hind-limb muscles in the cat.

The Journal of Physiology, 389(1):675–689.

Caylor, J., Reddy, R., Yin, S., Cui, C., Huang, M., Huang, C., Rao, R., Baker, D. G., Simmons, A., Souza, D., Narouze, S., Vallejo, R., and Lerman, I. (2019).

Spinal cord stimulation in chronic pain: Evidence and theory for mechanisms of action.

Bioelectronic Medicine, 5:12.

Celik, Y., Stuart, S., Woo, W. L., and Godfrey, A. (2021).
Gait analysis in neurological populations: Progression in the use of wearables.
Medical Engineering & Physics, 87:9–29.

Chaki, J. and Woźniak, M. (2023).
Deep learning for neurodegenerative disorder (2016 to 2022): A systematic review.
Biomedical Signal Processing and Control, 80:104223.

Chen, B., Zheng, E., Wang, Q., and Wang, L. (2015).
A new strategy for parameter optimization to improve phase-dependent locomotion mode recognition.
Neurocomputing, 149:585–593.

Chen, C., Fu, Z., Chen, Z., Jin, S., Cheng, Z., Jin, X., and Hua, X.-S. (2019).
HoMM: Higher-order Moment Matching for Unsupervised Domain Adaptation.

Chen, T., Kornblith, S., Norouzi, M., and Hinton, G. (2020).
A simple framework for contrastive learning of visual representations.
In *Proceedings of the 37th International Conference on Machine Learning*, volume 119 of *ICML'20*, pages 1597–1607. JMLR.org.

Cheng, R., Sui, Y., Sayenko, D., and Burdick, J. W. (2019).
Motor control after human SCI through activation of muscle synergies under spinal cord stimulation.
IEEE transactions on neural systems and rehabilitation engineering : a publication of the IEEE Engineering in Medicine and Biology Society, 27(6):1331–1340.

Choi, E., Schuetz, A., Stewart, W. F., and Sun, J. (2017).
Using recurrent neural network models for early detection of heart failure onset.

Journal of the American Medical Informatics Association : JAMIA, 24(2):361–370.

Choi, J. T., Jensen, P., Nielsen, J. B., and Bouyer, L. J. (2016).

Error signals driving locomotor adaptation: Cutaneous feedback from the foot is used to adapt movement during perturbed walking.

The Journal of Physiology, 594(19):5673–5684.

Chollet, F. (2017).

Xception: Deep learning with depthwise separable convolutions.

Chopek, J. W., Nascimento, F., Beato, M., Brownstone, R. M., and Zhang, Y. (2018).

Sub-populations of spinal V3 interneurons form focal modules of layered pre-motor microcircuits.

Cell Reports, 25(1):146–156.e3.

Chopin, S. F. and Buerger, A. A. (1976).

Instrumental avoidance conditioning in the Spinal rat.

Brain Research Bulletin, 1(2):177–183.

Christiansen, L. and Perez, M. A. (2018).

Targeted-plasticity in the corticospinal tract after human spinal cord injury.

Neurotherapeutics : the journal of the American Society for Experimental NeuroTherapeutics, 15(3):618–627.

Chu, L., Li, Q., Yang, B., Chen, L., Shen, C., and Wang, D. (2023).

Exploring the essence of compound fault diagnosis: A novel multi-label domain adaptation method and its application to bearings.

Heliyon, 9(3):e14545.

Ciompi, F., de Hoop, B., van Riel, S. J., Chung, K., Scholten, E. T., Oudkerk, M., de Jong, P. A., Prokop, M., and van Ginneken, B. (2015).

Automatic classification of pulmonary peri-fissural nodules in computed tomography using an ensemble of 2D views and a convolutional neural network out-of-the-box. *Medical Image Analysis*, 26(1):195–202.

Clarke, R. L., Smith, R. F., and Justesen, D. R. (1985).
An infrared device for detecting locomotor activity.
Behavior Research Methods, Instruments, & Computers, 17(5):519–525.

Collie, A., Keating, C., Pezzullo, L., Gabbe, B., Cooper, J., Brown, D., Olver, J., McCartin, F., and Trethewey, P. (2010).
Brain and spinal cord injury in Australia – economic cost and burden of disease.
Injury Prevention, 16(Suppl 1):A25–A26.

Colombo, R., Pisano, F., Micera, S., Mazzone, A., Delconte, C., Carrozza, M. C., Dario, P., and Minuco, G. (2008).
Assessing mechanisms of recovery during robot-aided neurorehabilitation of the upper limb.
Neurorehabilitation and neural repair, 22(1):50–63.

Conway, B. A., Hultborn, H., and Kiehn, O. (1987).
Proprioceptive input resets central locomotor rhythm in the spinal cat.
Experimental Brain Research, 68(3).

Cordo, P. J. and Nashner, L. M. (1982).
Properties of postural adjustments associated with rapid arm movements.
Journal of neurophysiology, 47(2):287–302.

Cote, M. P., Murray, L. M., and Knikou, M. (2018).
Spinal control of locomotion: Individual neurons, their circuits and functions.
Frontiers in physiology, 9:784.

Cote, M. P., Murray, M., and Lemay, M. A. (2017).

Rehabilitation strategies after spinal cord injury: Inquiry into the mechanisms of success and failure.

Journal of neurotrauma, 34(10):1841–1857.

Côté-Allard, U., Fall, C. L., Campeau-Lecours, A., Gosselin, C., Laviolette, F., and Gosselin, B. (2017).

Transfer learning for sEMG hand gestures recognition using convolutional neural networks.

In *2017 IEEE International Conference on Systems, Man, and Cybernetics (SMC)*, pages 1663–1668.

Côté-Allard, U., Fall, C. L., Drouin, A., Campeau-Lecours, A., Gosselin, C., Glette, K., Laviolette, F., and Gosselin, B. (2019).

Deep Learning for Electromyographic Hand Gesture Signal Classification Using Transfer Learning.

IEEE Transactions on Neural Systems and Rehabilitation Engineering, 27(4):760–771.

Côté-Allard, U., Gagnon-Turcotte, G., Phinyomark, A., Glette, K., Scheme, E., Laviolette, F., and Gosselin, B. (2021).

A Transferable Adaptive Domain Adversarial Neural Network for Virtual Reality Augmented EMG-Based Gesture Recognition.

IEEE Transactions on Neural Systems and Rehabilitation Engineering, 29:546–555.

Courtine, G., Bunge, M. B., Fawcett, J. W., Grossman, R. G., Kaas, J. H., Lemon, R., Maier, I., Martin, J., Nudo, R. J., Ramon-Cueto, A., Rouiller, E. M., Schnell, L., Wannier, T., Schwab, M. E., and Edgerton, V. R. (2007a).

Can experiments in nonhuman primates expedite the translation of treatments for spinal cord injury in humans?

Nature Medicine, 13(5):561–566.

Courtine, G., Gerasimenko, Y., van den Brand, R., Yew, A., Musienko, P., Zhong, H., Song, B., Ao, Y., Ichiyama, R. M., Lavrov, I., Roy, R. R., Sofroniew, M. V., and Edgerton, V. R. (2009).

Transformation of nonfunctional spinal circuits into functional states after the loss of brain input.

Nature neuroscience, 12(10):1333–42.

Courtine, G., Harkema, S. J., Dy, C. J., Gerasimenko, Y. P., and Dyhre-Poulsen, P. (2007b).

Modulation of multisegmental monosynaptic responses in a variety of leg muscles during walking and running in humans.

The Journal of physiology, 582(Pt 3):1125–39.

Courtine, G., Roy, R. R., Raven, J., Hodgson, J., McKay, H., Yang, H., Zhong, H., Tuszynski, M. H., and Edgerton, V. R. (2005).

Performance of locomotion and foot grasping following a unilateral thoracic corticospinal tract lesion in monkeys (Macaca mulatta).

Brain : a journal of neurology, 128(Pt 10):2338–58.

Courtine, G. and Sofroniew, M. V. (2019).

Spinal cord repair: Advances in biology and technology.

Nature medicine, 25(6):898–908.

Courtine, G., Song, B., Roy, R. R., Zhong, H., Herrmann, J. E., Ao, Y., Qi, J., Edgerton, V. R., and Sofroniew, M. V. (2008).

Recovery of supraspinal control of stepping via indirect propriospinal relay connections after spinal cord injury.

Nature medicine, 14(1):69–74.

Cowley, K. C. and Schmidt, B. J. (1995).

Effects of inhibitory amino acid antagonists on reciprocal inhibitory interactions during rhythmic motor activity in the in vitro neonatal rat spinal cord.

Journal of Neurophysiology, 74(3):1109–1117.

Cowley, K. C., Zaporozhets, E., and Schmidt, B. J. (2010).

Propriospinal transmission of the locomotor command signal in the neonatal rat.

Annals of the New York Academy of Sciences, 1198(1):42–53.

Crone, S. A., Quinlan, K. A., Zagoraiou, L., Droho, S., Restrepo, C. E., Lundfald, L., Endo, T., Setlak, J., Jessell, T. M., Kiehn, O., and Sharma, K. (2008).

Genetic ablation of V2a ipsilateral interneurons disrupts left-right locomotor coordination in mammalian spinal cord.

Neuron, 60(1):70–83.

Crone, S. A., Zhong, G., Harris-Warrick, R., and Sharma, K. (2009).

In mice lacking V2a interneurons, gait depends on speed of locomotion.

Journal of Neuroscience, 29(21):7098–7109.

Curt, A., Keck, M. E., and Dietz, V. (1998).

Functional outcome following spinal cord injury: Significance of motor-evoked potentials and ASIA scores.

Archives of Physical Medicine and Rehabilitation, 79(1):81–86.

Curt, A., Van Hedel, H. J., Klaus, D., Dietz, V., and Group, E.-S. S. (2008).

Recovery from a spinal cord injury: Significance of compensation, neural plasticity, and repair.

Journal of neurotrauma, 25(6):677–85.

Danner, S. M., Hofstoetter, U. S., Freundl, B., Binder, H., Mayr, W., Rattay, F., and Minassian, K. (2015).

Human spinal locomotor control is based on flexibly organized burst generators.
Brain : a journal of neurology, 138(3):577–588.

Danner, S. M., Shevtsova, N. A., Frigon, A., and Rybak, I. A. (2017).
Computational modeling of spinal circuits controlling limb coordination and gaits in quadrupeds.
Elife, 6.

Danner, S. M., Wilshin, S. D., Shevtsova, N. A., and Rybak, I. A. (2016).
Central control of interlimb coordination and speed-dependent gait expression in quadrupeds.
The Journal of Physiology, 594(23):6947–6967.

Danner, S. M., Zhang, H., Shevtsova, N. A., Borowska-Fielding, J., Deska-Gauthier, D., Rybak, I. A., and Zhang, Y. (2019).
Spinal V3 interneurons and Left–Right coordination in mammalian locomotion.
Frontiers in Cellular Neuroscience, 13(516).

Darrow, D., Balser, D., Netoff, T. I., Krassioukov, A., Phillips, A., Parr, A., and Samadani, U. (2019).
Epidural spinal cord stimulation facilitates immediate restoration of dormant motor and autonomic supraspinal pathways after chronic neurologically complete spinal cord injury.
Journal of neurotrauma, 36(15):2325–2336.

De Fazio, R., Mastronardi, V. M., De Vittorio, M., and Visconti, P. (2023).
Wearable Sensors and Smart Devices to Monitor Rehabilitation Parameters and Sports Performance: An Overview.
Sensors (Basel, Switzerland), 23(4):1856.

de Graaf, G., Postmus, D., Westerink, J., and Buskens, E. (2018).
The early economic evaluation of novel biomarkers to accelerate their translation into clinical applications.
Cost Effectiveness and Resource Allocation : C/E, 16:23.

De Guzman, C. P., Roy, R. R., Hodgson, J. A., and Reggie Edgerton, V. (1991).
Coordination of motor pools controlling the ankle musculature in adult spinal cats during treadmill walking.
Brain Research, 555(2):202–214.

De Leon, R. D., Hodgson, J. A., Roy, R. R., and Edgerton, V. R. (1998a).
Full weight-bearing hindlimb standing following stand training in the adult spinal cat.
Journal of Neurophysiology, 80(1):83–91.

De Leon, R. D., Hodgson, J. A., Roy, R. R., and Edgerton, V. R. (1998b).
Locomotor capacity attributable to step training versus spontaneous recovery after spinalization in adult cats.
Journal of Neurophysiology, 79(3):1329–1340.

de Leon, R. D., Reinkensmeyer, D. J., Timoszyk, W. K., London, N. J., Roy, R. R., and Reggie Edgerton, V. (2002).
Chapter 11 Use of robotics in assessing the adaptive capacity of the rat lumbar spinal cord.
In McKerracher, L., Doucet, G., and Rossignol, S., editors, *Progress in Brain Research*, volume 137, pages 141–149. Elsevier.

de Leon, R. D., Roy, R. R., and Edgerton, V. R. (2001).
Is the recovery of stepping following spinal cord injury mediated by modifying existing neural pathways or by generating new pathways? A perspective.
Physical therapy, 81(12):1904–11.

de Leon, R. D., Tamaki, H., Hodgson, J. A., Roy, R. R., and Edgerton, V. R. (1999).
Hindlimb locomotor and postural training modulates glycinergic inhibition in the spinal cord of the adult spinal cat.
Journal of neurophysiology, 82(1):359–69.

Demir, F., Bajaj, V., Ince, M. C., Taran, S., and Şengür, A. (2019).
Surface EMG signals and deep transfer learning-based physical action classification.
Neural Computing and Applications, 31(12):8455–8462.

Den Otter, A. R., Geurts, A. C. H., Mulder, Th., and Duysens, J. (2007).
Abnormalities in the temporal patterning of lower extremity muscle activity in hemiparetic gait.
Gait & Posture, 25(3):342–352.

Deng, J., Dong, W., Socher, R., Li, L.-J., Li, K., and Fei-Fei, L. (2009).
ImageNet: A large-scale hierarchical image database.
In *2009 IEEE Conference on Computer Vision and Pattern Recognition*, pages 248–255.

Desautels, T. A., Choe, J., Gad, P., Nandra, M. S., Roy, R. R., Zhong, H., Tai, Y. C., Edgerton, V. R., and Burdick, J. W. (2015).
An active learning algorithm for control of epidural electrostimulation.
IEEE transactions on bio-medical engineering, 62(10):2443–2455.

Deserno, T. M. and Marx, N. (2016).
Computational Electrocardiography: Revisiting Holter ECG Monitoring.
Methods of Information in Medicine, 55(4):305–311.

Dhawale, A. K., Smith, M. A., and Olveczky, B. P. (2017).
The role of variability in motor learning.
Annual review of neuroscience, 40:479–498.

Di Giorgio, AM. (1929).

Persistenza, nell'animale spinale, di asimmetrie posturali e motorie di origine cerebellare.

Arch Fisiol, 27:519–542.

Di Nardo, F., Morbidoni, C., Cucchiarelli, A., and Fioretti, S. (2021).

Influence of EMG-signal processing and experimental set-up on prediction of gait events by neural network.

Biomedical Signal Processing and Control, 63:102232.

Di Nardo, F., Morbidoni, C., and Fioretti, S. (2024).

Surface electromyographic signals collected during long-lasting ground walking of young able-bodied subjects.

Dickson, A., Allan, D., and O'carroll, R. (2008).

Biographical disruption and the experience of loss following a spinal cord injury: An interpretative phenomenological analysis.

Psychology & Health, 23(4):407–425.

Dietz, V. (2002).

Locomotor activity in spinal man: Significance of afferent input from joint and load receptors.

Brain : a journal of neurology, 125(12):2626–2634.

Dietz, V., Colombo, G., Jensen, L., and Baumgartner, L. (1995).

Locomotor capacity of spinal cord in paraplegic patients.

Annals of Neurology, 37(5):574–582.

Dietz, V. and Fouad, K. (2014).

Restoration of sensorimotor functions after spinal cord injury.

Brain : a journal of neurology, 137(Pt 3):654–67.

Dietz, V. and Muller, R. (2004).

Degradation of neuronal function following a spinal cord injury: Mechanisms and countermeasures.

Brain : a journal of neurology, 127(Pt 10):2221–31.

DiMarco, A. F., Kowalski, K. E., Hromyak, D. R., and Geertman, R. T. (2014).

Long-term follow-up of spinal cord stimulation to restore cough in subjects with spinal cord injury.

The Journal of Spinal Cord Medicine, 37(4):380–388.

Dimitrijevic, M. M., Dimitrijevic, M. R., Illis, L. S., Nakajima, K., Sharkey, P. C., and Sherwood, A. M. (1986).

Spinal cord stimulation for the control of spasticity in patients with chronic spinal cord injury: I. Clinical observations.

Central nervous system trauma : journal of the American Paralysis Association, 3(2):129–44.

Dimitrijevic, M. R., Gerasimenko, Y., and Pinter, M. M. (1998).

Evidence for a spinal central pattern generator in humansa.

Annals of the New York Academy of Sciences, 860(1 NEURONAL MECH):360–376.

Dimitrijevic, M. R. and Kakulas, B. A. (2020).

Spinal cord injuries, human neuropathology and neurophysiology.

Acta myologica : myopathies and cardiomyopathies : official journal of the Mediterranean Society of Myology, 39(4):353–358.

Ding, Y., Kastin, A. J., and Pan, W. (2005).

Neural plasticity after spinal cord injury.

Current pharmaceutical design, 11(11):1441–1450.

Diop, M., Epstein, D., and Gaggero, A. (2021).
Quality of life, health and social costs of patients with spinal cord injury: A systematic review.
European Journal of Public Health, 31(Supplement_3):ckab165.177.

Ditthapron, A., Agu, E. O., and Lammert, A. C. (2021).
Learning from Limited Data for Speech-based Traumatic Brain Injury (TBI) Detection.
In *2021 20th IEEE International Conference on Machine Learning and Applications (ICMLA)*, pages 1482–1486.

Djenoune, L., Khabou, H., Joubert, F., Quan, F. B., Nunes Figueiredo, S., Bodineau, L., Del Bene, F., Burcklé, C., Tostivint, H., and Wyart, C. (2014).
Investigation of spinal cerebrospinal fluid-contacting neurons expressing PKD2L1: Evidence for a conserved system from fish to primates.
Frontiers in Neuroanatomy, 8.

Domingo, A., Al-Yahya, A. A., Asiri, Y., Eng, J. J., Lam, and Spinal Cord Injury Rehabil, T. (2012).
A systematic review of the effects of pharmacological agents on walking function in people with spinal cord injury.
Journal of Neurotrauma, 29(5):865–879.

Donati, A. R., Shokur, S., Morya, E., Campos, D. S., Moioli, R. C., Gitti, C. M., Augusto, P. B., Tripodi, S., Pires, C. G., Pereira, G. A., Brasil, F. L., Gallo, S., Lin, A. A., Takigami, A. K., Aratanha, M. A., Joshi, S., Bleuler, H., Cheng, G., Rudolph, A., and Nicolelis, M. A. (2016).
Long-term training with a brain-machine interface-based gait protocol induces partial neurological recovery in paraplegic patients.

Scientific reports, 6:30383.

Donelan, J. M. and Pearson, K. G. (2004).

Contribution of force feedback to ankle extensor activity in decerebrate walking cats.

Journal of Neurophysiology, 92(4):2093–2104.

Dosovitskiy, A., Beyer, L., Kolesnikov, A., Weissenborn, D., Zhai, X., Unterthiner, T., Dehghani, M., Minderer, M., Heigold, G., Gelly, S., Uszkoreit, J., and Houlsby, N. (2021/2021).

An image is worth 16x16 words: Transformers for image recognition at scale.

Dougherty, K. J. and Kiehn, O. (2010).

Firing and cellular properties of V2a interneurons in the rodent spinal cord.

Journal of Neuroscience, 30(1):24–37.

Dougherty, K. J., Zagoraiou, L., Satoh, D., Rozani, I., Doobar, S., Arber, S., Jessell, T. M., and Kiehn, O. (2013).

Locomotor rhythm generation linked to the output of spinal shox2 excitatory interneurons.

Neuron, 80(4):920–933.

Du, Y., Jin, W., Wei, W., Hu, Y., and Geng, W. (2017).

Surface EMG-Based Inter-Session Gesture Recognition Enhanced by Deep Domain Adaptation.

Sensors, 17(3):458.

Duan, N., Liu, L.-Z., Yu, X.-J., Li, Q., and Yeh, S.-C. (2019).

Classification of multichannel surface-electromyography signals based on convolutional neural networks.

Journal of Industrial Information Integration, 15:201–206.

Dumont, R. J., Okonkwo, D. O., Verma, S., Hurlbert, R. J., Boulos, P. T., Ellegala, D. B., and Dumont, A. S. (2001).

Acute spinal cord injury, part I: Pathophysiologic mechanisms.

Clinical neuropharmacology, 24(5):254–64.

Duru, P. O., Tillakaratne, N. J., Kim, J. A., Zhong, H., Stauber, S. M., Pham, T. T., Xiao, M. S., Edgerton, V. R., and Roy, R. R. (2015).

Spinal neuronal activation during locomotor-like activity enabled by epidural stimulation and 5-hydroxytryptamine agonists in spinal rats.

Journal of neuroscience research, 93(8):1229–39.

Duysens, J. (1977).

Reflex control of locomotion as revealed by stimulation of cutaneous afferents in spontaneously walking premammillary cats.

Journal of Neurophysiology, 40(4):737–751.

Duysens, J. and Pearson, K. G. (1976).

The role of cutaneous afferents from the distal hindlimb in the regulation of the step cycle of thalamic cats.

Experimental Brain Research, 24(3).

Duysens, J. and Pearson, K. G. (1980).

Inhibition of flexor burst generation by loading ankle extensor muscles in walking cats.

Brain Research, 187(2):321–332.

Dy, C. J., Gerasimenko, Y. P., Edgerton, V. R., Dyhre-Poulsen, P., Courtine, G., and Harkema, S. J. (2010).

Phase-dependent modulation of percutaneously elicited multisegmental muscle responses after spinal cord injury.

Journal of neurophysiology, 103(5):2808–20.

Dyck, J., Lanuza, G. M., and Gosgnach, S. (2012).
Functional characterization of dI6 interneurons in the neonatal mouse spinal cord.
Journal of Neurophysiology, 107(12):3256–3266.

Dzeladini, F., van den Kieboom, J., and Ijspeert, A. (2014).
The contribution of a central pattern generator in a reflex-based neuromuscular model.
Frontiers in human neuroscience, 8:371.

Eccles, J. C., Kostyuk, P. G., and Schmidt, R. F. (1962).
Central pathways responsible for depolarization of primary afferent fibres.
The Journal of Physiology, 161(2):237–257.

Edgerton, V. R., Courtine, G., Gerasimenko, Y. P., Lavrov, I., Ichiyama, R. M., Fong, A. J., Cai, L. L., Otoshi, C. K., Tillakaratne, N. J., Burdick, J. W., and Roy, R. R. (2008).
Training locomotor networks.
Brain research reviews, 57(1):241–54.

Edgerton, V. R., de Leon, R. D., Tillakaratne, N., Recktenwald, M. R., Hodgson, J. A., and Roy, R. R. (1997a).
Use-dependent plasticity in spinal stepping and standing.
Advances in neurology, 72:233–247.

Edgerton, V. R. and Gad, P. (2022).
Spinal automaticity of movement control and its role in recovering function after spinal injury.
Expert Review of Neurotherapeutics.

Edgerton, V. R., Grillner, S., Sjöström, A., and Zangger, P. (1976).
Central generation of locomotion in vertebrates.

In Herman, R. M., Grillner, S., Stein, P. S. G., and Stuart, D. G., editors, *Neural Control of Locomotion*, pages 439–464. Springer US, Boston, MA.

Edgerton, V. R. and Harkema, S. (2011).

Epidural stimulation of the spinal cord in spinal cord injury: Current status and future challenges.

Expert Review of Neurotherapeutics, 11(10):1351–1353.

Edgerton, V. R., Kim, S. J., Ichiyama, R. M., Gerasimenko, Y. P., and Roy, R. R. (2006).

Rehabilitative therapies after spinal cord injury.

Journal of neurotrauma, 23(3-4):560–570.

Edgerton, V. R., Leon, R. D., Harkema, S. J., Hodgson, J. A., London, N., Reinkensmeyer, D. J., Roy, R. R., Talmadge, R. J., Tillakaratne, N. J., Timoszyk, W., and Tobin, A. (2001a).

Retraining the injured spinal cord.

The Journal of physiology, 533(Pt 1):15–22.

Edgerton, V. R. and Roy, R. R. (2009a).

Activity-dependent plasticity of spinal locomotion: Implications for sensory processing.

Exercise and sport sciences reviews, 37(4):171–8.

Edgerton, V. R. and Roy, R. R. (2009b).

Robotic training and spinal cord plasticity.

Brain research bulletin, 78(1):4–12.

Edgerton, V. R. and Roy, R. R. (2010).

Spasticity: A switch from inhibition to excitation.

Nature Medicine, 16(3):270–271.

Edgerton, V. R. and Roy, R. R. (2012).

A new age for rehabilitation.

European journal of physical and rehabilitation medicine, 48(1):99–109.

Edgerton, V. R., Roy, R. R., and de Leon, R. D. (2001b).

Neural darwinism in the mammalian spinal cord.

In Patterson, M. M. and Grau, J. W., editors, *Spinal Cord Plasticity: Alterations in Reflex Function*, pages 185–206. Springer US, Boston, MA.

Edgerton, V. R., Roy, R. R., De Leon Niranjala Tillakaratne, R., and Hodgson, J. A. (1997b).

Does motor learning occur in the spinal cord?

The Neuroscientist, 3(5):287–294.

Edgerton, V. R., Roy, R. R., Hodgson, J. A., Prober, R. J., De Guzman, C. P., and De Leon, R. (1991).

A physiological basis for the development of rehabilitative strategies for spinally injured patients.

The Journal of The American Paraplegia Society, 14(4):150–157.

Edgerton, V. R., Tillakaratne, N. J., Bigbee, A. J., de Leon, R. D., and Roy, R. R. (2004).

Plasticity of the spinal neural circuitry after injury.

Annual review of neuroscience, 27:145–67.

Edgley, S. A. and Jankowska, E. (1987).

An interneuronal relay for group I and II muscle afferents in the midlumbar segments of the cat spinal cord.

The Journal of Physiology, 389(1):647–674.

Edlund, J. A. (2019).

Numerical Investigation of Spinal Neuron Facilitation with Multi-Electrode Epidural Stimulation.

Thesis, California Institute of Technology.

Eisdorfer, J. T., Smit, R. D., Keefe, K. M., Lemay, M. A., Smith, G. M., and Spence, A. J. (2020).
Epidural electrical stimulation: A review of plasticity mechanisms that are hypothesized to underlie enhanced recovery from spinal cord injury with stimulation.
Frontiers in molecular neuroscience, 13:163.

El-Nouby, A., Touvron, H., Caron, M., Bojanowski, P., Douze, M., Joulin, A., Laptev, I., Neverova, N., Synnaeve, G., Verbeek, J., and Jegou, H. (2021).
XCiT: Cross-covariance image transformers.

Eldele, E., Ragab, M., Chen, Z., Wu, M., Kwoh, C. K., Li, X., and Guan, C. (2021).
Time-series representation learning via temporal and contextual contrasting.
In *Proceedings of the Thirtieth International Joint Conference on Artificial Intelligence, IJCAI-21*, pages 2352–2359.

Endo, M., Nerrise, F., Zhao, Q., Sullivan, E. V., Fei-Fei, L., Henderson, V. W., Pohl, K. M., Poston, K. L., and Adeli, E. (2024).
Data-driven discovery of movement-linked heterogeneity in neurodegenerative diseases.
Nature Machine Intelligence, 6(9):1034–1045.

Escobar-Juárez, E., Schillaci, G., Hermosillo-Valadez, J., and Lara-Guzmán, B. (2016).
A self-organized internal models architecture for coding Sensory–Motor schemes.
Frontiers in Robotics and AI, 3.

Esfandiari, N., Babavalian, M. R., Moghadam, A.-M. E., and Tabar, V. K. (2014).
Review: Knowledge discovery in medicine: Current issue and future trend.
Expert Systems With Applications, 41(9):4434–4463.

Etlin, A., Blivis, D., Ben-Zwi, M., and Lev-Tov, A. (2010).

Long and short multifunicular projections of sacral neurons are activated by sensory input to produce locomotor activity in the absence of supraspinal control.

The Journal of neuroscience : the official journal of the Society for Neuroscience, 30(31):10324–36.

Fahr, P., Buchanan, J., and Wordsworth, S. (2019).

A Review of the Challenges of Using Biomedical Big Data for Economic Evaluations of Precision Medicine.

Applied Health Economics and Health Policy, 17(4):443–452.

Farooqui, A. A. (2010).

Neurochemical Aspects of Neurotraumatic and Neurodegenerative Diseases.

Springer Science & Business Media.

Fawaz, H. I., Forestier, G., Weber, J., Idoumghar, L., and Muller, P.-A. (2018).

Transfer learning for time series classification.

In *2018 IEEE International Conference on Big Data (Big Data)*, pages 1367–1376.

Fawcett, J. W., Curt, A., Steeves, J. D., Coleman, W. P., Tuszynski, M. H., Lammertse, D., Bartlett, P. F., Blight, A. R., Dietz, V., Ditunno, J., Dobkin, B. H., Havton, L. A., Ellaway, P. H., Fehlings, M. G., Privat, A., Grossman, R., Guest, J. D., Kleitman, N., Nakamura, M., Gaviria, M., and Short, D. (2007).

Guidelines for the conduct of clinical trials for spinal cord injury as developed by the ICCP panel: Spontaneous recovery after spinal cord injury and statistical power needed for therapeutic clinical trials.

Spinal cord : the official journal of the International Medical Society of Paraplegia, 45(3):190–205.

Federico, P. and Perez, M. A. (2017).

Altered corticospinal function during movement preparation in humans with spinal cord injury.

The Journal of physiology, 595(1):233–245.

Feldman, A. G., Levin, M. F., Garofolini, A., Piscitelli, D., and Zhang, L. (2021).

Central pattern generator and human locomotion in the context of referent control of motor actions.

Clinical Neurophysiology, 132(11):2870–2889.

Feng, J. (2001).

Is the integrate-and-fire model good enough?–a review.

Neural Networks: The Official Journal of the International Neural Network Society, 14(6-7):955–975.

Feraboli-Lohnherr, D., Barthe, J. Y., and Orsal, D. (1999).

Serotonin-induced activation of the network for locomotion in adult spinal rats.

Journal of neuroscience research, 55(1):87–98.

Feraboli-Lohnherr, D., Orsal, D., Yakovleff, A., Gimenez Y Ribotta, M., and Privat, A. (1997).

Recovery of locomotor activity in the adult chronic spinal rat after sublesional transplantation of embryonic nervous cells: Specific role of serotonergic neurons.

Experimental Brain Research, 113(3):443–454.

Fidelin, K., Djenoune, L., Stokes, C., Prendergast, A., Gomez, J., Baradel, A., Del Bene, F., and Wyart, C. (2015).

State-Dependent Modulation of Locomotion by GABAergic Spinal Sensory Neurons.

Current biology : CB, 25(23):3035–3047.

Filli, L., Engmann, A. K., Zorner, B., Weinmann, O., Moraitis, T., Gullo, M., Kasper, H., Schneider, R., and Schwab, M. E. (2014).

Bridging the gap: A reticulo-propriospinal detour bypassing an incomplete spinal cord injury.

Journal of Neuroscience, 34(40):13399–13410.

Fink, A. J. P., Croce, K. R., Huang, Z. J., Abbott, L. F., Jessell, T. M., and Azim, E. (2014).

Presynaptic inhibition of spinal sensory feedback ensures smooth movement.

Nature, 509(7498):43–48.

Flash, T. and Hochner, B. (2005).

Motor primitives in vertebrates and invertebrates.

Current opinion in neurobiology, 15(6):660–6.

Flynn, J., Conn, V., Boyle, K., Hughes, D., Watanabe, M., Velasquez, T., Goulding, M., Callister, R., and Graham, B. (2017).

Anatomical and molecular properties of long descending propriospinal neurons in mice.

Frontiers in Neuroanatomy, 11(5).

Flynn, J. R., Graham, B. A., Galea, M. P., and Callister, R. J. (2011).

The role of propriospinal interneurons in recovery from spinal cord injury.

Neuropharmacology, 60(5):809–822.

Fong, A. J., Cai, L. L., Otoshi, C. K., Reinkensmeyer, D. J., Burdick, J. W., Roy, R. R., and Edgerton, V. R. (2005).

Spinal cord-transected mice learn to step in response to quipazine treatment and robotic training.

The Journal of neuroscience : the official journal of the Society for Neuroscience, 25(50):11738–47.

Formento, E., Minassian, K., Wagner, F., Mignardot, J. B., Le Goff-Mignardot, C. G., Rowald, A., Bloch, J., Micera, S., Capogrosso, M., and Courtine, G. (2018).

Electrical spinal cord stimulation must preserve proprioception to enable locomotion in humans with spinal cord injury.

Nature Neuroscience, 21(12):1728–1741.

Forssberg, H. (1979).

Stumbling corrective reaction: A phase-dependent compensatory reaction during locomotion.

Journal of Neurophysiology, 42(4):936–953.

Forssberg, H., Grillner, S., and Halbertsma, J. (1980a).

The locomotion of the low spinal cat I. Coordination within a hindlimb.

Acta Physiologica Scandinavica, 108(3):269–281.

Forssberg, H., Grillner, S., Halbertsma, J., and Rossignol, S. (1980b).

The locomotion of the low spinal cat. II. Interlimb coordination.

Acta Physiologica Scandinavica, 108(3):283–295.

Forssberg, H., Grillner, S., and Rossignol, S. (1975).

Phase dependent reflex reversal during walking in chronic spinal cats.

Brain Research, 85(1):103–107.

Fouad, K., Rank, M. M., Vavrek, R., Murray, K. C., Sanelli, L., and Bennett, D. J. (2010).

Locomotion after spinal cord injury depends on constitutive activity in serotonin receptors.

Journal of Neurophysiology, 104(6):2975–2984.

Freyvert, Y., Yong, N. A., Morikawa, E., Zdunowski, S., Sarino, M. E., Gerasimenko, Y., Edgerton, V. R., and Lu, D. C. (2018).

Engaging cervical spinal circuitry with non-invasive spinal stimulation and buspirone to restore hand function in chronic motor complete patients.

Scientific Reports, 8(1).

Froemke, R. C. and Dan, Y. (2002).

Spike-timing-dependent synaptic modification induced by natural spike trains.

Nature, 416(6879):433–438.

Fu, X. and Guan, C. (2023).

Gait Pattern Recognition Based on Supervised Contrastive Learning Between EEG and EMG.

In *2023 45th Annual International Conference of the IEEE Engineering in Medicine & Biology Society (EMBC)*, pages 1–4.

Fung, J., Stewart, J. E., and Barbeau, H. (1990).

The combined effects of clonidine and cyproheptadine with interactive training on the modulation of locomotion in spinal cord injured subjects.

Journal of the neurological sciences, 100(1-2):85–93.

Gackière, F. and Vinay, L. (2014).

Serotonergic modulation of post-synaptic inhibition and locomotor alternating pattern in the spinal cord.

Frontiers in Neural Circuits, 8(102).

Gad, P., Choe, J., Nandra, M. S., Zhong, H., Roy, R. R., Tai, Y.-C., and Edgerton, V. R. (2013a).

Development of a multi-electrode array for spinal cord epidural stimulation to facilitate stepping and standing after a complete spinal cord injury in adult rats.

Journal of NeuroEngineering and Rehabilitation, 10(1):2.

Gad, P., Choe, J., Shah, P., Garcia-Alias, G., Rath, M., Gerasimenko, Y., Zhong, H., Roy, R. R., and Edgerton, V. R. (2013b).

Sub-threshold spinal cord stimulation facilitates spontaneous motor activity in spinal rats.

Journal of NeuroEngineering and Rehabilitation, 10:108–108.

Gad, P., Gerasimenko, Y., Zdunowski, S., Turner, A., Sayenko, D., Lu, D. C., and Edgerton, V. R. (2017).

Weight bearing over-ground stepping in an exoskeleton with non-invasive spinal cord neuromodulation after motor complete paraplegia.

Frontiers in Neuroscience, 11.

Gad, P., Kreydin, E., Zhong, H., and Edgerton, V. R. (2020).

Enabling respiratory control after severe chronic tetraplegia: An exploratory case study.

Journal of Neurophysiology, 124(3):774–780.

Gad, P., Lavrov, I., Shah, P., Zhong, H., Roy, R. R., Edgerton, V. R., and Gerasimenko, Y. (2013c).

Neuromodulation of motor-evoked potentials during stepping in spinal rats.

Journal of neurophysiology, 110(6):1311–22.

Gad, P., Lee, S., Terrafranca, N., Zhong, H., Turner, A., Gerasimenko, Y., and Edgerton, V. R. (2018).

Noninvasive activation of cervical spinal networks after severe paralysis.

Journal of Neurotrauma.

Gad, P., Roy, R. R., Choe, J., Creagmile, J., Zhong, H., Gerasimenko, Y., and Edgerton, V. R. (2015).

Electrophysiological biomarkers of neuromodulatory strategies to recover motor function after spinal cord injury.

Journal of neurophysiology, 113(9):3386–96.

Ganapathy, M. K., Reddy, V., and Tadi, P. (2021).
Neuroanatomy, spinal cord morphology.
In *StatPearls*. StatPearls Publishing Copyright © 2021, StatPearls Publishing LLC., Treasure Island (FL).

Ganapathy, N., Swaminathan, R., and Deserno, T. M. (2018).
Deep Learning on 1-D Biosignals: A Taxonomy-based Survey.
Yearbook of Medical Informatics, 27(1):98–109.

Ganea, K., Liebl, C., Sterlemann, V., Müller, M. B., and Schmidt, M. V. (2007).
Pharmacological validation of a novel home cage activity counter in mice.
Journal of Neuroscience Methods, 162(1):180–186.

Ganin, Y., Ustinova, E., Ajakan, H., Germain, P., Larochelle, H., Laviolette, F., Marchand, M., and Lempitsky, V. (2016).
Domain-adversarial training of neural networks.

Garro, F., Chiappalone, M., Buccelli, S., De Michieli, L., and Semprini, M. (2021).
Neuromechanical Biomarkers for Robotic Neurorehabilitation.
Frontiers in Neurorobotics, 15:742163.

Genewsky, A., Heinz, D. E., Kaplick, P. M., Kilonzo, K., and Wotjak, C. T. (2017).
A simplified microwave-based motion detector for home cage activity monitoring in mice.
Journal of Biological Engineering, 11(1):36.

Gérardin, C., Wajsbürt, P., Vaillant, P., Bellamine, A., Carrat, F., and Tannier, X. (2022).
Multilabel classification of medical concepts for patient clinical profile identification.
Artificial Intelligence in Medicine, 128:102311.

Gerasimenko, Y., Gad, P., Sayenko, D., McKinney, Z., Gorodnichev, R., Puhov, A., Moshonkina, T., Savochin, A., Selionov, V., Shigueva, T., Tomilovskaya, E., Kozlovskaya, I., and Edgerton, V. R. (2016a).

Integration of sensory, spinal, and volitional descending inputs in regulation of human locomotion.

Journal of neurophysiology, 116(1):98–105.

Gerasimenko, Y., Gorodnichev, R., Moshonkina, T., Sayenko, D., Gad, P., and Reggie Edgerton, V. (2015a).

Transcutaneous electrical spinal-cord stimulation in humans.

Annals of physical and rehabilitation medicine, 58(4):225–231.

Gerasimenko, Y., Gorodnichev, R., Puhov, A., Moshonkina, T., Savochin, A., Selionov, V., Roy, R. R., Lu, D. C., and Edgerton, V. R. (2015b).

Initiation and modulation of locomotor circuitry output with multisite transcutaneous electrical stimulation of the spinal cord in noninjured humans.

Journal of neurophysiology, 113(3):834–42.

Gerasimenko, Y., Kozlovskaya, I., and Edgerton, V. R. (2016b).

Sensorimotor regulation of movements: Novel strategies for the recovery of mobility.

Human Physiology, 42(1):90–102.

Gerasimenko, Y., Musienko, P., Bogacheva, I., Moshonkina, T., Savochin, A., Lavrov, I., Roy, R. R., and Edgerton, V. R. (2009).

Propriospinal bypass of the serotonergic system that can facilitate stepping.

The Journal of neuroscience : the official journal of the Society for Neuroscience, 29(17):5681–9.

Gerasimenko, Y., Preston, C., Zhong, H., Roy, R. R., Edgerton, V. R., and Shah, P. K. (2019).

Rostral lumbar segments are the key controllers of hindlimb locomotor rhythmicity in the adult spinal rat.

Journal of Neurophysiology, 122(2):585–600.

Gerasimenko, Y., Roy, R. R., and Edgerton, V. R. (2008).

Epidural stimulation: Comparison of the spinal circuits that generate and control locomotion in rats, cats and humans.

Experimental neurology, 209(2):417–25.

Gerasimenko, Y., Sayenko, D., Gad, P., Kozesnik, J., Moshonkina, T., Grishin, A., Pukhov, A., Moiseev, S., Gorodnichev, R., Selionov, V., Kozlovskaya, I., and Edgerton, V. R. (2018).

Electrical spinal stimulation, and imagining of lower limb movements to modulate brain-spinal connectomes that control locomotor-like behavior.

Frontiers in physiology, 9:1196.

Gerasimenko, Y., Sayenko, D., Gad, P., Liu, C. T., Tillakaratne, N. J. K., Roy, R. R., Kozlovskaya, I., and Edgerton, V. R. (2017).

Feed-forwardness of spinal networks in posture and locomotion.

The Neuroscientist : a review journal bringing neurobiology, neurology and psychiatry, 23(5):441–453.

Gerasimenko, Y. P., Ichiyama, R. M., Lavrov, I. A., Courtine, G., Cai, L., Zhong, H., Roy, R. R., and Edgerton, V. R. (2007).

Epidural spinal cord stimulation plus quipazine administration enable stepping in complete spinal adult rats.

Journal of neurophysiology, 98(5):2525–36.

Gerasimenko, Y. P., Lavrov, I. A., Courtine, G., Ichiyama, R. M., Dy, C. J., Zhong, H., Roy, R. R., and Edgerton, V. R. (2006).

Spinal cord reflexes induced by epidural spinal cord stimulation in normal awake rats. *Journal of neuroscience methods*, 157(2):253–63.

Gerasimenko, Y. P., Lu, D. C., Modaber, M., Zdunowski, S., Gad, P., Sayenko, D. G., Morikawa, E., Haakana, P., Ferguson, A. R., Roy, R. R., and Edgerton, V. R. (2015c). Noninvasive reactivation of motor descending control after paralysis. *Journal of neurotrauma*, 32(24):1968–80.

Ghosh, M. and Pearse, D. D. (2014). The role of the serotonergic system in locomotor recovery after spinal cord injury. *Frontiers in neural circuits*, 8:151.

Ghosh, S. K. (2020). Camillo Golgi (1843 –1926): Scientist extraordinaire and pioneer figure of modern neurology. *Anatomy & Cell Biology*, 53(4):385–392.

Giboin, L.-S., Tokuno, C., Kramer, A., Henry, M., and Gruber, M. (2020). Motor learning induces time-dependent plasticity that is observable at the spinal cord level. *The Journal of Physiology*, 598(10):1943–1963.

Gill, M., Linde, M., Fautsch, K., Hale, R., Lopez, C., Veith, D., Calvert, J., Beck, L., Garlanger, K., Edgerton, R., Sayenko, D., Lavrov, I., Thoreson, A., Grahn, P., and Zhao, K. (2020a). Epidural electrical stimulation of the lumbosacral spinal cord improves trunk stability during seated reaching in two humans with severe thoracic spinal cord injury. *Frontiers in systems neuroscience*, 14:79.

Gill, M. L., Grahn, P. J., Calvert, J. S., Linde, M. B., Lavrov, I. A., Strommen, J. A., Beck, L. A., Sayenko, D. G., Van Straaten, M. G., Drubach, D. I., Veith, D. D., Thoreson, A. R., Lopez, C., Gerasimenko, Y. P., Edgerton, V. R., Lee, K. H., and Zhao, K. D. (2018).
Neuromodulation of lumbosacral spinal networks enables independent stepping after complete paraplegia.
Nature medicine, 24(11):1677–1682.

Gill, M. L., Linde, M. B., Hale, R. F., Lopez, C., Fautsch, K. J., Calvert, J. S., Veith, D. D., Beck, L. A., Garlanger, K. L., Sayenko, D. G., Lavrov, I. A., Thoreson, A. R., Grahn, P. J., and Zhao, K. D. (2020b).
Alterations of spinal epidural stimulation-enabled stepping by descending intentional motor commands and proprioceptive inputs in humans with spinal cord injury.
Frontiers in systems neuroscience, 14:590231.

Giszter, S. F. (2015).
Motor primitives–new data and future questions.
Current opinion in neurobiology, 33:156–165.

Giszter, S. F. and Hart, C. B. (2013).
Motor primitives and synergies in the spinal cord and after injury–the current state of play.
Annals of the New York Academy of Sciences, 1279:114–26.

GlobalData (2023).
Wearable Tech – Thematic Research.
https://www.globaldata.com/store/report/wearable-tech-theme-analysis/.

Goetz, C., Pivetta, C., and Arber, S. (2015).
Distinct limb and trunk premotor circuits establish laterality in the spinal cord.
Neuron, 85(1):131–144.

Goldberger, A. L., Amaral, L. A. N., Glass, L., Hausdorff, J. M., Ivanov, P. Ch., Mark, R. G., Mietus, J. E., Moody, G. B., Peng, C.-K., and Stanley, H. E. (2000).
PhysioBank, PhysioToolkit, and PhysioNet: Components of a new research resource for complex physiologic signals.
Circulation, 101(23):e215–e220.

Goldshmit, Y., Lythgo, N., Galea, M. P., and Turnley, A. M. (2008).
Treadmill training after spinal cord hemisection in mice promotes axonal sprouting and synapse formation and improves motor recovery.
Journal of neurotrauma, 25(5):449–65.

Gong, C., Zheng, X., Guo, F., Wang, Y., Zhang, S., Chen, J., Sun, X., Shah, S. Z. A., Zheng, Y., Li, X., Yin, Y., Li, Q., Huang, X., Guo, T., Han, X., Zhang, S.-C., Wang, W., and Chen, H. (2021).
Human spinal GABA neurons alleviate spasticity and improve locomotion in rats with spinal cord injury.
Cell Reports, 34(12):108889.

Gossard, J. P., Brownstone, R. M., Barajon, I., and Hultborn, H. (1994).
Transmission in a locomotor-related group Ib pathway from hindlimb extensor muscles in the cat.
Experimental Brain Research, 98(2).

Goulding, M. (2009).
Circuits controlling vertebrate locomotion: Moving in a new direction.
Nature Reviews Neuroscience, 10(7):507–518.

Goulding, M., Bourane, S., Garcia-Campmany, L., Dalet, A., and Koch, S. (2014).
Inhibition downunder: An update from the spinal cord.
Current Opinion in Neurobiology, 26:161–166.

Gradwell, M. A., Ozeri-Engelhard, N., Eisdorfer, J. T., Laflamme, O. D., Gonzalez, M., Upadhyay, A., Aoki, A., Shrier, T., Gandhi, M., Abbas-Zadeh, G., Oputa, O., Thackray, J. K., Ricci, M., Yusuf, N., Keating, J., Imtiaz, Z., Alomary, S. A., Katz, J., Haas, M., Hernandez, Y., Akay, T., and Abraira, V. (2023).

Multimodal sensory control of motor performance by glycinergic interneurons of the spinal cord deep dorsal horn.

bioRxiv : the preprint server for biology.

Grau, J. W. (2014).

Learning from the spinal cord: How the study of spinal cord plasticity informs our view of learning.

Neurobiology of learning and memory, 108:155–71.

Greene, B. R., McGrath, D., O'Neill, R., O'Donovan, K. J., Burns, A., and Caulfield, B. (2010).

An adaptive gyroscope-based algorithm for temporal gait analysis.

Medical & Biological Engineering & Computing, 48(12):1251–1260.

Greiner, N., Barra, B., Schiavone, G., Lorach, H., James, N., Conti, S., Kaeser, M., Fallegger, F., Borgognon, S., Lacour, S., Bloch, J., Courtine, G., and Capogrosso, M. (2021).

Recruitment of upper-limb motoneurons with epidural electrical stimulation of the cervical spinal cord.

Nature communications, 12(1):435.

Grider, M. H., Jessu, R., and Kabir, R. (2024).

Physiology, Action Potential.

In *StatPearls*. StatPearls Publishing, Treasure Island (FL).

Griener, A., Zhang, W., Kao, H., Haque, F., and Gosgnach, S. (2017).

Anatomical and electrophysiological characterization of a population of dI6 interneurons in the neonatal mouse spinal cord.

Neuroscience, 362:47–59.

Griener, A., Zhang, W., Kao, H., Wagner, C., and Gosgnach, S. (2015).

Probing diversity within subpopulations of locomotor-related V0 interneurons.

Developmental Neurobiology, 75(11):1189–1203.

Grillner, S. (2011).

Control of locomotion in bipeds, tetrapods, and fish.

Comprehensive Physiology.

Grillner, S. (2021).

The execution of movement: A spinal affair.

Journal of Neurophysiology, 125(2):693–698.

Grillner, S. and Dubuc, R. (1988).

Control of locomotion in vertebrates: Spinal and supraspinal mechanisms.

Advances in neurology, 47:425–53.

Grillner, S. and El Manira, A. (2020).

Current principles of motor control, with special reference to vertebrate locomotion.

Physiological reviews, 100(1):271–320.

Grillner, S. and Rossignol, S. (1978).

On the initiation of the swing phase of locomotion in chronic spinal cats.

Brain Research, 146(2):269–277.

Grillner, S. and Zangger, P. (1975).

How detailed is the central pattern generation for locomotion?

Brain Research, 88(2):367–371.

Grillner, S. and Zangger, P. (1979).

On the central generation of locomotion in the low spinal cat.

Experimental Brain Research, 34(2).

Gross, M. K., Dottori, M., and Goulding, M. (2002).

Lbx1 specifies somatosensory association interneurons in the dorsal spinal cord.

Neuron, 34(4):535–549.

Grossmann, K. S., Giraudin, A., Britz, O., Zhang, J., and Goulding, M. (2010).

Genetic dissection of rhythmic motor networks in mice.

In *Breathe, Walk and Chew: The Neural Challenge: Part I*, volume 187 of *Progress in Brain Research*, pages 19–37. Elsevier.

Guan, Y., Bradley, K., Parker, J. L., Krames, E. S., and Linderoth, B. (2018).

Chapter 15 - spinal cord stimulation: Mechanisms of action.

In Krames, E. S., Peckham, P. H., and Rezai, A. R., editors, *Neuromodulation (Second Edition)*, pages 161–178. Academic Press.

Guertin, P., Angel, M. J., Perreault, M. C., and McCrea, D. A. (1995).

Ankle extensor group I afferents excite extensors throughout the hindlimb during fictive locomotion in the cat.

The Journal of Physiology, 487(1):197–209.

Guiho, T., Baker, S. N., and Jackson, A. (2021).

Epidural and transcutaneous spinal cord stimulation facilitates descending inputs to upper-limb motoneurons in monkeys.

Journal of Neural Engineering, 18(4):046011.

Hagglund, M., Dougherty, K. J., Borgius, L., Itohara, S., Iwasato, T., and Kiehn, O. (2013).

Optogenetic dissection reveals multiple rhythmogenic modules underlying locomotion.

Proceedings of the National Academy of Sciences of the United States of America, 110(28):11589–94.

Han, C. E., Arbib, M. A., and Schweighofer, N. (2008).
Stroke rehabilitation reaches a threshold.
PLoS computational biology, 4(8):e1000133.

HaoChen, J. Z., Wei, C., Gaidon, A., and Ma, T. (2022).
Provable guarantees for self-supervised deep learning with spectral contrastive loss.

Haque, F., Rancic, V., Zhang, W., Clugston, R., Ballanyi, K., and Gosgnach, S. (2018).
WT1-Expressing interneurons regulate Left–Right alternation during mammalian locomotor activity.
The Journal of Neuroscience, 38(25):5666–5676.

Harbeau, H., Fung, J., Leroux, A., and Ladouceur, M. (2002).
Chapter 2 A review of the adaptability and recovery of locomotion after spinal cord injury.
In McKerracher, L., Doucet, G., and Rossignol, S., editors, *Progress in Brain Research*, volume 137, pages 9–25. Elsevier.

Harkema, S., Gerasimenko, Y., Hodes, J., Burdick, J., Angeli, C., Chen, Y., Ferreira, C., Willhite, A., Rejc, E., Grossman, R. G., and Edgerton, V. R. (2011).
Effect of epidural stimulation of the lumbosacral spinal cord on voluntary movement, standing, and assisted stepping after motor complete paraplegia: A case study.
The Lancet, 377(9781):1938–1947.

Harnie, J., Doelman, A., de Vette, E., Audet, J., Desrochers, E., Gaudreault, N., and Frigon, A. (2019).
The recovery of standing and locomotion after spinal cord injury does not require task-specific training.

Elife, 8.

Harrow-Mortelliti, M., Reddy, V., and Jimsheleishvili, G. (2021).

Physiology, spinal cord.

In *StatPearls*. StatPearls Publishing Copyright © 2021, StatPearls Publishing LLC., Treasure Island (FL).

Hart, B. L. (1971).

Facilitation by strychnine of reflex walking in spinal dogs.

Physiology & Behavior, 6(5):627–628.

Hart, C. B. and Giszter, S. F. (2010).

A neural basis for motor primitives in the spinal cord.

The Journal of neuroscience : the official journal of the Society for Neuroscience, 30(4):1322–36.

Harvey, L. A. (2016).

Physiotherapy rehabilitation for people with spinal cord injuries.

Journal of Physiotherapy, 62(1):4–11.

Hayashi, T., Kato, Y., and Nozaki, D. (2020).

Divisively normalized integration of multisensory error information develops motor memories specific to vision and proprioception.

The Journal of neuroscience : the official journal of the Society for Neuroscience, 40(7):1560–1570.

He, K., Zhang, X., Ren, S., and Sun, J. (2015).

Deep residual learning for image recognition.

Heald, E., Hart, R., Kilgore, K., and Peckham, P. H. (2017).

Characterization of volitional electromyographic signals in the lower extremity after motor complete spinal cord injury.
Neurorehabilitation and neural repair, 31(6):583–591.

Hebb, D. O. (2005).
The Organization of Behavior: A Neuropsychological Theory.
Psychology press.

Heckman, C. J. and Enoka, R. M. (2012).
Motor unit.
Comprehensive Physiology.

Heesoo, S., Sangseok, L., and Sael, L. (2022).
Cross-Attention Model for Multi-modal Bio-Signal Processing.
In *2022 IEEE International Conference on Big Data and Smart Computing (BigComp)*, pages 43–46.

Heng, C. and de Leon, R. D. (2007).
The rodent lumbar spinal cord learns to correct errors in hindlimb coordination caused by viscous force perturbations during stepping.
The Journal of neuroscience : the official journal of the Society for Neuroscience, 27(32):8558–62.

Heng, C. and de Leon, R. D. (2009).
Treadmill training enhances the recovery of normal stepping patterns in spinal cord contused rats.
Experimental neurology, 216(1):139–147.

Hennig, J. A., Golub, M. D., Lund, P. J., Sadtler, P. T., Oby, E. R., Quick, K. M., Ryu, S. I., Tyler-Kabara, E. C., Batista, A. P., Yu, B. M., and Chase, S. M. (2018).

Constraints on neural redundancy.

eLife, 7.

Herrity, A. N., Williams, C. S., Angeli, C. A., Harkema, S. J., and Hubscher, C. H. (2018).

Lumbosacral spinal cord epidural stimulation improves voiding function after human spinal cord injury.

Scientific reports, 8(1):8688.

Hicks, A. L. and Ginis, K. A. M. (2008).

Treadmill training after spinal cord injury: It's not just about the walking.

Journal of Rehabilitation Research and Development, 45(2):241–248.

Hochman, S. (2007).

Spinal cord.

Current Biology, 17(22):R950–R955.

Hochman, S., Shreckengost, J., Kimura, H., and Quevedo, J. (2010).

Presynaptic inhibition of primary afferents by depolarization: Observations supporting nontraditional mechanisms.

Annals of the New York Academy of Sciences, 1198(1):140–152.

Hodgkin, A. L. and Huxley, A. F. (1952).

Currents carried by sodium and potassium ions through the membrane of the giant axon of Loligo.

The Journal of Physiology, 116(4):449–472.

Hodgson, J. A., Roy, R. R., Leon, R. D., Dobkin, B., and Edgerton, V. R. (1994).

Can the mammalian lumbar spinal cord learn a motor task?

Medicine & Science in Sports & Exercise, 26(12).

Hofer, A. S. and Schwab, M. E. (2019).

Enhancing rehabilitation and functional recovery after brain and spinal cord trauma with electrical neuromodulation.

Current opinion in neurology, 32(6):828–835.

Hofstoetter, U. S., Freundl, B., Binder, H., and Minassian, K. (2018).

Common neural structures activated by epidural and transcutaneous lumbar spinal cord stimulation: Elicitation of posterior root-muscle reflexes.

PLOS ONE, 13(1):e0192013.

Hole, K. J. and Ahmad, S. (2021).

A thousand brains: Toward biologically constrained AI.

SN Applied Sciences, 3(8):743.

Hoo, Z. H., Candlish, J., and Teare, D. (2017).

What is an ROC curve?

Emergency Medicine Journal, 34(6):357–359.

Hornung, J.-P. (2003).

The human raphe nuclei and the serotonergic system.

Journal of Chemical Neuroanatomy, 26(4):331–343.

Hosna, A., Merry, E., Gyalmo, J., Alom, Z., Aung, Z., and Azim, M. A. (2022).

Transfer learning: A friendly introduction.

Journal of Big Data, 9(1).

Hosseini, E. A., Nguyen, K. P., and Joiner, W. M. (2017).

The decay of motor adaptation to novel movement dynamics reveals an asymmetry in the stability of motion state-dependent learning.

PLoS computational biology, 13(5):e1005492.

Hounsgaard, J., Hultborn, H., Jespersen, B., and Kiehn, O. (1988).

Bistability of alpha-motoneurones in the decerebrate cat and in the acute spinal cat after intravenous 5-hydroxytryptophan.
The Journal of Physiology, 405(1):345–367.

Hsieh, F. H. and Giszter, S. F. (2011).
Robot-driven spinal epidural stimulation compared with conventional stimulation in adult spinalized rats.
In *2011 Annual International Conference of the IEEE Engineering in Medicine and Biology Society*. IEEE.

Hu, C., Ju, R., Shen, Y., Zhou, P., and Li, Q. (2016).
Clinical decision support for Alzheimer's disease based on deep learning and brain network.
In *2016 IEEE International Conference on Communications (ICC)*, pages 1–6.

Huang, D. and Chen, B. (2019).
Surface EMG Decoding for Hand Gestures Based on Spectrogram and CNN-LSTM.
In *2019 2nd China Symposium on Cognitive Computing and Hybrid Intelligence (CCHI)*, pages 123–126.

Huang, H., Kuiken, T. A., and Lipschutz, R. D. (2009).
A strategy for identifying locomotion modes using surface electromyography.
IEEE transactions on bio-medical engineering, 56(1):65–73.

Hubli, M. and Dietz, V. (2013).
The physiological basis of neurorehabilitation - locomotor training after spinal cord injury.
Journal of NeuroEngineering and Rehabilitation, 10(1):5.

Hultborn, H., Denton, M. E., Wienecke, J., and Nielsen, J. B. (2003).

Variable amplification of synaptic input to cat spinal motoneurones by dendritic persistent inward current.

The Journal of Physiology, 552(3):945–952.

Hultborn, H., Jankowska, E., and Lindström, S. (1971a).

Recurrent inhibition of interneurones monosynaptically activated from group Ia afferents.

The Journal of Physiology, 215(3):613–636.

Hultborn, H., Jankowska, E., Lindström, S., and Roberts, W. (1971b).

Neuronal pathway of the recurrent facilitation of motoneurones.

The Journal of Physiology, 218(2):495–514.

Hultborn, H., Meunier, S., Pierrot-Deseilligny, E., and Shindo, M. (1987).

Changes in presynaptic inhibition of Ia fibres at the onset of voluntary contraction in man.

The Journal of Physiology, 389(1):757–772.

Husch, A., Dietz, S. B., Hong, D. N., and Harris-Warrick, R. M. (2014).

Adult spinal V2a interneurons show increased excitability and serotonin-dependent bistability.

Journal of Neurophysiology, 113(4):1124–1134.

Husch, A., Van Patten, G. N., Hong, D. N., Scaperotti, M. M., Cramer, N., and Harris-Warrick, R. M. (2012).

Spinal cord injury induces serotonin supersensitivity without increasing intrinsic excitability of mouse V2a interneurons.

Journal of Neuroscience, 32(38):13145–13154.

Ichiyama, R. M., Courtine, G., Gerasimenko, Y. P., Yang, G. J., van den Brand, R., Lavrov, I. A., Zhong, H., Roy, R. R., and Edgerton, V. R. (2008a).

Step training reinforces specific spinal locomotor circuitry in adult spinal rats.
The Journal of neuroscience : the official journal of the Society for Neuroscience, 28(29):7370–5.

Ichiyama, R. M., Gerasimenko, Y., Jindrich, D. L., Zhong, H., Roy, R. R., and Edgerton, V. R. (2008b).
Dose dependence of the 5-HT agonist quipazine in facilitating spinal stepping in the rat with epidural stimulation.
Neuroscience letters, 438(3):281–285.

Ichiyama, R. M., Gerasimenko, Y. P., Zhong, H., Roy, R. R., and Edgerton, V. R. (2005).
Hindlimb stepping movements in complete spinal rats induced by epidural spinal cord stimulation.
Neuroscience letters, 383(3):339–44.

Idri, A., Benhar, H., Fernández-Alemán, J. L., and Kadi, I. (2018).
A systematic map of medical data preprocessing in knowledge discovery.
Computer Methods and Programs in Biomedicine, 162:69–85.

Inanici, F., Brighton, L. N., Samejima, S., Hofstetter, C. P., and Moritz, C. T. (2021).
Transcutaneous spinal cord stimulation restores hand and arm function after spinal cord injury.
IEEE Transactions on Neural Systems and Rehabilitation Engineering, 29:310–319.

Inanici, F., Samejima, S., Gad, P., Edgerton, V. R., Hofstetter, C. P., and Moritz, C. T. (2018).
Transcutaneous electrical spinal stimulation promotes long-term recovery of upper extremity function in chronic tetraplegia.
IEEE Transactions on Neural Systems and Rehabilitation Engineering, 26(6):1272–1278.

Ismail Fawaz, H., Forestier, G., Weber, J., Idoumghar, L., and Muller, P.-A. (2019).
Deep learning for time series classification: A review.
Data Mining and Knowledge Discovery, 33(4):917–963.

Ismail Fawaz, H., Lucas, B., Forestier, G., Pelletier, C., Schmidt, D. F., Weber, J., Webb, G. I., Idoumghar, L., Muller, P.-A., and Petitjean, F. (2020).
InceptionTime: Finding AlexNet for time series classification.
Data Mining and Knowledge Discovery, 34(6):1936–1962.

Issa, S. and Khaled, A. R. (2022).
Lower Limb Movement Recognition Using EMG Signals.
In Abraham, A., Gandhi, N., Hanne, T., Hong, T.-P., Nogueira Rios, T., and Ding, W., editors, *Intelligent Systems Design and Applications*, Lecture Notes in Networks and Systems, pages 336–345, Cham. Springer International Publishing.

Iwahara, T., Atsuta, Y., Garcia-Rill, E., and Skinner, R. D. (1992).
Spinal cord stimulation-induced locomotion in the adult cat.
Brain Research Bulletin, 28(1):99–105.

Iwana, B. K. and Uchida, S. (2021).
An empirical survey of data augmentation for time series classification with neural networks.
PLOS ONE, 16(7):e0254841.

Jacobs, B. L. and Fornal, C. A. (1993).
5-HT and motor control: A hypothesis.
Trends in Neurosciences, 16(9):346–352.

Jacobs, B. L., MartíN-Cora, F. J., and Fornal, C. A. (2002).
Activity of medullary serotonergic neurons in freely moving animals.

Brain Research Reviews, 40(1-3):45–52.

James, N. D., McMahon, S. B., Field-Fote, E. C., and Bradbury, E. J. (2018).
Neuromodulation in the restoration of function after spinal cord injury.
The Lancet Neurology, 17(10):905–917.

Jankowska, E. (1992).
Interneuronal relay in spinal pathways from proprioceptors.
Progress in Neurobiology, 38(4):335–378.

Jankowska, E. (2001).
Spinal interneuronal systems: Identification, multifunctional character and reconfigurations in mammals.
The Journal of Physiology, 533(1):31–40.

Jankowska, E. (2008).
Spinal interneuronal networks in the cat: Elementary components.
Brain Research Reviews, 57(1):46–55.

Jankowska, E. (2013a).
Spinal interneurons.
In *Neuroscience in the 21st Century: From Basic to Clinical*, pages 1063–1099. Springer New York.

Jankowska, E. (2013b).
Spinal reflexes.
In *Neuroscience in the 21st Century: From Basic to Clinical*, pages 1463–1484. Springer New York.

Jankowska, E., Bannatyne, B. A., Stecina, K., Hammar, I., Cabaj, A., and Maxwell, D. J. (2009).

Commissural interneurons with input from group I and II muscle afferents in feline lumbar segments: Neurotransmitters, projections and target cells.

The Journal of Physiology, 587(2):401–418.

Jankowska, E. and Edgley, S. A. (2010).

Functional subdivision of feline spinal interneurons in reflex pathways from group Ib and II muscle afferents; an update.

European Journal of Neuroscience, 32(6):881–893.

Jankowska, E., Jukes, M. G. M., Lund, S., and Lundberg, A. (1967).

The Effect of DOPA on the Spinal Cord 6. Half-centre organization of interneurones transmitting effects from the flexor reflex afferents.

Acta Physiologica Scandinavica, 70(3-4):389–402.

Jankowska, E., Lundberg, A., Roberts, W. J., and Stuart, D. (1974).

A long propriospinal system with direct effect on motoneurones and on interneurones in the cat lumbosacral cord.

Experimental Brain Research, 21(2).

Jankowska, E., McCrea, D., Rudomín, P., and Sykova, E. (1981).

Observations on neuronal pathways subserving primary afferent depolarization.

Journal of Neurophysiology, 46(3):506–516.

Jankowska, E. and McCrea, D. A. (1983).

Shared reflex pathways from Ib tendon organ afferents and Ia muscle spindle afferents in the cat.

The Journal of Physiology, 338(1):99–111.

Jankowska, E. and Puczynska, A. (2008).

Interneuronal activity in reflex pathways from group II muscle afferents is monitored by dorsal spinocerebellar tract neurons in the cat.

Journal of Neuroscience, 28(14):3615–3622.

Jasiewicz, J. M., Allum, J. H. J., Middleton, J. W., Barriskill, A., Condie, P., Purcell, B., and Li, R. C. T. (2006).
Gait event detection using linear accelerometers or angular velocity transducers in able-bodied and spinal-cord injured individuals.
Gait & Posture, 24(4):502–509.

Jayaraman, C., Mummidisetty, C. K., Mannix-Slobig, A., McGee Koch, L., and Jayaraman, A. (2018).
Variables influencing wearable sensor outcome estimates in individuals with stroke and incomplete spinal cord injury: A pilot investigation validating two research grade sensors.
Journal of NeuroEngineering and Rehabilitation, 15(1):19.

Jazayeri, S. B., Beygi, S., Shokraneh, F., Hagen, E. M., and Rahimi-Movaghar, V. (2015).
Incidence of traumatic spinal cord injury worldwide: A systematic review.
European spine journal : official publication of the European Spine Society, the European Spinal Deformity Society, and the European Section of the Cervical Spine Research Society, 24(5):905–18.

Jean-Francois, P., Hanne Borger, R., Rasmus Kordt, C., and Anders Victor, P. (2013).
Modulation of the intrinsic properties of motoneurons by serotonin.
Current Pharmaceutical Design, 19(24):4371–4384.

Jensen, M. P. and Brownstone, R. M. (2019).
Mechanisms of spinal cord stimulation for the treatment of pain: Still in the dark after 50 years.
European Journal of Pain, 23(4):652–659.

Jiang, N., Pradhan, A., and He, J. (2022).

Gesture Recognition and Biometrics ElectroMyogram (GRABMyo).

Jiang, Y. Q., Zaaimi, B., and Martin, J. H. (2016).

Competition with primary sensory afferents drives remodeling of corticospinal axons in mature spinal motor circuits.

Journal of Neuroscience, 36(1):193–203.

Jilge, B., Minassian, K., Rattay, F., Pinter, M. M., Gerstenbrand, F., Binder, H., and Dimitrijevic, M. R. (2004).

Initiating extension of the lower limbs in subjects with complete spinal cord injury by epidural lumbar cord stimulation.

Experimental brain research, 154(3):308–26.

Jin, B., Alam, M., Tierno, A., Zhong, H., Roy, R. R., Gerasimenko, Y., Lu, D. C., and Edgerton, V. R. (2021).

Serotonergic facilitation of forelimb functional recovery in rats with cervical spinal cord injury.

Neurotherapeutics : the journal of the American Society for Experimental NeuroTherapeutics.

Jo, H. J. and Perez, M. A. (2019).

Changes in motor-evoked potential latency during grasping after tetraplegia.

Journal of Neurophysiology, 122(4):1675–1684.

Jo, H. J. and Perez, M. A. (2020).

Corticospinal-motor neuronal plasticity promotes exercise-mediated recovery in humans with spinal cord injury.

Brain : a journal of neurology.

Johansson, D., Malmgren, K., and Alt Murphy, M. (2018).
Wearable sensors for clinical applications in epilepsy, Parkinson's disease, and stroke: A mixed-methods systematic review.
Journal of Neurology, 265(8):1740–1752.

Johnson, E. O., Babis, G. C., Soultanis, K. C., and Soucacos, P. N. (2008).
Functional neuroanatomy of proprioception.
Journal of Surgical Orthopaedic Advances, 17(3):159–164.

Johnson, K. T. and Picard, R. W. (2020).
Advancing Neuroscience through Wearable Devices.
Neuron, 108(1):8–12.

Joshi, D., Nakamura, B. H., and Hahn, M. E. (2015).
High energy spectrogram with integrated prior knowledge for EMG-based locomotion classification.
Medical Engineering & Physics, 37(5):518–524.

Kachuee, M., Hoffman, H., D. Moore, L., Damavandi, H. G., Homsey, T., Moatamed, B., Hosseini, A., Huang, R., Leiter, J. C., Sarrafzadeh, M., and Lu, D. C. (2018).
Predicting the effects of epidural stimulation to improve hand function in patients with spinal cord injury: An active learning-based solution using dynamic sample weighting.
bioRxiv : the preprint server for biology, page 341719.

Kandel, E. R., Schwartz, J. H., Jessell, T. M., Siegelbaum, S., Hudspeth, A. J., and Mack, S. (2000).
Principles of Neural Science, volume 4.
McGraw-hill New York.

Kania, A., Johnson, R. L., and Jessell, T. M. (2000).

Coordinate roles for LIM homeobox genes in directing the dorsoventral trajectory of motor axons in the vertebrate limb.

Cell, 102(2):161–173.

Karthick, P. A., Venugopal, G., and Ramakrishnan, S. (2016).

Analysis of Muscle Fatigue Progression using Cyclostationary Property of Surface Electromyography Signals.

Journal of Medical Systems, 40(1):28.

Kathe, C., Skinnider, M. A., Hutson, T. H., Regazzi, N., Gautier, M., Demesmaeker, R., Komi, S., Ceto, S., James, N. D., Cho, N., Baud, L., Galan, K., Matson, K. J. E., Rowald, A., Kim, K., Wang, R., Minassian, K., Prior, J. O., Asboth, L., Barraud, Q., Lacour, S. P., Levine, A. J., Wagner, F., Bloch, J., Squair, J. W., and Courtine, G. (2022).

The neurons that restore walking after paralysis.

Nature.

Kempsell, K. E., Ball, G., and Szakmany, T. (2016).

Issues in biomarker identification, validation and development for disease diagnostics in Public Health.

Expert Review of Molecular Diagnostics, 16(4):383–386.

Khristy, W., Ali, N. J., Bravo, A. B., de Leon, R., Roy, R. R., Zhong, H., London, N. J. L., Edgerton, V. R., and Tillakaratne, N. J. K. (2009).

Changes in GABAA receptor subunit gamma 2 in extensor and flexor motoneurons and astrocytes after spinal cord transection and motor training.

Brain Research, 1273:9–17.

Kiehn, O. (2016).

Decoding the organization of spinal circuits that control locomotion.

Nature Reviews Neuroscience, 17(4):224–238.

Kim, D., Murray, M., and Simansky, K. J. (2001).

The serotonergic 5-HT2C agonist m-Chlorophenylpiperazine increases weight-supported locomotion without development of tolerance in rats with spinal transections.

Experimental Neurology, 169(2):496–500.

Kim, P., Lee, J., and Shin, C. S. (2021).

Classification of Walking Environments Using Deep Learning Approach Based on Surface EMG Sensors Only.

Sensors, 21(12):4204.

Kingma, D. P. and Ba, J. (2017).

Adam: A method for stochastic optimization.

Kirshblum, S., Millis, S., McKinley, W., and Tulsky, D. (2004).

Late neurologic recovery after traumatic spinal cord injury.

Archives of physical medicine and rehabilitation, 85(11):1811–7.

Kirshblum, S. C., Priebe, M. M., Ho, C. H., Scelza, W. M., Chiodo, A. E., and Wuermser, L. A. (2007).

Spinal cord injury medicine. 3. Rehabilitation phase after acute spinal cord injury.

Archives of physical medicine and rehabilitation, 88(3 Suppl 1):S62–70.

Knikou, M. (2008).

The H-reflex as a probe: Pathways and pitfalls.

Journal of Neuroscience Methods, 171(1):1–12.

Knikou, M., Dixon, L., Santora, D., and Ibrahim, M. M. (2015).

Transspinal constant-current long-lasting stimulation: A new method to induce cortical and corticospinal plasticity.

Journal of Neurophysiology, 114(3):1486–1499.

Kobayakawa, K., Depetro, K. A., Zhong, H., Pham, B., Hara, M., Harada, A., Nogami, J., Ohkawa, Y., and Edgerton, V. R. (2019).
Locomotor training increases synaptic structure with high NGL-2 expression after spinal cord hemisection.
Neurorehabilitation and Neural Repair, 33(3):225–231.

Koch, S. C., Del Barrio, M. G., Dalet, A., Gatto, G., Günther, T., Zhang, J., Seidler, B., Saur, D., Schüle, R., and Goulding, M. (2017).
RORβ spinal interneurons gate sensory transmission during locomotion to secure a fluid walking gait.
Neuron, 96(6):1419–1431.e5.

Koelstra, S., Muhl, C., Soleymani, M., Lee, J.-S., Yazdani, A., Ebrahimi, T., Pun, T., Nijholt, A., and Patras, I. (2012).
DEAP: A Database for Emotion Analysis ;Using Physiological Signals.
IEEE Transactions on Affective Computing, 3(1):18–31.

Kontson, K., Marcus, I., Myklebust, B., and Civillico, E. (2017).
Targeted box and blocks test: Normative data and comparison to standard tests.
PLoS ONE, 12(5):e0177965.

Kreydin, E., Zhong, H., Latack, K., Ye, S., Edgerton, V. R., and Gad, P. (2020).
Transcutaneous electrical spinal cord neuromodulator (TESCoN) improves symptoms of overactive bladder.
Frontiers in systems neuroscience, 14:1.

Kriellaars, D. J., Brownstone, R. M., Noga, B. R., and Jordan, L. M. (1994).
Mechanical entrainment of fictive locomotion in the decerebrate cat.

Journal of Neurophysiology, 71(6):2074–2086.

Krishnan, S. and Athavale, Y. (2018).

Trends in biomedical signal feature extraction.

Biomedical Signal Processing and Control, 43:41–63.

Kristiansen, M., Odderskær, N., and Kristensen, D. H. (2019).

Effect of body weight support on muscle activation during walking on a lower body positive pressure treadmill.

Journal of Electromyography and Kinesiology, 48:9–16.

Krizhevsky, A., Sutskever, I., and Hinton, G. E. (2012).

ImageNet classification with deep convolutional neural networks.

In Pereira, F., Burges, C., Bottou, L., and Weinberger, K., editors, *Advances in Neural Information Processing Systems*, volume 25. Curran Associates, Inc.

Krucoff, M. O., Rahimpour, S., Slutzky, M. W., Edgerton, V. R., and Turner, D. A. (2016).

Enhancing nervous system recovery through neurobiologics, neural interface training, and neurorehabilitation.

Frontiers in Neuroscience, 10:584.

Kumar, V., Lalotra, G. S., Sasikala, P., Rajput, D. S., Kaluri, R., Lakshmanna, K., Shorfuzzaman, M., Alsufyani, A., and Uddin, M. (2022).

Addressing Binary Classification over Class Imbalanced Clinical Datasets Using Computationally Intelligent Techniques.

Healthcare, 10(7):1293.

Kumru, H., Flores, A., Rodriguez-Canon, M., Edgerton, V. R., Garcia, L., Benito-Penalva, J., Navarro, X., Gerasimenko, Y., Garcia-Alias, G., and Vidal, J. (2021).

Cervical electrical neuromodulation effectively enhances hand motor output in healthy subjects by engaging a use-dependent intervention.

Journal of clinical medicine, 10(2).

Kuo, I. Y. and Ehrlich, B. E. (2015).

Signaling in Muscle Contraction.

Cold Spring Harbor Perspectives in Biology, 7(2):a006023.

Kyeong, S., Shin, W., Yang, M., Heo, U., Feng, J.-r., and Kim, J. (2019).

Recognition of walking environments and gait period by surface electromyography.

Frontiers of Information Technology & Electronic Engineering, 20(3):342–352.

Labella, L., Niechaj, A., and Rossignol, S. (1992).

Low-threshold, short-latency cutaneous reflexes during fictive locomotion in the ?semi-chronic? spinal cat.

Experimental Brain Research, 91(2).

Lai, H. C., Seal, R. P., and Johnson, J. E. (2016).

Making sense out of spinal cord somatosensory development.

Development (Cambridge, England), 143(19):3434–3448.

Laliberte, A. M., Farah, C., Steiner, K. R., Tariq, O., and Bui, T. V. (2022).

Changes in sensorimotor connectivity to dI3 interneurons in relation to the postnatal maturation of grasping.

Frontiers in Neural Circuits, 15.

Laliberte, A. M., Goltash, S., Lalonde, N. R., and Bui, T. V. (2019).

Propriospinal neurons: Essential elements of locomotor control in the intact and possibly the injured spinal cord.

Frontiers in Cellular Neuroscience, 13.

Lalonde, N. R. and Bui, T. V. (2021).

Do spinal circuits still require gating of sensory information by presynaptic inhibition after spinal cord injury?

Current Opinion in Physiology, 19:113–118.

Lam, T. and Pearson, K. G. (2001).

Proprioceptive Modulation of Hip Flexor Activity During the Swing Phase of Locomotion in Decerebrate Cats.

Journal of Neurophysiology, 86(3):1321–1332.

Lamy, J.-C., Russmann, H., Shamim, E. A., Meunier, S., and Hallett, M. (2010).

Paired associative stimulation induces change in presynaptic inhibition of ia terminals in wrist flexors in humans.

Journal of Neurophysiology, 104(2):755–764.

Landry, E. S., Lapointe, N. P., Rouillard, C., Levesque, D., Hedlund, P. B., and Guertin, P. A. (2006).

Contribution of spinal 5-HT1A and 5-HT7 receptors to locomotor-like movement induced by 8-OH-DPAT in spinal cord-transected mice.

The European journal of neuroscience, 24(2):535–46.

Längkvist, M., Karlsson, L., and Loutfi, A. (2014).

A review of unsupervised feature learning and deep learning for time-series modeling.

Pattern Recognition Letters, 42:11–24.

Lanuza, G. M., Gosgnach, S., Pierani, A., Jessell, T. M., and Goulding, M. (2004).

Genetic identification of spinal interneurons that coordinate left-right locomotor activity necessary for walking movements.

Neuron, 42(3):375–386.

Latash, M. L., Levin, M. F., Scholz, J. P., and Schöner, G. (2010).

Motor control theories and their applications.

Medicina (Kaunas, Lithuania), 46(6):382–392.

Lathe, R. (2023).

Restricted access data in the neurosciences: Are the restrictions always justified?

Frontiers in Neuroscience, 16:975795.

Lavrov, I., Courtine, G., Dy, C. J., van den Brand, R., Fong, A. J., Gerasimenko, Y., Zhong, H., Roy, R. R., and Edgerton, V. R. (2008a).

Facilitation of stepping with epidural stimulation in spinal rats: Role of sensory input.

The Journal of neuroscience : the official journal of the Society for Neuroscience, 28(31):7774–80.

Lavrov, I., Dy, C. J., Fong, A. J., Gerasimenko, Y., Courtine, G., Zhong, H., Roy, R. R., and Edgerton, V. R. (2008b).

Epidural stimulation induced modulation of spinal locomotor networks in adult spinal rats.

The Journal of neuroscience : the official journal of the Society for Neuroscience, 28(23):6022–9.

Lavrov, I., Gerasimenko, Y. P., Ichiyama, R. M., Courtine, G., Zhong, H., Roy, R. R., and Edgerton, V. R. (2006).

Plasticity of spinal cord reflexes after a complete transection in adult rats: Relationship to stepping ability.

Journal of neurophysiology, 96(4):1699–710.

Layne, C. S., Mulavara, A. P., McDonald, P. V., Pruett, C. J., Kozlovskaya, I. B., and Bloomberg, J. J. (2001).

Effect of long-duration spaceflight on postural control during self-generated perturbations.

Journal of applied physiology (Bethesda, Md. : 1985), 90(3):997–1006.

Layne, C. S. and Spooner, B. S. (1990).

EMG analysis of human postural responses during parabolic flight microgravity episodes.

Aviation, space, and environmental medicine, 61(11):994–8.

Le-Khac, P. H., Healy, G., and Smeaton, A. F. (2020).

Contrastive Representation Learning: A Framework and Review.

IEEE Access, 8:193907–193934.

Leblond, H., Espérance, M., Orsal, D., and Rossignol, S. (2003).

Treadmill locomotion in the intact and spinal mouse.

The Journal of Neuroscience, 23(36):11411.

Lee, K. Y., Ratté, S., and Prescott, S. A. (2019).

Excitatory neurons are more disinhibited than inhibitory neurons by chloride dysregulation in the spinal dorsal horn.

eLife, 8.

Levi, M., Attias, I., and Kontorovich, A. (2021).

Domain invariant adversarial learning.

CoRR, abs/2104.00322.

Levy, W. J., McCaffrey, M., and Hagichi, S. (1987).

Motor evoked potential as a predictor of recovery in chronic spinal cord injury.

Neurosurgery, 20(1):138–42.

Li, A. C., Prabhudesai, M., Duggal, S., Brown, E., and Pathak, D. (2023).

Your diffusion model is secretly a zero-shot classifier.

Li, S., Sui, X., Fu, J., Fu, H., Luo, X., Feng, Y., Xu, X., Liu, Y., Ting, D. S. W., and Goh, R. S. M. (2021a).

Few-Shot Domain Adaptation with Polymorphic Transformers.

In de Bruijne, M., Cattin, P. C., Cotin, S., Padoy, N., Speidel, S., Zheng, Y., and Essert, C., editors, *Medical Image Computing and Computer Assisted Intervention – MICCAI 2021*, pages 330–340, Cham. Springer International Publishing.

Li, S., Xie, M., Gong, K., Liu, C. H., Wang, Y., and Li, W. (2021b).

Transferable semantic augmentation for domain adaptation.

Li, W.-Y., Deng, L.-X., Zhai, F.-G., Wang, X.-Y., Li, Z.-G., and Wang, Y. (2022a).

Chx10+V2a interneurons in spinal motor regulation and spinal cord injury.

Neural Regeneration Research, 18(5):933–939.

Li, X., Ngu, A. H. H., and Metsis, V. (2022b).

TTS-CGAN: A transformer time-series conditional GAN for biosignal data augmentation.

Li, Y., Zhang, W., Zhang, Q., and Zheng, N. (2021c).

Transfer Learning-Based Muscle Activity Decoding Scheme by Low-frequency sEMG for Wearable Low-cost Application.

IEEE Access, 9:22804–22815.

Liew, S.-L., Lo, B. P., Donnelly, M. R., Zavaliangos-Petropulu, A., Jeong, J. N., Barisano, G., Hutton, A., Simon, J. P., Juliano, J. M., Suri, A., Wang, Z., Abdullah, A., Kim, J., Ard, T., Banaj, N., Borich, M. R., Boyd, L. A., Brodtmann, A., Buetefisch, C. M., Cao, L., Cassidy, J. M., Ciullo, V., Conforto, A. B., Cramer, S. C., Dacosta-Aguayo, R., de la Rosa, E., Domin, M., Dula, A. N., Feng, W., Franco, A. R., Geranmayeh, F., Gramfort, A., Gregory, C. M., Hanlon, C. A., Hordacre, B. G., Kautz, S. A., Khlif, M. S., Kim, H., Kirschke, J. S., Liu, J., Lotze, M., MacIntosh, B. J., Mataró, M., Mohamed, F. B.,

Nordvik, J. E., Park, G., Pienta, A., Piras, F., Redman, S. M., Revill, K. P., Reyes, M., Robertson, A. D., Seo, N. J., Soekadar, S. R., Spalletta, G., Sweet, A., Telenczuk, M., Thielman, G., Westlye, L. T., Winstein, C. J., Wittenberg, G. F., Wong, K. A., and Yu, C. (2022).

A large, curated, open-source stroke neuroimaging dataset to improve lesion segmentation algorithms.

Scientific Data, 9(1):320.

Little, J. W., Micklesen, P., Umlauf, R., and Britell, C. (1989).

Lower Extremity Manifestations of Spasticity in Chronic Spinal Cord Injury.

American Journal of Physical Medicine & Rehabilitation, 68(1):32.

Liu, P., Zhang, X., He, X., Jiang, Z., Wang, Q., and Lu, Y. (2021).

Spinal GABAergic neurons are under feed-forward inhibitory control driven by Aδ and C fibers in Gad2 td-Tomato mice.

Molecular Pain, 17:1744806921992620.

Liu, Q. and Xue, H. (2021).

Adversarial Spectral Kernel Matching for Unsupervised Time Series Domain Adaptation.

In *Twenty-Ninth International Joint Conference on Artificial Intelligence*, volume 3, pages 2744–2750.

Liu, S., Liu, S., Cai, W., Pujol, S., Kikinis, R., and Feng, D. (2014).

Early diagnosis of Alzheimer's disease with deep learning.

In *2014 IEEE 11th International Symposium on Biomedical Imaging (ISBI)*, pages 1015–1018.

Liu, S., Wang, X., Xiang, Y., Xu, H., Wang, H., and Tang, B. (2022).

Multi-channel fusion LSTM for medical event prediction using EHRs.

Journal of Biomedical Informatics, 127:104011.

Liu, Z., Ma, Q., Ma, P., and Wang, L. (2023).
Temporal-Frequency Co-training for Time Series Semi-supervised Learning.
Proceedings of the AAAI Conference on Artificial Intelligence, 37(7):8923–8931.

Long, M., CAO, ZHANGJIE., Wang, J., and Jordan, M. I. (2018).
Conditional Adversarial Domain Adaptation.
In *Advances in Neural Information Processing Systems*, volume 31. Curran Associates, Inc.

Lorach, H., Galvez, A., Spagnolo, V., Martel, F., Karakas, S., Intering, N., Vat, M., Faivre, O., Harte, C., Komi, S., Ravier, J., Collin, T., Coquoz, L., Sakr, I., Baaklini, E., Hernandez-Charpak, S. D., Dumont, G., Buschman, R., Buse, N., Denison, T., van Nes, I., Asboth, L., Watrin, A., Struber, L., Sauter-Starace, F., Langar, L., Auboiroux, V., Carda, S., Chabardes, S., Aksenova, T., Demesmaeker, R., Charvet, G., Bloch, J., and Courtine, G. (2023).
Walking naturally after spinal cord injury using a brain-spine interface.
Nature, 618(7963):126–133.

Lotze, M. and Cohen, L. G. (2006).
Volition and imagery in neurorehabilitation.
Cognitive and behavioral neurology : official journal of the Society for Behavioral and Cognitive Neurology, 19(3):135–40.

Lu, D. C., Edgerton, V. R., Modaber, M., AuYong, N., Morikawa, E., Zdunowski, S., Sarino, M. E., Sarrafzadeh, M., Nuwer, M. R., Roy, R. R., and Gerasimenko, Y. (2016).
Engaging cervical spinal cord networks to reenable volitional control of hand function in tetraplegic patients.
Neurorehabilitation and neural repair, 30(10):951–962.

Lu, D. C., Niu, T., and Alaynick, W. A. (2015).
Molecular and cellular development of spinal cord locomotor circuitry.
Frontiers in Molecular Neuroscience, 8(25).

Lu, Z., Narayan, A., and Yu, H. (2020).
A Deep Learning Based End-to-End Locomotion Mode Detection Method for Lower Limb Wearable Robot Control.
In *2020 IEEE/RSJ International Conference on Intelligent Robots and Systems (IROS)*, pages 4091–4097.

Luft, A., Bastian, A. J., and Dietz, V. (2016).
Learning in the damaged Brain/Spinal cord: Neuroplasticity.
In Reinkensmeyer, D. J. and Dietz, V., editors, *Neurorehabilitation Technology*, pages 3–17. Springer International Publishing, Cham.

Lundberg, A., Malmgren, K., and Schomburg, E. D. (1987).
Reflex pathways from group II muscle afferents.
Experimental Brain Research, 65(2):294–306.

Lundberg, S. M. and Lee, S.-I. (2017).
A Unified Approach to Interpreting Model Predictions.
In *Advances in Neural Information Processing Systems*, volume 30. Curran Associates, Inc.

Lundfald, L., Restrepo, C. E., Butt, S. J. B., Peng, C.-Y., Droho, S., Endo, T., Zeilhofer, H. U., Sharma, K., and Kiehn, O. (2007).
Phenotype of V2-derived interneurons and their relationship to the axon guidance molecule EphA4 in the developing mouse spinal cord.
European Journal of Neuroscience, 26(11):2989–3002.

Lüscher, C. and Malenka, R. C. (2012).

NMDA receptor-dependent long-term potentiation and long-term depression (LTP/LTD).

Cold Spring Harbor perspectives in biology, 4(6):a005710.

Lymberis, A. (2003).

Smart wearables for remote health monitoring, from prevention to rehabilitation: Current R&D, future challenges.

In *4th International IEEE EMBS Special Topic Conference on Information Technology Applications in Biomedicine, 2003.*, pages 272–275.

Lynskey, J. V., Belanger, A., and Jung, R. (2008).

Activity-dependent plasticity in spinal cord injury.

Journal of rehabilitation research and development, 45(2):229–240.

MacDonald, D. B. (2006).

Intraoperative motor evoked potential monitoring: Overview and update.

Journal of Clinical Monitoring and Computing, 20(5):347–377.

Mahrous, A., Birch, D., Heckman, C. J., and Tysseling, V. (2024).

Muscle Spasms after Spinal Cord Injury Stem from Changes in Motoneuron Excitability and Synaptic Inhibition, Not Synaptic Excitation.

The Journal of Neuroscience: The Official Journal of the Society for Neuroscience, 44(1):e1695232023.

Mahrous, A. A., Mousa, M. H., and Elbasiouny, S. M. (2019).

The mechanistic basis for successful spinal cord stimulation to generate steady motor outputs.

Frontiers in cellular neuroscience, 13:359.

Maier, I. C., Ichiyama, R. M., Courtine, G., Schnell, L., Lavrov, I., Edgerton, V. R., and Schwab, M. E. (2009).

Differential effects of anti-Nogo-A antibody treatment and treadmill training in rats with incomplete spinal cord injury.

Brain : a journal of neurology, 132(6):1426–1440.

Makino, H., Hwang, E. J., Hedrick, N. G., and Komiyama, T. (2016).

Circuit mechanisms of sensorimotor learning.

Neuron, 92(4):705–721.

Marchal-Crespo, L. and Reinkensmeyer, D. J. (2009).

Review of control strategies for robotic movement training after neurologic injury.

Journal of neuroengineering and rehabilitation, 6:20.

Marino, R. J., Ditunno, J. F., Jr., Donovan, W. H., and Maynard, F., Jr. (1999).

Neurologic recovery after traumatic spinal cord injury: Data from the Model Spinal Cord Injury Systems.

Archives of physical medicine and rehabilitation, 80(11):1391–6.

Markin, S. N., Klishko, A. N., Shevtsova, N. A., Lemay, M. A., Prilutsky, B. I., and Rybak, I. A. (2010).

Afferent control of locomotor CPG: Insights from a simple neuromechanical model.

Annals of the New York Academy of Sciences, 1198:21–34.

Martin, P. H. and Unwin, D. M. (1980).

A microwave doppler radar activity monitor.

Behavior Research Methods & Instrumentation, 12(5):517–520.

Martinez, M., Delivet-Mongrain, H., Leblond, H., and Rossignol, S. (2012).

Incomplete spinal cord injury promotes durable functional changes within the spinal locomotor circuitry.

Journal of Neurophysiology, 108(1):124–134.

Massetti, J. and Stein, D. M. (2018).

Spinal cord injury.

In White, J. L. and Sheth, K. N., editors, *Neurocritical Care for the Advanced Practice Clinician*, pages 269–288. Springer International Publishing, Cham.

Matsoukas, C., Haslum, J. F., Söderberg, M., and Smith, K. (2021).

Is it Time to Replace CNNs with Transformers for Medical Images?

Maynard, F. M., Jr., Bracken, M. B., Creasey, G., Ditunno, J. F., Jr., Donovan, W. H., Ducker, T. B., Garber, S. L., Marino, R. J., Stover, S. L., Tator, C. H., Waters, R. L., Wilberger, J. E., and Young, W. (1997).

International standards for neurological and functional classification of spinal cord injury. American spinal injury association.

Spinal cord : the official journal of the International Medical Society of Paraplegia, 35(5):266–74.

Mazzone, G. L., Mohammadshirazi, A., Aquino, J. B., Nistri, A., and Taccola, G. (2021).

GABAergic mechanisms can redress the tilted balance between excitation and inhibition in damaged spinal networks.

Molecular Neurobiology, 58(8):3769–3786.

McCulloch, W. S. and Pitts, W. (1943).

A logical calculus of the ideas immanent in nervous activity.

The bulletin of mathematical biophysics, 5(4):115–133.

McDermott, J. E., Wang, J., Mitchell, H., Webb-Robertson, B.-J., Hafen, R., Ramey, J., and Rodland, K. D. (2013).

Challenges in Biomarker Discovery: Combining Expert Insights with Statistical Analysis of Complex Omics Data.

Expert opinion on medical diagnostics, 7(1):37–51.

McKay, W. B., Ovechkin, A. V., Vitaz, T. W., Terson de Paleville, D. G. L., and Harkema, S. J. (2011).

Long-lasting involuntary motor activity after spinal cord injury.

Spinal Cord, 49(1):87–93.

McPherson, J. G., Miller, R. R., and Perlmutter, S. I. (2015).

Targeted, activity-dependent spinal stimulation produces long-lasting motor recovery in chronic cervical spinal cord injury.

Proceedings of the National Academy of Sciences of the United States of America, 112(39):12193–8.

Megia Garcia, A., Serrano-Munoz, D., Taylor, J., Avendano-Coy, J., and Gomez-Soriano, J. (2020).

Transcutaneous spinal cord stimulation and motor rehabilitation in spinal cord injury: A systematic review.

Neurorehabilitation and neural repair, 34(1):3–12.

Mekhail, N., Visnjevac, O., Azer, G., Mehanny, D. S., Agrawal, P., and Foorsov, V. (2018).

Spinal cord stimulation 50 years later: ¡em¿Clinical outcomes of spinal cord stimulation based on randomized clinical Trials—A systematic Review¡/em&gt.

Regional Anesthesia & Pain Medicine, 43(4):391.

Mendes, C. S., Bartos, I., Marka, Z., Akay, T., Marka, S., and Mann, R. S. (2015).

Quantification of gait parameters in freely walking rodents.

BMC biology, 13:50.

Merel, J., Botvinick, M., and Wayne, G. (2019).

Hierarchical motor control in mammals and machines.

Nature communications, 10(1):5489.

Merzon, L., Malevich, T., Zhulikov, G., Krasovskaya, S., and MacInnes, W. J. (2019). Temporal Limitations of the Standard Leaky Integrate and Fire Model. *Brain Sciences*, 10(1):16.

Meuwissen, K. P., de Vries, L. E., Gu, J. W., Zhang, T. C., and Joosten, E. A. (2020). Burst and Tonic Spinal Cord Stimulation Both Activate Spinal GABAergic Mechanisms to Attenuate Pain in a Rat Model of Chronic Neuropathic Pain. *Pain Practice*, 20(1):75–87.

Micera, S., Caleo, M., Chisari, C., Hummel, F. C., and Pedrocchi, A. (2020). Advanced neurotechnologies for the restoration of motor function. *Neuron*, 105(4):604–620.

Migliorini, C., Tonge, B., and Taleporos, G. (2008). Spinal cord injury and mental health. *Australian & New Zealand Journal of Psychiatry*, 42(4):309–314.

Mignardot, J.-B., Le Goff, C. G., van den Brand, R., Capogrosso, M., Fumeaux, N., Vallery, H., Anil, S., Lanini, J., Fodor, I., Eberle, G., Ijspeert, A., Schurch, B., Curt, A., Carda, S., Bloch, J., von Zitzewitz, J., and Courtine, G. (2017). A multidirectional gravity-assist algorithm that enhances locomotor control in patients with stroke or spinal cord injury. *Science Translational Medicine*, 9(399).

Militskova, A., Mukhametova, E., Fatykhova, E., Sharifullin, S., Cuellar, C. A., Calvert, J. S., Grahn, P. J., Baltina, T., and Lavrov, I. (2020). Supraspinal and afferent signaling facilitate spinal sensorimotor network excitability after discomplete spinal cord injury: A case report.

Serotonin Receptors in Neurobiology, 14:552.

Minassian, K., Bayart, A., Lackner, P., Binder, H., Freundl, B., and Hofstoetter, U. S. (2023).

Rare phenomena of central rhythm and pattern generation in a case of complete spinal cord injury.

Nature Communications, 14(1):3276.

Minassian, K. and Hofstoetter, U. S. (2016).

Spinal cord stimulation and augmentative control strategies for leg movement after spinal paralysis in humans.

CNS Neuroscience & Therapeutics, 22(4):262–270.

Minassian, K., Hofstoetter, U. S., Danner, S. M., Mayr, W., McKay, W. B., Tansey, K., and Dimitrijevic, M. R. (2013).

Mechanisms of rhythm generation of the human lumbar spinal cord in response to tonic stimulation without and with step-related sensory feedback.

Biomedical Engineering / Biomedizinische Technik, 58(SI-1-Track-A).

Minassian, K., Hofstoetter, U. S., Dzeladini, F., Guertin, P. A., and Ijspeert, A. (2017).

The human central pattern generator for locomotion: Does it exist and contribute to walking?

The Neuroscientist : a review journal bringing neurobiology, neurology and psychiatry, 23(6):649–663.

Minassian, K., Jilge, B., Rattay, F., Pinter, M. M., Binder, H., Gerstenbrand, F., and Dimitrijevic, M. R. (2004).

Stepping-like movements in humans with complete spinal cord injury induced by epidural stimulation of the lumbar cord: Electromyographic study of compound muscle action potentials.

Spinal cord : the official journal of the International Medical Society of Paraplegia, 42(7):401–16.

Minassian, K., McKay, W. B., Binder, H., and Hofstoetter, U. S. (2016).
Targeting lumbar spinal neural circuitry by epidural stimulation to restore motor function after spinal cord injury.
Neurotherapeutics : the journal of the American Society for Experimental NeuroTherapeutics, 13(2):284–294.

Minassian, K., Persy, I., Rattay, F., Pinter, M. M., Kern, H., and Dimitrijevic, M. R. (2007).
Human lumbar cord circuitries can be activated by extrinsic tonic input to generate locomotor-like activity.
Human movement science, 26(2):275–95.

Miotto, R., Wang, F., Wang, S., Jiang, X., and Dudley, J. T. (2018).
Deep learning for healthcare: Review, opportunities and challenges.
Briefings in Bioinformatics, 19(6):1236–1246.

Mitchell, W. G., Dee, E. C., and Celi, L. A. (2021).
Generalisability through local validation: Overcoming barriers due to data disparity in healthcare.
BMC Ophthalmology, 21(1):228.

Moran-Rivard, L., Kagawa, T., Saueressig, H., Gross, M. K., Burrill, J., and Goulding, M. (2001).
Evx1 is a postmitotic determinant of V0 interneuron identity in the spinal cord.
Neuron, 29(2):385–399.

Moraud, E. M., Capogrosso, M., Formento, E., Wenger, N., DiGiovanna, J., Courtine, G., and Micera, S. (2016).

Mechanisms underlying the neuromodulation of spinal circuits for correcting gait and balance deficits after spinal cord injury.

Neuron, 89(4):814–28.

Morbidoni, C., Cucchiarelli, A., Agostini, V., Knaflitz, M., Fioretti, S., and Di Nardo, F. (2021).

Machine-Learning-Based Prediction of Gait Events From EMG in Cerebral Palsy Children.

IEEE Transactions on Neural Systems and Rehabilitation Engineering, 29:819–830.

Morbidoni, C., Cucchiarelli, A., Fioretti, S., and Di Nardo, F. (2019).

A Deep Learning Approach to EMG-Based Classification of Gait Phases during Level Ground Walking.

Electronics, 8(8):894.

Mortimer, J. T. and Bhadra, N. (2018).

Chapter 6 - fundamentals of electrical stimulation.

In Krames, E. S., Peckham, P. H., and Rezai, A. R., editors, *Neuromodulation (Second Edition)*, pages 71–82. Academic Press.

Mouchnino, L. and Blouin, J. (2013).

When standing on a moving support, cutaneous inputs provide sufficient information to plan the anticipatory postural adjustments for gait initiation.

PLoS ONE, 8(2):e55081.

Mounis, S. Y. A., Azlan, N. Z., and Fatai, S. (2017).

Progress based assist-as-needed control strategy for upper-limb rehabilitation.

In *2017 IEEE Conference on Systems, Process and Control (ICSPC)*, pages 65–70.

Müller, T., Brohmann, H., Pierani, A., Heppenstall, P. A., Lewin, G. R., Jessell, T. M., and Birchmeier, C. (2002).

The homeodomain factor lbx1 distinguishes two major programs of neuronal differentiation in the dorsal spinal cord.

Neuron, 34(4):551–562.

Muradeli, J. (2020).

Ssqueezepy.

GitHub. Note: https://github.com/OverLordGoldDragon/ssqueezepy/.

Murg, M., Binder, H., and Dimitrijevic, M. (2000).

Epidural electric stimulation of posterior structures of the human lumbar spinal cord: 1. muscle twitches – a functional method to define the site of stimulation.

Spinal cord : the official journal of the International Medical Society of Paraplegia, 38(7):394–402.

Murray, K. C., Nakae, A., Stephens, M. J., Rank, M., D'Amico, J., Harvey, P. J., Li, X., Harris, R. L. W., Ballou, E. W., Anelli, R., Heckman, C. J., Mashimo, T., Vavrek, R., Sanelli, L., Gorassini, M. A., Bennett, D. J., and Fouad, K. (2010).

Recovery of motoneuron and locomotor function after spinal cord injury depends on constitutive activity in 5-HT2C receptors.

Nature Medicine, 16(6):694–700.

Musienko, P. E., Bogacheva, I. N., and Gerasimenko, Y. P. (2007).

Significance of peripheral feedback in the generation of stepping movements during epidural stimulation of the spinal cord.

Neuroscience and Behavioral Physiology, 37(2):181–190.

Musienko, P. E., Bogacheva, I. N., Savochin, A. A., Kilimnik, V. A., Gorskiĭ, O. V., Nikitin, O. A., and Gerasimenko Ia, P. (2013).

Non-invasive transcutaneous spinal cord stimulation facilitates locomotor activity in decerebrated and spinal cats.

Rossiiskii fiziologicheskii zhurnal imeni I.M. Sechenova / Rossiiskaia akademiia nauk, 99(8):917–27.

Musienko, P. E., Gorskii, O. V., Kilimnik, V. A., Kozlovskaya, I. B., Courtine, G., Edgerton, V. R., and Gerasimenko, Yu. P. (2015).

Regulation of Posture and Locomotion in Decerebrate and Spinal Animals.

Neuroscience and Behavioral Physiology, 45(2):229–237.

Mussa-Ivaldi, F. A. and Bizzi, E. (2000).

Motor learning through the combination of primitives.

Philosophical transactions of the Royal Society of London. Series B, Biological sciences, 355(1404):1755–69.

Musselman, K. E., Shah, M., and Zariffa, J. (2018).

Rehabilitation technologies and interventions for individuals with spinal cord injury: Translational potential of current trends.

Journal of neuroengineering and rehabilitation, 15(1):40.

Nagaraj, A., Shears, E., and de Vaan, M. (2020).

Improving data access democratizes and diversifies science.

Proceedings of the National Academy of Sciences, 117(38):23490–23498.

Nahid, N., Rahman, A., and Ahad, M. (2020).

Deep Learning Based Surface EMG Hand Gesture Classification for Low-Cost Myoelectric Prosthetic Hand.

In *2020 Joint 9th International Conference on Informatics, Electronics & Vision (ICIEV) and 2020 4th International Conference on Imaging, Vision & Pattern Recognition (icIVPR)*, pages 1–8.

Nakamura, Y., Kurabe, M., Matsumoto, M., Sato, T., Miyashita, S., Hoshina, K., Kamiya, Y., Tainaka, K., Matsuzawa, H., Ohno, N., and Ueno, M. (2023).

Cerebrospinal fluid-contacting neuron tracing reveals structural and functional connectivity for locomotion in the mouse spinal cord.
eLife, 12:e83108.

Nam, K. Y., Kim, H. J., Kwon, B. S., Park, J.-W., Lee, H. J., and Yoo, A. (2017).
Robot-assisted gait training (Lokomat) improves walking function and activity in people with spinal cord injury: A systematic review.
Journal of NeuroEngineering and Rehabilitation, 14(1):24.

Nas, K., Yazmalar, L., Şah, V., Aydın, A., and Öneş, K. (2015).
Rehabilitation of spinal cord injuries.
World Journal of Orthopedics, 6(1):8–16.

Nascimento, F., Broadhead, M. J., Tetringa, E., Tsape, E., Zagoraiou, L., and Miles, G. B. (2020).
Synaptic mechanisms underlying modulation of locomotor-related motoneuron output by premotor cholinergic interneurons.
eLife, 9.

Naud, R., Marcille, N., Clopath, C., and Gerstner, W. (2008).
Firing patterns in the adaptive exponential integrate-and-fire model.
Biological Cybernetics, 99(4):335–347.

Naumann, L. B. and Sprekeler, H. (2020).
Presynaptic inhibition rapidly stabilises recurrent excitation in the face of plasticity.
PLOS Computational Biology, 16(8):e1008118.

Nazmi, N., Abdul Rahman, M. A., Yamamoto, S.-I., and Ahmad, S. A. (2019).
Walking gait event detection based on electromyography signals using artificial neural network.

Biomedical Signal Processing and Control, 47:334–343.

Negi, S., CBS Negi, P., Sharma, S., and Sharma, N. (2020).
Electromyographic and Acceleration Signals-Based Gait Phase Analysis for Multiple Terrain Classification Using Deep Learning.

Neyshabur, B., Sedghi, H., and Zhang, C. (2020).
What is being transferred in transfer learning?
In *Advances in Neural Information Processing Systems*, volume 33, pages 512–523. Curran Associates, Inc.

Nguyen, L., Agaronnik, N., Ferrone, M. L., Katz, J. N., and Schoenfeld, A. J. (2021).
Evaluating ambulatory function as an outcome following treatment for spinal metastases: A systematic review.
The spine journal : official journal of the North American Spine Society, 21(9):1430–1439.

Ni, Y., Nawabi, H., Liu, X., Yang, L., Miyamichi, K., Tedeschi, A., Xu, B., Wall, N. R., Callaway, E. M., and He, Z. (2014).
Characterization of long descending premotor propriospinal neurons in the spinal cord.
Journal of Neuroscience, 34(28):9404–9417.

Nie, Y., Nguyen, N. H., Sinthong, P., and Kalagnanam, J. (2023).
A Time Series is Worth 64 Words: Long-term Forecasting with Transformers.

Niu, J., Ding, L., Li, J. J., Kim, H., Liu, J., Li, H., Moberly, A., Badea, T. C., Duncan, I. D., Son, Y.-J., Scherer, S. S., and Luo, W. (2013).
Modality-based organization of ascending somatosensory axons in the direct dorsal column pathway.
The Journal of neuroscience : the official journal of the Society for Neuroscience, 33(45):17691–17709.

Niu, S., Liu, Y., Wang, J., and Song, H. (2020).

A Decade Survey of Transfer Learning (2010–2020).

IEEE Transactions on Artificial Intelligence, 1(2):151–166.

Nizam Uddin, A. (2012).

Biosensors assisted automated rehabilitation systems: A systematic review.

International Journal of the Physical Sciences, 7(1).

Nógrádi, A. and Vrbová, G. (2013).

Anatomy and Physiology of the Spinal Cord.

In *Madame Curie Bioscience Database [Internet]*. Landes Bioscience.

Oni-Orisan, A., Kaushal, M., Li, W., Leschke, J., Ward, B. D., Vedantam, A., Kalinosky, B., Budde, M. D., Schmit, B. D., Li, S. J., Muqeet, V., and Kurpad, S. N. (2016).

Alterations in cortical sensorimotor connectivity following complete cervical spinal cord injury: A prospective resting-state fMRI study.

PLoS One, 11(3):e0150351.

Onifer, S. M., Smith, G. M., and Fouad, K. (2011).

Plasticity after spinal cord injury: Relevance to recovery and approaches to facilitate it.

Neurotherapeutics : the journal of the American Society for Experimental NeuroTherapeutics, 8(2):283–93.

Orban De Xivry, J. J. and Ethier, V. (2008).

Neural correlates of internal models.

Journal of Neuroscience, 28(32):7931–7932.

Oyinbo, C. A. (2011).

Secondary injury mechanisms in traumatic spinal cord injury: A nugget of this multiply cascade.

Acta neurobiologiae experimentalis, 71(2):281–99.

Ozdemir, M. A., Kisa, D. H., Guren, O., and Akan, A. (2022).
Hand gesture classification using time–frequency images and transfer learning based on CNN.
Biomedical Signal Processing and Control, 77:103787.

Özyurt, M. G., Ojeda-Alonso, J., Beato, M., and Nascimento, F. (2022).
In vitro longitudinal lumbar spinal cord preparations to study sensory and recurrent motor microcircuits of juvenile mice.
Journal of Neurophysiology, 128(3):711–726.

Pantelopoulos, A. and Bourbakis, N. G. (2010).
A survey on wearable sensor-based systems for health monitoring and prognosis.
IEEE Transactions on Systems, Man, and Cybernetics, Part C (Applications and Reviews), 40(1):1–12.

Park, H., Han, S., Sung, J., Hwang, S., Youn, I., and Kim, S.-J. (2023).
Classification of gait phases based on a machine learning approach using muscle synergy.
Frontiers in Human Neuroscience, 17.

Park, H., Latash, E. M., Molkov, Y. I., Klishko, A. N., Frigon, A., Deweerth, S. P., and Prilutsky, B. I. (2019).
Cutaneous sensory feedback from paw pads affects lateral balance control during split-belt locomotion in the cat.
Journal of Experimental Biology, 222(14):jeb198648.

Parker, J. L., Obradovic, M., Hesam Shariati, N., Gorman, R. B., Karantonis, D. M., Single, P. S., Laird-Wah, J., Bickerstaff, M., and Cousins, M. J. (2020).

Evoked compound action potentials reveal spinal cord dorsal column neuroanatomy. *Neuromodulation: Technology at the Neural Interface*, 23(1):82–95.

Paszke, A., Gross, S., Massa, F., Lerer, A., Bradbury, J., Chanan, G., Killeen, T., Lin, Z., Gimelshein, N., Antiga, L., Desmaison, A., Köpf, A., Yang, E., DeVito, Z., Raison, M., Tejani, A., Chilamkurthy, S., Steiner, B., Fang, L., Bai, J., and Chintala, S. (2019). PyTorch: An Imperative Style, High-Performance Deep Learning Library.

Patel, S., Park, H., Bonato, P., Chan, L., and Rodgers, M. (2012). A review of wearable sensors and systems with application in rehabilitation. *Journal of neuroengineering and rehabilitation*, 9:21.

Pathak, Y. J., Greenleaf, W., Verhagen Metman, L., Kubben, P., Sarma, S., Pepin, B., Lautner, D., DeBates, S., Benison, A. M., Balasingh, B., and Ross, E. (2021). Digital Health Integration With Neuromodulation Therapies: The Future of Patient-Centric Innovation in Neuromodulation. *Frontiers in Digital Health*, 3:618959.

Pearson, K. G. (2008). Role of sensory feedback in the control of stance duration in walking cats. *Brain Research Reviews*, 57(1):222–227.

Pearson, K. G. and Collins, D. F. (1993). Reversal of the influence of group Ib afferents from plantaris on activity in medial gastrocnemius muscle during locomotor activity. *Journal of Neurophysiology*, 70(3):1009–1017.

Pearson, K. G., Ramirez, J. M., and Jiang, W. (1992). Entrainment of the locomotor rhythm by group Ib afferents from ankle extensor muscles in spinal cats.

Experimental Brain Research, 90(3).

Pearson, KG. (1993).

Common principles of motor control in vertebrates and invertebrates.

Annual review of neuroscience, 16(1):265–297.

Pernold, K., Iannello, F., Low, B. E., Rigamonti, M., Rosati, G., Scavizzi, F., Wang, J., Raspa, M., Wiles, M. V., and Ulfhake, B. (2019).

Towards large scale automated cage monitoring – Diurnal rhythm and impact of interventions on in-cage activity of C57BL/6J mice recorded 24/7 with a non-disrupting capacitive-based technique.

PLOS ONE, 14(2):e0211063.

Perrier, J. F. (2005).

Synaptic release of serotonin induced by stimulation of the raphe nucleus promotes plateau potentials in spinal motoneurons of the adult turtle.

Journal of Neuroscience, 25(35):7993–7999.

Perry, S., Larhammar, M., Vieillard, J., Nagaraja, C., Hilscher, M. M., Tafreshiha, A., Rofo, F., Caixeta, F. V., and Kullander, K. (2019).

Characterization of dmrt3-derived neurons suggest a role within locomotor circuits.

The Journal of Neuroscience, 39(10):1771–1782.

Petersen, J. A., Spiess, M., Curt, A., Dietz, V., and Schubert, M. (2012).

Spinal Cord Injury: One-Year Evolution of Motor-Evoked Potentials and Recovery of Leg Motor Function in 255 Patients.

Neurorehabilitation and Neural Repair, 26(8):939–948.

Pham, B. N., Luo, J., Anand, H., Kola, O., Salcedo, P., Nguyen, C., Gaunt, S., Zhong, H., Garfinkel, A., Tillakaratne, N., and Edgerton, V. R. (2020).

Redundancy and multifunctionality among spinal locomotor networks.
Journal of neurophysiology, 124(5):1469–1479.

Pierani, A., Moran-Rivard, L., Sunshine, M. J., Littman, D. R., Goulding, M., and Jessell, T. M. (2001).
Control of interneuron fate in the developing spinal cord by the progenitor homeodomain protein dbx1.
Neuron, 29(2):367–384.

Pillai, A., Mansouri, A., Behringer, R., Westphal, H., and Goulding, M. (2007).
Lhx1 and Lhx5 maintain the inhibitory-neurotransmitter status of interneurons in the dorsal spinal cord.
Development (Cambridge, England), 134(2):357–366.

Pinter, M., Gerstenbrand, F., and Dimitrijevic, M. (2000).
Epidural electrical stimulation of posterior structures of the human lumbosacral cord: 3. Control of spasticity.
Spinal cord : the official journal of the International Medical Society of Paraplegia, 38(9):524–531.

Pizzolato, C., Gunduz, M. A., Palipana, D., Wu, J., Grant, G., Hall, S., Dennison, R., Zafonte, R. D., Lloyd, D. G., and Teng, Y. D. (2021).
Non-invasive approaches to functional recovery after spinal cord injury: Therapeutic targets and multimodal device interventions.
Experimental neurology, 339:113612.

Pocratsky, A. M., Shepard, C. T., Morehouse, J. R., Burke, D. A., Riegler, A. S., Hardin, J. T., Beare, J. E., Hainline, C., States, Gregory, Jr., Brown, B. L., Whittemore, S. R., and Magnuson, D. S. (2020).

Long ascending propriospinal neurons provide flexible, context-specific control of interlimb coordination.

eLife, 9.

Pradhan, A., He, J., and Jiang, N. (2022).

Multi-day dataset of forearm and wrist electromyogram for hand gesture recognition and biometrics.

Scientific Data, 9(1):733.

Prager, J. P. (2010).

What does the mechanism of spinal cord stimulation tell us about complex regional pain syndrome?

Pain Medicine, 11(8):1278–1283.

Prajapati, S. K., Gage, W. H., Brooks, D., Black, S. E., and McIlroy, W. E. (2011).

A novel approach to ambulatory monitoring: Investigation into the quantity and control of everyday walking in patients with subacute stroke.

Neurorehabilitation and Neural Repair, 25(1):6–14.

Prochazka, A. (1999).

Chapter 11 quantifying proprioception.

In Binder, M. D., editor, *Progress in Brain Research*, volume 123, pages 133–142. Elsevier.

Prochazka, A., Gosgnach, S., Capaday, C., and Geyer, H. (2017).

Chapter 6 - neuromuscular models for locomotion.

In Sharbafi, M. A. and Seyfarth, A., editors, *Bioinspired Legged Locomotion*, pages 401–453. Butterworth-Heinemann.

Prochazka, A., Trend, P., Hulliger, M., and Vincent, S. (1989).

Chapter 6 Ensemble proprioceptive activity in the cat step cycle: Towards a representative look-up chart.

In Allum, J. H. J. and Hulliger, M., editors, *Progress in Brain Research*, volume 80, pages 61–74. Elsevier.

Prut, Y. and Fetz, E. E. (1999).

Primate spinal interneurons show pre-movement instructed delay activity.

Nature, 401(6753):590–594.

Public Health Agency of Canada (2013).

Chronic Diseases and Injuries in Canada.

https://www.canada.ca/en/public-health/services/reports-publications/health-promotion-chronic-disease-prevention-canada-research-policy-practice/vol-33-no-3-2013/economic-burden-traumatic-spinal-cord-injury-canada.html.

Pulvermüller, F., Tomasello, R., Henningsen-Schomers, M. R., and Wennekers, T. (2021).

Biological constraints on neural network models of cognitive function.

Nature reviews. Neuroscience, 22(8):488–502.

Qi, X., Wang, J., Chen, Y., Shi, Y., and Zhang, L. (2023).

LipsFormer: Introducing lipschitz continuity to vision transformers.

Quinlan, K. A. and Kiehn, O. (2007).

Segmental, synaptic actions of commissural interneurons in the mouse spinal cord.

Journal of Neuroscience, 27(24):6521–6530.

Rabby, M. F., Tu, Y., Hossen, M. I., Lee, I., Maida, A. S., and Hei, X. (2021).

Stacked LSTM based deep recurrent neural network with kalman smoothing for blood glucose prediction.

BMC Medical Informatics and Decision Making, 21(1):101.

Rabchevsky, A. G., Patel, S. P., and Springer, J. E. (2011).
Pharmacological interventions for spinal cord injury: Where do we stand? How might we step forward?
Pharmacology & Therapeutics, 132(1):15–29.

Rabe, N., Gezelius, H., Vallstedt, A., Memic, F., and Kullander, K. (2009).
Netrin-1-dependent spinal interneuron subtypes are required for the formation of left-right alternating locomotor circuitry.
Journal of Neuroscience, 29(50):15642–15649.

Radhakrishna, M., Steuer, I., Prince, F., Roberts, M., Mongeon, D., Kia, M., Dyck, S., Matte, G., Vaillancourt, M., and Guertin, P. A. (2017).
Double-blind, placebo-controlled, randomized phase I/IIa study (safety and efficacy) with Buspirone/Levodopa/Carbidopa (SpinalonTM) in subjects with complete AIS A or motor-complete AIS B spinal cord injury.
Current pharmaceutical design, 23(12):1789–1804.

Ragab, M., Eldele, E., Tan, W. L., Foo, C.-S., Chen, Z., Wu, M., Kwoh, C.-K., and Li, X. (2023).
ADATIME: A Benchmarking Suite for Domain Adaptation on Time Series Data.
ACM Transactions on Knowledge Discovery from Data, 17(8):1–18.

Rahimian, E., Zabihi, S., Atashzar, S. F., Asif, A., and Mohammadi, A. (2020).
Surface EMG-Based Hand Gesture Recognition via Hybrid and Dilated Deep Neural Network Architectures for Neurorobotic Prostheses.
Journal of Medical Robotics Research, 05(01n02):2041001.

Rahman, M. A., Tharu, N. S., Gustin, S. M., Zheng, Y.-P., and Alam, M. (2022).
Trans-Spinal Electrical Stimulation Therapy for Functional Rehabilitation after Spinal Cord Injury: Review.

Journal of Clinical Medicine, 11(6):1550.

Rajan, D. and Thiagarajan, J. J. (2018).
A Generative Modeling Approach to Limited Channel ECG Classification.
In *2018 40th Annual International Conference of the IEEE Engineering in Medicine and Biology Society (EMBC)*, pages 2571–2574.

Rancic, V. and Gosgnach, S. (2021).
Recent insights into the rhythmogenic core of the locomotor CPG.
International Journal of Molecular Sciences, 22(3):1394.

Rath, M., Vette, A. H., Ramasubramaniam, S., Li, K., Burdick, J., Edgerton, V. R., Gerasimenko, Y. P., and Sayenko, D. G. (2018).
Trunk Stability Enabled by Noninvasive Spinal Electrical Stimulation after Spinal Cord Injury.
Journal of Neurotrauma, 35(21):2540–2553.

Rattay, F., Minassian, K., and Dimitrijevic, M. (2000).
Epidural electrical stimulation of posterior structures of the human lumbosacral cord: 2. quantitative analysis by computer modeling.
Spinal cord : the official journal of the International Medical Society of Paraplegia, 38(8):473–489.

Redfern, W. S., Tse, K., Grant, C., Keerie, A., Simpson, D. J., Pedersen, J. C., Rimmer, V., Leslie, L., Klein, S. K., Karp, N. A., Sillito, R., Chartsias, A., Lukins, T., Heward, J., Vickers, C., Chapman, K., and Armstrong, J. D. (2017).
Automated recording of home cage activity and temperature of individual rats housed in social groups: The Rodent Big Brother project.
PLOS ONE, 12(9):e0181068.

Reinkensmeyer, D. J., Burdet, E., Casadio, M., Krakauer, J. W., Kwakkel, G., Lang, C. E., Swinnen, S. P., Ward, N. S., and Schweighofer, N. (2016).

Computational neurorehabilitation: Modeling plasticity and learning to predict recovery.

Journal of neuroengineering and rehabilitation, 13(1):42.

Reinkensmeyer, D. J., Guigon, E., and Maier, M. A. (2012).

A computational model of use-dependent motor recovery following a stroke: Optimizing corticospinal activations via reinforcement learning can explain residual capacity and other strength recovery dynamics.

Neural networks : the official journal of the International Neural Network Society, 29–30:60–9.

Rejc, E., Angeli, C., and Harkema, S. (2015).

Effects of lumbosacral spinal cord epidural stimulation for standing after chronic complete paralysis in humans.

PLoS One, 10(7):e0133998.

Rejc, E., Angeli, C. A., Atkinson, D., and Harkema, S. J. (2017a).

Motor recovery after activity-based training with spinal cord epidural stimulation in a chronic motor complete paraplegic.

Scientific reports, 7(1):13476.

Rejc, E., Angeli, C. A., Bryant, N., and Harkema, S. J. (2017b).

Effects of stand and step training with epidural stimulation on motor function for standing in chronic complete paraplegics.

Journal of neurotrauma, 34(9):1787–1802.

Richens, J. G., Lee, C. M., and Johri, S. (2020).

Improving the accuracy of medical diagnosis with causal machine learning.

Nature Communications, 11(1):3923.

Rodgers, M. M., Alon, G., Pai, V. M., and Conroy, R. S. (2019).

Wearable technologies for active living and rehabilitation: Current research challenges and future opportunities.

Journal of Rehabilitation and Assistive Technologies Engineering, 6:2055668319839607.

Rose, F. D., Dell, P. A., and Love, S. (1985).

Doppler shift radar monitoring of activity of rats in a behavioural test situation.

Physiology & Behavior, 35(1):85–87.

Rosenblatt, F. (1958).

The perceptron: A probabilistic model for information storage and organization in the brain.

Psychological Review, 65(6):386–408.

Rossignol, S., Bouyer, L., Barthélemy, D., Langlet, C., and Leblond, H. (2002).

Recovery of locomotion in the cat following spinal cord lesions.

Brain Research Reviews, 40(1-3):257–266.

Rossignol, S. and Drew, T. (1986).

Phasic modulation of reflexes during rhythmic activity.

In Grillner, S., Stein, P. S. G., Stuart, D. G., Forssberg, H., and Herman, R. M., editors, *Neurobiology of Vertebrate Locomotion: Proceedings of an International Symposium Held at the Wenner-Gren Center, Stockholm, June 17th – 19th, 1985*, pages 517–534. Palgrave Macmillan UK, London.

Rossignol, S., Dubuc, R., and Gossard, J.-P. (2006).

Dynamic sensorimotor interactions in locomotion.

Physiological Reviews, 86(1):89–154.

Rossignol, S. and Frigon, A. (2011).
Recovery of locomotion after spinal cord injury: Some facts and mechanisms.
Annual review of neuroscience, 34:413–40.

Rossignol, S., Giroux, N., Chau, C., Marcoux, J., Brustein, E., and Reader, T. A. (2001).
Pharmacological aids to locomotor training after spinal injury in the cat.
The Journal of Physiology, 533(1):65–74.

Rowald, A., Komi, S., Demesmaeker, R., Baaklini, E., Hernandez-Charpak, S. D., Paoles, E., Montanaro, H., Cassara, A., Becce, F., Lloyd, B., Newton, T., Ravier, J., Kinany, N., D'Ercole, M., Paley, A., Hankov, N., Varescon, C., McCracken, L., Vat, M., Caban, M., Watrin, A., Jacquet, C., Bole-Feysot, L., Harte, C., Lorach, H., Galvez, A., Tschopp, M., Herrmann, N., Wacker, M., Geernaert, L., Fodor, I., Radevich, V., Van Den Keybus, K., Eberle, G., Pralong, E., Roulet, M., Ledoux, J.-B., Fornari, E., Mandija, S., Mattera, L., Martuzzi, R., Nazarian, B., Benkler, S., Callegari, S., Greiner, N., Fuhrer, B., Froeling, M., Buse, N., Denison, T., Buschman, R., Wende, C., Ganty, D., Bakker, J., Delattre, V., Lambert, H., Minassian, K., van den Berg, C. A. T., Kavounoudias, A., Micera, S., Van De Ville, D., Barraud, Q., Kurt, E., Kuster, N., Neufeld, E., Capogrosso, M., Asboth, L., Wagner, F. B., Bloch, J., and Courtine, G. (2022).
Activity-dependent spinal cord neuromodulation rapidly restores trunk and leg motor functions after complete paralysis.
Nature Medicine, 28(2):260–271.

Roy, F. D., Bosgra, D., and Stein, R. B. (2014).
Interaction of transcutaneous spinal stimulation and transcranial magnetic stimulation in human leg muscles.
Experimental Brain Research, 232(6):1717–1728.

Roy, R. R., Harkema, S. J., and Edgerton, V. R. (2012).

Basic concepts of activity-based interventions for improved recovery of motor function after spinal cord injury.

Archives of physical medicine and rehabilitation, 93(9):1487–97.

Roy, R. R., Hodgson, J. A., Lauretz, S. D., Pierotti, D. J., Gayek, R. J., and Edgerton, V. R. (1992).

Chronic spinal cord-injured cats: Surgical procedures and management.

Laboratory animal science, 42(4):335–343.

Rudomin, P. (1990).

Presynaptic inhibition of muscle spindle and tendon organ afferents in the mammalian spinal cord.

Trends in Neurosciences, 13(12):499–505.

Rudomin, P. (2009).

In search of lost presynaptic inhibition.

Experimental Brain Research, 196(1):139–151.

Rudomin, P. and Schmidt, R. F. (1999).

Presynaptic inhibition in the vertebrate spinal cord revisited.

Experimental Brain Research, 129(1):1–37.

Rybak, I. A., Dougherty, K. J., and Shevtsova, N. A. (2015).

Organization of the mammalian locomotor CPG: Review of computational model and circuit architectures based on genetically identified spinal Interneurons(1,2,3).

eNeuro, 2(5).

Rybak, I. A., Shevtsova, N. A., Lafreniere-Roula, M., and McCrea, D. A. (2006).

Modelling spinal circuitry involved in locomotor pattern generation: Insights from deletions during fictive locomotion.

The Journal of physiology, 577(Pt 2):617–39.

Ryu, H. X. and Kuo, A. D. (2021).

An optimality principle for locomotor central pattern generators.

Scientific Reports, 11(1):13140.

Sabharwal, S. (2013).

Essentials of Spinal Cord Medicine.

Demos Medical Publishing.

Sakurai, A., Tamvacakis, A. N., and Katz, P. S. (2016).

Recruitment of polysynaptic connections underlies functional recovery of a neural circuit after lesion.

eneuro, 3(4):ENEURO.0056–16.

Salarian, A., Russmann, H., Vingerhoets, F. J. G., Dehollain, C., Blanc, Y., Burkhard, P. R., and Aminian, K. (2004).

Gait assessment in Parkinson's disease: Toward an ambulatory system for long-term monitoring.

IEEE transactions on bio-medical engineering, 51(8):1434–1443.

Salomon, J. A., Haagsma, J. A., Davis, A., de Noordhout, C. M., Polinder, S., Havelaar, A. H., Cassini, A., Devleesschauwer, B., Kretzschmar, M., Speybroeck, N., Murray, C. J. L., and Vos, T. (2015).

Disability weights for the Global Burden of Disease 2013 study.

The Lancet Global Health, 3(11):e712–e723.

Sapir, T. (2004).

Pax6 and engrailed 1 regulate two distinct aspects of renshaw cell development.

Journal of Neuroscience, 24(5):1255–1264.

Sarvamangala, D. R. and Kulkarni, R. V. (2022).

Convolutional neural networks in medical image understanding: A survey.

Evolutionary Intelligence, 15(1):1–22.

Saueressig, H., Burrill, J., and Goulding, M. (1999).

Engrailed-1 and netrin-1 regulate axon pathfinding by association interneurons that project to motor neurons.

Development (Cambridge, England), 126(19):4201–4212.

Savithri, C. N., Priya, E., and Sudharsanan, J. (2021).

Classification of sEMG signal-based arm action using convolutional neural network.

In Priya, E. and Rajinikanth, V., editors, *Signal and Image Processing Techniques for the Development of Intelligent Healthcare Systems*, pages 241–259. Springer Singapore, Singapore.

Sayenko, D. G., Rath, M., Ferguson, A. R., Burdick, J. W., Havton, L. A., Edgerton, V. R., and Gerasimenko, Y. P. (2019).

Self-Assisted Standing Enabled by Non-Invasive Spinal Stimulation after Spinal Cord Injury.

Journal of Neurotrauma, 36(9):1435–1450.

Schmid, W., Fan, Y., Chi, T., Golanov, E., Regnier-Golanov, A. S., Austerman, R. J., Podell, K., Cherukuri, P., Bentley, T., Steele, C. T., Schodrof, S., Aazhang, B., and Britz, G. W. (2021).

Review of wearable technologies and machine learning methodologies for systematic detection of mild traumatic brain injuries.

Journal of Neural Engineering, 18(4):041006.

Schmidt, B. J. and Jordan, L. M. (2000).

The role of serotonin in reflex modulation and locomotor rhythm production in the mammalian spinal cord.
Brain Research Bulletin, 53(5):689–710.

Schmit, B. D., McKenna-Cole, A., and Rymer, W. Z. (2000).
Flexor reflexes in chronic spinal cord injury triggered by imposed ankle rotation.
Muscle & Nerve, 23(5):793–803.

Schneider, S., Popp, W. L., Brogioli, M., Albisser, U., Demkó, L., Debecker, I., Velstra, I.-M., Gassert, R., and Curt, A. (2018).
Reliability of Wearable-Sensor-Derived Measures of Physical Activity in Wheelchair-Dependent Spinal Cord Injured Patients.
Frontiers in Neurology, 9:1039.

Schomburg, E. D., Petersen, N., Barajon, I., and Hultborn, H. (1998).
Flexor reflex afferents reset the step cycle during fictive locomotion in the cat.
Experimental Brain Research, 122(3):339–350.

Seanez, I. and Capogrosso, M. (2021).
Motor improvements enabled by spinal cord stimulation combined with physical training after spinal cord injury: Review of experimental evidence in animals and humans.
Bioelectronic medicine, 7(1):16.

Segev, I. (1990).
Computer study of presynaptic inhibition controlling the spread of action potentials into axonal terminals.
Journal of neurophysiology, 63 5:987–98.

Selvaraju, R. R., Cogswell, M., Das, A., Vedantam, R., Parikh, D., and Batra, D. (2019).

Grad-CAM: Visual explanations from deep networks via gradient-based localization. *International Journal of Computer Vision*, 128(2):336–359.

Sengul, G. and Watson, C. (2012a).
Chapter 6 - spinal cord: Regional anatomy, cytoarchitecture and chemoarchitecture.
In Mai, J. K. and Paxinos, G., editors, *The Human Nervous System (Third Edition)*, pages 186–232. Academic Press, San Diego.

Sengul, G. and Watson, C. (2012b).
Chapter 7 - spinal cord: Connections.
In Mai, J. K. and Paxinos, G., editors, *The Human Nervous System (Third Edition)*, pages 233–258. Academic Press, San Diego.

Sezer, N., Akkus, S., and Ugurlu, F. G. (2015).
Chronic complications of spinal cord injury.
World journal of orthopedics, 6(1):24–33.

Shah, P. K., Garcia-Alias, G., Choe, J., Gad, P., Gerasimenko, Y., Tillakaratne, N., Zhong, H., Roy, R. R., and Edgerton, V. R. (2013).
Use of quadrupedal step training to re-engage spinal interneuronal networks and improve locomotor function after spinal cord injury.
Brain : a journal of neurology, 136(Pt 11):3362–77.

Shah, P. K., Gerasimenko, Y., Shyu, A., Lavrov, I., Zhong, H., Roy, R. R., and Edgerton, V. R. (2012).
Variability in step training enhances locomotor recovery after a spinal cord injury.
European Journal of Neuroscience, 36(1):2054–2062.

Shanmuganathan, V., Yesudhas, H. R., Khan, M. S., Khari, M., and Gandomi, A. H. (2020).

R-CNN and wavelet feature extraction for hand gesture recognition with EMG signals. *Neural Computing and Applications*, 32(21):16723–16736.

Shenoy, K. V., Sahani, M., and Churchland, M. M. (2013).
Cortical control of arm movements: A dynamical systems perspective.
Annual review of neuroscience, 36:337–59.

Sherrington, C. S. (1906).
Observations on the scratch-reflex in the spinal dog.
The Journal of physiology, 34(1-2):1.

Sherrington, C. S. (1910).
Flexion-reflex of the limb, crossed extension-reflex, and reflex stepping and standing.
The Journal of physiology, 40(1-2):28.

Shimizu-Okabe, C., Kobayashi, S., Kim, J., Kosaka, Y., Sunagawa, M., Okabe, A., and Takayama, C. (2022).
Developmental formation of the GABAergic and glycinergic networks in the mouse spinal cord.
International Journal of Molecular Sciences, 23(2).

Shin, H.-C., Roth, H. R., Gao, M., Lu, L., Xu, Z., Nogues, I., Yao, J., Mollura, D., and Summers, R. M. (2016).
Deep Convolutional Neural Networks for Computer-Aided Detection: CNN Architectures, Dataset Characteristics and Transfer Learning.
IEEE Transactions on Medical Imaging, 35(5):1285–1298.

Silipo, R. and Marchesi, C. (1998).
Artificial neural networks for automatic ECG analysis.
IEEE Transactions on Signal Processing, 46(5):1417–1425.

Simis, M., Doruk Camsari, D., Imamura, M., Filippo, T. R. M., Rubio De Souza, D., Battistella, L. R., and Fregni, F. (2021).

Electroencephalography as a Biomarker for Functional Recovery in Spinal Cord Injury Patients.

Frontiers in Human Neuroscience, 15:548558.

Simonyan, K. and Zisserman, A. (2015).

Very deep convolutional networks for large-scale image recognition.

Smith, L. H., Hargrove, L. J., Lock, B. A., and Kuiken, T. A. (2011).

Determining the optimal window length for pattern recognition-based myoelectric control: Balancing the competing effects of classification error and controller delay.

IEEE transactions on neural systems and rehabilitation engineering : a publication of the IEEE Engineering in Medicine and Biology Society, 19(2):186–192.

Solnik, S., Rider, P., Steinweg, K., DeVita, P., and Hortobágyi, T. (2010).

Teager-Kaiser energy operator signal conditioning improves EMG onset detection.

European journal of applied physiology, 110(3):489–498.

Soteropoulos, D. S. (2018).

Corticospinal gating during action preparation and movement in the primate motor cortex.

Journal of neurophysiology, 119(4):1538–1555.

Soviany, P., Ionescu, R. T., Rota, P., and Sebe, N. (2022).

Curriculum Learning: A Survey.

International Journal of Computer Vision, 130(6):1526–1565.

Spiess, M. R., Müller, R. M., Rupp, R., Schuld, C., and Van Hedel, H. J. A. (2009).

Conversion in ASIA impairment scale during the first year after traumatic spinal cord injury.

Journal of Neurotrauma, 26(11):2027–2036.

Squair, J. W., Gautier, M., Sofroniew, M. V., Courtine, G., and Anderson, M. A. (2021).
Engineering spinal cord repair.
Current opinion in biotechnology, 72:48–53.

Stam, F. J., Hendricks, T. J., Zhang, J., Geiman, E. J., Francius, C., Labosky, P. A., Clotman, F., and Goulding, M. (2012).
Renshaw cell interneuron specialization is controlled by a temporally restricted transcription factor program.
Development (Cambridge, England), 139(1):179–190.

Starkey, M. L., Bleul, C., Kasper, H., Mosberger, A. C., Zorner, B., Giger, S., Gullo, M., Buschmann, F., and Schwab, M. E. (2014).
High-impact, self-motivated training within an enriched environment with single animal tracking dose-dependently promotes motor skill acquisition and functional recovery.
Neurorehabilitation and neural repair, 28(6):594–605.

Steele, A. G., Atkinson, D. A., Varghese, B., Oh, J., Markley, R. L., and Sayenko, D. G. (2021).
Characterization of spinal sensorimotor network using transcutaneous spinal stimulation during voluntary movement preparation and performance.
Journal of Clinical Medicine, 10(24):5958.

Steeves, J. D., Kramer, J. K., Fawcett, J. W., Cragg, J., Lammertse, D. P., Blight, A. R., Marino, R. J., Ditunno, J. F., Jr., Coleman, W. P., Geisler, F. H., Guest, J., Jones, L., Burns, S., Schubert, M., van Hedel, H. J., Curt, A., and Group, E. S. (2011).
Extent of spontaneous motor recovery after traumatic cervical sensorimotor complete spinal cord injury.

Spinal cord : the official journal of the International Medical Society of Paraplegia, 49(2):257–65.

Stein, R. B. (1995).

Presynaptic inhibition in humans.

Progress in Neurobiology, 47(6):533–544.

Stein, R. B. and Capaday, C. (1988).

The modulation of human reflexes during functional motor tasks.

Trends in Neurosciences, 11(7):328–332.

Stepien, A. E., Tripodi, M., and Arber, S. (2010).

Monosynaptic rabies virus reveals premotor network organization and synaptic specificity of cholinergic partition cells.

Neuron, 68(3):456–472.

Stewart, J. E., Barbeau, H., and Gauthier, S. (1991).

Modulation of locomotor patterns and spasticity with clonidine in spinal cord injured patients.

Canadian Journal of Neurological Sciences / Journal Canadien des Sciences Neurologiques, 18(3):321–332.

Stifani, N. (2014).

Motor neurons and the generation of spinal motor neurons diversity.

Frontiers in Cellular Neuroscience, 8(293).

Stimberg, M., Brette, R., and Goodman, D. F. (2019).

Brian 2, an intuitive and efficient neural simulator.

eLife, 8:e47314.

Storm, F. A., Buckley, C. J., and Mazzà, C. (2016).

Gait event detection in laboratory and real life settings: Accuracy of ankle and waist sensor based methods.

Gait & Posture, 50:42–46.

Strominger, N. L., Demarest, R. J., and Laemle, L. B. (2012).

Reflexes and Muscle Tone.

In Strominger, N. L., Demarest, R. J., and Laemle, L. B., editors, *Noback's Human Nervous System, Seventh Edition: Structure and Function*, pages 143–154. Humana Press, Totowa, NJ.

Stuart, D. G. and Hultborn, H. (2008).

Thomas Graham Brown (1882–1965), Anders Lundberg (1920–), and the neural control of stepping.

Brain Research Reviews, 59(1):74–95.

Stubbs, P. W., Nielsen, J. F., Sinkjaer, T., and Mrachacz-Kersting, N. (2011a).

Crossed spinal soleus muscle communication demonstrated by H-reflex conditioning.

Muscle & Nerve, 43(6):845–850.

Stubbs, P. W., Nielsen, J. F., Sinkjær, T., and Mrachacz-Kersting, N. (2011b).

Phase modulation of the short-latency crossed spinal response in the human soleus muscle.

Journal of Neurophysiology, 105(2):503–511.

Sui, Y., Yue, Y., and W. Burdick, J. (2017).

Correlational dueling bandits with application to clinical treatment in large decision spaces.

In *Proceedings of the Twenty-Sixth International Joint Conference on Artificial Intelligence*, pages 2793–2799.

Suzuki, K. (2017).

Overview of deep learning in medical imaging.

Radiological Physics and Technology, 10(3):257–273.

Suzuki, K., Horiba, I., Sugie, N., and Nanki, M. (2004).

Extraction of left ventricular contours from left ventriculograms by means of a neural edge detector.

IEEE Transactions on Medical Imaging, 23(3):330–339.

Suzuki, K., Rockey, D. C., and Dachman, A. H. (2010).

CT colonography: Advanced computer-aided detection scheme utilizing MTANNs for detection of "missed" polyps in a multicenter clinical trial.

Medical Physics, 37(1):12–21.

Syed, S. T., Gerber, B. S., and Sharp, L. K. (2013).

Traveling Towards Disease: Transportation Barriers to Health Care Access.

Journal of community health, 38(5):976–993.

Szabo, N. E., Da Silva, R. V., Sotocinal, S. G., Zeilhofer, H. U., Mogil, J. S., and Kania, A. (2015).

Hoxb8 intersection defines a role for lmx1b in excitatory dorsal horn neuron development, spinofugal connectivity, and nociception.

Journal of Neuroscience, 35(13):5233–5246.

Szegedy, C., Vanhoucke, V., Ioffe, S., Shlens, J., and Wojna, Z. (2016).

Rethinking the Inception Architecture for Computer Vision.

In *2016 IEEE Conference on Computer Vision and Pattern Recognition (CVPR)*, pages 2818–2826.

Taccola, G., Salazar, B. H., Apicella, R., Hogan, M. K., Horner, P. J., and Sayenko, D. (2020).

Selective antagonism of A1 adenosinergic receptors strengthens the neuromodulation of the sensorimotor network during epidural spinal stimulation.
Frontiers in Systems Neuroscience, 14.

Taccola, G., Sayenko, D., Gad, P., Gerasimenko, Y., and Edgerton, V. R. (2018).
And yet it moves: Recovery of volitional control after spinal cord injury.
Progress in neurobiology, 160:64–81.

Takeoka, A. (2020).
Proprioception: Bottom-up directive for motor recovery after spinal cord injury.
Neuroscience Research, 154:1–8.

Takeoka, A. and Arber, S. (2019).
Functional local proprioceptive feedback circuits initiate and maintain locomotor recovery after spinal cord injury.
Cell Reports, 27(1):71–85.e3.

Takeoka, A., Vollenweider, I., Courtine, G., and Arber, S. (2014).
Muscle spindle feedback directs locomotor recovery and circuit reorganization after spinal cord injury.
Cell, 159(7):1626–1639.

Talpalar, A. E., Bouvier, J., Borgius, L., Fortin, G., Pierani, A., and Kiehn, O. (2013).
Dual-mode operation of neuronal networks involved in left–right alternation.
Nature, 500(7460):85–88.

Tate, D. G., Wheeler, T., Lane, G. I., Forchheimer, M., Anderson, K. D., Biering-Sorensen, F., Cameron, A. P., Santacruz, B. G., Jakeman, L. B., Kennelly, M. J., Kirshblum, S., Krassioukov, A., Krogh, K., Mulcahey, M. J., Noonan, V. K., Rodriguez, G. M., Spungen, A. M., Tulsky, D., and Post, M. W. (2020).

Recommendations for evaluation of neurogenic bladder and bowel dysfunction after spinal cord injury and/or disease.

The Journal of Spinal Cord Medicine, 43(2):141–164.

Terashi, H., Taguchi, T., Ueta, Y., Okubo, Y., Mitoma, H., and Aizawa, H. (2020).

Analysis of non-invasive gait recording under free-living conditions in patients with Parkinson's disease: Relationship with global cognitive function and motor abnormalities.

BMC Neurology, 20(1):161.

Thau, L., Reddy, V., and Singh, P. (2021).

Anatomy, central nervous system.

In *StatPearls*. StatPearls Publishing Copyright © 2021, StatPearls Publishing LLC., Treasure Island (FL).

Thomas, S. L., Wakerman, J., and Humphreys, J. S. (2015).

Ensuring equity of access to primary health care in rural and remote Australia - what core services should be locally available?

International Journal for Equity in Health, 14(1):111.

Tillakaratne, N. J. K., De Leon, R. D., Hoang, T. X., Roy, R. R., Edgerton, V. R., and Tobin, A. J. (2002).

Use-dependent modulation of inhibitory capacity in the feline lumbar spinal cord.

The Journal of Neuroscience, 22(8):3130–3143.

Tillakaratne, N. J. K., Duru, P., Fujino, H., Zhong, H., Xiao, M. S., Edgerton, V. R., and Roy, R. R. (2014).

Identification of interneurons activated at different inclines during treadmill locomotion in adult rats.

Journal of Neuroscience Research, 92(12):1714–1722.

Tillakaratne, N. J. K., Guu, J. J., De Leon, R. D., Bigbee, A. J., London, N. J., Zhong, H., Ziegler, M. D., Joynes, R. L., Roy, R. R., and Edgerton, V. R. (2010).

Functional recovery of stepping in rats after a complete neonatal spinal cord transection is not due to regrowth across the lesion site.

Neuroscience, 166(1):23–33.

Timoszyk, W. K., de Leon, R. D., London, N., Roy, R. R., Edgerton, V. R., and Reinkensmeyer, D. J. (2002).

The rat lumbosacral spinal cord adapts to robotic loading applied during stance.

Journal of Neurophysiology, 88(6):3108–3117.

Toda, H., Maruyama, T., and Tada, M. (2020).

Indoor vs. Outdoor Walking: Does It Make Any Difference in Joint Angle Depending on Road Surface?

Frontiers in Sports and Active Living, 2.

Tolmacheva, A., Savolainen, S., Kirveskari, E., Lioumis, P., Kuusela, L., Brandstack, N., Ylinen, A., Makela, J. P., and Shulga, A. (2017).

Long-term paired associative stimulation enhances motor output of the tetraplegic hand.

Journal of neurotrauma, 34(18):2668–2674.

Tosney, K. W., Hotary, K. B., and Lance-Jones, C. (1995).

Specifying the target identity of motoneurons.

BioEssays : news and reviews in molecular, cellular and developmental biology, 17(5):379–382.

Trieschmann, R. B. (1988).

Spinal Cord Injuries: Psychological, Social, and Vocational Rehabilitation.

Demos Medical Publishing.

Tripodi, M., Stepien, A. E., and Arber, S. (2011).
Motor antagonism exposed by spatial segregation and timing of neurogenesis.
Nature, 479(7371):61–66.

Truchon, C., Fallah, N., Santos, A., Vachon, J., Noonan, V. K., and Cheng, C. L. (2017).
Impact of therapy on recovery during rehabilitation in patients with traumatic spinal cord injury.
Journal of neurotrauma, 34(20):2901–2909.

Tuan, Akay, T., Loubani, O., Thomas, Thomas, and Robert (2013).
Circuits for grasping: Spinal dI3 interneurons mediate cutaneous control of motor behavior.
Neuron, 78(1):191–204.

Urbin, M. A., Ozdemir, R. A., Tazoe, T., and Perez, M. A. (2017).
Spike-timing-dependent plasticity in lower-limb motoneurons after human spinal cord injury.
Journal of neurophysiology, 118(4):2171–2180.

Van De Crommert, H. W. A. A., Mulder, T., and Duysens, J. (1998).
Neural control of locomotion: Sensory control of the central pattern generator and its relation to treadmill training.
Gait & Posture, 7(3):251–263.

Van Den Brand, R., Heutschi, J., Barraud, Q., Digiovanna, J., Bartholdi, K., Huerlimann, M., Friedli, L., Vollenweider, I., Moraud, E. M., Duis, S., Dominici, N., Micera, S., Musienko, P., and Courtine, G. (2012).
Restoring voluntary control of locomotion after paralyzing spinal cord injury.
Science (New York, N.Y.), 336(6085):1182–1185.

van den Brand, R., Mignardot, J. B., von Zitzewitz, J., Le Goff, C., Fumeaux, N., Wagner, F., Capogrosso, M., Martin Moraud, E., Micera, S., Schurch, B., Curt, A., Carda, S., Bloch, J., and Courtine, G. (2015).

Neuroprosthetic technologies to augment the impact of neurorehabilitation after spinal cord injury.

Annals of physical and rehabilitation medicine, 58(4):232–237.

van Hedel, H. J. A. and Dietz, V. (2010).

Rehabilitation of locomotion after spinal cord injury.

Restorative Neurology and Neuroscience, 28(1):123–134.

Van Rossum, G. and Drake, F. L. (2009).

Python 3 Reference Manual.

CreateSpace, Scotts Valley, CA.

Vargas Luna, J. L., Brown, J., Krenn, M. J., McKay, B., Mayr, W., Rothwell, J. C., and Dimitrijevic, M. R. (2021).

Neurophysiology of epidurally evoked spinal cord reflexes in clinically motor-complete posttraumatic spinal cord injury.

Experimental Brain Research, 239(8):2605–2620.

Vaswani, A., Shazeer, N., Parmar, N., Uszkoreit, J., Jones, L., Gomez, A. N., Kaiser, Ł., and Polosukhin, I. (2017).

Attention is all you need.

In Guyon, I., Luxburg, U. V., Bengio, S., Wallach, H., Fergus, R., Vishwanathan, S., and Garnett, R., editors, *Advances in Neural Information Processing Systems*, volume 30. Curran Associates, Inc.

Wagner, F. B., Mignardot, J. B., Le Goff-Mignardot, C. G., Demesmaeker, R., Komi, S., Capogrosso, M., Rowald, A., Seanez, I., Caban, M., Pirondini, E., Vat, M., McCracken,

L. A., Heimgartner, R., Fodor, I., Watrin, A., Seguin, P., Paoles, E., Van Den Keybus, K., Eberle, G., Schurch, B., Pralong, E., Becce, F., Prior, J., Buse, N., Buschman, R., Neufeld, E., Kuster, N., Carda, S., von Zitzewitz, J., Delattre, V., Denison, T., Lambert, H., Minassian, K., Bloch, J., and Courtine, G. (2018).

Targeted neurotechnology restores walking in humans with spinal cord injury.

Nature, 563(7729):65–71.

Wagner, M. J. and Smith, M. A. (2008).

Shared internal models for feedforward and feedback control.

The Journal of neuroscience : the official journal of the Society for Neuroscience, 28(42):10663–73.

Wainberg, M., Barbeau, H., and Gauthier, S. (1990).

The effects of cyproheptadine on locomotion and on spasticity in patients with spinal cord injuries.

Journal of Neurology, Neurosurgery & Psychiatry, 53(9):754–763.

Wang, H., Pujos-Guillot, E., Comte, B., de Miranda, J. L., Spiwok, V., Chorbev, I., Castiglione, F., Tieri, P., Watterson, S., McAllister, R., de Melo Malaquias, T., Zanin, M., Rai, T. S., and Zheng, H. (2021).

Deep learning in systems medicine.

Briefings in Bioinformatics, 22(2):1543–1559.

Wang, H. and Raj, B. (2017).

On the Origin of Deep Learning.

Wang, Q., Chen, W., and Markopoulos, P. (2014).

Literature review on wearable systems in upper extremity rehabilitation.

In *IEEE-EMBS International Conference on Biomedical and Health Informatics (BHI)*, pages 551–555.

Wang, Q., Markopoulos, P., Yu, B., Chen, W., and Timmermans, A. (2017).
Interactive wearable systems for upper body rehabilitation: A systematic review.
Journal of neuroengineering and rehabilitation, 14(1):20.

Wayne, P., Gow, B., Hausdorff, J., Peng, C.-K., Lipsitz, L., Ahn, A., Novak, V., and Manor, B. (2021).
Tai Chi, Physiological Complexity, and Healthy Aging - Gait.

Wayne, P. M., Manor, B., Novak, V., Costa, M. D., Hausdorff, J. M., Goldberger, A. L., Ahn, A. C., Yeh, G. Y., Peng, C.-K., Lough, M., Davis, R. B., Quilty, M. T., and Lipsitz, L. A. (2013).
A Systems Biology Approach to Studying Tai Chi, Physiological Complexity and Healthy Aging: Design and Rationale of a Pragmatic Randomized Controlled Trial.
Contemporary clinical trials, 34(1):21–34.

Weidner, N., Ner, A., Salimi, N., and Tuszynski, M. H. (2001).
Spontaneous corticospinal axonal plasticity and functional recovery after adult central nervous system injury.
Proceedings of the National Academy of Sciences, 98(6):3513–3518.

Wenger, N., Moraud, E. M., Gandar, J., Musienko, P., Capogrosso, M., Baud, L., Le Goff, C. G., Barraud, Q., Pavlova, N., Dominici, N., Minev, I. R., Asboth, L., Hirsch, A., Duis, S., Kreider, J., Mortera, A., Haverbeck, O., Kraus, S., Schmitz, F., DiGiovanna, J., van den Brand, R., Bloch, J., Detemple, P., Lacour, S. P., Bezard, E., Micera, S., and Courtine, G. (2016).
Spatiotemporal neuromodulation therapies engaging muscle synergies improve motor control after spinal cord injury.
Nature medicine, 22(2):138–45.

Wenig, P., Schmidl, S., and Papenbrock, T. (2022).

TimeEval: A benchmarking toolkit for time series anomaly detection algorithms.
Proceedings of the VLDB Endowment, 15(12):3678–3681.

Werner, C., Easthope, C. A., Curt, A., and Demkó, L. (2021).
Towards a Mobile Gait Analysis for Patients with a Spinal Cord Injury: A Robust Algorithm Validated for Slow Walking Speeds.
Sensors (Basel, Switzerland), 21(21).

Whiting, H. T. A. and Bernshtein, N. A. (1984).
Human Motor Actions : Bernstein Reassessed / Edited by H.T.A. Whiting.
Advances in Psychology (Amsterdam, Netherlands) ; 17. North-Holland : Sole distributors for the U.S.A. and Canada, Elsevier Science Pub. Co, Amsterdam ; New York.

Willis, W. D. (2006).
John Eccles' studies of spinal cord presynaptic inhibition.
Progress in Neurobiology, 78(3):189–214.

Wolbrecht, E. T., Chan, V., Reinkensmeyer, D. J., and Bobrow, J. E. (2008).
Optimizing compliant, model-based robotic assistance to promote neurorehabilitation.
IEEE transactions on neural systems and rehabilitation engineering : a publication of the IEEE Engineering in Medicine and Biology Society, 16(3):286–97.

Wolpaw, J. R. and Carp, J. S. (1990).
Memory traces in spinal cord.
Trends in Neurosciences, 13(4):137–142.

Wolpaw, J. R. and Tennissen, A. M. (2001).
Activity-dependent spinal cord plasticity in health and disease.
Annual Review of Neuroscience, 24(1):807–843.

Wolpert, D. M., Ghahramani, Z., and Jordan, M. I. (1995).
An internal model for sensorimotor integration.
Science (New York, N.Y.), 269(5232):1880.

Wosiak, A., Glinka, K., and Zakrzewska, D. (2018).
Multi-label classification methods for improving comorbidities identification.
Computers in Biology and Medicine, 100:279–288.

Wu, H., Petitpré, C., Fontanet, P., Sharma, A., Bellardita, C., Quadros, R. M., Jannig, P. R., Wang, Y., Heimel, J. A., Cheung, K. K. Y., Wanderoy, S., Xuan, Y., Meletis, K., Ruas, J., Gurumurthy, C. B., Kiehn, O., Hadjab, S., and Lallemend, F. (2021a).
Distinct subtypes of proprioceptive dorsal root ganglion neurons regulate adaptive proprioception in mice.
Nature Communications, 12(1).

Wu, H., Xiao, B., Codella, N., Liu, M., Dai, X., Yuan, L., and Zhang, L. (2021b).
CvT: Introducing convolutions to vision transformers.
In *2021 IEEE/CVF International Conference on Computer Vision (ICCV)*, pages 22–31.

Xiong, D., Zhang, D., Zhao, X., and Zhao, Y. (2021).
Deep Learning for EMG-based Human-Machine Interaction: A Review.
IEEE/CAA Journal of Automatica Sinica, 8(3):512–533.

Ye, R. and Dai, Q. (2021).
Implementing transfer learning across different datasets for time series forecasting.
Pattern Recognition, 109:107617.

Yi, C., Chen, H., Xu, Y., Zhou, Y., Du, J., Cui, L., and Tan, H. (2024).
TADA: Temporal-aware Adversarial Domain Adaptation for patient outcomes forecasting.

Expert Systems with Applications, 238:122184.

Ying, Z., Roy, R. R., Edgerton, V. R., and Gomez-Pinilla, F. (2005).
Exercise restores levels of neurotrophins and synaptic plasticity following spinal cord injury.
Experimental neurology, 193(2):411–9.

Yoo, Y., Brosch, T., Traboulsee, A., Li, D. K. B., and Tam, R. (2014).
Deep Learning of Image Features from Unlabeled Data for Multiple Sclerosis Lesion Segmentation.
In Wu, G., Zhang, D., and Zhou, L., editors, *Machine Learning in Medical Imaging*, Lecture Notes in Computer Science, pages 117–124, Cham. Springer International Publishing.

York, J. M., Blevins, N. A., McNeil, L. K., and Freund, G. G. (2013).
Mouse short- and long-term locomotor activity analyzed by video tracking software.
Journal of visualized experiments : JoVE, (76):e50252.

Young, A. L., Marinescu, R. V., Oxtoby, N. P., Bocchetta, M., Yong, K., Firth, N. C., Cash, D. M., Thomas, D. L., Dick, K. M., Cardoso, J., van Swieten, J., Borroni, B., Galimberti, D., Masellis, M., Tartaglia, M. C., Rowe, J. B., Graff, C., Tagliavini, F., Frisoni, G. B., Laforce, R., Finger, E., de Mendonça, A., Sorbi, S., Warren, J. D., Crutch, S., Fox, N. C., Ourselin, S., Schott, J. M., Rohrer, J. D., and Alexander, D. C. (2018).
Uncovering the heterogeneity and temporal complexity of neurodegenerative diseases with Subtype and Stage Inference.
Nature Communications, 9(1):4273.

Young, C. W., Young, M. S., Li, Y. C., and Lin, M. T. (1996).
A new ultrasonic method for measuring minute motion activities on rats.
Journal of Neuroscience Methods, 70(1):45–49.

Young, W. (2015).

Electrical stimulation and motor recovery.

Cell transplantation, 24(3):429–46.

Yue, Z., Wang, Y., Duan, J., Yang, T., Huang, C., Tong, Y., and Xu, B. (2022).

TS2Vec: Towards Universal Representation of Time Series.

Proceedings of the AAAI Conference on Artificial Intelligence, 36(8):8980–8987.

Yuste, R. (2015).

From the neuron doctrine to neural networks.

Nature Reviews. Neuroscience, 16(8):487–497.

Zagoraiou, L., Akay, T., Martin, J. F., Brownstone, R. M., Jessell, T. M., and Miles, G. B. (2009).

A cluster of cholinergic premotor interneurons modulates mouse locomotor activity.

Neuron, 64(5):645–662.

Zehr, E. P. and Stein, R. B. (1999).

What functions do reflexes serve during human locomotion?

Progress in Neurobiology, 58(2):185–205.

Zhang, H., Liu, Y., Zhou, K., Wei, W., and Liu, Y. (2021).

Restoring sensorimotor function through neuromodulation after spinal cord injury: Progress and remaining challenges.

Frontiers in Neuroscience, 15.

Zhang, J., Guillermo, Britz, O., Wang, Z., Valerie, Zhang, Y., Velasquez, T., Francisco, Frank, E., and Goulding, M. (2014).

V1 and V2b interneurons secure the alternating flexor-extensor motor activity mice require for limbed locomotion.

Neuron, 82(1):138–150.

Zhang, X., Wu, L., Zhang, X., Chen, X., Li, C., and Chen, X. (2023).
Multi-source domain generalization and adaptation toward cross-subject myoelectric pattern recognition.
Journal of Neural Engineering, 20(1):016050.

Zhang, X., Zhao, Z., Tsiligkaridis, T., and Zitnik, M. (2022).
Self-Supervised Contrastive Pre-Training For Time Series via Time-Frequency Consistency.
In *Advances in Neural Information Processing Systems*.

Zhang, Y., Narayan, S., Geiman, E., Lanuza, G. M., Velasquez, T., Shanks, B., Akay, T., Dyck, J., Pearson, K., Gosgnach, S., Fan, C.-M., and Goulding, M. (2008).
V3 spinal neurons establish a robust and balanced locomotor rhythm during walking.
Neuron, 60(1):84–96.

Zhao, Y., Wang, J., Zhang, Y., Liu, H., Chen, Z., Lu, Y., Dai, Y., Xu, L., and Gao, S. (2021).
Flexible and Wearable EMG and PSD Sensors Enabled Locomotion Mode Recognition for IoHT-Based In-Home Rehabilitation.
IEEE Sensors Journal, 21(23):26311–26319.

Zhao, Y., Wong, Z. S.-Y., and Tsui, K. L. (2018).
A Framework of Rebalancing Imbalanced Healthcare Data for Rare Events' Classification: A Case of Look-Alike Sound-Alike Mix-Up Incident Detection.
Journal of Healthcare Engineering, 2018:6275435.

Zheng, Y., Mao, Y. R., Yuan, T. F., Xu, D. S., and Cheng, L. M. (2020).
Multimodal treatment for spinal cord injury: A sword of neuroregeneration upon neuromodulation.

Neural regeneration research, 15(8):1437–1450.

Zholudeva, L. V., Abraira, V. E., Satkunendrarajah, K., McDevitt, T. C., Goulding, M. D., Magnuson, D. S. K., and Lane, M. A. (2021).
Spinal interneurons as gatekeepers to neuroplasticity after injury or disease.
The Journal of Neuroscience, 41(5):845–854.

Zhong, G., Droho, S., Crone, S. A., Dietz, S., Kwan, A. C., Webb, W. W., Sharma, K., and Harris-Warrick, R. M. (2010).
Electrophysiological characterization of V2a interneurons and their locomotor-related activity in the neonatal mouse spinal cord.
Journal of Neuroscience, 30(1):170–182.

Zhong, H., Roy, R. R., Nakada, K. K., Zdunowski, S., Khalili, N., de Leon, R. D., and Edgerton, V. R. (2012).
Accommodation of the spinal cat to a tripping perturbation.
Frontiers in physiology, 3:112.

Zhou, Y., Zia Ur Rehman, R., Hansen, C., Maetzler, W., Del Din, S., Rochester, L., Hortobágyi, T., and Lamoth, C. J. C. (2020).
Classification of Neurological Patients to Identify Fallers Based on Spatial-Temporal Gait Characteristics Measured by a Wearable Device.
Sensors, 20(15):4098.

Zhuang, F., Qi, Z., Duan, K., Xi, D., Zhu, Y., Zhu, H., Xiong, H., and He, Q. (2021).
A Comprehensive Survey on Transfer Learning.
Proceedings of the IEEE, 109(1):43–76.

Ziegler, M. D., Zhong, H., Roy, R. R., and Edgerton, V. R. (2010).
Why variability facilitates spinal learning.

The Journal of neuroscience : the official journal of the Society for Neuroscience, 30(32):10720–6.

Zouitni, C., Sabri, M. A., and Aarab, A. (2023).

A Comparison Between LSTM and Transformers for Image Captioning.

In Motahhir, S. and Bossoufi, B., editors, *Digital Technologies and Applications*, Lecture Notes in Networks and Systems, pages 492–500, Cham. Springer Nature Switzerland.